ORBIT™
A FOUNDATION SERIES

ARTIFICIAL SPACE DEBRIS

Nicholas L. Johnson
and Darren S. McKnight

Please Return to
Dr. Mark Hoover



ORBIT™
A FOUNDATION SERIES

ARTIFICIAL SPACE DEBRIS

by
Nicholas L. Johnson
and
Darren S. McKnight

with Foreword by
Donald J. Kessler

ORBIT BOOK COMPANY

MALABAR, FLORIDA
1987

Original Edition 1987

Printed and Published by
ORBIT BOOK COMPANY, INC.
2005 Township Road
Malabar, Florida 32950

Copyright© 1987 by
ORBIT BOOK COMPANY, INC.

All rights reserved. No part of this book may be reproduced in any form or by any means, electronic or mechanical, including information storage and retrieval systems without permission in writing from the publisher.

No liability is assumed with respect to the use of this information contained herein.

Printed in the United States of America.

This book represents the views of the authors and does not necessarily reflect the official opinion of the United States Department of Defense, the Department of the Air Force, or the National Aeronautics and Space Administration.

Library of Congress Cataloging in Publication Data

Johnson, Nicholas L.
Artificial space debris.

Includes bibliographies and index.
1. Space debris.
I. McKnight, Darren S.
II. Title.
TL1489.J64 1987 629.4'16 86-31247
ISBN 0-89464-012-7
10 9 8 7 6 5 4 3 2

We dedicate this book to future space travelers. May our foresight in controlling the growth of artificial space debris provide boundless opportunities for the exploration of the cosmos for generations to come.

Series editor
Edwin F. Strother, Ph.D.

Contents

Foreword vii
Preface ix
1. ***Space Debris Overview*** 1
References 8
2. ***Sources of Space Debris*** 9
Operational Activities 9
Satellite Deterioration 12
Satellite Fragmentations 13
Satellite Fragmentations of Unknown Causes 20
Summary 23
References 24
3. ***Definition and Analysis of the Space Debris Environment*** 25
Measurement of Size and Dispersion 26
Conversion From RCS to Mass 31
Mass and Velocity Distributions 33
Gabbard Diagrams 38
Satellite Fragmentation Event (SAFE) Test 52
Debris Heading Plots 53
Treating a Debris Cloud as a Continuum 55
Determining Breakup Time 58
Simulation of Satellite Breakups 60
Future Measurement Devices 61
Summary 65
References 65
4. ***Hazards From Space Debris*** 67
Impact Theory 68
Debris Models 69
Hazard to Geosynchronous Satellites 77
Summary 81
References 83
5. ***Space Debris Issues*** 85
Recognition of the Space Debris Problem 85
Living With the Present Environment 87
Cleaning Up the Environment 90
Summary 99
References 101
List of Illustrations 103
List of Tables 107
Glossary 109
Index 111

Foreword

During the first 20 years of the space program, there was a perception that the world was successfully placing satellites into an empty, limitless space, and that the North American Aerospace Defense Command (NORAD) was keeping close track of each of these satellites. The measure of our success could be seen in the NASA publication, *Satellite Situation Report*. For example, on 30 April 1976 this report maintained that there were 3,866 objects in orbit, placed there by 17 different countries or organizations. Additional information on what could have been interpreted as very successful launches was found in the footnotes. For example, footnotes 23 and 25 read "110 objects have been identified as having been launched with 1974-089A, 1974-089B, and 1974-089C," and "15 objects have been identified as having been launched with 1975-004A." Why had these launches placed so many objects into orbit? Into what orbits were they placed, and how long would they stay there? These were questions that were rarely asked, even by the serious space observers.

We now know that these, and similar footnotes in the *Satellite Situation Report,* were the most visible public hint of a major process occurring in low Earth orbit: satellite breakups and explosions. As of 30 April 1976 over 40 satellites had fragmented in low Earth orbit, accounting for about half of the catalogued objects in orbit and an unmeasured number of objects too small to be detected by NORAD radars. Yet, few people were aware that any breakups had occurred. Satellites 1974-089B and 1975-004B were both Delta rocket second stages which had exploded in orbit. The latter of these two had successfully placed Landsat 2 into orbit more than a year before it exploded in early 1976. By April 1976 only a small fraction of the fragments had been catalogued. This explosion represented the fourth time that the Delta second stage had exploded in orbit. Yet, the fact that it had exploded was unknown even to the builders of a Delta rocket. Three more Delta second stages would explode in orbit before the issue could be brought to the attention of the proper people, and a solution found. Since 1981 none of the Delta second stages have exploded in orbit.

We are now beginning to recognize that while space may be infinite, Earth orbital space is a finite natural resource that must be managed properly if it is to be continually used. So limited is this resource that a single breakup can sufficiently increase the risk to future satellites that design changes would be required to ensure adequate reliability. This is especially true for large spacecraft which require high reliability, such as NASA's planned space station. Part of the space station design already includes shields to protect the more vulnerable areas against impacts from small fragments. Consequently, satellite breakups are now taken much more seriously. For example, within days of the discovery of an Ariane third stage explosion on 13 November 1986, NASA was alerted and quickly notified its European counterparts. By May 1987 a probable cause had been determined, and new operating procedures were being developed to ensure that similar explosions would not occur in the future.

This is the first book to address the orbital debris problem. Its authors were some of the key people who gathered data on satellite breakups and helped ensure that the space community was aware of their causes and consequences. The book contains sufficient technical information and references to introduce a serious researcher to what is known and not known; yet, it is written so that the nontechnical reader can understand the issues. A proper understanding of the issues will become increasingly important as various governments and organizations begin to write and implement policy. A poorly conceived policy could reduce our access to space just as surely as an uncontrolled growth in orbital debris.

This book will help determine future responsible actions by the space community as activities in space increase and new problems are identified.

DONALD J. KESSLER

NASA
Houston, Texas

Digitized by Google

Preface

In his foreword to this book, Donald J. Kessler recalled that during the first two decades of the space age scant notice was paid to the gradually increasing Earth satellite population. An occasional technical paper would appear in scientific journals examining some obtuse, astrodynamical characteristic of orbiting particle clouds. No perspective was given of the macroscopic changes occurring in the skies above us. In the early morning hours of 29 June 1961, when the Transit 4A rocket body unexpectedly blew itself apart only a few hours after launch, the Earth's satellite population instantly increased by more than a factor of four. Since then Earth's satellite population has increased yet another twentyfold.

The primary objective of this volume is to heighten the awareness of the public at large and the space-faring community in particular to the growing hazards of artificial space debris. We do not paint an apocalyptic picture. Clearly, the present Earth satellite environment poses little threat to the operation of both manned and unmanned satellites. However, the trends of the past 30 years are undeniable. If we do not modify our activities in Earth orbit and adopt a conscious policy aimed at curbing the growth of the debris population, we will bestow upon future generations an ominous legacy.

The authors are encouraged by the widening recognition of the artificial space debris issue. Today, when only 5% of the more than 7,000 trackable objects in orbit about the Earth represent functioning satellites, scientists, engineers, spacecraft owners and operators, lawyers, and even politicians are realizing that we dare not conduct our space business as usual. We must vigorously continue to expand our knowledge of the complex near Earth environment and to devise new techniques to work in harmony with it.

Two individuals stand out in the brief history of artificial space debris studies. John R. Gabbard, as a civilian analyst at NORAD headquarters in Colorado Springs, was instrumental first in identifying the occurrences of satellite fragmentations and later in developing unique methods for evaluating the space environment. His detailed records and dedication for over 25 years laid the foundation for our present understanding of artificial space debris. Donald J. Kessler, NASA's chief scientist on space debris, has been directly responsible for bringing the issue of space debris to the attention of officials not only in the U.S. space program but also in space programs around the world. Through diligent effort, he has brought together the theoreticians and the practitioners. We are indebted to him for his critical review of this book. The authors have been privileged to work with these talented gentlemen for many years and wish to express thanks for their guidance and their friendship.

We would especially like to thank Dr. Joseph Angelo for his suggestion that this project be undertaken to consolidate the current issues and technical developments of artificial space debris. His encouragement in the early stages of this work was vital to its completion. Behind every book is a small army of unsung professionals. We extend our thanks to Alison McKnight and Joy Marnell for converting our rough handwritten manuscript into a legible document and to Lori Ullery, Jamie Nehmer, and Laura DeHart for the final typesetting. Thanks also to Mary Roberts and Dr. Edwin Strother at Krieger Publishing Company for the fine-tuning of the manuscript.

Finally, we wish to thank our families for their love and support during this project: Beth, Kevin, Alison, Joy, and Eric.

Chapter 1

Space Debris Overview

There are more things in heaven and earth, Horatio, than are dreamt of in your philosophy.

Shakespeare, **Hamlet,** I.v.

The term *space debris* immediately raises a mental picture of meteoroid swarms, asteroid belts, and ejecta from comets as they pass close to the sun. Even before the space age began, science fiction tale and cinema had advised us of the dangers of space debris: the penetration of a life-sustaining spacesuit, the damage to manned spaceships, or even the destruction of extraterrestrial outposts on airless celestial bodies. Although ever-present, these dangers were considered remote and acceptable hazards, an unavoidable risk in man's conquest of the universe.

The hazards posed by natural space debris to the near Earth environment were evaluated in detail during the 1960s as both manned and unmanned spacecraft entered space in increasing numbers. These studies found that about 200 kg of meteoroid mass were always moving through a volume within 2,000 km of the Earth (1). Fortunately, most meteoroids are less than 0.1 mm in diameter, permitting the use of effective, low-cost shields in the construction of satellites. The Apollo and Skylab spacecraft were designed to withstand impacts from meteoroids as large as 3 mm in diameter (2). Impacts from particles of this size were expected in Earth orbit only at intervals greater than 1,000 years per m^2 of cross-sectional area.

Soviet experience with their Salyut space station (one-fourth the size of Skylab) over several years indicates the station encounters up to 200 tiny particles every 100 revolutions about the Earth, i.e., about every 6 days (3). For larger particles which might actually penetrate the space station, Salyut's reserve of atmosphere will protect the crew for short periods of time. If the hole is the size of a pinhead, a day will elapse before all the atmosphere has escaped. If the hole is larger, say the size of a pencil, the crew will still have over an hour to make their escape or repair the breach.

Thus the hazard from the natural debris environment has been assessed as acceptable. Of growing concern, however, are the dangers posed by artificial or man-made space debris. Of all the artificial satellites now circling the Earth, less than 5% represent operational, functioning satellites. The remainder constitute an orbiting junkyard of dead satellites, spent rocket stages, discarded equipment, and fragments from satellite breakups.

Since Sputnik 1 invaded the cosmos in 1957, over 18,000 man-made satellites have been tracked and cataloged by the U.S.-Canadian North American Aerospace Defense Command (NORAD). More importantly, the number of known objects in Earth orbit has been increasing steadily. Since the beginning of the 1980s, the Earth's known satellite population has been increasing at a rate of 230 satellites per year (Figure 1.1), despite an annual average international space launch rate of 121.

On the surface these figures do not appear incongruent. For example, if every space launch on the average leaves a payload and a rocket body in orbit, then a population growth rate of approximately 240 satellites per year is to be expected. However, over one-third of all space missions (primarily Soviet) are still very short-lived,

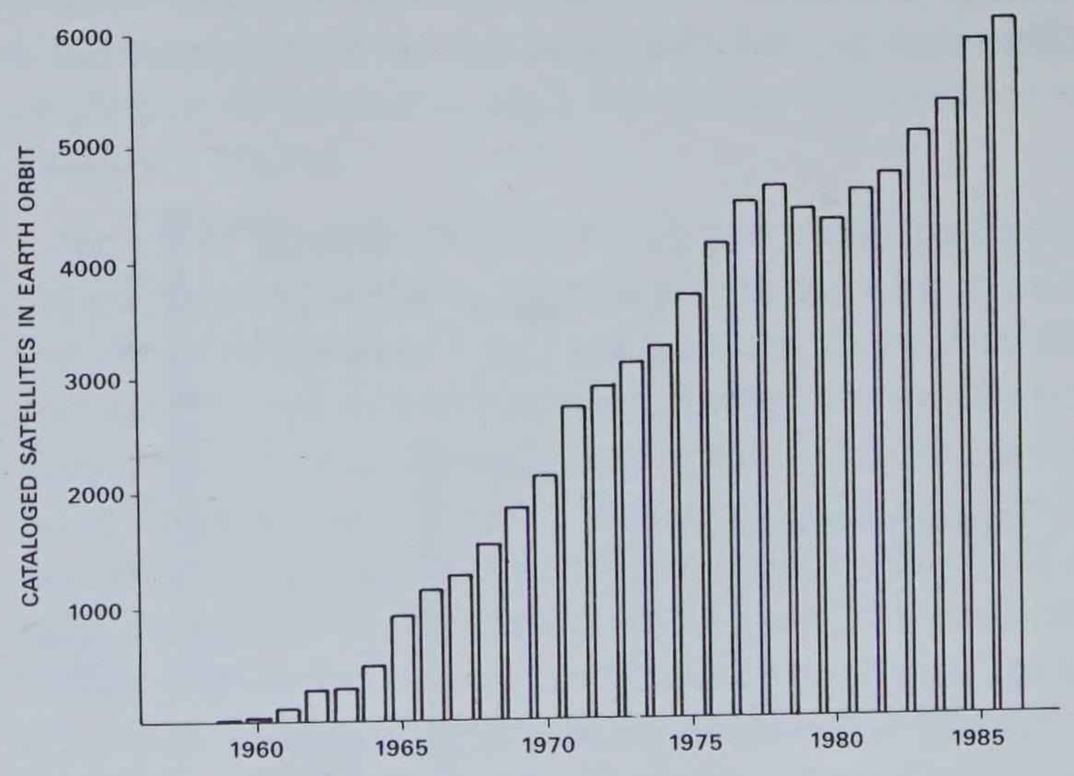


Figure 1.1 With the exception of the period of solar maximum (1979-1980), the known Earth satellite population has been increasing at an annual rate of more than 300 satellites during the past dozen years.

resulting in the reentry of both the payload and the final rocket body within only a few months. For example, the payloads and associated rocket bodies of 37 of the 103 space missions of 1986 were no longer in Earth orbit at the end of that year. In addition, NORAD data indicates man-made objects decay and reenter the atmosphere at the rate of about one a day. What then is the source of this space debris which continues to multiply?

Artificial space debris is the product of (1) normal satellite operations, (2) the deterioration of satellites, and (3) the fragmentation or breakup of satellites. D. J. Kessler of NASA estimates that artificial space debris may account for as much as 2,000 metric tons in Earth orbit today (2). For comparison, the world's most active space-faring country, the Soviet Union, conducts 80% of all space launchings and currently places about 850 metric tons (payloads and rocket bodies) into Earth orbit annually (4). Also noteworthy is a one-third increase in mass to orbit by the U.S.S.R. between 1976 and 1984 while the Soviet space launch rate remained virtually unchanged (99 launches in 1976, 97 launches in 1984).

Each of the three debris categories mentioned above will be discussed in greater detail in succeeding chapters, but it is important to note here that almost one-half of all space debris now in orbit originated during satellite fragmentations. The 90+ recognized fragmentation events (events not associated with any nondestructive operations) are responsible for over one-third of all satellites cataloged since the dawn of the space age (Figure 1.2).

Before the relative hazards between natural and artificial space debris can be compared, deficiencies in our understanding of the artificial space debris environment need to be addressed. The primary data acquisition system for artificial space debris is the NORAD network of conventional dish and phased-array radars scattered around the world. The specific characteristics of this vital network are provided in Chapter 3. In general the sensitivity of the NORAD network is limited to particles 8 cm in diameter and larger at very low altitudes with decreasing sensitivity at higher altitudes. Hence data on very small debris must be acquired through other, sometimes indirect, means. In the larger (greater than 1 cm diameter) sizes, however, the estimated artificial debris flux already exceeds the natural debris flux by one order of magnitude or more (5).

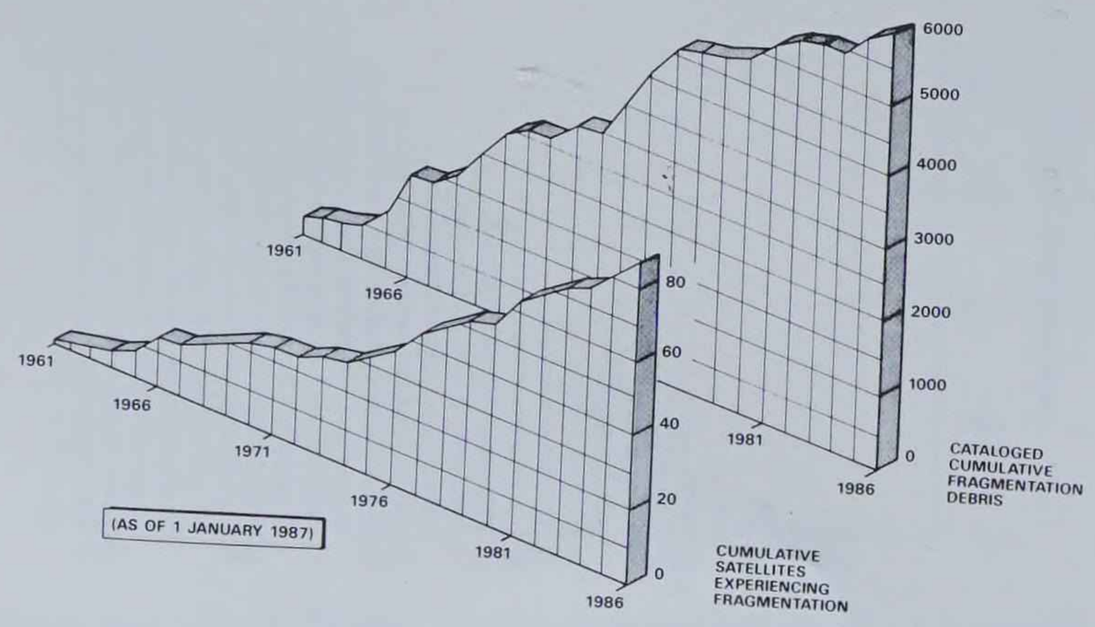


Figure 1.2 Satellite fragmentations account for almost half of all known Earth satellites now in orbit. *Courtesy of Teledyne Brown Engineering.*

Because artificial space debris is not uniformly distributed about the Earth, detailed hazard assessments must consider the operating altitudes and orbital inclinations of their subject payloads. Figure 1.3 illustrates the distribution of the known Earth satellite population. The orbits of virtually all Earth satellites can be characterized as low altitude, semisynchronous, or geosynchronous. Low altitude satellites are those objects in orbits below 5,000 km (orbital periods of 200 minutes and less). This is the most densely populated region of near Earth space and is used for remote sensing, oceanographic, navigation, meteorological, military support, and manned missions.

Semisynchronous satellites, as their name implies, circle the Earth only twice each day, maintaining fixed daily groundtracks with respect to the Earth. Their orbital periods are actually 718 minutes instead of 720 minutes to account for the Earth's movement about the Sun. Semisynchronous orbits can be of two types: circular or highly elliptical. Circular semisynchronous orbits reside 20,000 km above the Earth and are currently used only by the United States and the U.S.S.R. for the latest generation of navigation satellites.

Alternatively, a 718 minute orbital period can be obtained with a perigee near 400 km and an apogee near 40,000 km, i.e., a mean altitude of 20,000 km. This type of orbit with a perigee usually located deep in the Southern Hemisphere and an apogee high above the Northern Hemisphere, was pioneered by the Soviet Union in the 1960s and is currently used by the United States and the U.S.S.R. for communications and strategic surveillance missions. These orbits offer the advantage of complete coverage of the North Polar regions when used at inclinations near 63 degrees where precession of the argument of perigee is retarded. Highly elliptical, near semisynchronous orbits are also used at lower inclinations as transfer orbits for geosynchronous satellites. Only 6% of the cataloged objects now in orbit are in near semisynchronous orbits (6).

Geosynchronous satellites circle the Earth every 1,436 minutes, thereby matching their orbital periods with the rotational period of the Earth. Equatorial geosynchronous satellites appear fixed in the sky and are referred to as geostationary satellites. Although the number of trackable near geostationary satellites is still quite modest (on the order of 300), the fact that these

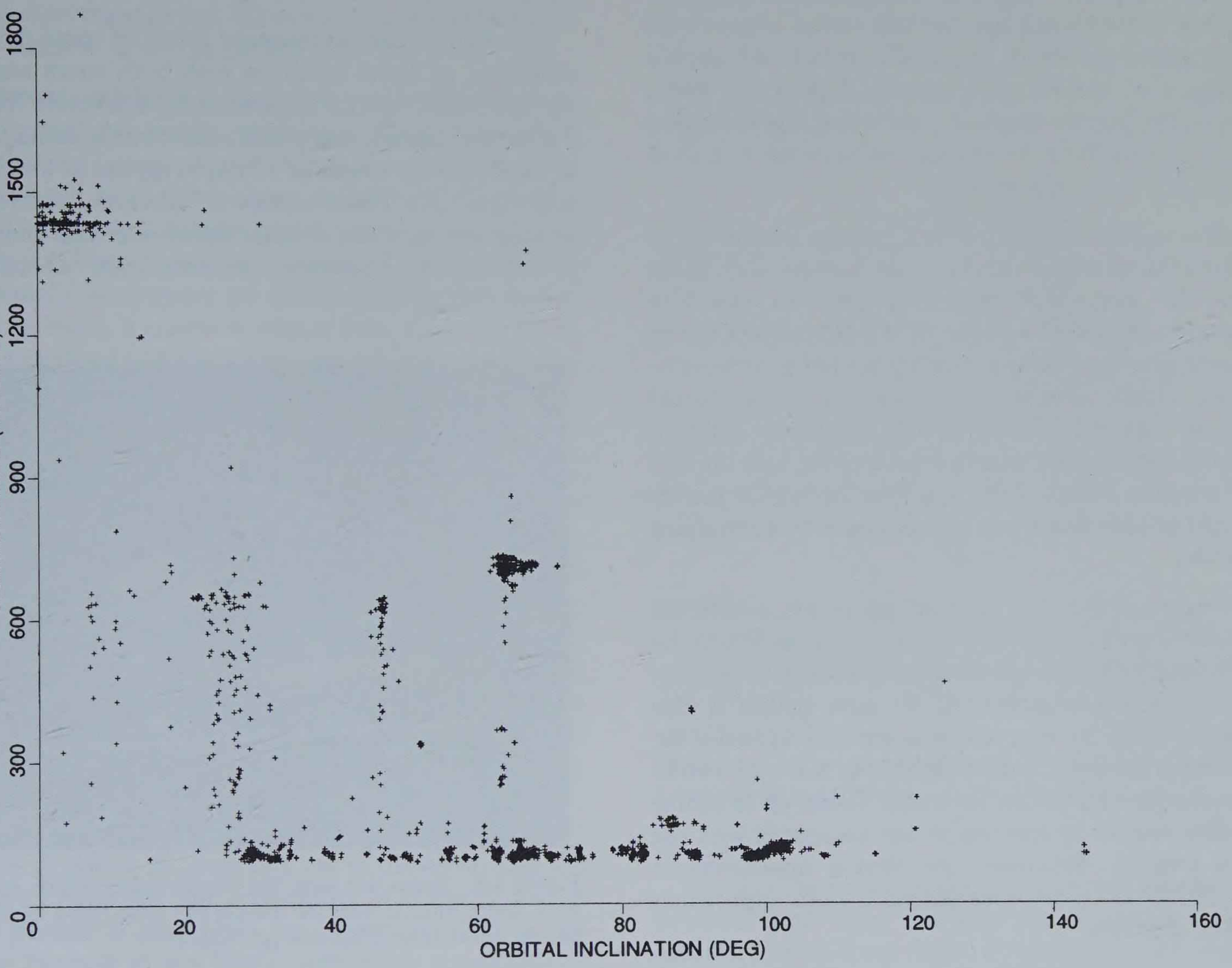


Figure 1.3 Although roughly uniform at low altitudes, the distribution of Earth satellites at high altitudes clearly represents the results of a few specific mission profiles.

satellites are at similar altitudes in virtually a single orbital plane has raised concerns of congestion in the geostationary "ring" (7, 8). As will be shown later, the density of spacecraft in the geostationary ring is still low and spacecraft hazards are mitigated by the very small relative velocities.

The consequences of space debris are diverse, but all have operational and economic influences on those interested in exploiting the near Earth environment. One of the prime motivations behind the establishment of NORAD's space surveillance and tracking mission was to be able to distinguish between satellites and reentering ballistic missile warheads. Today with more than 7,000 satellites in orbit about the Earth, this simple requirement has reached almost Herculean proportions. Every day over 35,000 individual observations are made by NORAD ground-based sensors. Each observation is forwarded to NORAD Headquarters in Cheyenne Mountain overlooking Colorado Springs, Colorado. Here the observations must be checked against the entire satellite catalog to determine if each represents a known or an unknown object.

Very low altitude objects which are about to reenter the Earth's atmosphere, particularly those with a cross-section of more than 1 m^2, are watched more carefully and are tracked at every opportunity to obtain the best prediction of their likely reentry point. Large objects often break up upon reentry or may actually skip across the upper layers of the atmosphere, landing hundreds or even thousands of kilometers away from the predicted impact site. In both cases, without constant monitoring a country might misinterpret an unexpected shower of particles as an attack by an adversary. The United States routinely notifies the U.S.S.R. of any significant satellite reentry over Soviet territory even if the satellite is of Soviet origin.

Another NORAD task of increasing difficulty involves providing collision avoidance information to satellite operators. In 1962 when less than 300 known objects were in orbit about the Earth, the likelihood of two objects colliding was almost infinitesimal. Ten years later, however, the known satellite population had increased tenfold, and collision avoidance was no longer ignored as a statistical improbability.

Today, collision avoidance is routinely conducted in support of three mission areas. Prior to every U.S. space launch the planned orbital trajectory of the new spacecraft is compared with the *NORAD Satellite Catalog* to ensure that the new spacecraft does not pass close to a known satellite. Due to the considerable computational resources required to accomplish this task, collision avoidance windows are usually generated for only the first few hours after launch. After that time the satellite merely relies on the odds that it will not get struck by a damaging projectile.

In the case of the U.S. manned spacecraft, additional precautions are taken. Potential near approaches to the U.S. Shuttle by known satellites are calculated every day. When an object is projected to pass within a few kilometers of the Shuttle, special attention is afforded the encounter. However, to date the Shuttle is not known to have performed a collision avoidance maneuver to escape a possible impact by any object not associated with the Shuttle mission. Whenever the Shuttle maneuvers in space, NORAD recomputes potential close approaches by other satellites.

Geosynchronous satellites represent a third subject of concern for collision avoidance. Because satellites in nonperfect geostationary orbits (usually dead payloads and rocket bodies) drift east or west along the geostationary ring, they frequently will pass close to operational satellites. Although relative velocities are quite low compared to lower altitude satellite encounters, even a slow bumping could irreparably damage a delicate communications satellite. Consequently, NORAD provides orbital data to satellite operators who can then evaluate the possibility of a collision of their satellite with a piece of space junk. This data is also useful to satellite operators when planning to move a spacecraft from one location to another. Due to increased uncertainty in the precise positions of high altitude satellites, some geosynchronous satellites have already performed collision avoidance maneuvers when the projected passage volume was less than the positional uncertainty volume (9).

The jobs of the crews who man the Space Surveillance Center in Cheyenne Mountain and the worldwide sensors 24 hours a day, 7 days a week, would be considerably easier were it not for man-made debris. New radar and electro-optical sensors as well as new computers are now being acquired - at great expense - in part due to the need to monitor the ever-growing satellite population.

More direct consequences of artificial space debris are collisions of Earth satellites with both small and large debris. Small debris, particles with diameters less than 1 mm, will usually not cause catastrophic damage, even at hypervelocity speeds of 10 km/s, typical of low altitude collisions (10). These collisions, however, can result in gradual degradation of solar panel electrical generation or of highly machined surfaces such as telescope

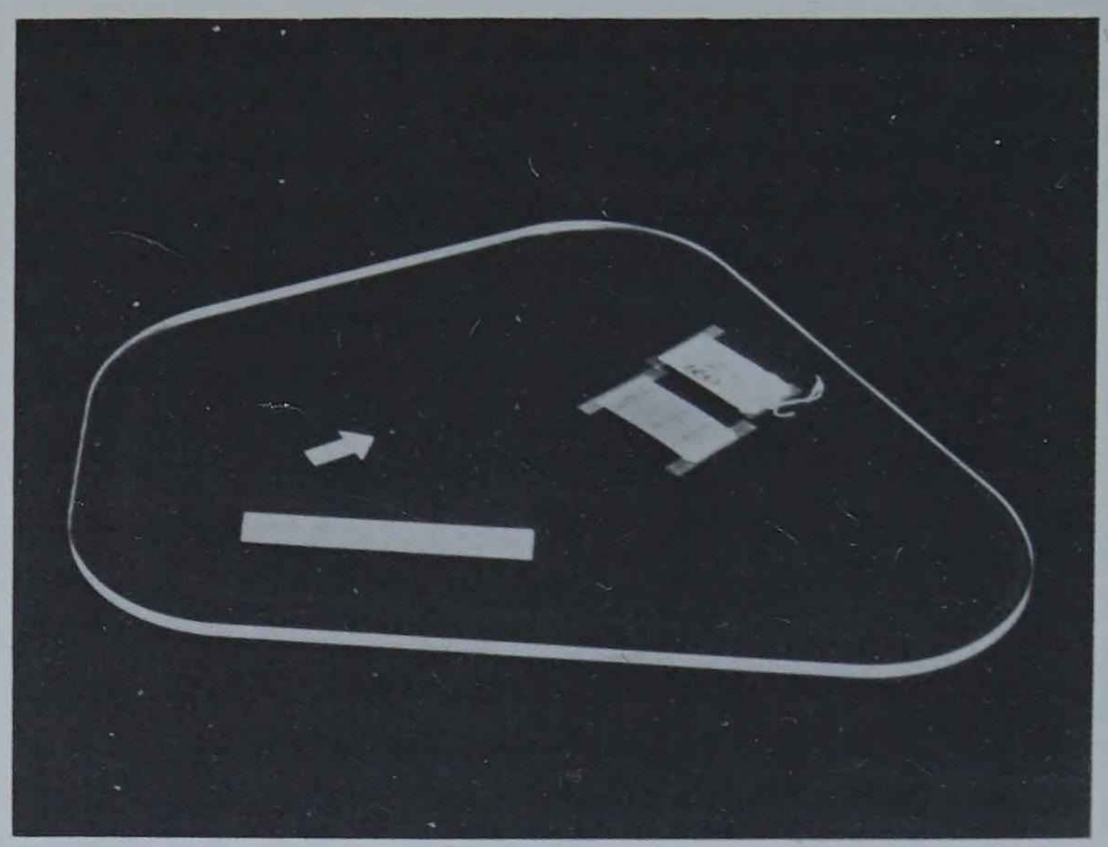


Figure 1.4 From this view the impact crater which appeared on a Space Shuttle window during the 1983 flight of STS-7 is barely noticeable. *Courtesy of NASA.*

Figure 1.5 In this closeup view of the STS-7 Shuttle window impact crater, substrate fracturing is apparent. See Plate 1. *Courtesy of NASA.*

reflectors. A single impact by a submillimeter particle on a U.S. Shuttle window (Figures 1.4 and 1.5) in 1983 did not endanger the crew but did necessitate the replacement of the window at a cost of $50,000.

Collisions with large space debris can be characterized as highly energetic events, resulting in damage exceeding even that of conventional explosive charges. Such collisions can have either direct or indirect effects. If a piece of large debris collides with a working satellite, that satellite will likely cease functioning. The economic and operational consequences are obvious and immediate. On the other hand, a collision with a large rocket body or defunct payload will likely generate millions of particles 1 mm or more in diameter which will in turn pose even greater hazards to operating satellites.

One of the primary objectives of determining the extent of the space debris background is to be able to calculate the probability of collision of a particular satellite with debris of varying sizes. The probability of collision, which is addressed at length later in this volume, is a function of the satellite's cross-sectional area and the debris flux to which the satellite is exposed. Since the debris flux is not uniform in near Earth space, the altitude and, to a lesser extent, the inclination of the subject satellite also affect the resultant probability of collision. To satisfy crew safety requirements, NASA has calculated that the Space Station must be able to withstand hypervelocity impacts of debris as large as 1 cm in diameter. For the station's design life, the probability of colliding with a larger particle is acceptably low, assuming there is not a large increase in low Earth orbit space activities.

Orbiting space debris not only poses hazards to operational spacecraft but also is beginning to affect our observations of the heavens. Artificial Earth satellites now invariably corrupt celestial photographs with exposure times of 90 minutes or more (11). The space debris population will be a double hazard to any space-based telescope, obstructing its view as well as creating a collision hazard. It has been estimated that there is about a 1% chance that the Hubble Space Telescope will be significantly damaged by a piece of space debris during its 17-year mission. Additionally, many instruments on this telescope will be distracted or confused by the many artificial satellites crossing their fields-of-view. As a result the instruments may malfunction or perform poorly (12).

As indicated at the beginning of this chapter, the growth of the known Earth satellite population is cause for concern for future space operations. Despite the apparent vastness of near Earth space, it is all too finite. Like the terrestrial oceans, the sea of space cannot be subjected to indiscriminate abuse by man with impunity. Without a more reasoned approach to space operations, the space environment will become increasingly inhospitable.

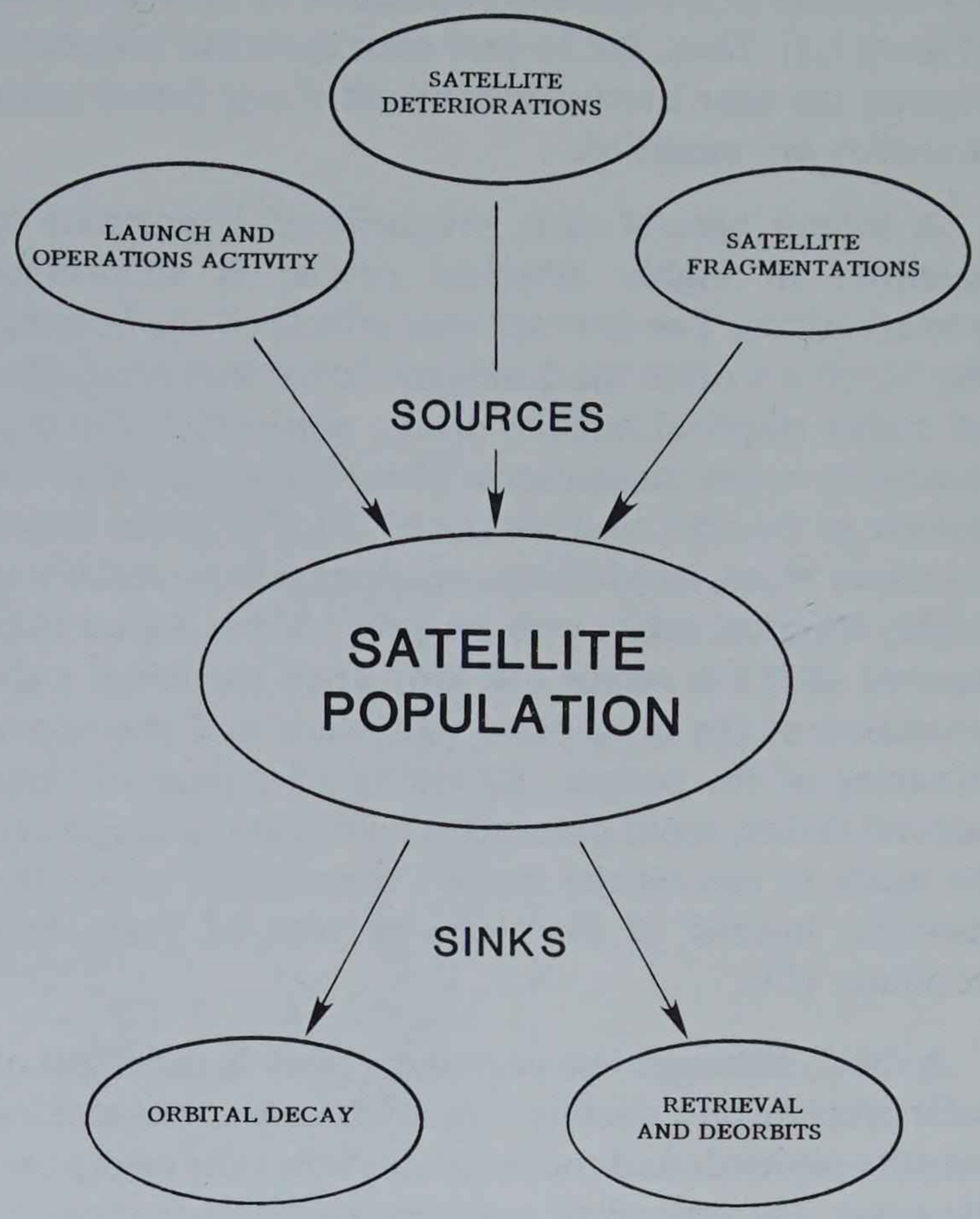


Figure 1.6 The growth of the Earth satellite population is governed by a variety of sources and sinks.

Natural processes provide some relief to the debris problem and help mitigate the polluting activities associated with space flight. Orbital decay, for example, is a natural sink for the removal of space debris and can be caused in three ways (Figure 1.6). The first and foremost is obviously atmospheric drag. Below 500 km, the density of the atmosphere is sufficient to impart significant retarding forces to Earth satellites. While the actual effect of atmospheric drag is dependent upon the satellite's mass and cross-sectional area (i.e., ballistic coefficient), virtually all satellites below 500 km will reenter the Earth's atmosphere within a span of several years.

At higher altitudes the importance of atmospheric drag is considerably less. For example, a satellite in a circular orbit at an altitude of 1,000 km can expect to remain in orbit 1,000 years or more. If, however, the area-to-mass ratio could be increased for spent rocket bodies or payloads no longer of use, these objects could be deorbited at an accelerated rate.

Atmospheric density at any altitude is not constant. Not only are there diurnal changes, but during solar maximum (i.e., increased sunspot activity) the atmosphere is heated, increasing atmospheric density at high altitudes. This effect, which led to the unexpectedly early demise of the U.S. Skylab in 1979, also explains

the decrease in the satellite population in 1979 and 1980 (Figure 1.1). Thus, the 11-year solar cycle can noticeably cleanse the near Earth environment if our future space activities are modified.

A second natural sink, primarily of importance to satellites in highly elliptical orbits, is solar-lunar perturbations. The gravitational effects of the Sun and the Moon are often the dominant factor in the behavior of highly elliptical satellite orbits, particularly those at moderate or low inclinations. These forces can cause the perigee of the orbit to either rise or fall. The Soviet Union routinely places its Molniya communications satellites in highly elliptical orbits with perigees 150 km higher than normal (600 km versus 450 km) when the initial right ascension of the orbit plane will result in a short-term lowering of the perigee. By taking advantage of these natural forces, spent geosynchronous transfer stages can be made to reenter the Earth's atmosphere after only months, instead of the years or tens of years now common (13).

A third, although less prominent, sink is the effect of solar pressure on a satellite. The effect of photons striking satellite payloads and rocket bodies is usually negligible. However, for very small particles, particularly those of a few grams or less, solar pressure can induce rapid orbital decay. Solar pressure appears to be a dominant force in quickly removing solid rocket motor effluents from the space environment (14).

The overall effect of natural sinks is not fully appreciated due to our imperfect understanding of the environment itself. Until recently, little attention has been paid to the Earth's small satellite population; that is, those satellites at the lower end of NORAD's sensitivity and those totally invisible to the NORAD space surveillance system (15). Whereas NORAD's mission is to keep track of all objects in space, preference is of course given to active satellite payloads and larger pieces of space debris.

In addition, the vast majority of NORAD sensors were designed for ballistic missile tracking instead of satellite tracking. Consequently, some sensors are range and sensitivity limited. For example, the older dish radars are capable of tracking only one or two satellites at a time, and thus play smaller roles in the space surveillance network. Although the newer phased-array radars can track hundreds of objects simultaneously, almost all are dedicated strategic warning sensors with only auxiliary space surveillance missions. Missile warning radar waveforms are also not always optimum for tracking small Earth satellites. Finally, missile warning radars are not designed to detect objects only a few centimeters or less in diameter.

Of perhaps equal frustration to the world scientific community is the absence of any satellite tracking data comparable to the NORAD satellite catalogs from the world's largest user of space, the Soviet Union. At the 1984 meeting of COSPAR in Graz, Austria, East European scientists bemoaned their inability to acquire satellite tracking data from the Soviet Union. As a result they had to rely on NORAD data, often several years old, for their analyses and investigations. Even the highly respected U.K. Royal Aircraft Establishment's (RAE) *Table of Earth Satellites,* which is published monthly and distributed around the world, depends primarily on satellite tracking data issued by NORAD.

Because radars rely on the reflection of a pulse of electromagnetic energy off a satellite target, they are particularly susceptible to altitude effects. While some NORAD radars can detect 5 cm diameter particles below 500 km, at an altitude of 1,000 km only particles 10 cm or more are usually detectable. This problem is of course accentuated at geosynchronous altitudes where objects less than 1 m in diameter may be invisible to radar as well as to optical and electro-optical sensors. For this reason the true near geosynchronous satellite population may be many times that now known.

As a result of these limitations, the magnitude of the so-called rain-down effect is important. Rain-down is the process of gradual altitude reduction due to any of the natural effects described earlier. Rain-down permits objects which were originally outside NORAD's sensitivity limits to be detected at lower altitudes. For example, 5 cm particles generated during a satellite explosion at 1,000 km would not normally be detected by the NORAD network until they had decayed to an altitude of perhaps 500 km. If the rate at which these particles "appear" is known, an estimate of the size of the debris reservoirs at higher altitudes could be made.

Without doubt the biggest obstacle facing the space debris issue is simple recognition. To date, no international guidelines or regulations pertaining to space debris exist. The closest the international space community has come to acknowledging the problem is to provide liability recourse in the event of damage caused by a space object. In the case of a collision with a small, untracked satellite, determining the national origin of the satellite would be all but impossible.

The only apparent regulation of space activity to date is through the International Telecommunications Union (ITU). The ITU assigns frequency bands for different satellite applications and in geostationary orbit governs the allocations of frequency locations. Although the intent of the latter regulation is to prevent radio frequency interference (RFI), the result is a de facto regulation of satellite positioning. The removal of spacecraft from geostationary orbit at their end-of-life is also recommended but is not yet mandatory.

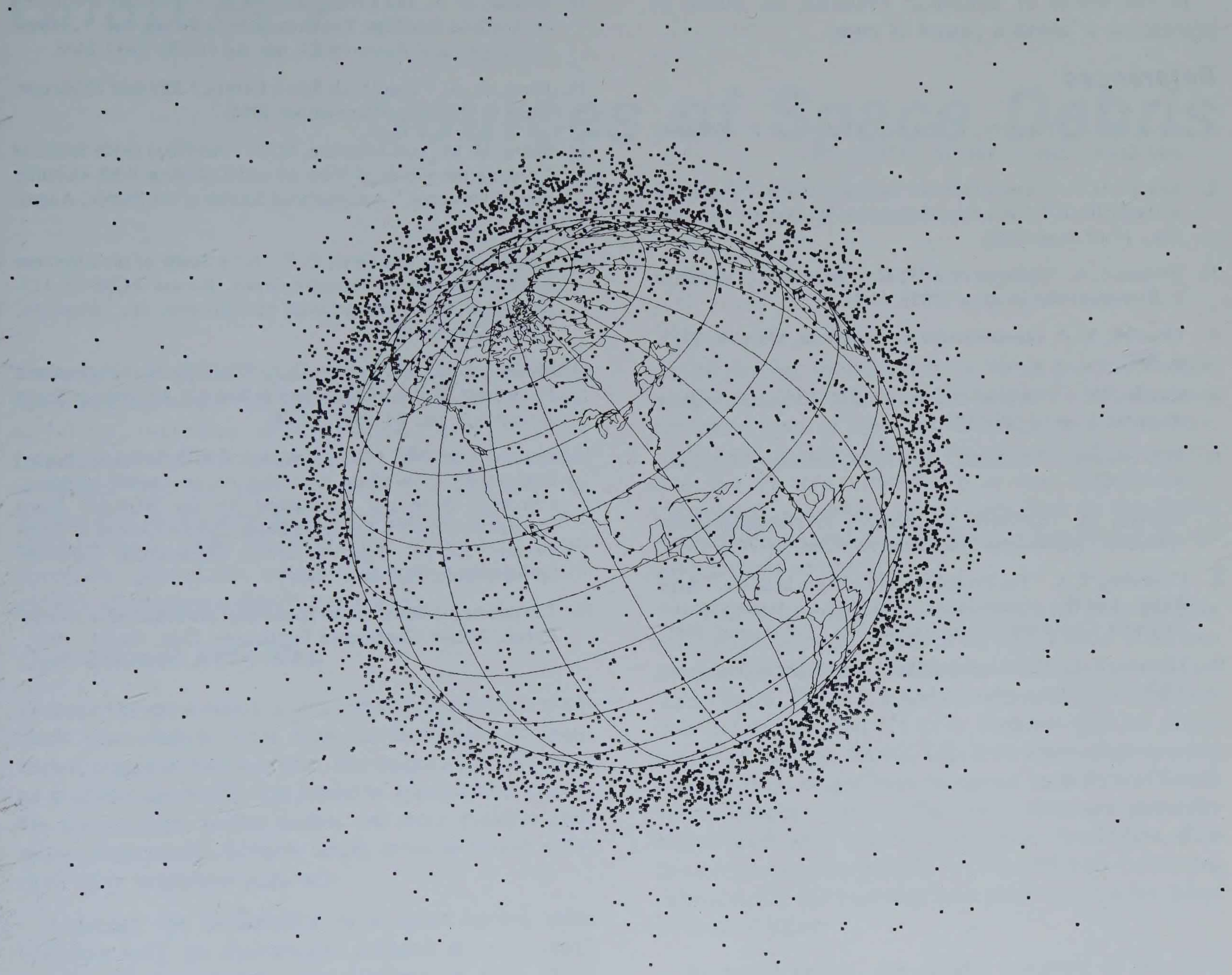


Figure 1.7 The state of the near Earth environment is graphically illustrated in this snapshot of the locations of all cataloged satellites in July 1987. *Courtesy of Teledyne Brown Engineering.*

The reluctance to recognize the space debris issue is paradoxically perhaps greatest among satellite owners and operators. A typical response came at the first national space debris conference hosted by NASA Johnson Space Center in 1982 (16). At that meeting a representative of a satellite operator would not acknowledge that a space debris problem existed, because in 25 years of experience no satellite was known to have been seriously disabled by space debris. While probably accurate (the causes of some satellite failures are still unknown; see Chapter 2), the assessment was at best short-sighted. Most agree that space debris currently poses only a slight hazard to space operations. However, unless some space activity philosophies are fundamentally modified, a serious space debris problem will develop. Regrettably, the definition of the present space environment is sufficiently poor to prevent a reasoned prediction of when space debris will begin to present more severe hazards.

Underlying the debate is the possibility that by the time space debris begins to affect space operations detrimentally, our ability to effect a remedy may be curtailed (Figure 1.7). Carried to its logical conclusion, space debris in Earth orbit could grow to the point where it is self-regenerative, i.e., the rate of debris generation by satellite-satellite collisions will exceed the rate of debris removal by natural sinks. This situation, called the Kessler syndrome after Donald J. Kessler of NASA who proposed the possibility (10), would result in a continual cloud of space debris about the Earth which could seriously impair our utilization of near Earth space. Cleaning up the environment at this stage might require a monumental undertaking.

In the words of Benjamin Franklin, an ounce of prevention is worth a pound of cure.

References

1. Zook, H. A.; Flaherty, R. E.; and Kessler, D. J. *Planetary and Space Sciences.* Vol. 18, 1970, p. 953.
2. Kessler, D. J. "Orbital Debris - Technical Issues." Presented at the SDIO/IST Space Experimentation Workshop, Orlando, Fla., 17-19 June 1986.
3. Berezovoi, A. "Memoirs on a 211-Day Spaceflight." *Aviatsiya I. Kosmonavtika* (August 1983): 40-41.
4. Glushko, V. P. *Kosmonavtika Encyclopedia.* Moscow, 1985, p. 498.
5. Kessler, D. J. "Orbital Debris Issues." *Advances in Space Research* 5, no. 2 (1985): 3-10.
6. *RCS Catalog.* USSPACECOM/J3SOS, Peterson AFB, Col., April 1987.
7. Hechler, M. "Collision Probabilities at Geosynchronous Altitudes." *Advances in Space Research* 5, no. 2 (1985): 47-57.
8. Chobotov, V. A. "The Probability of Collision in Space." AAS Paper 81-148, presented at AAS/AIAA Astrodynamics Specialist Conference, Lake Tahoe, Nev., 3-5 August 1981.
9. Johnson, N. L. "The Crowded Sky." *Spaceflight* 24 (December 1982).
10. Kessler, D. J., and Cour-Palais, B. G. "Collision Frequency of Artificial Satellites: The Creation of a Debris Belt." *Journal of Geophysical Research* 83, no. A6 (1978): 2637-2646.
11. Hoag, A. A. "Too Much Space Debris." *Sky and Telescope,* letter to the editor (September 1986).
12. Shara, M. M., and Johnston, M. D. "Artificial Earth Satellites Crossing the Fields of View of and Colliding With Orbiting Space Telescopes." Astronomical Society of the Pacific, August 1986.
13. Mueller, A. C., and Graf, O. F., Jr. *A Study of the Lifetimes of Geosynchronous Transfer Orbits.* Report ACM-TR-115, Analytical and Computational Mathematics, Inc., Houston, Tex., January 1979.
14. Mueller, A. C., and Kessler, D. J. "The Effects of Particulates From Solid Rocket Motors Fired in Space." *Advances in Space Research* 5, no. 2 (1985): 77-86.
15. Beginning in 1983 NASA contracted with Teledyne Brown Engineering to produce a catalog of very small satellites, especially those not maintained by the NORAD space surveillance network. See for example, *Sample Catalog of Small Objects,* 5th ed., Teledyne Brown Engineering, Colorado Springs, Col., February 1986.
16. The papers presented at this conference are collected in *Orbital Debris,* NASA Conference Publication 2360, NASA, 1985.

Chapter 2

Sources of Space Debris

The origins of artificial space debris are as varied as the satellites from which they emanate: namely, operational activities, satellite deterioration, and satellite fragmentations. An examination of each of these categories will not only illustrate and quantify the influence of debris generation mechanisms, but will also identify those areas where modest changes in space operation procedures could eventually mitigate the growth of the space debris population.

Operational Activities

Perhaps the most obvious and certainly the largest man-made space debris arises from the deposition of spent rocket stages in Earth orbits. The majority of the mass of artificial space debris is found in spent rocket stages. On the average, rocket bodies are more massive and, more importantly, possess larger cross-sectional areas than their respective payloads.

Although the probability of a spent rocket stage colliding with an operational payload is quite small because of the relatively few numbers of each, spent rocket stages represent a tremendous store of mass for future space debris. This debris could be produced by a collision between the rocket body and a much smaller piece of space debris. Because the flux of smaller space debris is considerably higher than that of functioning satellites, the probability of a debris-rocket body collision is similarly higher.

Rocket stages can be further subdivided into three categories: parking orbit stages, transfer orbit stages, and final stages. Any given launch profile may incorporate any or all of these vehicles. Parking orbit stages are designed to lift a payload and additional rocket stage(s) into a low Earth orbit, typically less than 400 km. From this orbital vantage point the payload can be maneuvered into a longer-lived low altitude orbit, a high altitude orbit, or an Earth-escape trajectory for missions to the moon and planets.

Parking orbit stages are typically large, possess high ballistic coefficients (most of their mass has been consumed), and decay very quickly. For example, a typical parking orbit stage for a Soviet geosynchronous or interplanetary mission is 12 m long and 4 m in diameter and has a mass of 4,000 kg. This equates to a ballistic coefficient of about 0.01 m^2/kg, which leads to reentry into the Earth's atmosphere in one or two days. Consequently, parking orbit stages pose no significant space debris hazard because they are removed from the environment so quickly.

Transfer orbit stages are usually smaller than parking orbit stages because they need only lift a lesser mass into a new orbit requiring a change in velocity of usually less than 2 km/s. The U.S. PAM transfer orbit stage measures only 2.3 m long and 1.5 m in diameter with an empty weight of less than 500 kg. Like their lower stage cousins, transfer orbit stages have moderate ballistic coefficient values (about 0.005 m^2/kg) since they are primarily hollow shells after successful operation. In addition, their low perigees (again typically less than 400 km) ensure that orbital decay will normally take place within a few years or tens of years.

As noted earlier, the careful selection of the right ascension of the transfer orbit stage's initial orbital plane can often greatly accelerate the decay process by taking advantage of solar-lunar perturbations (1, 2). An improper choice could lead to considerably longer lifetimes. Although small in number, transfer orbit stages could provide a critical coupling between the low altitude satellite population and high altitude satellites. If, for example, a transfer orbit stage fragmented either by a collision at low altitude or due to an on-board accident, much of its debris would be ejected into highly eccentric elliptical orbits. This debris could then induce fragmentations at high altitudes. Fortunately, in the case of geosynchronous transfer orbits ($i = 25°$ for U.S. launches and $i = 47°$ for Soviet launches), the argument of perigee precesses relatively rapidly. Therefore, the latitude of apogee will quickly drift away from the more densely populated equatorial regions, and the opportunities for colliding with geosynchronous satellites will occur infrequently. However, when they do pass through the geosynchronous region, the higher relative velocity between the geosynchronous satellites and

transfer orbit stages would create more debris in the case of a collision.

Of potential concern in this area is the reported performance of the European Space Agency's (ESA) Ariane upper stage. The first Ariane geosynchronous transfer stage is known to have experienced a fragmentation. More recent conversations with ESA personnel in 1986 and 1987 indicate that additional transfer stages broke up in 1985 and 1986. This being the case, the possibility of a breakup in geosynchronous orbit caused by debris may increase. The situation is compounded because Ariane vehicles use orbital inclinations of only 7 degrees, within the geosynchronous drift band. Solar-lunar perturbations will cause equatorial geosynchronous satellites to cycle through orbital inclinations of up to 15 degrees.

Since final orbit stages deliver payloads to their operational orbits, the orbit of the final stage will usually differ from that of the payload only slightly, the difference arising from the small change in velocity imparted to the payload at separation. Even so, the probability of the final stage colliding with the payload after a successful separation is almost negligible. However, because final orbit stages are often placed in long-lived orbits, they present excellent targets for smaller debris and thus become a source for secondary debris.

The removal of final orbit stages from Earth orbit could be accelerated at very small expense. Ideally, the stage could be designed to contain residual propellents after completing its payload delivery mission. If the propulsion unit were then reignited to produce a retrograde impulse, the final orbit stage's perigee could be lowered significantly. Reentry need not be immediate since a lower perigee, particularly one below 300 km, would effectively remove the rocket body from Earth orbit before a collision with another orbiting object would have much possibility of occurring. Even if the rocket body were struck and fragmented before reentry, had the vehicle been placed in an orbit of lower perigee, the majority of the subsequent debris itself would be in short-lived orbits and would be cleansed from the environment within a moderate time.

In addition to the rocket casings, some upper stages have recently come to be recognized as direct polluters of the near Earth environment. Modern solid fuel upper stages, particularly those used for injection to geosynchronous transfer and final orbits, are seeded with large quantities of aluminum which burn to aluminum oxide (AL_2O_3) to dampen burn rate instabilities (3). These particles, which are ejected through a wide range of flight path angles at velocities of up to 4 km/s, are usually no larger than 10 μm in diameter. As many as 10^{20} AL_2O_3 particles can be ejected during a single solid rocket motor firing (4).

Mueller and Kessler have shown that the AL_2O_3 flux immediately after an engine burn exceeds that of the meteoroid environment for similarly sized particles. Fortunately, solar pressure acts on these particles to remove up to 95% within a year of the firing. However, while in orbit the particles present a non-negligible hazard to some scientific equipment. When a 1.5 m^2 section of thermal blanket was returned from the Solar Max satellite following its repair by Shuttle astronauts, over 1,000 craters greater than 20 μm were discovered. Many of these craters were attributed to collisions with solid rocket AL_2O_3 effluents. At the operational altitude of Solar Max, AL_2O_3 particle lifetimes should be very short. This suggests that Solar Max penetrated a "new" cloud (highest particulate density) of AL_2O_3 particles created by a solid rocket firing or that there is a buildup of AL_2O_3 particles in near Earth space the physics of which is not yet fully understood.

Operational space debris also entails loose hardware which is intentionally or inadvertently ejected during satellite launch, operation, or recovery. Staging events between parking orbit and transfer orbit stages and between transfer orbit and final orbit stages are usually accomplished by explosive bolts. When these devices are activated, dozens of small fragments are produced. Motion pictures of Saturn V staging events reveal many particles flying away from both stages.

Occasionally some of the larger fragments are actually tracked and cataloged by NORAD. In December 1985, NORAD cataloged three pieces of debris in a Soviet parking orbit along with the parking orbit stage and an accompanying platform. Even more dramatically, in June 1986 when a Soviet nuclear power supply was moved to a high altitude storage orbit (see Chapter 5), more than two dozen pieces of debris were detected and cataloged. Three-fourths of these were found in orbits with perigees greater than 500 km, suggesting lifetimes varying from 3 to 1,000 years or more. Many more smaller, undetectable pieces were almost certainly generated during this maneuver.

The lifetime of staging debris and its consequent importance to the growth of the debris population are, of course, dependent upon the altitude of the deposition and the nature of the debris. Parking orbit and transfer orbit staging debris usually reenter the Earth's atmosphere within a short period of time.

A similar debris problem arises when a spacecraft is deorbited and returned to Earth. This applies not only to manned and man-related spaceships (i.e., unmanned resupply vehicles), but also to a large number (35 annually) of Soviet military reconnaissance and Earth resources spacecraft. Prior to 1984, NORAD historically would catalog four to five objects created during the

reentry process. The debris is generated by the ejection of equipment just prior to retrofire to reduce the mass of the spacecraft and thereby lessen propulsion requirements. In November 1984, NORAD was able to increase the overall sensitivity of its space surveillance network for low altitude objects by about an order of magnitude. Immediately, the observed number of debris spawned by Soviet satellites prior to reentry doubled.

Since staging and reentry events are normally explosive in nature, a large number of particles can be assumed to be produced. However, the limitations of the NORAD space surveillance network currently prohibit an accurate estimation of the true number of debris pieces generated. In the case of the nuclear power supply transfer noted above, this operation only produced an average of three to four pieces of observable debris. Since this was before NORAD's sensitivity was increased, the unseen operational debris population may be many times that of the known population.

The separation of a payload from its final rocket stage is usually a more gentle event due to the relative delicacy of many payloads. Many payloads are pushed away from the rocket with springs or similar devices. This usually results in a slight posigrade velocity increment, raising the orbit of the satellite slightly above that of the rocket and reducing the probability of collisions between the two at a later date (note that rocket bodies normally decay faster than their payloads).

Some of these payload deployment mechanisms themselves are cast off after use and become space debris. Sometimes special weights or yo-yos are used to spin up a satellite at deployment or stabilize it in a particular fashion. These also often become new satellites in their own right.

Once the payload has been properly separated, other debris can still be liberated. A frequent source of such debris is the intentional ejection of protective shields and covers over sensitive sensors, such as telescopes or attitude control and navigational sensors. Greater use of hinged covers or sliding sheaths could reduce this source of debris.

Planned experiments in space can also create considerable numbers of debris pieces. An example is the Westford needles experiments conducted in 1961 and 1963 (5). The project's goal was to release large quantities of small copper dipoles resonant at x-band and radio frequencies at a moderate altitude of 3,900 km. The first attempt in October 1961 was completely unsuccessful: no dipoles were dispensed. A second try in May 1963 was only marginally successful. Over 300 million dipoles, each about 2 cm long, were to be reeled out of a spinning canister. The dipoles were bonded together with an agent designed to deteriorate rapidly when exposed to solar radiation, thus freeing the individual dipoles. A "belt" of dipoles 8 km wide and 40 km deep was expected.

Unfortunately, payload separation did not occur properly, resulting in some free dipoles (which decayed as planned within a few years) but also resulting in clumps of dipoles. Of the 100 clumps cataloged by NORAD to date, 60 were still in orbit as of 1 January 1987. Since many of these clumps are at NORAD's sensitivity threshold for their altitudes, much more Westford space debris is probably still present, although the smaller debris would be expected to reenter more quickly.

Another example of planned satellite dispersal is a class of Soviet satellites believed to fulfill radar calibration missions (6, 7). Over a span of a few years these satellites eject up to 25 or more small objects which are then apparently used to calibrate large, ground-based radars in the Soviet Union. Since the objects are ejected at relatively low altitudes (below 500 km) and exhibit much higher ballistic coefficients than the parent satellite, this debris (as designated by NORAD) decays rather quickly and poses no long term threat to the near Earth environment.

Manned activity in space can also lead to both deliberate and inadvertent space debris. During its almost 5 years in space, the Soviet Salyut 6 space station was responsible for over 100 cataloged pieces of debris. In less than four years its successor, Salyut 7, had generated almost 200 pieces of debris (8). Most of this debris is small refuse and human waste. Larger items are loaded into Progress robot ships and are destroyed during reentry. Because of the low operating altitude of Salyut space stations (below 400 km) most of this debris reenters the atmosphere within a year.

More celebrated pieces of debris include Ed White's glove which drifted out of his Gemini spaceship during the first American space walk in June 1965 and a powered screwdriver lost during the repair of Solar Max. Also, during the examination of the Solar Max thermal blanket mentioned earlier, a single impact was discovered which penetrated three layers of the 17-layer blanket. Analysis of the resulting crater suggests the object was probably an ice particle from the Shuttle waste management system (9).

The final category of operational space debris is that of dead satellite payloads. Most satellites not specifically designed for recovery are simply left in Earth orbit to decay naturally. Exceptions are very large objects, such as Soviet space stations and unmanned resupply ships, which may partially survive reentry and cause damage on Earth. These vehicles are deliberately brought down over wide ocean areas where any debris will fall harmlessly into the sea. A controlled reentry was also eventually planned for the U.S. Skylab, but forces described in the preceding chapter prevented this.

Nevertheless, abandoned spacecraft in both low and high altitude orbits constitute one of the most severe hazards to space operations. As with their defunct rocket bodies, the dead satellites are more worrisome as sources of debris after impacts by smaller objects than as direct threats to operating spacecraft. Removal of dead satellites from Earth orbit can be an expensive proposition. Mass retrieval by the Shuttle is both impractical and in some cases dangerous to the crew. The inclusion of a deorbit propulsion system is technically straightforward, but it results in decreased payload weight and ultimately leads to increased costs.

Perhaps a cheaper solution for failing low altitude satellites and spent rocket stages is the erection of structures designed to increase the satellite's cross-sectional area and thus accelerate natural orbital decay. This could be effected by deployable panels or an inflatable balloon. A liability of this technique is that the higher cross-sectional area will increase the probability of colliding with existing debris, creating even more debris.

Satellite Deterioration

A little understood source of space debris comes from the gradual deterioration of old spacecraft and rocket bodies. The primary culprits in these deteriorations are atomic oxygen and solar radiation.

For many years atomic oxygen has been suspected as the agent behind the apparent stripping of paint from spacecraft surfaces. Over half of the impacts on the recovered Solar Max material are believed to have been caused by man-made debris, and many of these appear to be from tiny paint flecks (10). The impact on the Shuttle window during the STS-7 mission, depicted in Figures 1.4 and 1.5, was almost certainly a 0.2 mm diameter paint fleck (Figure 2.1). Spacecraft paint is usually required for thermal control rather than cosmetic reasons.

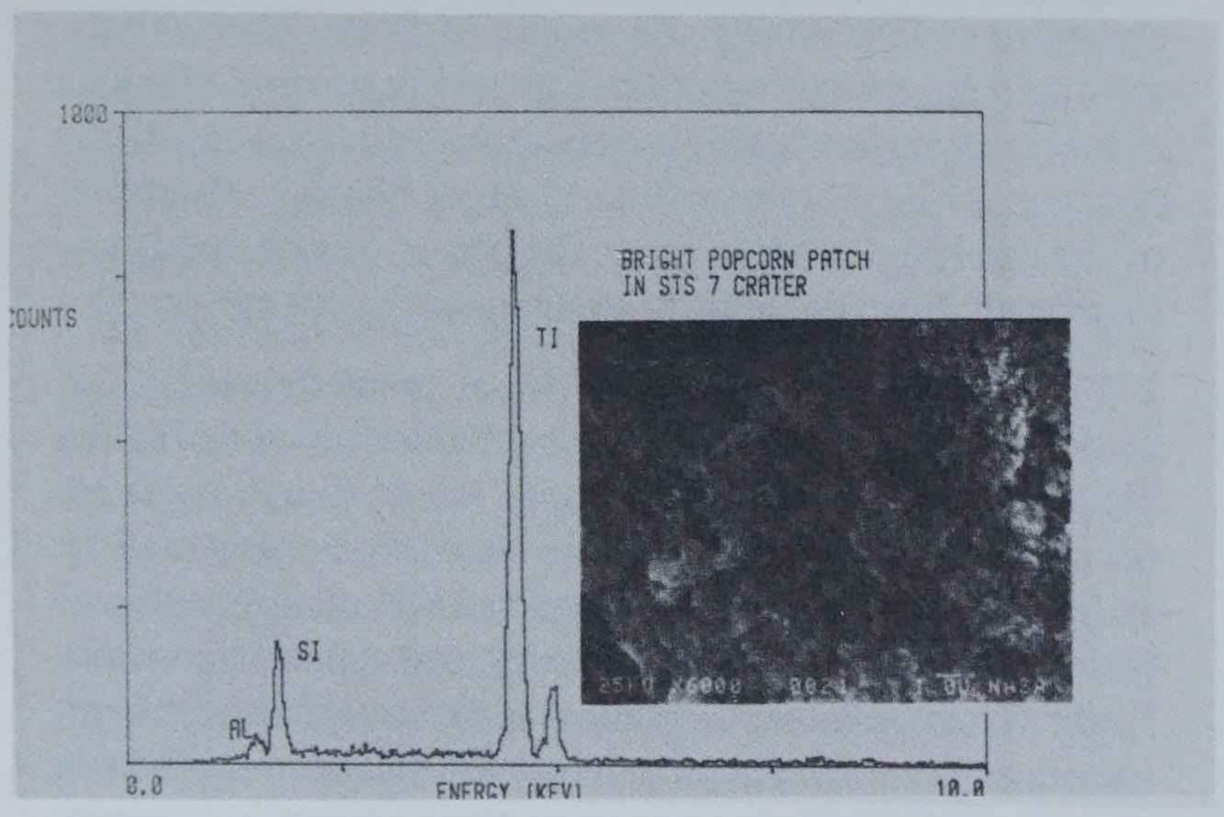


Figure 2.1 Examination of the STS-7 impact crater with an electron scanning microscope revealed material consistent with a fleck of spacecraft paint. *Courtesy of NASA.*

Although the density of atomic oxygen at even 500 km altitudes is quite low, the large volumes of space swept out by satellites traveling at speeds of up to 8 km/s provide ample opportunities for atomic oxygen encounters. Atomic oxygen can react with and degrade organic paint binders, allowing separation of small segments. Experience with the Shuttle at very low altitudes indicates this reaction can occur in very short periods. Some exposed surfaces in the Shuttle cargo bay have been stripped of paint in a single week-long mission. The large number of dead satellites in low Earth orbits may be considered as a substantial reservoir of space debris, continually raining down through the lower altitudes.

Other metallic and nonmetallic materials are also vulnerable to atomic oxygen. The thermal blankets returned from Solar Max were made of Kapton and aluminized mylar layers separated by a dacron net. After just over four years exposure in space, the outer Kapton layer was eroded from 75 μm thickness to 55 μm thickness by atomic oxygen (11).

Experiments flown on STS-5 and STS-8 indicate that atomic oxygen may be even more a hazard to spacecraft than previously believed (12). Extrapolation of data collected on these flights suggests that graphite-epoxy composite members of a planned NASA space station could lose more than half of their 0.15 cm thickness within 30 years to atomic oxygen alone. Solar arrays could lose their entire Kapton substrates during a single solar cycle, i.e., 11 years. Much of this material will find its way into the space environment in the form of microscopic particles which may then interfere with other spacecraft.

Repeated heating by solar radiation can induce thermal stresses and result in structural failures. Perhaps the clearest example of this phenomenon is the history of explosive fragmentations of Delta second stages (to be discussed in greater detail later in this chapter), apparently due to the inadvertent mixing of propellents when an internal membrane ruptured. Less dramatic effects may be caused by the loss of flexibility in plastics and polymers after years of exposure to solar radiation. Whereas the cause for the initial fragmentation of the 14 m diameter Pageos balloon after 10 years in space is still unknown, the reason for subsequent observed breakups of Pageos pieces may be due to a naturally induced spin-up of the now brittle pieces (13). Even the short-term exposure of unprotected satellite surfaces to solar radiation can cause considerable damage, as witnessed during the initial phase of the U.S. Skylab program (14).

Satellite Fragmentations

Clearly the single largest source of man-made space debris has been the fragmentation of over 80 satellites since 1961. In the intervening quarter century, satellite fragmentations have accounted for over one-third of all satellites cataloged and now constitute almost one-half of the known Earth satellite population.

Beginning in 1983 one of the authors, under the sponsorship of NASA, directed the first comprehensive effort to identify, to characterize, and to assess the probable cause of every known satellite breakup (15). A satellite breakup is defined as a debris-producing event which results in the disruption of the parent satellite. Therefore, normal operational events or satellite deteriorations regardless of the amount of debris produced are not considered breakups.

The purpose for trying to determine the causes of satellite fragmentations was two-fold. By understanding the mechanisms of the fragmentations, estimates could be made of the number of untrackable debris pieces. Models designed to simulate low and high intensity explosions and hypervelocity collisions could be exercised to predict the number of fragments of a given size range, their probable orbits, and the orbital evolution for each known breakup. Thus a better estimate of the present day environment can be obtained.

Secondly, by realizing and calling attention to the causes of satellite fragmentations, future breakups might be prevented. This philosophy was instrumental in NASA's investigation and ultimate solution to the Delta second stage breakup problem. Simple education of the space-faring organizations was also expected to decrease the number of unnecessary satellite breakups.

Causes for satellite breakups have been divided into the following three general categories: deliberate actions, accidental propulsion-related events, and unknown causes. The last category, which is also the largest, is a reflection of an inability to select a single, high probability cause for a satellite breakup. This condition may be due to a lack of telemetric data, lack of observational data, or the reluctance of the satellite owner/operator to cooperate during the breakup investigation.

Figure 2.2 vividly illustrates the relative influence of these breakup categories at five year intervals. Of particular concern to those involved in space operations is the trend toward more breakups. Fortunately, this trend has been mitigated somewhat by a decline in the average number of fragments observed after each event. Prior to 1975 the average number of trackable debris resulting from a satellite breakup was 100. Since then the number of debris per event has fallen to 35. Finally, Figure 2.2 also indicates the number of Western and Soviet satellites

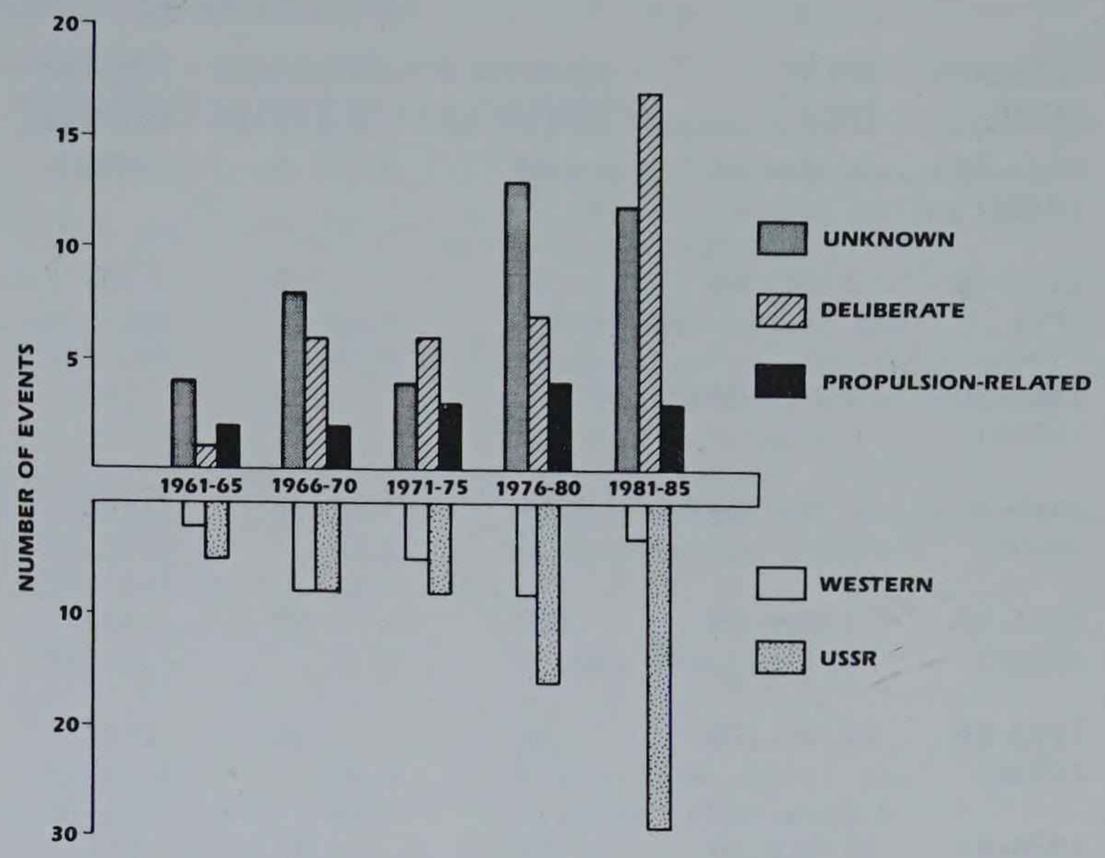


Figure 2.2 Unfortunately, the rate of satellite fragmentations has increased significantly during the past decade. *Courtesy of Teledyne Brown Engineering.*

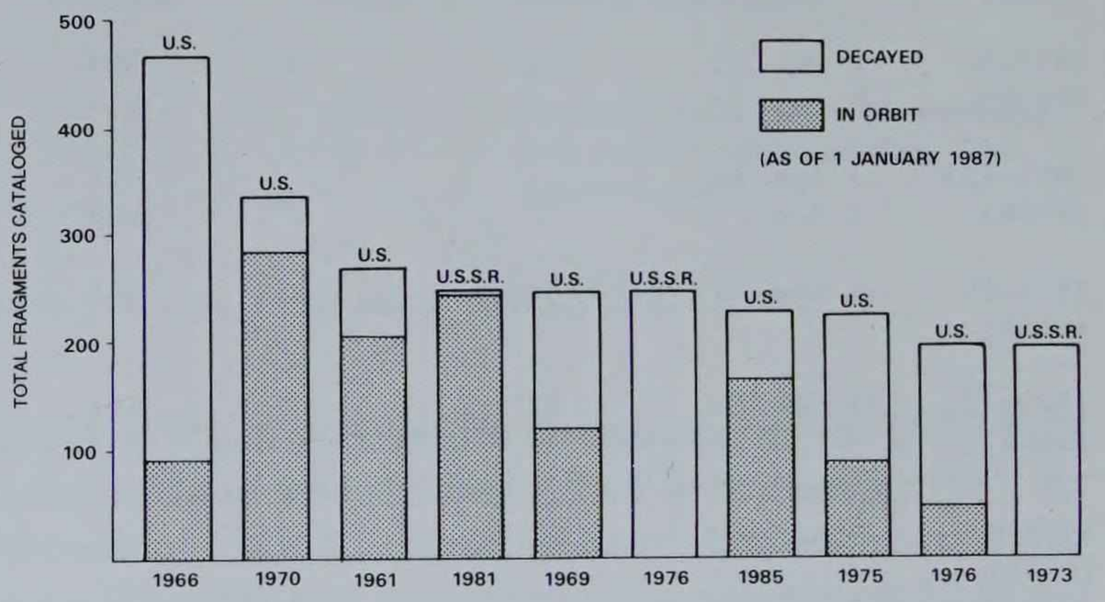


Figure 2.3 According to the *NORAD Satellite Catalog,* the 10 most prolific satellite fragmentations have accounted for more than 2,600 known pieces of debris. *Courtesy of Teledyne Brown Engineering.*

which have broken up. To date no Japanese, Chinese, or Indian satellites have fragmented. Figure 2.3 depicts the 10 most prolific breakups as of 1 January 1987.

Deliberate Satellite Fragmentations

Although the consequences of intentionally destroying a satellite in orbit are now known to be nontrivial, historically four rationales have been offered: structural testing, disposition of sensitive equipment, antisatellite (ASAT) tests, and self-defense. Table 2.1 lists the 34 satellite breakups assessed to have been the result of intentional acts.

Interestingly, all but three have belonged to the Soviet Union. Furthermore, 41% have been the result of ASAT and Strategic Defense Initiative (SDI) tests, 41% have been attributed to a single class of Soviet ocean surveillance satellites, 15% were destroyed when on-board

Table 2.1 Deliberate Satellite Breakups.

INTERN'L DESIG.	EVENT DATE	FRAGMENTS CATALOGED	FRAGMENTS IN ORBIT	BREAKUP ALTITUDE	INCL. (deg)	APOGEE/ PERIGEE(km)	ORBITAL PERIOD	COMMENTS
1964-70 (USSR)	5 Nov 64	96	0	UNK	51.23	233/188	88.7	Fragmented when reentry control was lost
1966-59 (US)	5 Jul 66	34	0	204	31.98	214/185	88.5	Planned structures test
1968-90 (USSR)	1 Nov 68	5	0	542	62.25	543/473	94.8	Only Soviet ASAT target to fragment immediately after test
1968-91 (USSR)	20 Oct 68	97	60	1994	62.33	2159/496	112.2	Soviet ASAT interceptor
1968-97 (USSR)	1 Nov 68	125	55	534	62.34	2139/534	112.4	Soviet ASAT interceptor
1970-89 (USSR)	23 Oct 70	97	44	1197	62.94	2132/529	112.3	Soviet ASAT interceptor
1970-91 (USSR)	30 Oct 70	42	31	565	62.83	2186/464	112.1	Soviet ASAT interceptor
1971-15 (USSR)	25 Feb 71	95	78	587	65.76	2200/575	113.5	Soviet ASAT interceptor
1971-106 (USSR)	3 Dec 71	29	0	231	65.88	1654/231	103.8	Soviet ASAT interceptor
1973-21 (USSR)	6 May 73	196	0	309	72.85	350/168	89.7	Fragmented when reentry control was lost
1974-103 (USSR)	17 Apr 75 2 Aug 75	50	0	437 433	65.04 65.05	444/424 442/414	93.3 93.1	First of Kosmos 699-class; two fragmentation events
1975-80 (USSR)	6 Sep 75	76	0	184	67.14	324/173	89.5	Fragmented when reentry control was lost
1975-102 (USSR)	25 Jan 76	62	0	441	65.02	442/430	93.3	Kosmos 699-class
1976-63 (USSR)	17 May 77	40	0	431	65.06	444/415	93.2	Kosmos 699-class
1976-72 (USSR)	25 Jul 76	248	0	209	67.15	353/172	89.8	Fragmented when reentry control was lost
1976-126 (USSR)	27 Dec 76	64	57	2088	65.84	2297/595	114.8	Soviet ASAT interceptor
1977-21 (USSR)	21 Dec 77	59	59	1133	65.85	1139/946	106.0	Soviet ASAT interceptor
1979-17 (US)	13 Sep 85	230	166	525	97.63	549/518	95.3	U.S. ASAT target
1979-33 (USSR)	17 Sep 79	1	0	403	65.03	405/382	92.4	Kosmos 699-class; at least 23 pieces decayed before being cataloged
1980-21 (USSR)	15 Jul 81	12	0	437	65.0	450/357	92.6	Kosmos 699-class
1980-30 (USSR)	18 Apr 80	45	25	986	65.84	1025/362	98.6	Soviet ASAT interceptor
1980-89 (USSR)	20 Jun 82 25 Aug 82	68	30	877 666	65.0 65.0	883/571 873/580	99.3 99.3	Kosmos 699-class; two fragmentation events
1981-24 (USSR)	14 Mar 81	1	0	UNK	65.8	1024/301	98.0	Soviet ASAT interceptor; at least 12-18 fragments decayed before being cataloged
1981-28 (USSR)	8 May 82 10 Aug 82	66	24	557 752	65.02 66.02	720/422 753/447	96.1 96.7	Kosmos 699-class; two fragmentation events

Table 2.1 continued on next page

Table 2.1 Deliberate Satellite Breakups (Continued).

INTERN'L DESIG.	EVENT DATE	FRAGMENTS CATALOGED	FRAGMENTS IN ORBIT	BREAKUP ALTITUDE	INCL. (deg)	APOGEE/ PERIGEE(km)	ORBITAL PERIOD	COMMENTS
1981-72 (USSR)	29 Sep 82	2	0	317	65.21	328/305	92.6	Kosmos 699-class; estimated 30 pieces decayed before being cataloged
1981-89 (USSR)	12 Jul 82 18 Sep 82	8	2	380 370	64.94 64.94	407/380 372/369	92.4 92.0	Kosmos 699-class; two fragmentation events; as many as 20 more fragments detected but not cataloged
1982-38 (USSR)	8 Aug 83 1 Feb 84 21 Feb 84	29	0	364 317 UNK	65.05 65.04 65.04	395/362 330/308 307/289	92.1 90.9 90.5	Kosmos 699-class; three fragmentation events
1982-88 (USSR)	20 Dec 83	32	0	333	65.0	342/315	91.1	Kosmos 699-class
1983-44 (USSR)	11 Mar 85 13 May 85	86	79	752 839	65.02 65.02	888/568 887/570	99.4 99.4	Kosmos 699-class; two fragmentation events
1984-83 (USSR)	23 Feb 86	45	4	428	65.03	439/408	93.0	Kosmos 699-class
1985-39 (USSR)	21 Jun 85	18	0	202	64.85	299/184	89.3	Fragmented when reentry control was lost
1985-82 (USSR)	18 Dec 86	18	17	408	65.04	418/404	92.8	Kosmos 699-class
1986-69 (US)	5 Sep 86	13 5	5 1	220 220	39.07 22.78	747/211 611/219	94.2 92.9	Planned collision of payload and rocket body during SDI-related test
TOTALS: 34 Breakups		2094	737		(35% of debris still in orbit as 1 January 1987)			

system failures prevented a controlled return to Earth of military reconnaissance satellites, and the remaining breakup was part of an American engineering test.

Antisatellite tests perhaps have received the widest publicity in terms of their effect on the space environment as well as the political environment. ASAT tests have accounted for almost 15% of all satellite breakup debris, but represented 20% of the breakup debris population as of 1 January 1987. Soviet ASAT tests which began in 1968 are characterized by the breakup of the ASAT interceptor itself as it fires its conventional warhead. In only one case has a Soviet ASAT target satellite fragmented due to ASAT activity and this occurred during the first successful Soviet test in November 1968 when 4 pieces of debris came off the target satellite (16).

The Soviet ASAT test program has been divided into Phase 1 (1968-1971) and Phase 2 (1976-1982). During Phase 1, 7 ASAT tests generated 490 pieces of detectable space debris, whereas the 13 Phase 2 ASAT tests produced only 169 catalogable debris. The reason for the sharp decline in Phase 2 was a change in the Soviet intercept profile which removed the interceptor (and presumably its debris) from orbit shortly after the intecept. The reason for this test change is unknown, but a response to world public opinion is a possibility.

The solitary American ASAT test resulting in a satellite breakup was the successful engagement of the DOD P-78 satellite by an air-launched ASAT in September 1985. By the end of 1986, 230 pieces of debris had been associated with the event and entered into the permanent NORAD satellite catalog. In September 1986 the intentional collision of two satellites during a test under the SDI program produced several hundred pieces of detectable debris, of which only 18 were cataloged. However, by selecting a low intercept altitude all known debris had naturally decayed by mid 1987.

Even before the first Soviet ASAT test, the U.S.S.R. began flying recoverable photographic reconnaissance satellites based on manned spacecraft hardware. Between 1962 and 1986, the Soviets orbited a total of 712 such spacecraft on military surveillance and Earth resources missions. Of these only 5 (0.7%) have encountered malfunctions severe enough to prevent a controlled reentry and landing in Soviet territory. Since each spacecraft is specifically designed to survive the rigors of reentry, the Soviet Union feels compelled to destroy the satellite in such cases to prevent its recovery by an unfriendly nation. In January 1987 a sixth deliberate destruction resulted in more than 800 detectable debris, of which 180 had been cataloged by 1 July 1987.

The five earlier satellite breakups of this type have accounted for 634 cataloged pieces of debris, almost

exactly the same as the 11 Soviet ASAT-related breakups. However, due to their very low operational altitudes none of this debris was still in orbit on 1 January 1987. Actually, each event creates much more debris than is ever cataloged, but because about half of the debris reenters the Earth's atmosphere within 1 hour and the other half within a few days or weeks, cataloging the debris is very difficult for NORAD.

In 1974 the Soviets began flying a new class of ocean surveillance satellites called EORSATs by the U.S. Department of Defense (DOD). About four months after the launch of the first of the series, Kosmos 699, the satellite broke up into several dozen fragments. Since then the majority of these satellites have encountered similar fates, and some have experienced multiple breakups. The rationale for this action is still not clear, but the consistency of the events and some of the earlier location patterns strongly suggest intent (17).

Normally, these satellites operate in nearly circular orbits with a mean altitude of 435 km. The early breakups occurred at this altitude or lower after natural orbital decay had been allowed to take over. However, since 1981 three of these satellites have been maneuvered into higher elliptical orbits before fragmenting. From these orbits the debris will remain in orbit for much longer periods. Also disquieting is the fact that special radar observations have revealed at least three times the number of cataloged debris fragments after a given event (18). The number of even smaller debris is unknown.

The only other known deliberate satellite breakup occurred on 5 July 1966 shortly after a Saturn 1B test flight. Some six hours after launch when the flight objectives had been accomplished, the pressure in the Saturn IVB upper stage was allowed to build and to rupture the tank in an engineering test of the vehicle's structural integrity. All debris reentered within 17 days, posing no significant hazard to the space environment.

A fourth reason to deliberately destroy an operating satellite is one of self-defense. Thus far neither the Soviet Union nor the United States has deployed self-defensive weapons in space. The nature of this space debris (amount, size and longevity) will depend heavily on the orbit of the target satellite and the type of negation mechanism, e.g., conventional explosives, kinetic vehicles, directed-energy weapons. The potential consequences of these techniques will be addressed later in this volume.

Propulsion-Related Satellite Fragmentations

In the late 1960s as the United States was striving to acquire reliable launch skills, the complexity of the task was apparent in numerous, often spectacular launch failures. The Shuttle, Titan, Atlas, and Delta disasters of 1985-1987 reminded all of us that access to space still relies upon quite fragile and volatile techniques. Although Soviet secrecy hides most of their own failures, overwhelming evidence indicates that they have similar accidents and failures on an all too regular basis.

Despite their vivid nature, launch vehicle failures before minimum orbital velocity has been obtained pose no threat to the space environment. However, malfunctions of orbital stages (parking, transfer, and final) can have a dramatic impact on the space debris population. Table 2.2 lists the 13 documented cases of upper stage failures believed caused by their propulsion systems. The generated breakup debris accounts for 30% of all satellite breakup debris and 33% of breakup debris still in orbit.

Launch vehicle breakups are often associated with the propulsion system and consequently can result in extremely dynamic events. Whether the propellents are cryogenic or hypergolic, they are selected for their high energy content. The creation of hundreds of trackable debris pieces in a single breakup is common.

As seen in Figure 2.2 the frequency of propulsion-related breakups is relatively constant, averaging about one breakup every two years. Six of the identified propulsion-related breakups (three each for the U.S. and the U.S.S.R.) occurred shortly after launch. In October 1965 a Titan transtage broke up, producing the largest number of debris objects cataloged with any satellite breakup. The November 1986 breakup of an Ariane upper stage will probably exceed this record (see the next section on unknown fragmentation causes).

The last such documented breakup was typical of an upper stage failure. On 8 December 1982 the Soviet Union launched a new Molniya communications satellite to replace a two-year-old Molniya approaching the end of its useful life. The satellite originated from the Baikonur Cosmodrome, site of all Soviet manned, lunar, and planetary launchings. It headed on a northeast azimuth into a low altitude parking orbit at an inclination of 62.8 degrees. Almost an hour after launch, after the transfer orbit stage had separated from the parking orbit stage and the two were flying over the northernmost tip of Antartica, south of the Falkland Islands, an on-board signal commanded the transfer orbit stage to ignite with the goal of placing the payload into a semisynchronous, highly elliptical orbit. For an as yet undisclosed reason, the propulsion unit did not fire successfully, and instead the vehicle was blown apart. Much of the debris which was thrown into a retrograde direction decayed within an hour. However, those trackable objects thrown forward entered new orbits with apogees almost 250 km higher than that of the parent satellite. Following Soviet tradition to hide failures whenever possible, the deceased satellite was given the next Kosmos satellite designator

Table 2.2 Propulsion-Related Satellite Breakups.

INTERN'L DESIG.	EVENT DATE	FRAGMENTS CATALOGED	FRAGMENTS IN ORBIT	BREAKUP ALTITUDE	INCL. (deg)	APOGEE/ PERIGEE(km)	ORBITAL PERIOD	COMMENTS
1962-βIota (USSR)	29 Oct 62	24	0	UNK	65.11	261/202	89.1	Mars probe upper stage failure
1963-47 (US)	27 Nov 63	17	14	UNK	29.94	1735/502	107.7	Centaur test flight
1965-82 (US)	15 Oct 65	467	91	739	32.6	791/708	99.8	Transtage fragmented soon after launch
1969-64 (US)	26 Jul 69	22	1	UNK	30.37	5445/271	147.2	Upper stage malfunction
1972-58 (US)	22 May 75	225	88	725	98.34	909/633	100.3	Delta second stage
1973-86 (US)	28 Dec 73	184	169	1513	102.05	1513/1504	116.2	Delta second stage
1974-89 (US)	20 Aug 75	138	130	1460	101.69	1460/1445	114.9	Delta second stage
1975-04 (US)	9 Feb 76 19 Jun 76	198	48	UNK 751	97.78 97.78	915/741 912/742	101.5 101.4	Delta second stage; two fragmentation events
1976-77 (US)	24 Dec 77	141	140	1510	102.02	1521/1506	116.3	Delta second stage
1977-65 (US)	14 Jul 77	159	96	1450	29.05	2027/536	111.2	Delta second stage
1978-26 (US)	27 Jan 81	185	164	905	98.85	912/903	103.1	Delta second stage
1981-88 (USSR)	11 Sep 81	2	2	649	62.82	13864/626	263.7	Upper stage failure; other pieces detected but not cataloged
1982-115 (USSR)	8 Dec 82	29	2	402	62.8	516/400	93.8	Upper stage failure
TOTALS:	13 Breakups	1791	945	(53% of debris still in orbit as of 1 January 1987)				

rather than using the Molniya 1-56 nomenclature as originally planned (19).

By far the most serious series of launch vehicle failures involved Delta second stages which experienced seven devastating breakups between 1973 and 1981. The average number of debris per event was a disturbing 175. Regrettably, due to the high orbits at the time of the breakups, 68% of the debris is still in orbit and most of it will remain so for many years to come. In fact, the debris from just those seven breakups represents almost one-third of all satellite breakup debris now in orbit.

The Delta second stage breakup phenomenon is a remarkable case history of the concern of a few individuals about the space environment and of their ability to halt the unnecessary pollution of near Earth space. Unlike the propulsion-related breakups noted earlier, Delta second stages did not fragment during operation but only after they had successfully completed their delivery missions and had been abandoned, some for as long as three years. As a result, although each event was dutifully recorded by NORAD, investigations into the incidents did not receive high priority by either NASA or the vehicle manufacturer, McDonnell Douglas.

A civilian analyst at NORAD/ADCOM in Colorado Springs, John Gabbard, became interested in satellite breakups following the very first breakup by the Transit 4A rocket body in 1961. He later developed the Gabbard diagram, an extremely useful analytical tool for satellite breakups (described at length in Chapter 3). Gabbard maintained a record of satellite breakups for NORAD/ADCOM and in 1978 provided a copy to Don Kessler of NASA's Space Environment Office. Kessler assigned launch vehicle types to each breakup and immediately noticed a number of energetic breakups involving Delta second stages (20).

With the appropriate management levels in NASA now alerted, an investigation was undertaken by both NASA and McDonnell Douglas (21). The apparently violent nature of the breakups led to a serious review of both the propulsion system and the self-destruct mechanism needed to destroy the vehicle in flight if it deviated excessively from the planned trajectory. The latter

potential cause was eventually assessed as a low probability cause and attention focused on the propulsion system.

Residual propellents in the Delta second stage rapidly became the prime candidate as the breakup energy source. Because the propellents were hypergolic (i.e., ignite on contact), a variety of scenarios involving inadvertent mixing were devised. Without fully understanding the cause and effect sequence, the obvious corrective action was to dispose of the residual propellents, after mission completion. This procedure was instituted in August 1981 and no Delta second stage has fragmented since that time. Under licensing agreements with the United States, Japan's current domestic space launch vehicle is modeled heavily after the Delta rocket. To minimize any unwarranted pollution of space, Japan has also instituted so-called depletion burns in its second stages.

A further analysis in 1985 of the Delta second stage breakup phenomenon was conducted by John Gabbard, then at Teledyne Brown Engineering, in support of NASA's debris assessment program (22). The troubling aspect of the Delta phenomenon was why some vehicles experienced breakups and others did not. At the time NASA began depletion burns with Delta second stages, 154 Deltas had been launched with a high success rate. Dozens of second stages were still in orbit without incident.

Gabbard's first clue came when he noticed the first Delta second stage to fragment came after a major vehicle redesign. In addition to the use of small solid-fuel boosters attached to the first stage and a new inertial guidance system, new propellents were selected for the second stage: nitrogen textroxide (N_2O_4) and Aerozine 50. The redesigned second stage tankage and the new propellents could explain why none of the previous stages had broken up, but why did only a handful of the new generation second stages fragment?

The final clues came when Gabbard realized that six of the seven Delta breakups had been launched from Vandenberg AFB into sun-synchronous orbits. Moreover, the time of launch, which governs the lumination conditions of a vehicle in a sun-synchronous orbit, of each was approximately 1000 hours local time. Only one other Delta second stage had been placed in a similar orbit and orbital analysis suggested it had performed a depletion burn for unknown reasons.

In hindsight, the redesign of the Delta second stage in 1972 laid the foundation for the ensuing catastrophes. The catalyst required to induce the breakup was a sun-synchronous orbit centered about 1000 hours local time. (Delta second stages in afternoon orbits have not fragmented.) The accepted hypothesis now suggests that solar heating causes either an overpressurization in the propellent tank (Figure 2.4) or thermal contraction and expansion degrades the common fuel/oxidizer bulkhead. In either case, residual N_2O_4 and Aerozine 50 are allowed to come into contact explosively.

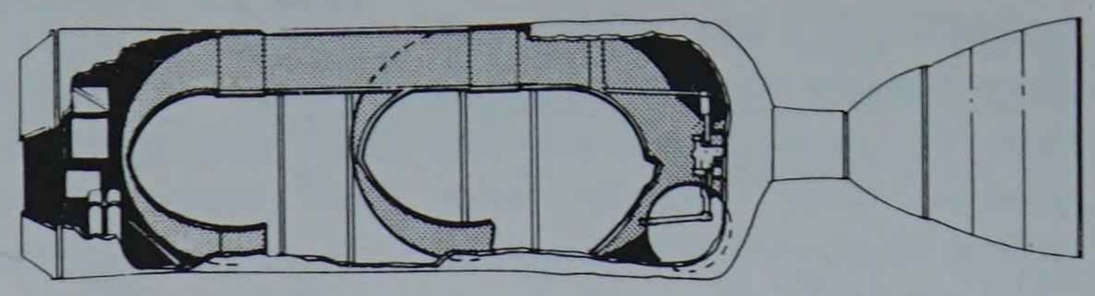


Figure 2.4 This schematic diagram of a Delta second stage illustrates the common bulkhead between the fuel and oxidizer tanks. A breach in this bulkhead is believed to be the cause of seven violent fragmentations. *Courtesy of Teledyne Brown Engineering.*

The remaining Delta second stage to break up was used to launch a Japanese geosynchronous satellite from Cape Canaveral. The breakup occurred less than six hours after launch; and although it does not fit the pattern of the Vandenberg launches, the cause of this failure is presumed to be similar to that of the other six.

The lesson to be learned from the Delta second stage experience is that perseverance and dedication can help overcome man's imperfection. Propulsion-related satellite breakups will inevitably continue into the future, but if we remain vigilant to what is happening in the cosmos, we can solve deficiencies before they get out of hand.

It should be noted that more than the 13 rocket bodies mentioned above have been the source of breakups since 1961. These other rockets, including Ablestar, Altair, Atlas, Agena, Ariane, and Soviet rockets, have fragmented for unknown reasons. Some have broken up on the day of launch, others much later. Their omission from this section (and inclusion in the last section) is due solely to a lack of information. It is logical to assume that some, but certainly not all, of these other rockets may have experienced propulsion-related breakups. Their breakup status will be updated as warranted by further analysis.

Collision-induced Satellite Fragmentations

Collision-induced satellite fragmentations are potentially the most threatening to the near Earth environment. A single hypervelocity collision could produce as many as one million fragments with diameters of 1 mm or more. More importantly, additions to the Earth satellite population also increase the probability that satellite-satellite collisions will take place, possibly triggering a vicious spiral of debris generation. Of course, hypervelocity collisions actually occur on a daily basis between very small natural and man-made particles (less than 1 mm in diameter) and the tracked satellite

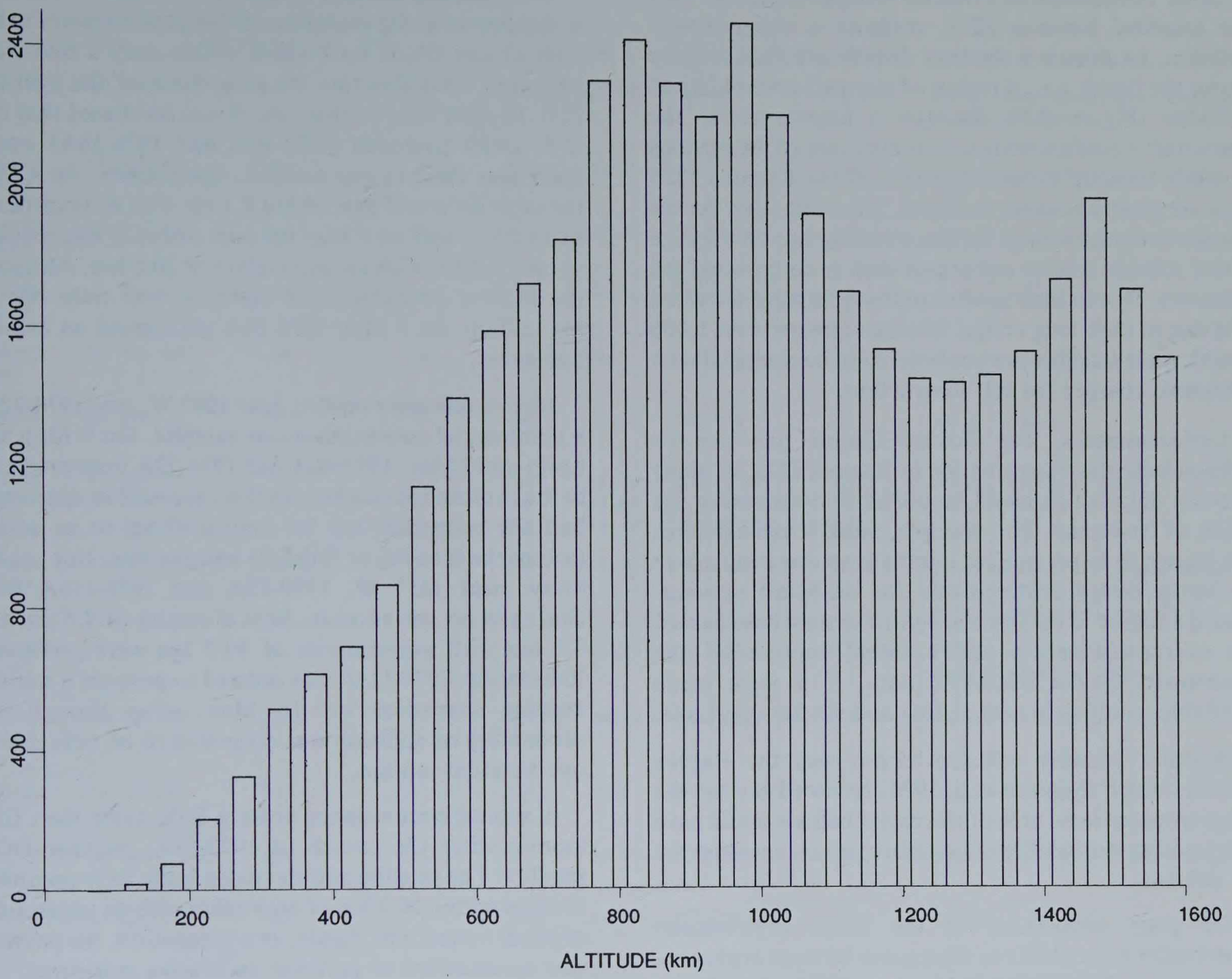


Figure 2.5 Based on data from the January 1987 *NORAD Satellite Catalog,* the altitude regime between 800 and 1,000 km is the most populous.

population. Since these events produce no significant secondary debris and do not affect the status of functioning satellites, they are of lesser concern to the space environmentalist.

Despite NORAD's considerable capabilities, this organization does not have the luxury of being able to watch two satellites intersect on a display screen and thus identify possible satellite collisions. Satellites are tracked normally for only a few minutes each day or even less. Breakups are recognized only when a cloud of unexpected satellites penetrates a radar coverage. The orbital characteristics of the debris are matched with known satellites and then the debris cloud is propagated via computer models back in time to determine the likely parent satellite.

Once the parent satellite has been identified, its orbit can be matched with the orbits of all other known satellites to ascertain the likelihood of a collision. To date this process has always produced negative results. It is statistically more likely that a collision will involve a large tracked object (e.g., an old rocket body or payload) and a small, untracked piece of debris. As will be illustrated later, even a small piece of debris could easily cause extensive spacecraft damage similar to that observed in many satellite breakups.

Although no satellite is definitely known to have experienced a breakup due to an accidental collision in space (the hypervelocity collisions of P-78 and the SDI experiment were intentional), at least one satellite is considered a strong candidate as a victim of space debris. On 24 July 1981 only seven weeks after launch, a Soviet Transit-type navigation satellite explosively fragmented. Over 240 pieces of debris have been cataloged to date, and its high altitude of 1,000 km makes it the second largest source of debris now in orbit.

Other circumstantial evidence leads to the belief that the satellite, Kosmos 1275, suffered a hypervelocity collision. Its altitude is the most densely populated regime about the Earth, i.e., a region of elevated probability of collision (Figure 2.5). Enough is known about the spacecraft's configuration to rule out some of the obvious possible breakup causes. Satellites of the Kosmos 1275 type are gravity gradient stablized. Therefore, they do not possess propulsion units for maneuvering nor do they use active attitude control techniques such as compressed gas thrusters. Due to their modest military intelligence value and due to their long orbital lifetimes (greater than 1,000 years), these satellites are not believed to be equipped with explosive charges for self-destruction.

Unfortunately, the Soviet Union has yet to acknowledge the fragmentation of Kosmos 1275, let alone provide data which could be useful in determining the cause of its demise. For example, most Soviet satellites are known to be pressurized internally to one atmosphere to lessen design requirements for on-board systems. Could a failure in the thermal control system have caused an overpressurization and eventual rupture of the spacecraft? Soviet telemetric data, if it were made available, could help answer that and similar questions.

Another possible collision victim was the Pageos satellite which fragmented in 1976. As noted earlier, the large cross-sectional area of this mylar balloon could have increased its probability of collision with an unseen piece of debris.

Of great importance to the space environment community is the ability to distinguish between explosion-induced and collision-induced satellite breakups. Theoretical analyses of the mechanics of these dissimilar happenings clearly indicate that the debris mass and velocity distributions are substantially different. Presently, however, our observational limitations hinder our ability to make these distinctions. In light of the first known (deliberate) hypervelocity collision in space (P-78) in September 1985, debris models are being revised with the hope of discovering the long sought, yet elusive, breakup "signature" of a hypervelocity collision. This topic is covered in succeeding chapters.

Not all collisions in space are hypervelocity. Collisions of much lower velocity can occur from improper staging during the launch process and in the geostationary ring. Occasionally, final rocket stages have bumped their payloads after release, for example, ECS 1 and its final stage in February 1979 (23). The number of fragments created in an event of this type is small. Moreover, the threat of this activity to the viability of satellite deployments ensures close attention by launcher organizations and quick resolution should an inherent problem arise.

Of increasing concern to the international community is the potential for collisions in the geostationary orbit. Three cases which took place within only a two week period in 1980 illustrate the magnitude of the problem (24). In early May of that year it was estimated that two U.S. DOD payloads (1973-40A and 1978-16A) would soon pass close to one another. Specifically, on 4 May the satellites would pass within 9.4 km with an uncertainty of 10.0 km, and on 8 May the miss distance was reduced to only 3.5 km with an uncertainty of 20.0 km. Although the highest probability of collision was only one in ten million, on 3 May 1978-16A performed an evasive maneuver.

Also in this same region, near 100° W, was 1974-22A, a commercial communications satellite. On 9 May and again on 15 May, 1973-40A and 1974-22A were predicted to make close approaches. In this case neither spacecraft had any propellent left for maneuvering, so no action (except the crossing of fingers!) was possible. Not too far away, near 135° W, 1979-53A and 1978-113A were closing in on one another. Miss distances of 9.6 km and 3.5 km with uncertainties of 40.7 km were predicted. Reluctantly, 1978-113A was ordered to perform a station-keeping maneuver on 15 May, even though the probability of collision was estimated to be only one in one hundred million.

A similar circumstance arose a little more than four months after the launch of 1979-53A, another DOD satellite. The satellite and its rocket body were predicted to come within 20.9 km of each other with an uncertainty of equal magnitude. Again, as a precaution, the payload was commanded to perform an evasive maneuver.

Although the amount of debris expected to be produced in each collision was small, the unique nature of the geostationary orbit makes it more susceptible to contamination by breakups than other regions of space. Our inability to track even modest-sized objects (less than 1 m in diameter) and the uncertainty of our measurements complicate the situation. In August 1970 the apogee motor of Skynet 1B failed, possibly creating a cloud of particles which periodically penetrate the geostationary ring. Two other spacecraft, the American RCA Satcom 3 and the Japanese ECS 2, were lost under similar circumstances in late 1979 and early 1980 (25). They, too, may have formed particle clouds capable of intercepting geostationary satellites. Such collisions would take place at relatively low velocities, well below that required for debris-intensive hypervelocity collisions.

Satellite Fragmentations of Unknown Causes

As in so many scientific endeavors, the unknown often outweighs the known. Table 2.3 lists 39 known satellite

Table 2.3 Satellite Breakups of Unknown Cause.

INTERN'L DESIG.	EVENT DATE	FRAGEMENTS CATALOGED	FRAGMENTS IN ORBIT	BREAKUP ALTITUDE	INCL. (deg)	APOGEE/ PERIGEE(km)	ORBITAL PERIOD	COMMENTS
1961-Omi (US)	29 Jun 61	269	206	950	66.81	998/880	103.8	First known satellite breakup; Ablestar rocket
1965-12 (USSR)	22 Feb 65	167	0	UNK	64.8	UNK	UNK	Unmanned Voskhod test flight
1965-20 (USSR)	15 Mar 65	147	26	1639	56.05	1827/260	106.0	Multiple payload test flight
1965-88 (USSR)	Nov 65	22	0	UNK	48.44	521/211	91.9	Kosmos 95
1966-12 (US)	15 Feb 66	38	0	UNK	96.5	268/147	88.6	Inflated sphere
1966-46 (US)	21 Jun 66	51	0	UNK	28.82	300/281	90.3	Atlas rocket
1966-56 (US)	12 Jul 75 20 Jan 76 Jun 78	76	8	5144 UNK UNK	85.28 85.07 84.60	5169/3201 5424/2934 5750/2629	180.1 179.9 180.1	Pageos balloon; three fragmentation events
1966-88 (USSR)	17 Sep 66	53	0	UNK	49.60	792/138	93.9	Fractional Orbit Bombardment System (FOBS) test; launch not acknowledged by USSR
1966-101 (USSR)	2 Nov 66	41	0	UNK	49.70	651/188	92.9	FOBS test; launch not acknowledged by USSR
1969-29 (USSR)	28 Mar 69	37	2	554	81.17	851/462	97.9	Meteor 1 rocket
1969-82 (US)	4 Oct 69	248	121	919	70.0	940/907	103.4	Agena D rocket
1970-25 (US)	17 Oct 70	337	284	1076	99.79	1094/1051	106.7	Agena D rocket
1973-17 (USSR)	3 Apr 73	25	0	224	51.48	224/195	88.9	Salyut 2 rocket
1974-74 (USSR)	26 Sep 74	19	0	355	70.9	456/259	91.7	Kosmos 686 rocket
1975-27 (US)	12 Mar 78	4	3	840	114.99	844/837	101.7	Delta second stage
1976-67 (USSR)	29 Sep 77	55	54	1911	65.85	2100/981	116.9	Soviet ASAT target; breakup not caused by ASAT test
1976-105 (USSR)	15 Mar 77	11	11	5678	63.16	39644/1352	718.9	First of Kosmos 862-class
1976-120 (USSR)	27 Nov 78	50	9	559	65.84	621/551	96.4	Soviet ASAT target; breakup not caused by ASAT test
1977-27 (USSR)	8 Jun 78	2	2	UNK	63.15	39035/1323	717.8	Kosmos 862-class
1977-47 (USSR)	30 Mar 79	1	1	3283	62.95	38723/1643	718.0	Kosmos 862-class
1977-68 (USSR)	24 Oct 77	4	4	UNK	62.94	39667/682	717.7	Kosmos 862-class
1978-83 (USSR)	10 Oct 78	4	4	UNK	62.84	39760/666	719.2	Kosmos 862-class
1979-58 (USSR)	Sep 79	5	5	UNK	62.86	39679/712	718.5	Kosmos 862-class
1979-77 (USSR)	9 Sep 79	5	5	8100	62.93	39754/574	717.2	Kosmos 862-class

Table 2.3 continued on next page

Table 2.3 Satellite Breakups of Unknown Cause (Continued).

INTERN'L DESIG.	EVENT DATE	FRAGEMENTS CATALOGED	FRAGMENTS IN ORBIT	BREAKUP ALTITUDE	INCL. (deg)	APOGEE/ PERIGEE(km)	ORBITAL PERIOD	COMMENTS
1979-104 (ESA)	Early 80	1	0	UNK	17.6	35839/189	631.9	Ariane Vl rocket; estimated 25 fragments
1980-57 (USSR)	14 May 81	2	2	UNK	62.64	39283/1083	718.0	Kosmos 862-class
1981-16 (USSR)	20 Oct 81	4	4	UNK	62.97	39401/362	717.9	Kosmos 862-class
1981-31 (USSR)	12 May 81	4	4	UNK	63.04	39743/649	718.5	Kosmos 862-class
1981-53 (USSR)	24 Jul 81	249	244	977	82.96	1014/961	104.8	Kosmos 1275
1981-58 (USSR)	Dec 86	2	2	UNK	67.1	37689/2664	717.8	Kosmos 862-class
1981-71 (USSR)	21 Nov 81	3	3	UNK	63.11	40109/721	727.4	Kosmos 862-class
1981-108 (USSR)	Jan 84	4	4	UNK	62.8	39085/1319	718.8	Kosmos 862-class
1982-55 (USSR)	21 Oct 85	33	33	986	65.84	1000/992	105.04	Soviet ASAT target; breakup not caused by ASAT test
1983-20 (USSR)	3 Sep 84	1	0	307	51.5	1230/220	99.3	Astron platform
1983-22 (US)	30 Dec 85	7	3	823	98.64	831/808	101.29	NOAA 8 (battery explosion?)
1983-38 (USSR)	12 Aug 83	4	4	UNK	63.29	39631/729	717.9	Kosmos 862-class
1983-70 (USSR)	9 Jul 83	2	2	UNK	62.92	39199/642	707.4	Kosmos 862-class; launch failure?
1985-94 (USSR)	22 Nov 85	11	11	1414	82.6	1430/1409	114.2	Kosmos 1691
1986-19 (ESA)	13 Nov 86	80	80	806	98.7	836/806	101.3	Ariane V16 rocket; estimated 470+ fragments
TOTALS:	39 Breakups	2078	1141	(55% of debris still in orbit as of 1 January 1987)				

breakups for which the cause has yet to be determined. This represents 45% of all known satellite fragmentations. Furthermore, the over 1,100 resultant pieces of debris still in orbit as of 1 January 1987 account for 18% of all cataloged satellites tracked by NORAD.

The grouping of these satellite breakups together in no way is meant to suggest that they share a common cause. Some are undoubtedly propulsion-related, some may have been intentional, and some may actually mask operational activities of which we are not aware. The recent breakup of the Ariane upper stage (1986-19C) may have been caused by propulsion-related forces. By 1 July 1987 330 pieces of debris from this event had been officially cataloged with more than 150 pieces awaiting cataloging. Interestingly, this Ariane upper stage was the first to enter a low altitude, sun-synchronous orbit and one which was almost identical to the Delta second stage orbits discussed previously, i.e., local sun-time of 1030.

The Kosmos 862-class satellite breakups may fall into the last category. These satellites are widely believed to form the backbone of the Soviet strategic early warning sensor system. After several years of experimentation, the U.S.S.R. apparently initiated operational deployment in 1976 with Kosmos 862. However, five months after launch, the spacecraft fragmented into at least 11 pieces and immediately began to drift off station. Because these satellites are in highly elliptical orbits with low altitudes only in the Southern Hemisphere, the ability of the NORAD space surveillance network to detect fragments less than 0.5 meter in diameter is limited. Since that event 13 other satellites of this class have experienced similar fates, accounting for one-third of all satellite breakups from unknown causes. Following the breakups, the satellites appear to be nonoperational.

The reason for these breakups is still unknown in the West. Deliberate destruction by the Soviets seems unnecessary since the spacecraft are not assumed capable of surviving reentry after their orbital lifetimes of tens of years. Another possibility is that a design flaw - one which had obviously eluded the Soviets for several years - caused the breakups, perhaps analagous to the Delta second stage breakups. These pieces may also be part of an auxiliary mission activated near the completion of the primary mission.

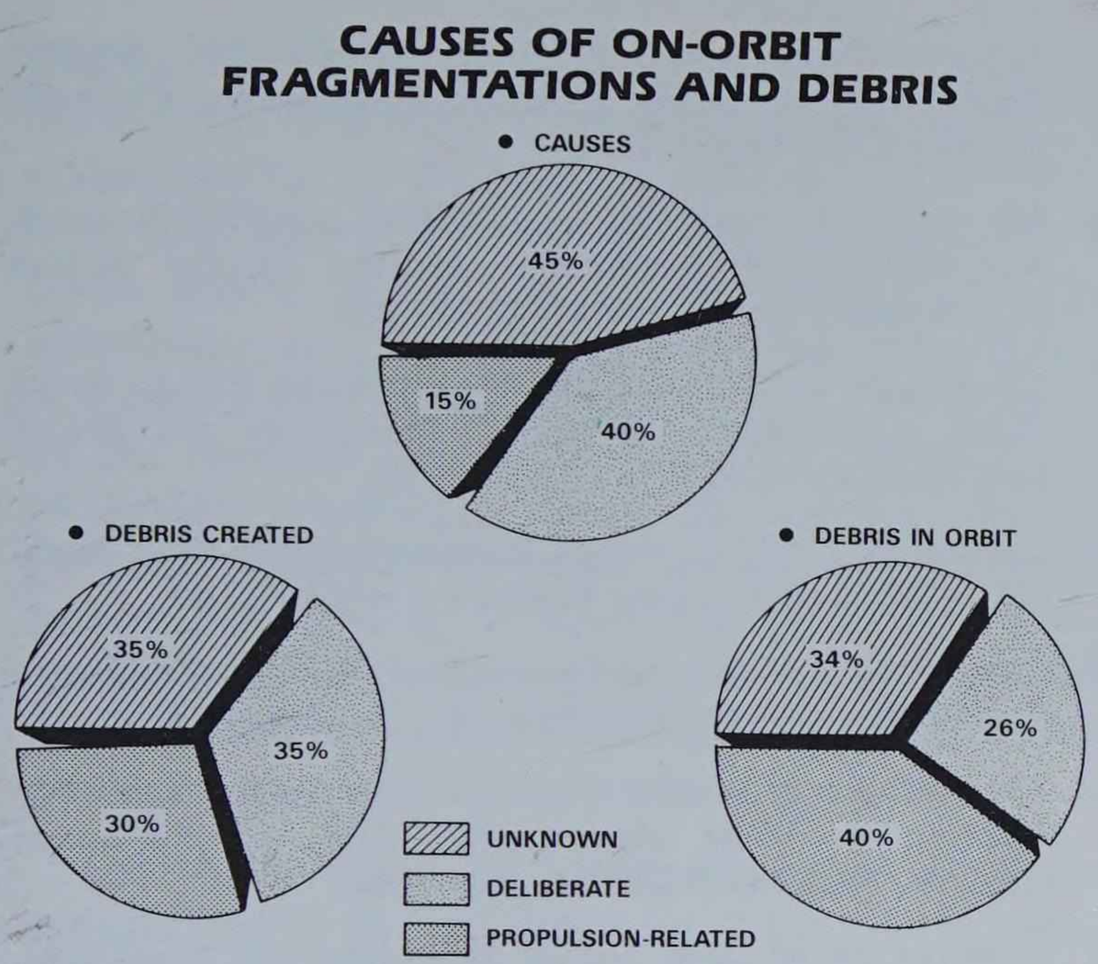


Figure 2.6 Despite numerous investigations, the causes for almost half of all satellite fragmentations are still unknown. Collisions with unseen space objects may be responsible for some of these breakups. *Courtesy of Teledyne Brown Engineering.*

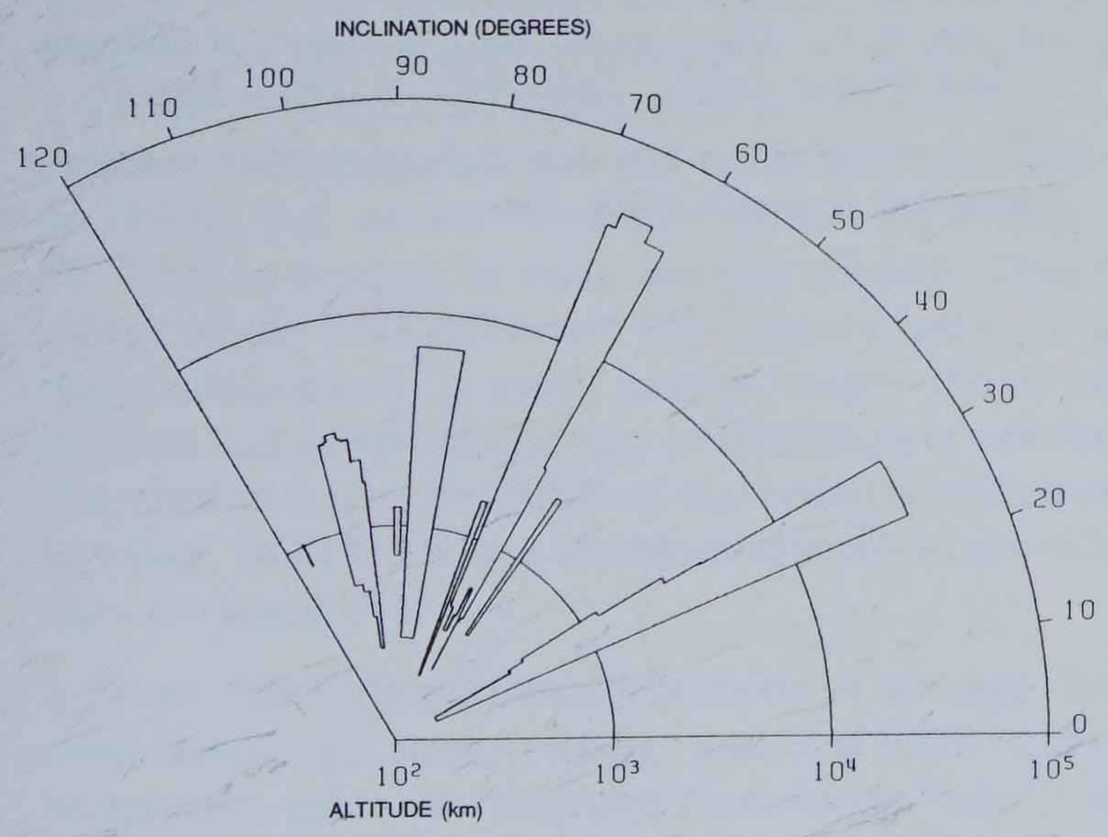


Figure 2.7 The regimes of most satellite fragments are relatively narrow and easily defined, yet virtually all Earth satellites have orbits that expose them to the hazard. *Courtesy of Teledyne Brown Engineering.*

Another oddity in this group of unknown breakup causes is the presence of three Soviet ASAT target satellites. Each of these satellites fragmented at least a year after its involvement with a Soviet ASAT test. The first two occurrences took place about a year apart in 1977 and 1978. Despite the low probability that two similar satellites could be accidentally struck by space debris in so short a time, both breakups were tagged by some analysts as potential collision victims. One of the rationales was that these satellites could be subjected to higher probabilities of collision with ASAT test debris due to the nature of their orbits.

Then in October 1985 a third Soviet ASAT target broke up. In the earlier cases, about 50 fragments were detected in comparison to only 33 fragments for the last one. The possibility that all three were struck by space debris large enough to cause substantial fragmentation is now considered to be remote. Other mechanisms are likely to be involved.

Summary

The sources of space debris are numerous. Today 95% of all known Earth satellites can be classified as space debris, but the untracked space debris population is certainly many times this. Breakup debris accounts for almost one-half of all satellites now tracked by NORAD, and 40% of this debris is the result of unknown causes (Figure 2.6). Despite the seemingly narrow regions of space contaminated with satellite breakup debris (Figure 2.7), all satellites pass through most of these regions on their daily travels about the Earth.

Using the *NORAD Satellite Catalog* as a database, the average number of objects in a unit volume of space at a given altitude may be calculated (Figure 2.8). This plot

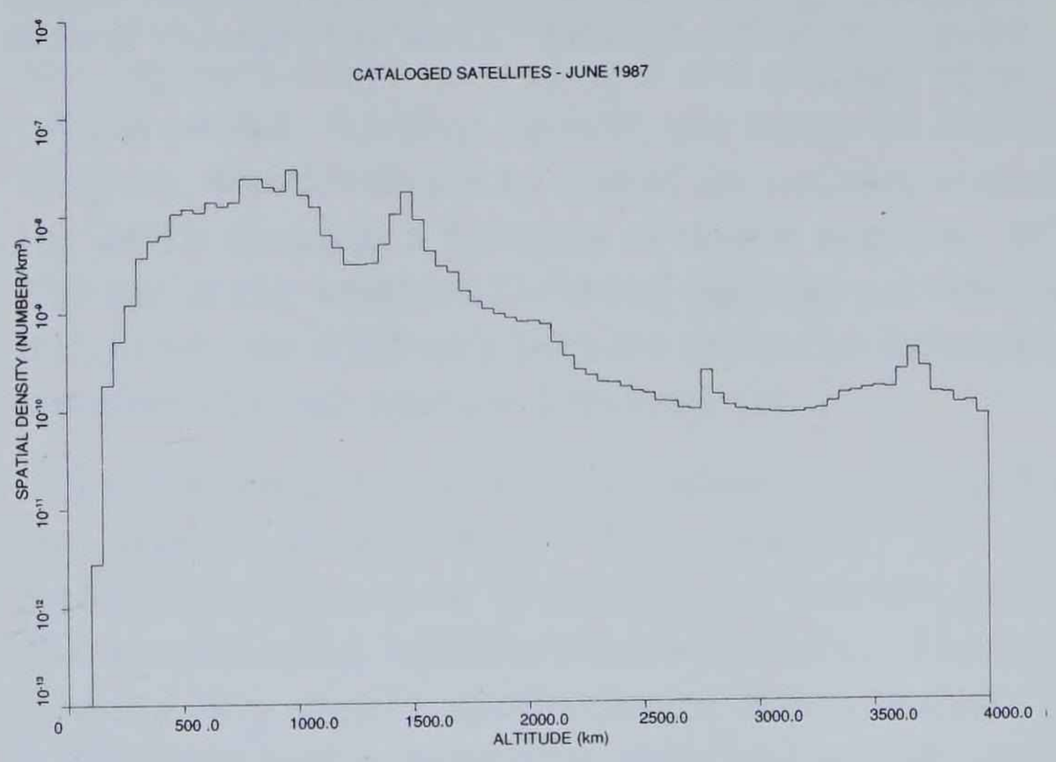


Figure 2.8 Calculation of the spatial density of known Earth satellites is necessary to evaluate the collision hazard in near Earth orbits.

of spatial density versus altitude is the most accurate and up-to-date representation of the debris environment. Some of the most prolific sources of space debris have only been recognized in recent years, e.g., solid rocket effluents, paint flecks. The question posed by D. J. Kessler of NASA is: What other sources exist of which we are simply not aware? Only better experimentation and modeling can answer this question. These are the subjects of the next two chapters.

References

1. Mueller, A. C., and Graf, O. F., Jr. *A Study of the Lifetimes of Geosynchronous Transfer Orbits.* Report ACM-TR-115, Analytical and Computational Mathematics, Inc., Houston, Tex., January 1979.
2. Johnson, N. L. "The Development and Deployment of Soviet Geosynchronous Satellites." *Journal of the British Interplanetary Society* 35, no. 10: 450-458.
3. Mueller, A. C., and Kessler, D. J. "The Effects of Particulates From Solid Rocket Motors Fired in Space." *Advances in Space Research* 5 (1985): 77-86.
4. Kessler, D. J. "Orbital Debris Issues." *Advances in Space Research* 5 (1985): 3-10.
5. Gabbard, J. R. *Spacetrack System Data Related to Some Non-routine Events Through May 1981.* NORAD/ADCOM Technical Memorandum 81-6, 30 June 1981.
6. *Soviet Space Programs: 1976-1980* (with supplementary data through 1983). Part 3, Unmanned Activities, Committee on Commerce, Science, and Transportation, U.S. Senate, May 1985, p. 1109
7. Johnson, N. L. *The Soviet Year in Space 1985.* Teledyne Brown Engineering, Colorado Springs, Col., January 1986, pp. 47-48.
8. *Satellite Catalog.* NORAD/J31SSO, Peterson AFB, Col., January 1986.
9. Kessler, D. J. NASA Johnson Space Center, Houston, Tex., 1986.
10. Schramm, L. S., et al. "Particles Associated With Impact Features in the Main Electronics Box (MEB) Thermal Blanket From the Solar Max Satellite." *Lunar and Planetary Sciences* XVII (1986).
11. Barrett, R. A., et al. "Impact Features and Projectile Flux on Returned Solar Max Material." *Lunar and Planetary Sciences.* XVII (1986).
12. Leger, L. J., and Visentine, J. T. "Protecting Spacecraft From Atomic Oxygen." *Aerospace America.* 24 (July 1986): 32-35.
13. Johnson, N. L., et al. *History of On-Orbit Satellite Fragmentations.* 2d ed., Report CS-USASDC-0001, Teledyne Brown Engineering, Colorado Springs, Col., February 1986, pp. 1-46—1-53.
14. Belew, L. F., ed. *Skylab, Our First Space Station.* NASA SP-400, NASA George C. Marshall Space Flight Center, Ala., 1977, p. 64.
15. Johnson, N. L., et al. *History of On-Orbit Satellite Fragmentations.* Teledyne Brown Engineering, Colorado Springs, Col., August 1984.
16. Johnson, N. L. "Artificial Satellite Break-ups (Part 2): Soviet Anti-Satellite Programme." *Journal of the British Interplanetary Society* 36 (1983): 357-362.
17. Johnson, N. L. "Artificial Satellite Break-ups (Part 1): Soviet Ocean Surveillance Satellites." *Journal of the British Interplanetary Society* 36 (1983): 51-58.
18. Johnson, N. L. "History and Consequences of On-Orbit Break-ups." *Advances in Space Research* 5 (1985): 11-19.
19. Johnson, N. L. *The Soviet Year in Space 1982.* Teledyne Brown Engineering, Colorado Springs, Col., January 1983, p. 11.
20. *The Explosion of Satellite 10704 and Other Delta Second Stage Rockets.* Technical Memorandum 81-5, Directorate of Analysis, NORAD/ADCOM, May 1981.
21. *Investigation of Delta Second Stage On-Orbit Explosions.* Document MDC-H0047, McDonnell Douglas Astronautics Co., Huntington Beach, Calif., April 1982.
22. Gabbard, J. R. *A Later Look at Delta Second Stage On-Orbit Explosions.* Technical Report CS85-BMDSC-00-24, Teleydne Brown Engineering, Colorado Springs, Col., March 1985.
23. "Industry Observer." *Aviation Week and Space Technology* (28 May 1979): 13.
24. Johnson, N. L. "The Crowded Sky, The Danger of Collisions in Geostationary Orbit." *Spaceflight* 24 (1982): 446-449.
25. "Japanese Lose Second Satcom." *Aviation Week and Space Technology* (3 March 1980): 234.

Chapter 3

Definition and Analysis of the Space Debris Environment

Despite over 30 years experience working in and monitoring near Earth space, our knowledge and understanding of this complex environment is still far from complete. Just as we continue to learn about the ocean depths and the interactions within the upper atmosphere, so, too, must we strive to unravel the nature of the space about us. Our primary source of information on the numbers, sizes, and orbits of space debris is NORAD's worldwide Space Surveillance Network (formerly known as the Space Detection and Tracking System, SPADATS). Although the Soviet Union must operate a similar tracking system, that country has never openly published an equivalent of the NORAD satellite catalogs.

The measurement of space debris by NORAD is complicated by the fact that most of the system was not designed and built with a debris-tracking capability in mind. This tracking system was developed to sense relatively large objects that might indicate an attack from an adversary and is comprised of radar (phased array and mechanical trackers) and optical devices. Additionally, the tracking of space debris is not presently the highest priority at NORAD. Their primary mission concerns tactical warning and attack assessment for continental defense, not the tracking of fragments from old satellites. To attempt to track *all* debris accurately would not only saturate the computational and analytical resources of NORAD, but would adversely affect the ability of NORAD to conduct its early warning mission. Thus the nature of the NORAD Space Surveillance Network and the availability of its assets cannot master the already difficult task of identifying very small objects of unknown characteristics. Despite technical and political roadblocks, however, NORAD does a commendable job of providing data on space debris.

Space debris data generally consists of average radar cross-sectional area (RCS) and satellite orbital parameters. Once the researcher receives the "what" and "where" of the debris, he must extrapolate other desired characteristics. Determining the mass of a debris fragment from its RCS value is made more difficult by uncertainties in five aspects of the debris: shape, orientation, tumble rate, reflectivity, and density. Furthermore, the RCS value itself is a function of the frequency of the probing radar. Particularly for small objects with diameters of the same order as the wavelength of the radar, corrections for Rayleigh effects are necessary.

Once the masses of the fragments from a satellite breakup are estimated, the data can be used in a number of ways. A widely used form of analysis is to construct a mass distribution curve. This curve plots mass versus the number of fragments greater than a respective fragment mass. Curves are then fit to these plots to help group the breakups into families. Exponential, power, and polynomial expressions have all been employed in this manner with success. The interpretation of the mass data requires a rigid mathematical approach and inherently includes a number of assumptions.

From the orbital elements of the debris and the parent satellite, the velocity imparted to each fragment can be calculated. The distribution of these changes in velocity (ΔV) with respect to mass is distinctive of different types of breakup mechanisms and can be represented graphically on a debris heading plot. Another powerful graphical approach using orbital parameters was developed by John Gabbard while at NORAD. The Gabbard diagram depicts the intensity of the breakup, and hence the initial character of the debris cloud, by plotting each fragment's apogee and perigee versus its orbital period. Another format, the weighted Gabbard diagram, was developed by one of the authors to exhibit the debris cloud as a function of debris size, i.e., RCS. The use of the weighted Gabbard diagram provides new insight into the difference between explosion-induced and collision-induced satellite breakups (1).

Some of these debris analysis methods are used to form the Satellite Fragmentation Event (SAFE) Test. The SAFE Test assesses the likelihood that a debris cloud is characteristic of a collision-induced breakup. The SAFE Test is a very specific application of debris analysis, but it illustrates how a number of analytical techniques may be combined.

All the previous methods of analysis discussed depict

the debris cloud as a set of individual particles with the characteristics of each object adding to the knowledge of the whole. In contrast, some analysis has been conducted which treats the resulting debris cloud from a fragmentation event as a continuum. Statistical mechanics can play a major role in this type of analysis. The simulation of satellite breakups, as discussed later in this chapter, provides yet another valuable tool for debris analysis. In the future additional measurement devices may lead to improved understanding of the breakup phenomena and the debris environment.

Measurement of Size and Dispersion

During the 1970s NORAD began to routinely provide RCS data in addition to orbital elements on space debris. The average RCS values are calculated from measurements made by the AN/FPS-85 phased array radar system at Eglin Air Force Base, Florida, at a UHF frequency of 442 MHz. This data is compiled by NORAD and published monthly along with the basic orbital parameters (inclination, period, apogee, and perigee) for each satellite still in orbit (2). Special sections of the current *RCS Catalog* sort all satellites by RCS and by each of the orbital parameters. These sorts allow quick evaluation of changes in the total observable Earth satellite population.

Another useful document published by NORAD is the *Satellite Catalog (SATCAT)*. Each *SATCAT* contains pertinent launch, orbit, and decay data for every Earth-orbiting satellite ever cataloged by NORAD. The first entry in all *SATCAT*s is 1957 Alpha-1, the Sputnik 1 rocket body, launched on 4 October 1957. In 1984-85 under the direction of one of the authors, the *NORAD SATCAT* was expanded to provide RCS data on decayed as well as in-orbit satellites. Thus, for the first time a document contains historical RCS data on space debris as well as satellite payloads. In early 1986 the *SATCAT* was again modified to accept RCS values from different frequency radars including L-band, C-band, and VHF radars.

The *NORAD SATCAT* has limited distribution, but a similar document, the *Satellite Situation Report,* is available to the general public through the Goddard Space Flight Center (GSFC) in Greenbelt, Maryland. Exact orbital parameter data can also be obtained from GSFC on any satellite tracked by NORAD. Data gathered from NORAD, GSFC, the Smithsonian Astrophysical

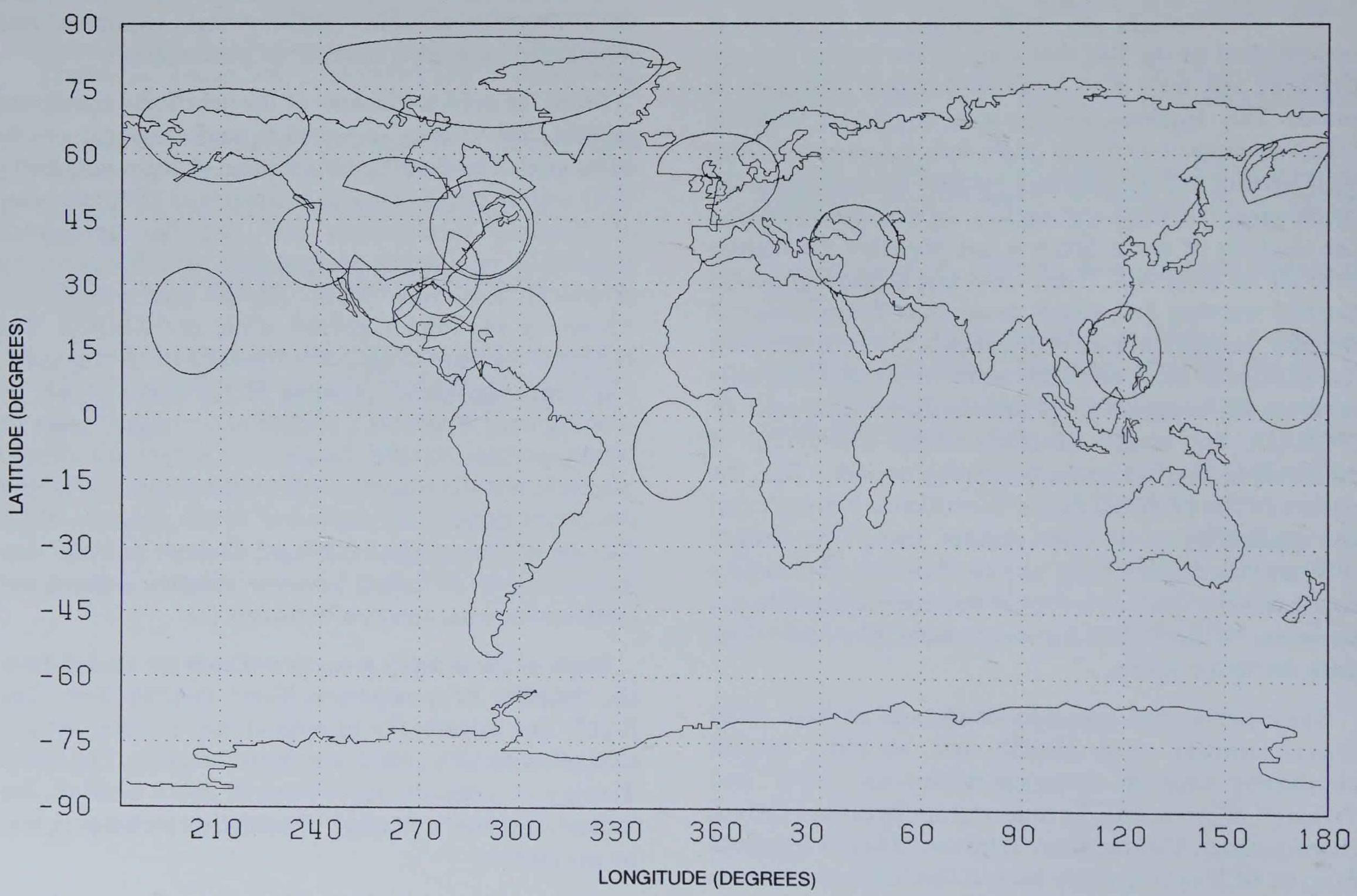


Figure 3.1 The worldwide NORAD Space Surveillance Network provides frequent coverage of low altitude satellites.

Table 3.1 NORAD Space Surveillance Sensors.

TYPE	NAME	LOCATION	OPERATING FREQUENCY	PRIMARY MISSION(s)
Dish Radar	ALTAIR (PACBAR 1)	Kwajalein Island, Pacific	415-440 MHz	Satellite tracking
	AN/FPQ-14	Antigua Island, Atlantic	5400-5900 MHz	Launch support; satellite tracking
	AN/FPQ-15	Ascension Island, Atlantic	5450-5900 MHz	Launch support; satellite tracking
	BMEWS Site 1	Thule, Greenland	400-450 MHz	Missile warning
	BMEWS Site 2	Clear, Alaska	400-450 MHz	Missile warning
	BMEWS Site 3	Fylingdales, England	400-450 MHz	Missile warning
	GPS-10 (PACBAR 2)	San Miguel, Phillipines	442 MHz	Satellite tracking
	Millstone	Westford, Massachusetts	1295 MHz	Satellite tracking
	AN/FPS-79	Pirinclik, Turkey	432 MHz	Missile test monitoring; satellite tracking
Phased Array Radar	COBRA DANE	Shemya Island, Alaska	1175-1375 MHz	Missile test monitoring; satellite tracking
	AN/FPS-85	Eglin AFB, Florida	437-447 MHz	Satellite tracking
	PARCS	Cavalier, North Dakota	420-450 MHz	Missile warning; satellite tracking
	PAVE PAWS East	Otis AFB, Massachusetts	420-450 MHz	Missile warning; satellite tracking
	PAVE PAWS West	Beale AFB, California	420-450 MHz	Missile warning; satellite tracking
	PAVE PAWS Southeast	Robins AFB, Georgia	420-450 MHz	Missile warning; satellite tracking
	PAVE PAWS Southwest	Goodfellow AFB, Texas	420-450 MHz	Missile warning; satellite tracking
Radar Fence	NAVSPASUR	Dahlgren, Virginia (Headquarters)	217 MHz	Satellite tracking (3 transmitters and 6 receivers across U.S. at 33° N lattitude)
Optical	Baker-Nunn	San Vito, Italy	Visible light	Satellite tracking (high altitude)
	Baker-Nunn	St. Margarets, Canada	Visible light	Satellite tracking (high altitude)
Electro-Optical	GEODSS Site 1	White Sands, New Mexico	Visible light	Satellite tracking (high altitude)
	GEODSS Site 2	Taegu, South Korea	Visible light	Satellite tracking (high altitude)
	GEODSS Site 3	Maui, Hawaii	Visible light	Satellite tracking (high altitude)
	GEODSS Site 4	Diego Garcia Island, Indian Ocean	Visible light	Satellite tracking (high altitude)

Table 3.2 Future NORAD Space Surveillance Sensors.

TYPE	NAME	LOCATION	OPERATIONAL DATE	REMARKS
Dish Radar	GPS-10 (PACBAR 3)	Saipan Island, Pacific	1989	Satellite tracking
Phased Array Radar	Thule Upgrade	Thule, Greenland	1988	Replace dish radar with PAVE PAWS type phased array radar
	Fylingdales Upgrade	Fylingdales, England	1992	Replace dish radar with PAVE PAWS type phased array radar
Electro-Optical	GEODSS Site 5	Portugal	1990+	Satellite tracking (high altitude); will complete GEODSS coverage of entire geostationary belt

Observatory, and NASA are combined in the *Satellite Handbook* (49).

The equipment used to measure and track Earth satellites includes a variety of conventional and phased array radars, photographic equipment (Baker-Nunn cameras), and electro-optical devices (GEODSS sites) (4). In all, 17 radars and 6 optical sensing systems comprise the NORAD space surveillance network (Figure 3.1, Tables 3.1 and 3.2). A modernization program currently underway will result in the conversion of two BMEWS (Ballistic Missile Early Warning System) sites from mechanical trackers to more capable phased array radars

and the deployment of a third mechanical tracker in the Pacific region and one more GEODSS site in Portugal.

This elaborate system provides reliable sensing of objects greater than 1 m in diameter up to geosynchronous orbit and as small as 8 cm at very low altitudes. Figure 3.2 shows NORAD's tracking capabilities and highlights the resolutions at different altitudes. From the figure it is obvious that any particle smaller than about 8 cm in diameter (0.005 m^2 assuming a circular cross-section) cannot be sensed reliably by NORAD at any altitude. The smallest fragment which can be measured at altitudes greater than 1,000 km is about 10 cm in diameter.

Partial reason for this limitation can easily be seen by observing the resolution of representative radars of the space surveillance network shown in Figure 3.3. Since no object may be cataloged unless two or more sensors can reliably track it, the network sensitivity is consequently less than the best radar in the system.

Even when an object can be measured and tracked, the error in the measurement may be so great that very little useful information is provided. It is generally accepted that the orbital element sets are much more accurate than the RCS data for debris-sized objects. A higher confidence in RCS values will be possible when NORAD begins publishing RCS data from multiple sensors, including those with different frequencies.

A statistical approach was taken by one of the authors to develop an RCS measurement uncertainty (standard error) for debris tracked by NORAD. A sample standard deviation was calculated for each object by examining monthly RCS values over a period of time (two years was selected). Using the chi-square probability distribution function, a 90% confidence interval was formed for the population standard deviation using the observed sample variance. The relationship used was

$$\sqrt{\frac{(n-1)s^2}{\chi^2_{0.95}(\nu)}} < \sigma < \sqrt{\frac{(n-1)s^2}{\chi^2_{0.05}(\nu)}} \qquad (3.1)$$

where
- n = number of samples
- $\nu = n-1$ = degrees of freedom (DF)
- $\chi^2_{0.95}(\nu)$ = chi-square value for ν DF at a 0.95 level of significance
- s = sample variance
- σ = population standard deviation

This analysis was also conducted on eight calibration spheres ranging from 30 to 110 centimeters in diameter. These spheres generally have high orbital inclinations (greater than 70 degrees) and orbital periods around 105 minutes. The population standard deviation was calculated, using the approach outlined above, to be 20% of the measured RCS value. The same analysis conducted

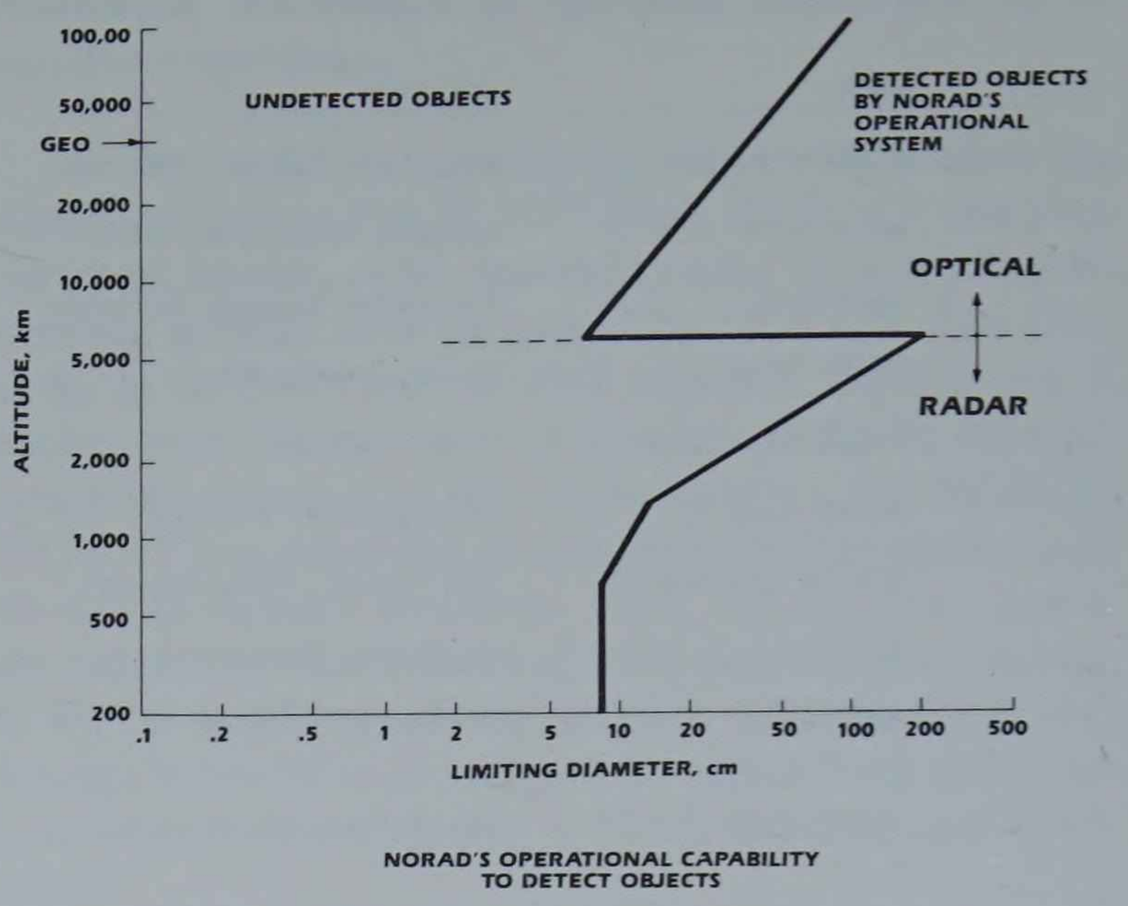


Figure 3.2 The overall sensitivity of the NORAD Space Surveillance Network is highly dependent on the altitude of the satellite. *Courtesy of D. J. Kessler, NASA Johnson Space Center.*

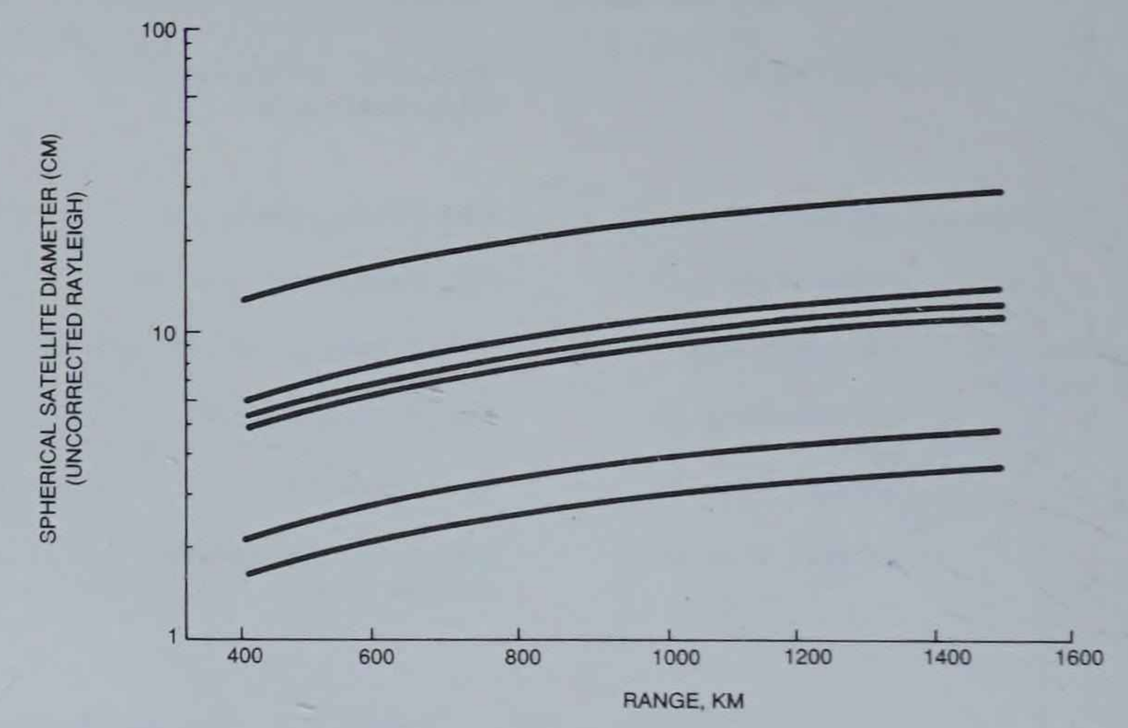


Figure 3.3 Since more than one NORAD sensor must be able to track a satellite before it can be cataloged, the overall network sensitivity is less than that of some individual radars. The curves above represent the sensitivities of specific NORAD radars. *Courtesy of Teledyne Brown Engineering.*

on the debris from the 12 breakups analyzed in reference 1 produced significantly worse results. Although only 12 breakups were studied, these breakups accounted for over 60% of the debris then in orbit. The debris population standard deviation was found to be 100% of the measured RCS value across the entire size spectrum. This is a factor of five worse than for the calibration spheres.

The measurement standard deviation for debris-like objects was expected to be much larger for the smaller particles, but in fact the value was nearly constant for all trackable debris. The reasons for the comparable standard deviations across the entire size range are both

operational and technical. At the high end of the size regime (1 m^2 or greater) the random orientation of the fragment will produce considerable statistical fluctuation due to the physical nature of the large object. These objects are more likely to be cylindrical, hemispherical, or panel-shaped so that a slight change in orientation may cause a marked change in cross-sectional area. On the other hand, the smaller objects (less than 1 m^2) are more likely to have cross-sectional areas which are less dependent on orientation. This improved physical architecture is offset by the rather poor radar resolution at these smaller sizes (mainly due to Rayleigh scattering).

Futhermore, the RCS measurement of debris-sized objects is a low priority task, resulting in a smaller database for examination. Yet another difficulty is the occasional loss of very small objects by NORAD. When such objects are "found" again, they may actually be different debris pieces from the same parent satellite. Hence, when new RCS data is taken, significant variations in the historical record can occur.

The problem of tasking became evident while making the calculations for developing the measurement standard deviation for debris analyzed in reference 1. Of the debris monitored for two years (January 1983 - December 1984) only 26% of the pieces had two or more different RCS values and, hence, were actually used to calculate the sample variance. Over 40% of the debris had no RCS value at all. The debris had either decayed before a valid measurement could be made or NORAD assigned a default value which means that the measurement was not completed for any of a variety of reasons. Over 30% of the debris had the same RCS value over the two-year period. Obviously, these smaller debris-sized objects do not have their RCS values remeasured and recalculated as often as is done for the larger fragments.

During this analysis it was also found that a very small percentage (3%) of particles apparently were "switched" from time to time. As an example, imagine that two satellites, 1085 and 2942, are in similar orbits and have RCS values of 0.1 and 10 m^2, respectively. If the satellites are in very close proximity to one another as they pass through a sensor's coverage, the sensor may cross-correlate the objects with the existing track files. Hence, satellite 1085 becomes 2942 and vice versa. This is called mistagging and is usually easily detected upon careful scrutiny of the data. As a result of mistagging, RCS values can fluctuate dramatically. Mistagging is most prominent when the debris cloud is densely packed soon after creation and before significant dispersion has occurred.

The factor of five difference between measurement standard deviations for calibration spheres and orbital space debris is significant. To calculate the shielding needed to protect a satellite from debris, the fragment mass must be known. If the cross-sectional area is in error by an order of magnitude, the mass calculations will merely amplify this error. This problem of mass representation from RCS values is of great concern for centimeter-sized particles.

Impact sensors have been used for years to measure meteoroids less than 1 mm in diameter. Some of these impact sensors have measured considerable fluxes in low Earth orbits, some of which have been attributed to solid rocket motor products. The first direct measurements of orbital debris were apparently taken in 1973-74 during the Skylab program when the returned Apollo command modules were carefully examined (6). The sensing matrix of impact sensors and ground radars leaves a measurement gap in the 1 mm to 10 cm size regime. Dedicated optical telescopes might be used to fill this gap. NASA saw a need for this capability and contracted with Lincoln Laboratories to use two of their GEODSS telescopes to investigate the 1 cm debris regime (7). The two 80 cm equatorially mounted cassegrain telescopes were linked to measure and track small, low altitude objects. This system had some capability to discriminate between meteors and artificial satellites. The video signals from the two telescopes were combined with an accurate time base to provide an estimate of the small satellite population. The preliminary conclusion suggested the nontrackable debris population of 1 cm or greater may be eight times that of the trackable population. This result is used by hazard models presented in Chapter 4.

In addition to ground-based telescopes, the Long Duration Exposure Facility (LDEF) will contribute much to the understanding of the nontrackable debris population. Deployed by the Shuttle in 1984, LDEF houses a series of 84 long duration experiments, some of which are dedicated to the measurement of near Earth debris (Figure 3.4). Experiment S0001, Space Debris Impact Experiment, on LDEF will measure impacting particles over a wide span of particle sizes (39). In the past, the piecing together of data from various impact sensors provided an incomplete understanding of the debris environment since different hardware was used each time. Experiment S0001 will use the same aluminum plate to measure the wide spectrum of impacts and thus produce a more comprehensive evaluation of the distribution of space debris and meteoroids.

Specifically, this experiment seeks "to establish the population and size distribution of meteoroids in the mass range from 10^{-10} to 10^{-4} grams, to establish the current population of man-made debris in the same mass range, and to obtain data on the physical properties (composition and density) of meteoroids" (39). The experiment uses trays located on all sides of the LDEF, i.e., along the circumference of the structure and on the nadir and zenith ends. It was scheduled to be retrieved

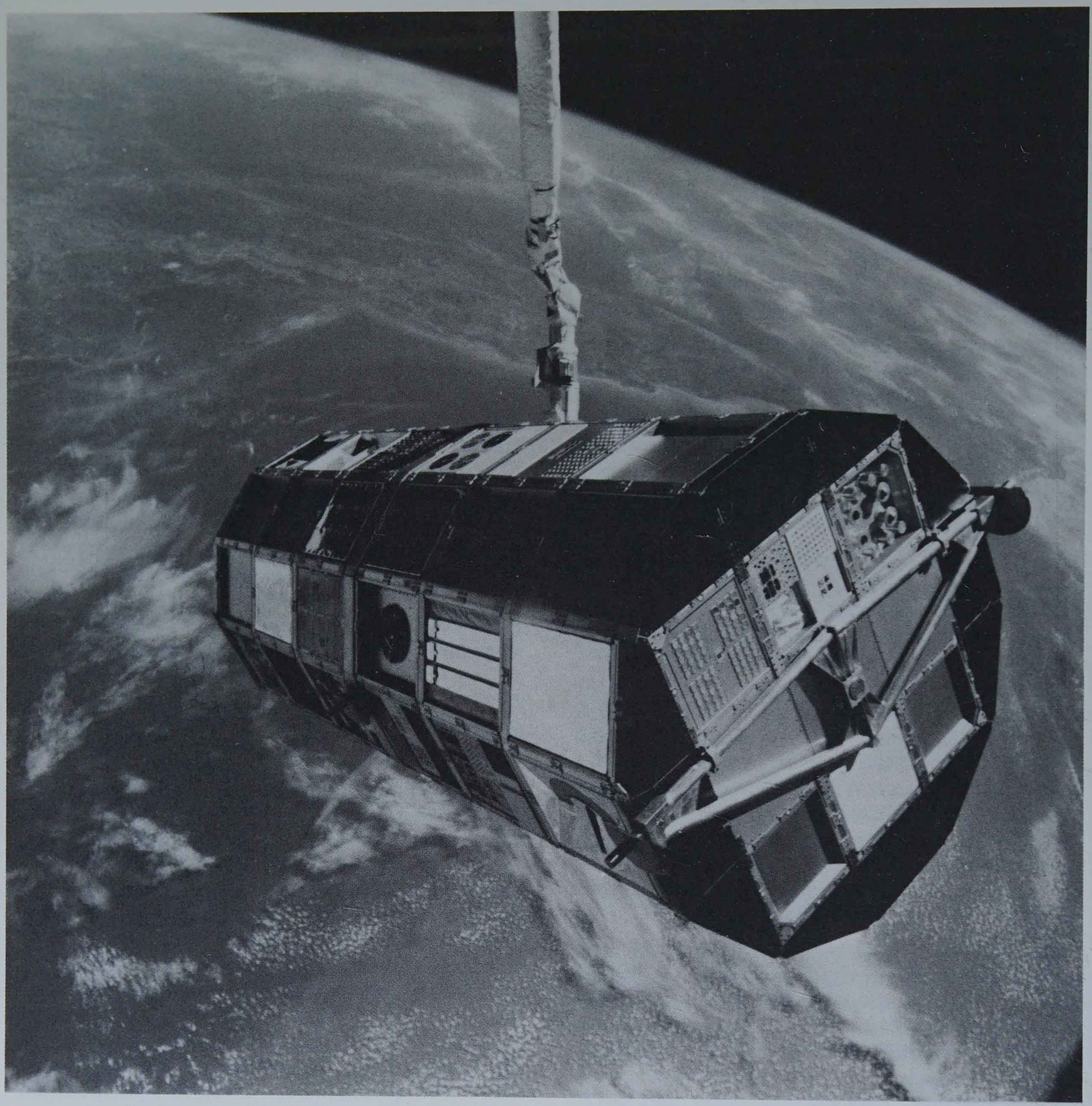


Figure 3.4 The Long Duration Exposure Facility (LDEF), deployed in 1984 by the Space Shuttle, will provide valuable data on the space debris environment when it is retrieved later in this decade. *Courtesy of NASA.*

by the U.S. Shuttle in 1985, but programmatic delays and then the Challenger accident in January 1986 have postponed its return to Earth. Retrieval of LDEF is a high priority when Shuttle flights resume. The results of the LDEF debris experiments should be available within a year after the termination of its flight.

The use of Lincoln Laboratory's GEODSS telescopes was a valuable effort which provided information not routinely available from NORAD. Similar experiments have been performed with the Perimeter Acquisition Radar Characterization System (PARCS) in North Dakota. Originally designed to track the reentry of small strategic weapons and associated debris (5), this radar system is actually part of NORAD's Space Surveillance Network. On three occasions, the last in May 1984, the sensitivity of the radar was increased significantly from its normal operations to assess better the very small debris population at low altitudes. The magnitude of this short-

lived debris flux can then be used to estimate the size of the debris "reservoirs" at higher altitudes. One of the debris models presented in Chapter 4 uses these observations as a major aspect of its population prediction process.

Another experiment using PARCS was conducted in conjunction with other NORAD radars. All systems monitored the debris from the breakup of satellite 1982-88A on 20 December 1983. PARCS detected and tracked over 130 objects while the NORAD network as a whole could only track and catalog 33 pieces (3). Thus, published NORAD data normally represents a highly conservative view of space debris in the near Earth environment.

The monitoring of the dispersion of debris is also a difficult task. The orbital element sets generated by NORAD are updated as required to maintain specified positional prediction accuracies. These accuracies typically range from a few kilometers to tens of kilometers. However, the nature of space debris, especially the nontrackable debris, often makes orbital decay by atmospheric drag and solar pressure a fast-acting agent for their removal. Trackable debris characteristically have area-to-mass ratios (A/M) on the order of 0.015 m^2/kg, while nontrackable debris on the average have even greater A/M ratios by a factor of 37.5 (10). In comparison, the Shuttle (empty) has an A/M ratio of only 0.002 m^2/kg (11) which is many times smaller than the A/M ratio for nontrackable debris.

The other major parameter in orbital decay problems is atmospheric density at the altitude of the orbiting object. Atmospheric density is also a function of the level of solar activity at any given altitude. Sehnal has shown that major reductions in the debris population can be associated with increased solar activity near solar maxima (10). This trend has also been analyzed quantitatively in simulation models (48).

The study of space debris and its dispersion is a complex and challenging task. Yet, information can be derived from the dispersion of debris which is germane to other astronomical processes. Reference 38 develops the use of Gabbard diagrams of long-lived breakups for the study of spherical harmonic resonances of the Earth. Anomalies of the fragments' orbits are noted at specific orbital periods which appear to correlate with the harmonic terms of the Earth's gravitational force field potential. These types of resonance forces also produce similar phenomena elsewhere in the universe. Resonance forces from Saturn's moons may have caused the particulates about Saturn to separate into discrete rings (38).

The size and spatial distribution of space debris can be used to predict collisional and breakup hazards for spacecraft (Chapter 4). Some of the basic limitations and constraints of the measurement of debris will be covered in the remainder of this chapter. The next four sections deal with the basic tools for debris analysis. First, RCS-to-mass conversion techniques will be discussed, followed by an outline of information on and methods for the consolidation of debris data of this type. A graphical tool, Gabbard diagrams, will be explained to show its usefulness in describing the characteristics of a debris cloud. Lastly, a number of these techniques are combined into a test to classify debris characteristics in an attempt to identify the cause of the breakup.

Conversion From RCS to Mass

The RCS value for an object depends greatly upon its composition, its shape, and its orientation. A flat plate can produce radically different RCS values depending on its orientation with respect to the observing radar as well as the geometry of the pass near the radar. The RCS value for a piece of debris has been seen to vary by as much as an order of magnitude from one month to the next in NORAD's RCS catalogs. This phenomenon is quite prevalent, particularly for tumbling rocket bodies, contributing to the large measurement standard deviation for space debris discussed earlier. Because of these variations, it is appropriate to take an average of all the RCS values recorded for a fragment and use the average RCS value to derive a mass for the object. This process is complicated by the fact that the RCS values provided by UHF FPS-85 radar at Eglin AFB are already averaged values.

Three methods of converting an RCS value to a mass can be employed. The first approach assumes that the RCS value represents the face of an irregularly shaped, almost circular disk. This circular disk is assumed to have some average characteristic thickness: 5 mm and 10 mm are reasonable values for many spacecraft structures. The thickness is selected to be representative of the thickness of the bulk of material used to construct the satellite being analyzed. Obviously, the more we know about the parent satellite the more we know about its debris. The RCS value is taken to be equal to the area of the circular face of the disk ($\pi d^2/4$) so the proposed diameter may be found directly.

The circular disk approach forces the assumption that the object has a spherical shape when the characteristic thickness exceeds the calculated diameter. The calculated diameter then becomes the diameter of the assumed sphere. Next the volume of these two shapes can be calculated directly which in turn will lead to the mass of the fragment if a mass density is estimated. Spacecraft are normally made of materials that primarily fall into three density regimes: approximately 2.0 gm/cm^3 for circuit board material; 2.7 gm/cm^3 for aluminum, glass,

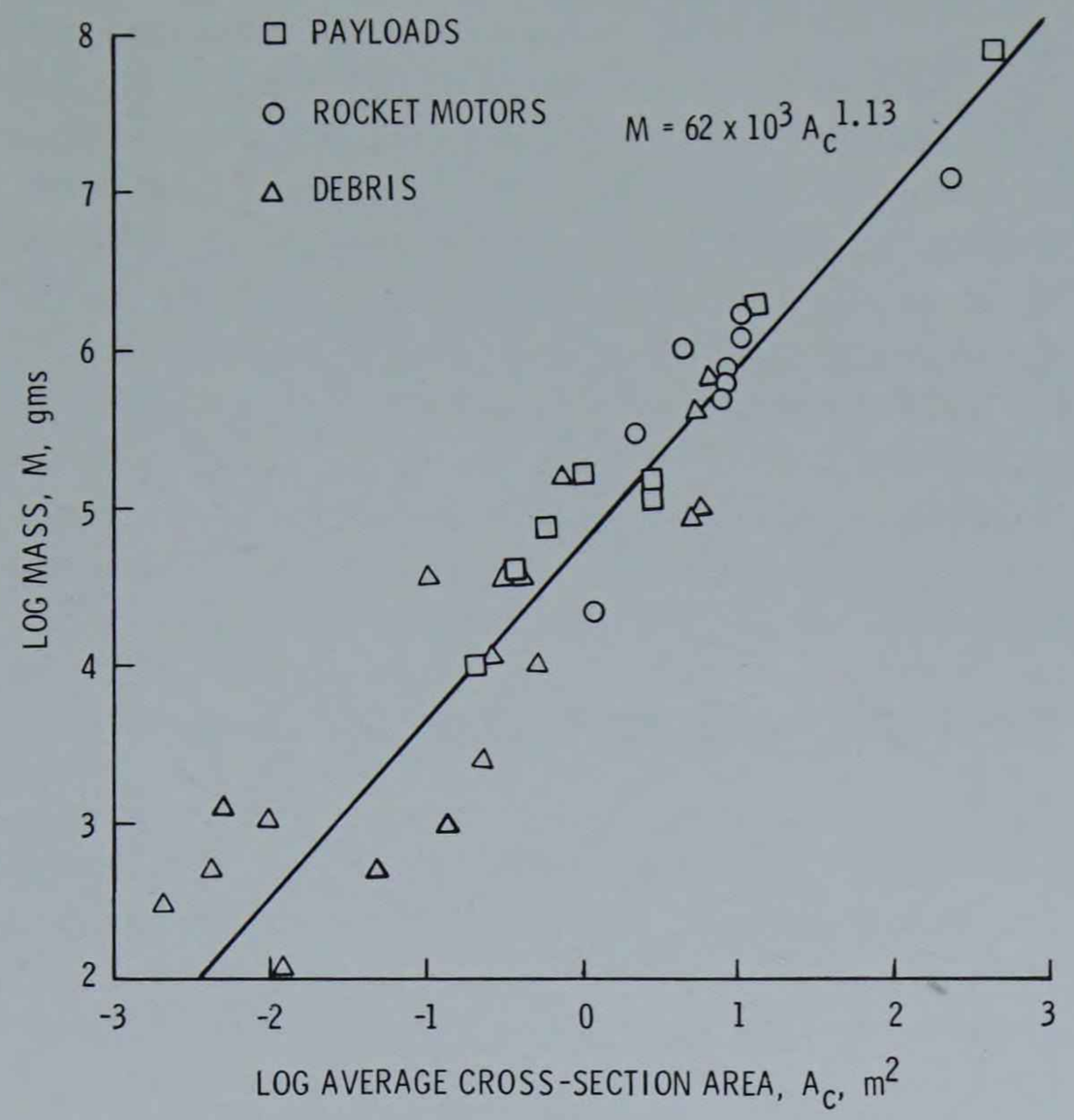


Figure 3.5 The mass of an Earth satellite can be approximated by its average cross-sectional area. *Developed by D. J. Kessler, NASA Johnson Space Center.*

and basalt; and 8.0 gm/cm³ for steel. These densities produce a wide variation of possibilities, and one must assign a specific composition to the debris under examination.

One way to handle this problem is to apply a parametric approach and use all three densities to provide a range of possible masses. Again, if the researcher knows precisely the structure of a satellite which has broken up, he may decide that one end of the extreme is more appropriate than the other. For example, a short duration spacecraft made in the 1960s with no solar panels, no honeycomb construction, and a cumbersome propulsion system may suggest an average density closer to the high end of the parametric values. An example using this technique will be presented at the end of this section.

The second approach was developed by D. J. Kessler and B. G. Cour-Palais (13). Here the logarithmic cross-sectional areas were plotted against the logarithmic mass for representative payloads, rocket motors, and for debris from the breakup of a Centaur D-1T rocket (Figure 3.5). From this graph the following relationship was found:

$$M = 62 \times 10^3 (A_c)^{1.13} \qquad (3.2)$$

where M = mass of satellite in grams
A_c = average radar cross-section in m^2

The exponential value 1.13 falls between the two extremes of 1.0 and 1.5, where 1.0 would hold for hollow structures with walls of a constant thickness and 1.5 would hold for structures having a constant mass density.

One of the present authors repeated this exercise using exclusively Soviet spacecraft and rocket bodies distributed over three orders of magnitude in mass and found virtually the same mass-to-RCS relationship. This method is used later in one of the debris population/collision hazard models.

The third and final technique, the building block approach, uses characteristics of both of the first two methods. The building block approach assumes that the RCS value measured is the area of the face of a cube. This cube will have a density equal to the total mass of the parent satellite divided by the total volume of the parent satellite, i.e., the spacecraft density. The building block approach assumes that variations in density and structure will be randomly distributed throughout the resulting debris. The successful use of the building block approach depends heavily on knowledge about the parent satellite as does the circular disc technique. The building block approach is also similar to the second conversion technique since it uses an averaging process to determine a fragment's mass. All three methods have been used to convert from cross-sectional area to mass for the fragments from the hypervelocity impact tests in reference 17. From the actual debris, the approach used by Kessler and Cour-Palais was found to be most accurate.

Conversion Processes

Two illustrative examples of the use of these RCS-to-mass conversion processes follow. These examples highlight some of the difficulties in the analysis of space debris.

Example 1

During the early research in support of reference 1, the building block approach was developed. The circular disk technique was originally employed to analyze debris from satellite breakups and the building block approach came out of an attempt to improve upon this method.

Originally six satellite breakups were selected for analysis to try to distinguish between collision-induced and explosion-induced satellite breakups through debris analysis. Three of the breakups were of unknown cause and three were known to be propulsion-related, i.e. explosion-induced. One proposed method to distinguish between breakups was to compare the mass accounted for by RCS measurements for each breakup. Using the parametric circular disk approach, the RCS values for all the trackable debris from each breakup were converted to their mass equivalents, summed, and compared to the estimated mass of the parent satellite. The results from this analysis are presented in Table 3.3.

Of the utmost importance in this analysis is the recognition that less mass might be present for a breakup if it occurred at a low altitude where a portion of the

Table 3.3 Trackable Mass Versus Satellite Mass (Circular Disk).

Satellite Breakup	Trackable Mass (kg) 2.0 g/cm³	2.7 g/cm³	8.0 g/cm³	Mass of Satellite (kg)	Ratio (Measured to Actual)
1981-53A	2519	3395	10074	800	3.1/4.2/12.6
1976-120A	175	236	697	700	0.25/0.34/1.0
1976-67A	333	445	1330	700	0.48/0.64/1.9
1982-115A	743	1006	2972	2240	0.33/0.45/1.3
1978-26B	1234	1687	—	350	3.5/4.8
1976-77B	1734	2365	—	350	5.0/6.8

Table 3.4 Trackable Mass Versus Actual Mass (Building Block).

Satellite Breakup	Density (g/cm³)	Trackable Mass (kg)	Actual Mass (kg)	Ratio (Measured to Actual)
1981-53A	0.189	4633	700	6.62
1976-120A	0.055	277	700	0.40
1976-67A	0.055	299	700	0.43
1982-115A	0.180	618	2240	0.28
1978-26B	0.017	186	350	0.53
1976-77B	0.017	208	350	0.59

debris may have decayed quickly or if the breakup occurred at a high altitude where the small debris could not be sensed by NORAD radars. Therefore, it was expected that all the ratios would be less than 1.0 since some debris will undoubtedly be unaccounted for. The large range of values found for the ratios are thought to be due to decay of debris, RCS-to-mass conversion errors, the inaccuracy of the RCS data, uncertainty of spacecraft materials, and unique characteristics of each spacecraft. (Note that calculations for U.S. spacecraft only use the lower two density values.)

Since information about Soviet spacecraft is often limited, a new mass representation approach was developed. This new technique was the building block approach described earlier. The results acquired using this method for the same six satellite breakups are provided in Table 3.4. With the exception of 1981-53A, the mass ratios appear more credible than the results from the circular disk approach.

From this analysis it became obvious that mass accountability alone could not provide a means to distinguish mechanisms for breakups due to the uncertainties involved. On the other hand, this attempt produced an alternate mass representation method which proved useful in a mass distribution curve normalization procedure which will be covered later.

Example 2

The difference in the three RCS-to-mass conversion techniques can best be seen by conducting a short example problem. Consider a cylindrically shaped American satellite with a length of 6 m, a diameter of 2 m, a weight of 625 kg, and a characteristic thickness of 10 mm. Once this satellite fragments, the resulting debris may have its RCS values converted to masses by any of the three techniques outlined previously. The RCS values for 1 m² and for 0.1 m² fragments with their respective mass conversions are displayed in Table 3.5

Table 3.5 Comparison of Fragment Mass Values.

RCS (m²)	Circular Disk Method 2.0/2.7/8.0 g/cm³ (kg)	Average Method $M = 62(RCS)^{1.13}$ (kg)	Building Block Method $\varrho = 0.033$ g/cm³ (kg)
1.0	2.0/2.7/8.0	62	33
0.1	0.2/.27/0.8	4.6	1.0

Mass and Velocity Distributions

Mass and velocity distribution curves are used to organize large groups of data and characterize trends in that data. Trends are characterized by fitting curves to the data. Many ways exist to derive the mass data (as shown in the previous section) and many more ways are available to fit curves to this data. Families of curves may be used to distinguish types and magnitudes of fragmentation events. First, experimental data for explosions and hypervelocity collisions will be examined. The information from these developments will then be compared to mass distribution curves for actual observed debris data.

Explosion Data

Reference 14 provides a development of mass distribution data for low and high intensity explosions. A low intensity explosion is defined as one in which the "charge is not in direct contact with the spacecraft structure," such as a pressure vessel explosion. For a high intensity explosion the charge is in direct contact with the spacecraft structure, such as ignition of excess fuel or the detonation of an explosive charge. In general, high intensity explosions will be larger in magnitude regardless of the physical situation which triggered the fragmentation.

Experiments were conducted to obtain data for high intensity explosions whereas the fragments from an exploded Atlas missile were used to derive experimental results for low intensity explosions. Both mass distributions for the two magnitudes of explosions follow exponential laws of the form

$$N = N_o \exp\left[-c(m_f)^{1/2}\right] \tag{3.3}$$

where N = number of fragments of mass greater than or equal to m_f
N_o = total number of fragments
c = a constant (controls the slope of the curve)
m_f = fragment mass

The high intensity explosions have larger values of both c and N_o than low intensity explosions. A larger c means that the slope of the curve is steeper and a larger N_o means that numerically there are more fragments resulting from the explosion. The values for c ranged from 0.23 to 0.44 while N_o ranged from 6,921 to 33,880. The value for N_o is dependent on the mass and structure of the parent satellite in addition to the intensity of the explosion. The smallest fragment measured from the explosion experiments was 30 mg (about 0.3 cm diameter sphere for density of 2.7 gm/cm^3), but for most explosions, over 30% of the mass was not recovered.

It should be noted that the two classifications of low and high intensity explosions are used to represent two regions on a continuum of possibilities. The steepness of the mass distribution curves for these two cases forms a regime of slopes which may be broadly categorized merely as explosions. This distinction is important when trying to compare mass distribution curves of known explosions to fragmentation events of unknown cause.

The results from the explosion experiments were compared with fragmentation theory. From this analysis it was apparent that theory underestimates the total number of fragments produced. Even though the theory is slightly conservative, it is still useful since it can be used to predict results for structures with different thicknesses. The development of this theory may be found in reference 15.

An additional term may be added to the exponential equation to compensate for the different spacecraft structures (1). This new term, the shift factor, is part of the constant c from eq. 3.3. The exponential law now becomes

$$N = N_o \exp\left[-b\ SF\ (m_f)^{1/2}\right] \qquad (3.4)$$

where N, N_o, and m_f are defined as earlier and
b = differentiating term
SF = shift factor = $10\varrho/m_l$ (ϱ is the spacecraft density as defined earlier, and m_l is the mass of the smallest fragment)

Using this proposed analysis method, the differentiating term b is 10.5 for low intensity explosions. Due to the lack of data, the differentiating term for the high intensity explosion was not calculated, but it is known to be larger than the low intensity term by definition. This method of creating a mass distribution was developed to assist in distinguishing between different types of breakups (explosion-induced versus collision-induced). Unfortunately, this method has proven to be too subjective due to the uncertainty in measurements and the varying magnitude of explosion events.

The velocity of the resulting fragments from an explosion is a function of the magnitude of the fragmentation event. The velocities of fragments for low and high intensity explosions average about 100 m/s and 3 km/s, respectively. There appears to be no dependence of velocity on the mass of the fragment, unlike debris from hypervelocity impacts.

Hypervelocity Impact Data

Hypervelocity impact tests have been conducted to investigate the survivability of reentry vehicles, the toughness of armored vehicles, and the penetration of satellites (40). A vast majority of these analyses are classified, but there are enough studies in the public domain to provide a good perspective on the collision phenomenon between space debris and a satellite. Many hypervelocity impact tests were conducted at the NASA Langley Research Center in the mid-1970s. Data from other tests conducted at the Arnold Engineering and Development Center (AEDC) was compiled by Physical Sciences Incorporated (PSI) (17) and then reanalyzed by Lockheed (18).

The AEDC hypervelocity tests used aluminum projectiles travelling at speeds of 3 to 5 km/s and impacting small spacecraft-type structures. At these velocities, the impact phenomenology may still allow the target and the projectile to be treated as solids throughout the entire fragmentation process as a rough estimate. As the impacting velocity approaches 20 km/s, the liquid state is encountered routinely, while for velocities above this, vaporization of material becomes a major part of the fragmentation process (41). The targets were segmented aluminum cylinders with fittings for circuitry located at numerous points throughout their structure to represent a target similar to a typical satellite (Figures 3.6, 3.7, and 3.8).

The mass distribution curve for a hypervelocity collision may actually consist of two regions. At the very small fragment sizes (less than 1 cm for these tests) a power distribution law is observed. An exponential curve (of the same form as that associated with explosions) describes the upper end of the hypervelocity collision mass distribution curve. The constant b in eq. 3.4 takes on the value of 0.9067. That this differentiating factor is an order of magnitude smaller than the differentiating term for explosion-induced fragmentations is used in the SAFE test.

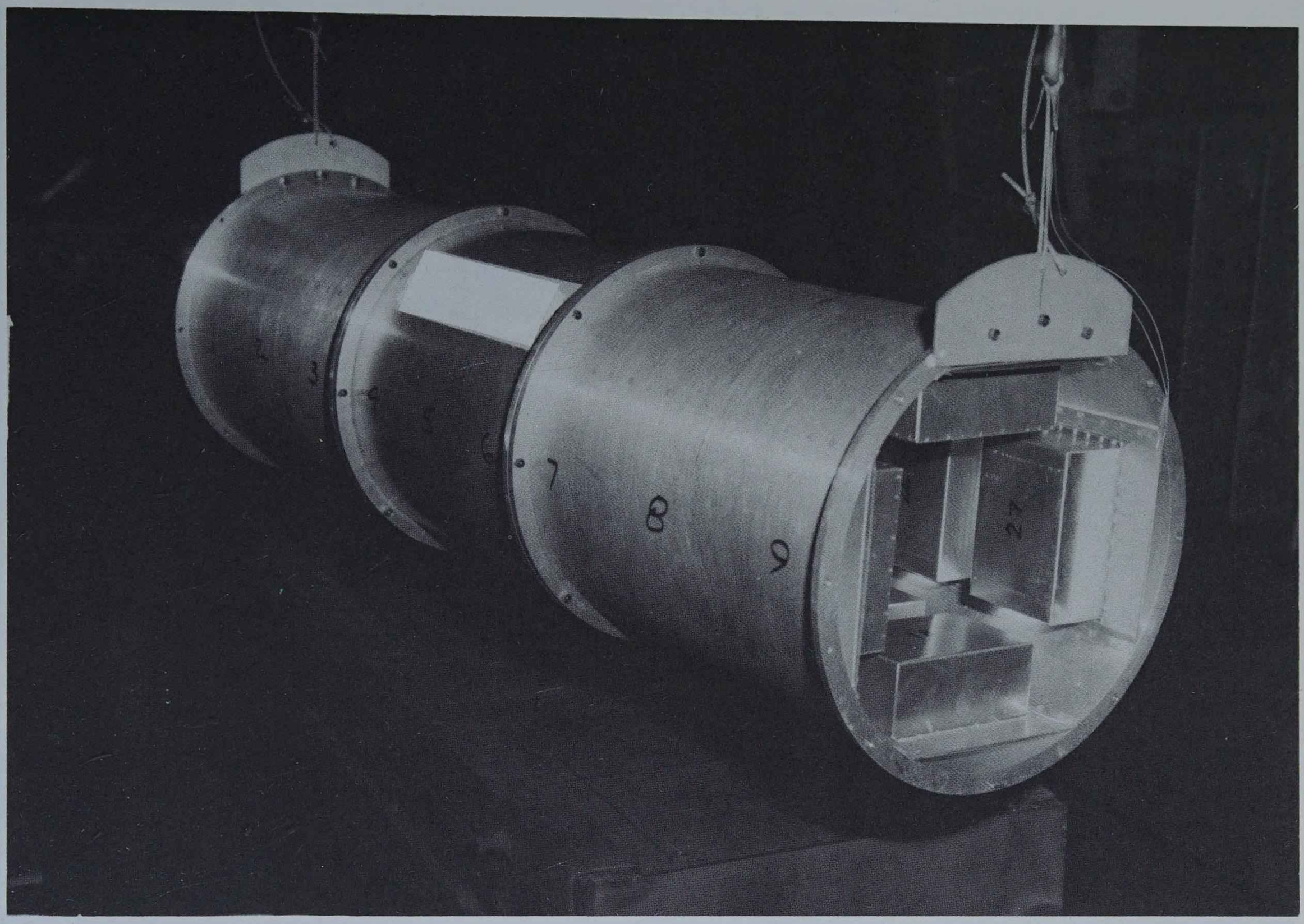


Figure 3.6 This hypervelocity impact target was designed to simulate a typical spacecraft structure. Note the interior boxes representing electronic systems.

The part of the mass distribution curve which follows a power law is of limited importance to the casual observer because these smaller fragments generally cannot be tracked by NORAD. For this reason, when observational debris data is reduced, this power law distribution may not substantially affect the mass distribution curve. It is important to note the physical explanation for this two-part distribution curve. The power law governs the ejecta fragments which are produced as a direct result of the collision (18). When an aluminum particle impacts a spacecraft with a relative velocity in the 9 to 11 km/s range, the instantaneous pressure may reach 5 megabars (46). The ejecta mass distribution takes the form

$$N = 0.447\ (m/m_e)^{-0.7496} \qquad (3.5)$$

where N = number of fragments with mass m or greater
m = fragment mass
m_e = total ejecta mass

The exponential law governs the larger fragments which break up as an indirect result of the collision. "The number of larger fragments [is] a direct function of the mass of the projectile and the mass and nature of the impacted object" (3).

As the result of a hypervelocity collision, the ejecta velocity may actually exceed the projectile velocity (18). This is not always true: the ejecta velocity depends on the size of the projectile and where it impacts the target (parent satellite). If the projectile penetrates the parent through a thin skin (low mass region), high ejecta velocities may be expected. On the other hand, if the projectile strikes a dense portion of the target, lower ejecta velocities may result.

The debris spray angle is also dependent on where the projectile hits the parent satellite. The debris spray angle is a measure of how much the paths of the ejecta vary from the path of the projectile. It is the angle between the projectile's path and the path of the debris as it leaves the parent satellite. A small debris spray angle would physically mean that most ejecta would leave the target almost along the same vector upon which the projectile

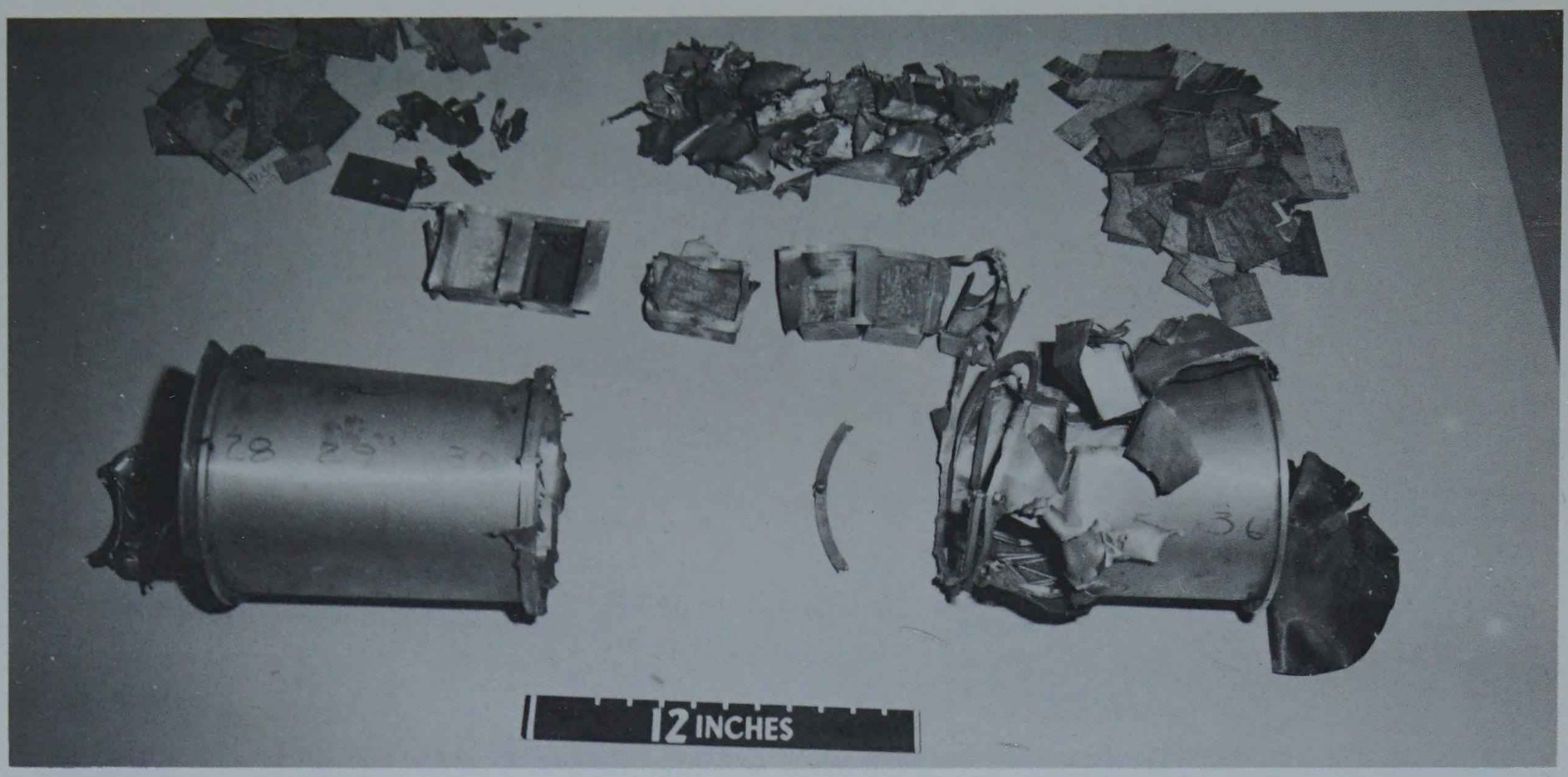


Figure 3.7 The mass ratio (projectile/target) during this hypervelocity impact test was 9%.



Figure 3.8 The same projectile type used in the test described in Figure 3.7 impacted a more massive target at the same velocity (the projectile to target mass ratio was 3% for this impact).

approached. A small debris spray angle (less than 20 degrees) exists when the projectile is greater than a tenth of the mass of the impacted satellite. This situation equates to when the projectile enters the target through a sparsely constructed area (e.g., thin skin) of the satellite. Hence, high ejecta velocities and small debris spray angles should occur in tandem for this type of collision.

The much more likely occurrence of a projectile striking a target at a dense portion results in lower ejecta velocities (between 10 and 100 m/s) and wide (approximately 90 degrees) debris spray angles. Characteristically, the smaller debris fragments have larger velocities, while the larger debris fragments have smaller velocities. Figure 3.9 shows a curve distinctive of the distribution of velocities versus mass for a collision where the projectile had a velocity of 3.5 km/s (3). The ratio of the mass of the projectile to the mass of the target is an important parameter and will be discussed more in Chapter 4. Note the destructiveness of the collisions in Figures 3.7 and 3.8 when the projectile mass was less than 10% of the target mass. These physical observations are useful for debris analysis and are important when assessing debris dispersion patterns using Gabbard diagrams.

The use of Gabbard diagrams for debris analysis provides a graphical approach to the difficult processes of determining the causes of satellite breakups, defining the debris cloud from a satellite breakup, and assessing how these debris clouds act over time. A basic understanding of orbit theory is necessary for a complete appreciation of the usefulness of Gabbard diagrams. Therefore, orbital perturbation equations will be reviewed briefly (19) before Gabbard diagrams are discussed at greater length.

Perturbation Theory

The equations of motion for an object in an elliptical orbit under the influence of a central force μ/r^2 per unit mass are well known. For Earth satellites, $\mu = 3.986 \times 10^5$ km^3/sec^2 and r is the radial distance of the Earth satellite from the center of the Earth. Some basic equations of orbital motion follow without proof (for example, see references 50 and 51).

$$p = a(1 - e^2) = h^2/\mu \tag{3.6}$$

where p = semi-latus rectum of the orbit
a = semimajor axis
e = eccentricity
h = total angular momentum
μ = gravitational constant

$$r = p/\left[1 + e\cos(f)\right] = a(1 - e^2)/\left[1 + e\cos(f)\right] \tag{3.7}$$

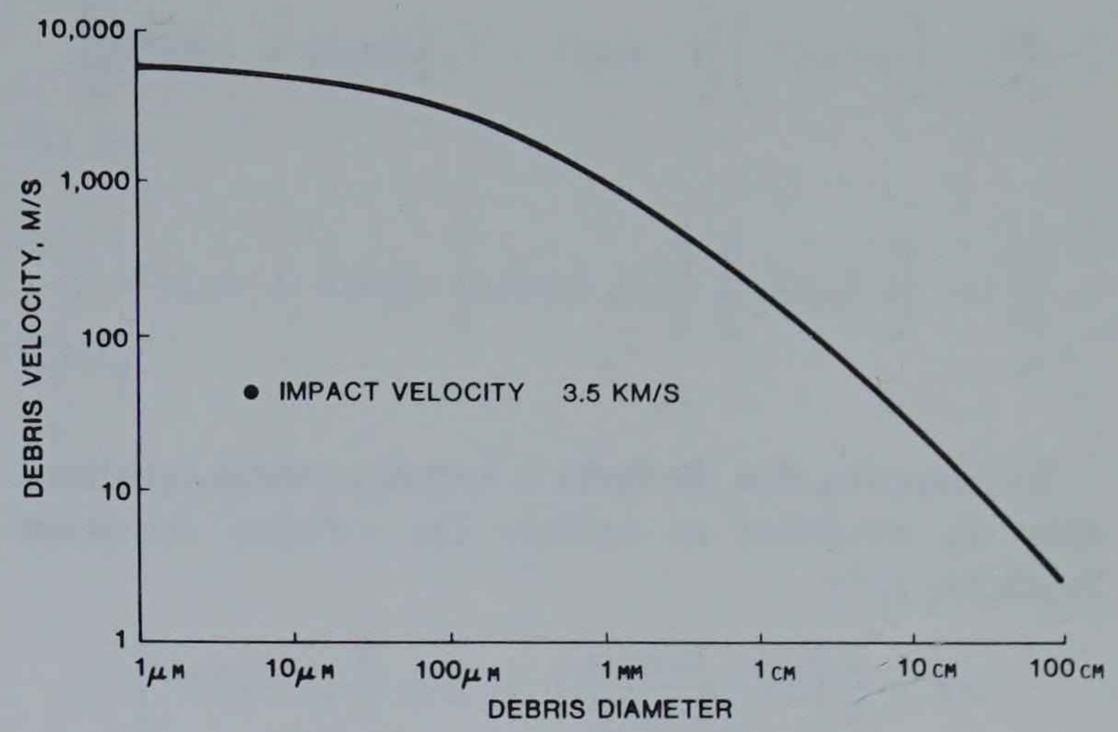


Figure 3.9 Hypervelocity impact tests have revealed the maximum ejection velocities of debris as a function of particle diameter. *Courtesy of Teledyne Brown Engineering.*

where f is the true anomaly, and

$$r = a\left[1 - e\cos(E)\right] \tag{3.8}$$

where E is the orbital eccentric anomaly.

Two more useful equations include

$$V = (2\mu/r - \mu/a)^{1/2} \tag{3.9}$$

where V is the velocity of satellite, and

$$T = 2\pi(a^3/\mu)^{1/2} \tag{3.10}$$

where T is the orbital period of the satellite.

Lagrange developed equations which predicted changes in orbital parameters (a, e, i, Ω, ω) due to external forces (in addition to the inverse square gravitational force). It is assumed that these external forces are small compared to gravity. The external force is considered to have the following three components. The radial force component is in the orbital plane along the radius vector and is denoted by f_r. The transverse component, which acts perpendicularly to r in the orbital plane, is denoted f_t (the transverse direction is found by rotating the radial vector 90 degrees counterclockwise in the orbital plane). The last component, f_n, represents the force normal to the orbital plane and is orthogonal to the first two components.

Again, the proof of the following derived equations will be left to the reader. Only the Lagrange equations pertinent to the use of the Gabbard diagrams are listed.

$$\frac{da}{dt} = \left[2a^2/(\mu p)^{1/2}\right]\left[f_r\, e\sin(f) + f_t\left[1 + e\cos(f)\right]\right]. \tag{3.11}$$

$$\frac{de}{dt} = \left[(p/\mu)^{1/2}\right]\left[f_r \sin(f) + f_t\left[\cos(f) + \cos(E)\right]\right]. \tag{3.12}$$

$$\frac{di}{dt} = \left[1/(\mu p)^{1/2}\right]\left[r\, f_n \cos(u)\right] \text{ where } u = \omega + f. \tag{3.13}$$

By assuming that the force is impulsive these equations may be modified to include the velocity imparted explicitly (37):

$$\Delta a = \frac{2}{n}\left[\Delta V_r \frac{e\sin(f)}{(1-e^2)^{1/2}} + \Delta V_t \frac{a}{r}(1-e^2)^{1/2}\right] \tag{3.14}$$

$$\Delta e = \frac{(1-e^2)^{1/2}}{na}\left[\Delta V_r \sin(f) + \Delta V_t \frac{a}{er}\left(1-e^2-\frac{r^2}{a^2}\right)\right] \tag{3.15}$$

$$\Delta i = \Delta V_n \left[\frac{r\cos(\omega+f)}{na^2(1-e^2)^{1/2}}\right] \tag{3.16}$$

These equations are often much more convenient to work with since delta velocities are implicit in the observables and are easier to calculate than forces. These equations are used later to solve for the delta velocities of debris fragments.

Gabbard Diagrams

The Gabbard diagram plots a satellite's apogee and perigee heights against its orbital period. For a satellite in a circular orbit the Gabbard diagram is a single point (Figure 3.10). A satellite in an elliptical orbit will have a Gabbard diagram with two points: the satellite's apogee and perigee heights aligned above its orbital period (Figure 3.11). Often "x" symbols are used to denote apogee and "+" symbols are used to denote perigee. Larger symbols are also sometimes used to denote the parent satellite's parameters at the time of the breakup. This is very helpful when examining a Gabbard diagram with many fragments.

When debris from a satellite breakup is plotted on a Gabbard diagram, the figure becomes more complex. In analyzing debris through the use of Gabbard diagrams, two distinct dispersion patterns are apparent and coincide with circular and elliptical parent satellite orbits. For a parent satellite with a circular or nearly circular orbit, the dispersion of the debris takes on the form of an X-shape. Figure 3.12 shows the Gabbard diagram for the breakup of satellite 1973-86B which had an apogee height of 1,512 km and a perigee height of 1,505 km.

The fragments depicted by the two arms which trail

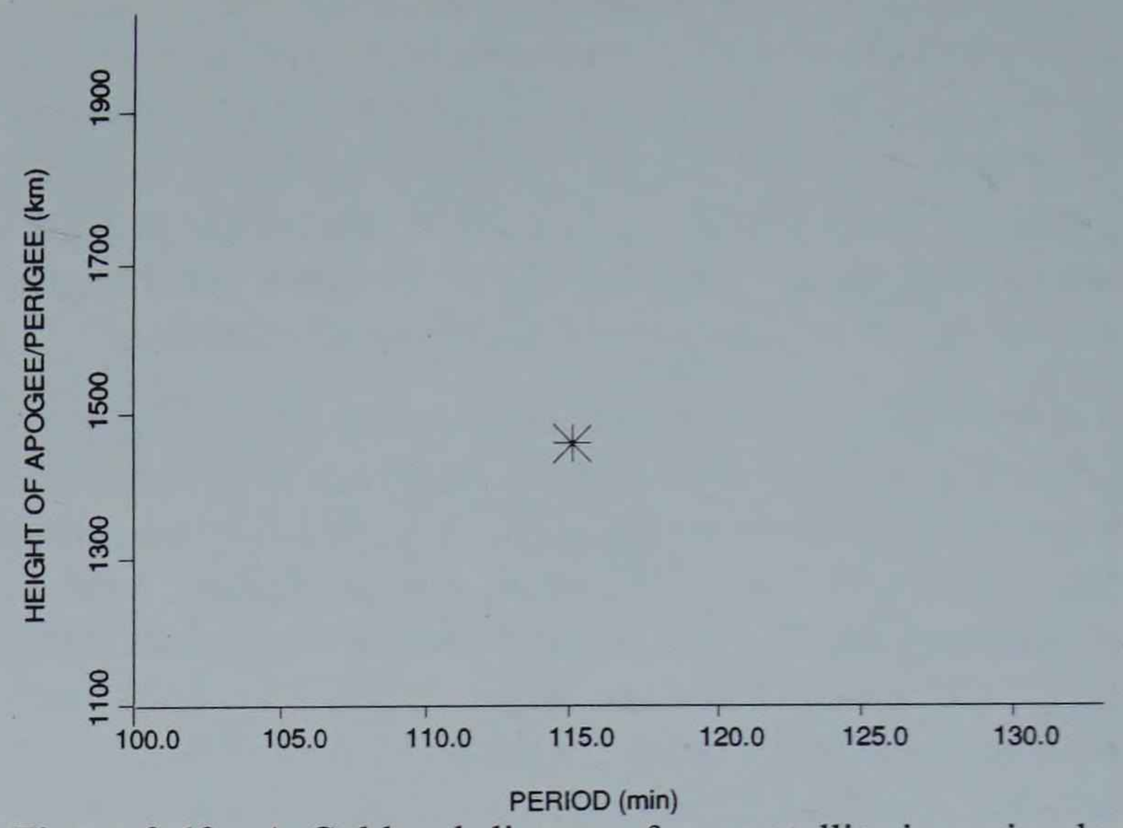


Figure 3.10 A Gabbard diagram for a satellite in a circular orbit at an altitude of nearly 1,500 km is depicted by a single point.

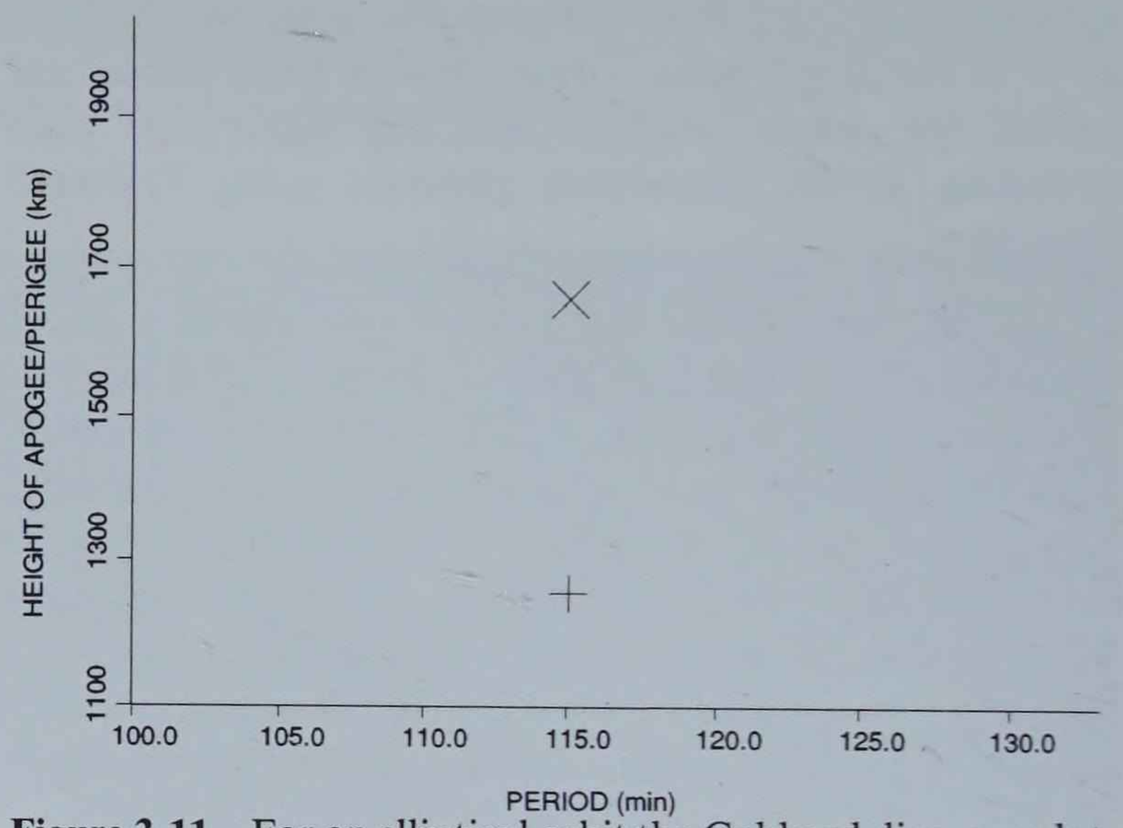


Figure 3.11 For an elliptical orbit the Gabbard diagram plots the apogee (×) and the perigee (+) against the orbital period.

to the left of the parent satellite's orbit received a net retrograde impulse from the breakup. Similarly, the debris which form the arms to the right of the parent satellite received a net posigrade impulse. The influence of these forces can be likened to one of the two impulses of a Hohmann transfer. The fragments which received a net retrograde force have the same apogee but varying perigees depending on the magnitude of the net retrograde force. It should be noted that the retrograde pieces have apogee altitudes similar to the perigees of the posigrade pieces. This observation solidifies the analogy with the impulse maneuvers: an impulse at perigee (apogee) does not affect perigee (apogee) height but only changes the apogee (perigee) height. For a circular orbit, the apogee and perigee are defined once the impulse occurs.

The dispersion of debris from the breakup of a satellite with an elliptical orbit may be analyzed using the same

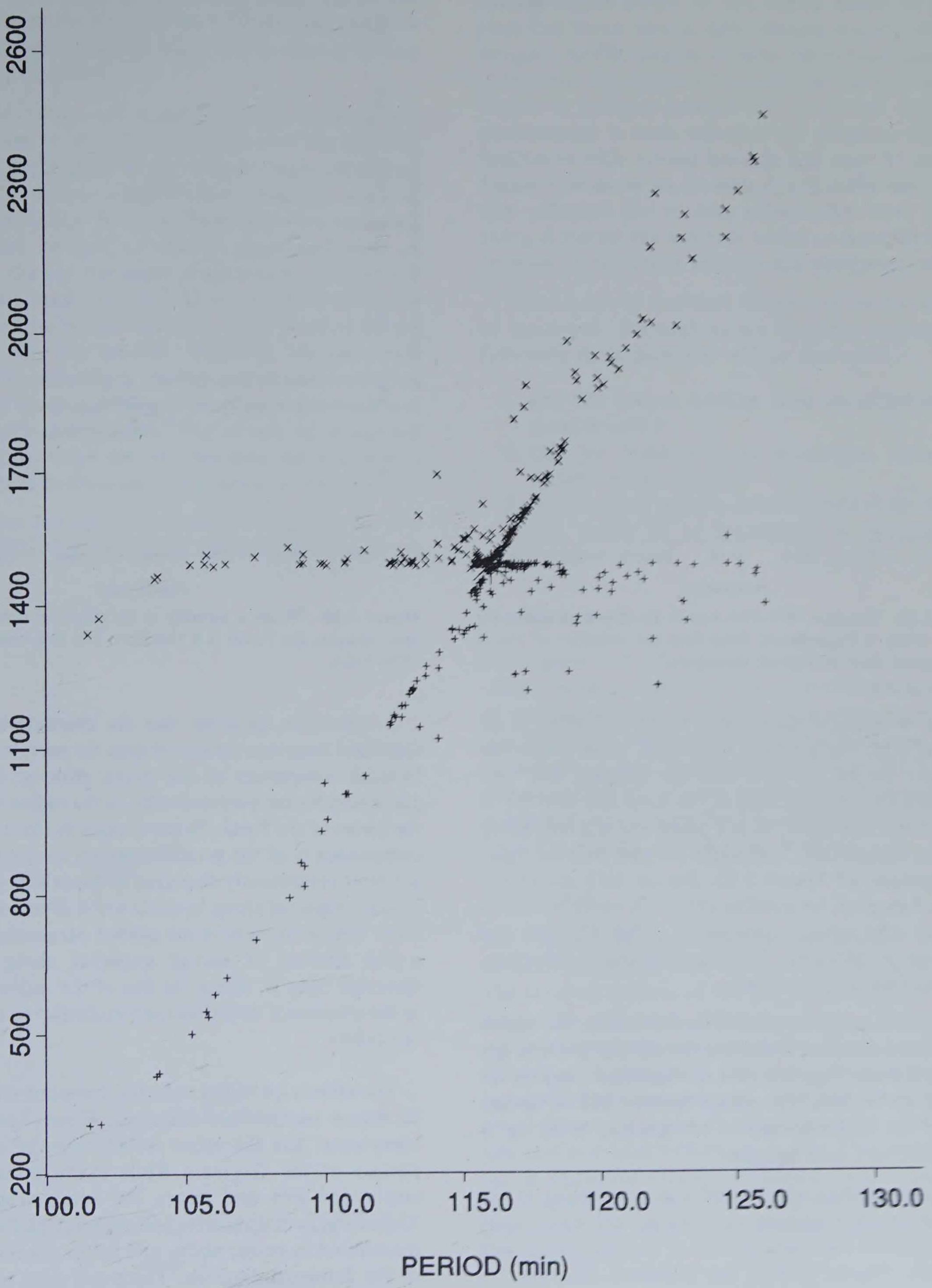


Figure 3.12 When a satellite in a nearly circular orbit fragments, the resultant debris is distributed in a characteristic X-pattern as shown here for the debris from satellite 1973-86B.

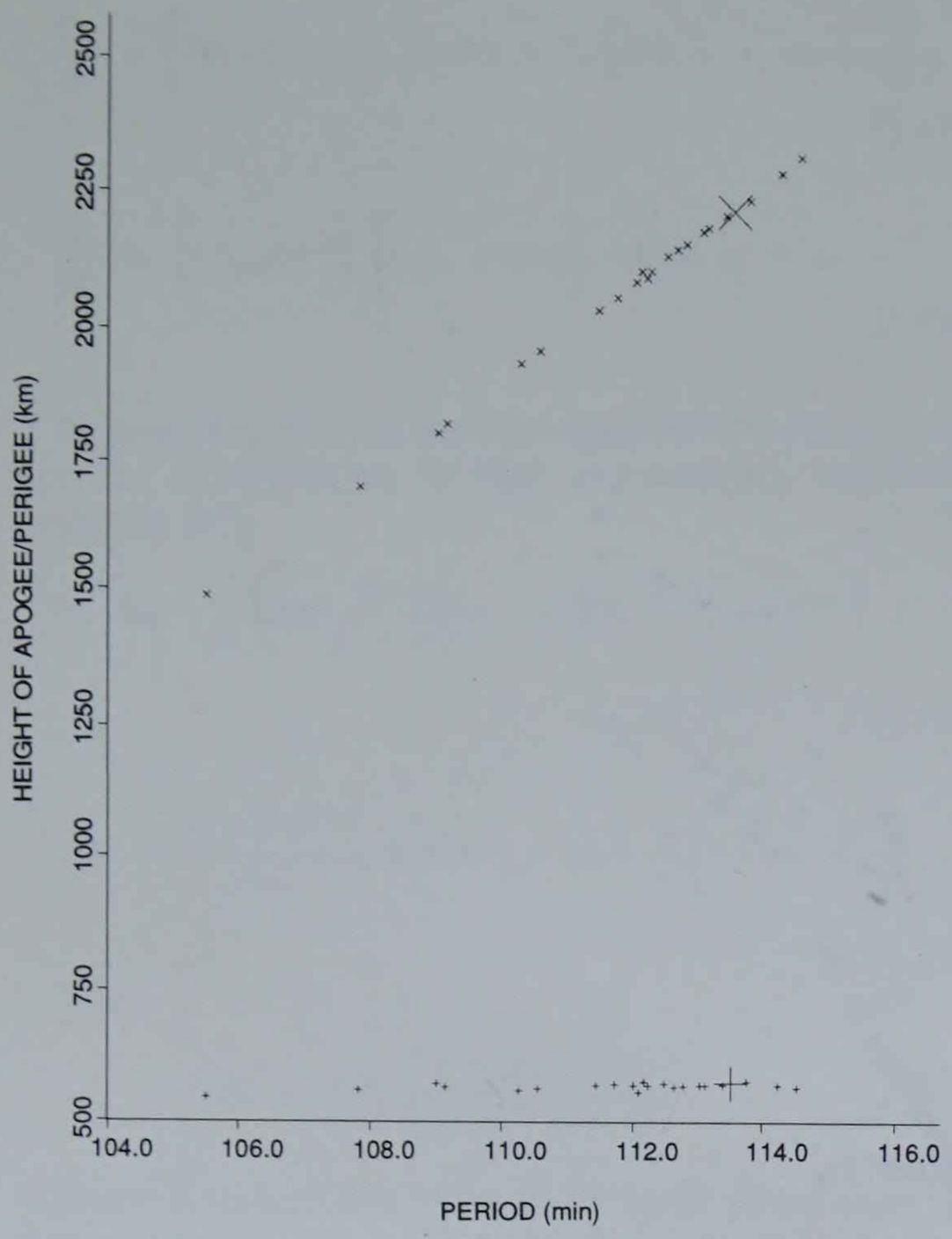


Figure 3.13 Satellite 1971-15A was in an elliptical orbit near perigee when it fragmented. Note that the majority of pieces were ejected in a retrograde direction.

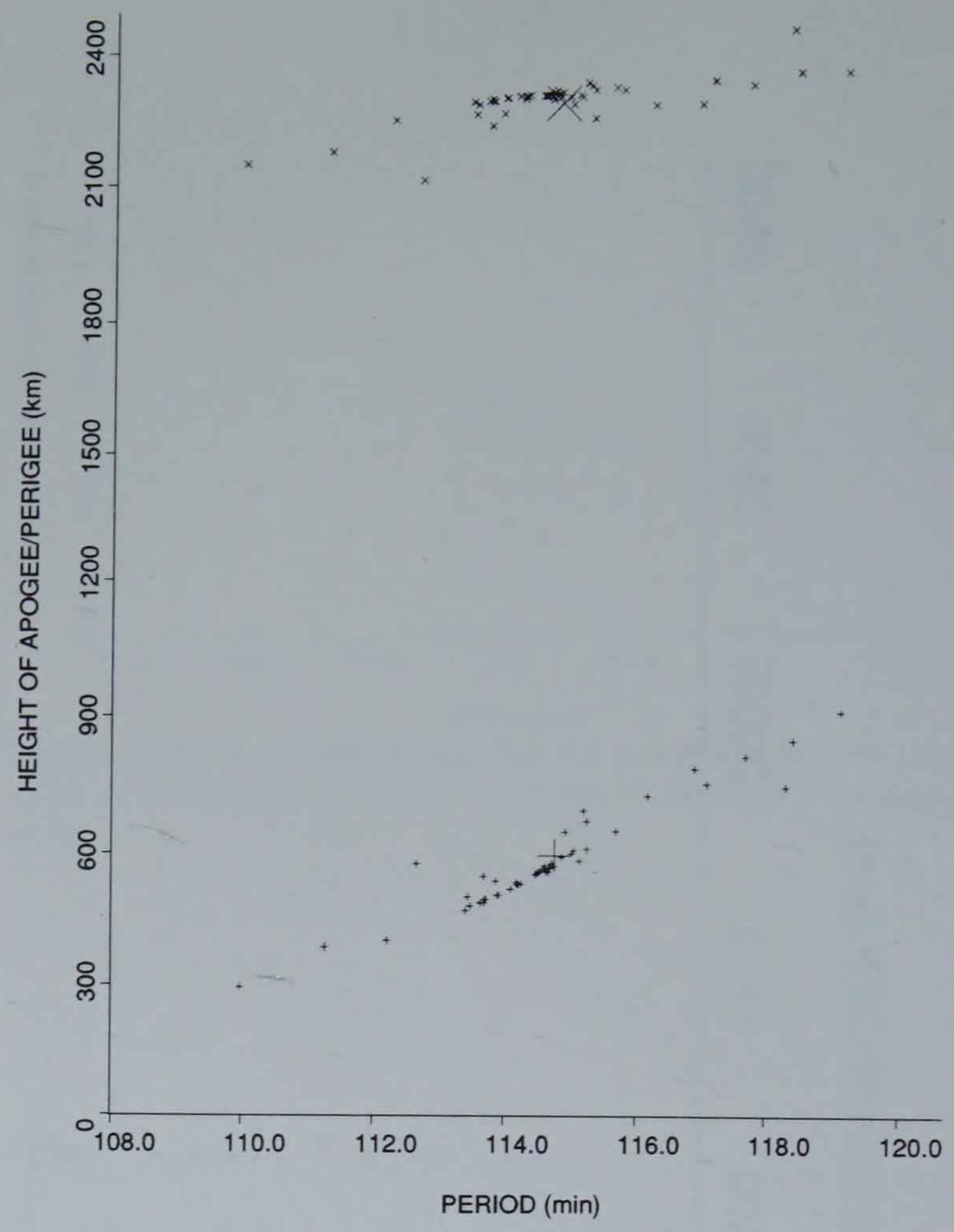


Figure 3.14 When a satellite in an elliptical orbit fragments near apogee, the result is a Gabbard like this one for satellite 1976-126A.

analogy to impulse maneuvers. When a satellite in an elliptical orbit fragments at its perigee, most fragments will have similar perigees and the apogees will vary depending on the magnitude of the force and whether or not the force was imparted in a posigrade or a retrograde direction. Graphically, one might imagine only the right-hand portion of Figure 3.12. Figure 3.13 shows the Gabbard diagram for satellite 1971-15A which was in an elliptical orbit (apogee/perigee = 2,200/575 km) and broke up at 587 km. This fragmentation, therefore, occurred very near perigee.

Breakup at apogee produces similar results: the higher arm keeps a constant altitude while the perigee arm has a positive slope. Figure 3.14 is the Gabbard diagram for breakup 1976-126A. The parent satellite had an apogee of 2,297 km and a perigee of 595 km and broke up at 2,088 km, very near apogee.

A fragmentation which occurs at some point in the orbit other than apogee or perigee will have some combination of the characteristics of the two families just discussed. Figure 3.15 is the Gabbard diagram for breakup 1977-65B which had an apogee and perigee of 2,027 km and 536 km, respectively. The satellite fragmented at an altitude of 1,450 km which corresponds to a true anomaly of 108 degrees.

It should be apparent that the characteristics of the Gabbard diagrams described thus far pertain only to the in-track component of the ejecta velocity, i.e., the in-plane component perpendicular to the radius vector from the center of the Earth. In many cases the in-track velocity component is of the greatest interest because its effects are most prominently displayed in the orbital parameters. Energy imparted along in the in-track direction will cause more visible changes in the orbital parameters than will a like amount of energy imparted along the radial direction (that is, along the line of the radius vector) or in the crosstrack direction (perpendicular to the plane of the orbit).

The effects of radial velocity components, however, do appear on Gabbard diagrams. A pure radial velocity component has the effect of altering the apogee and perigee of the fragment while maintaining the same semimajor axis and hence the same orbital period. Therefore, radial velocity components of the ejecta are manifested as points above and below the nominal arms of the Gabbard diagram. These are most pronounced, as would be expected, in the region of the parent satellite's pre-breakup orbital period. Because they appear to surround the parent satellite, they are sometimes referred to as halo debris. A second look at Figure 3.12 will reveal

halo fragments between the upper arms and between the lower arms. Again it should be remembered that for a symmetrical satellite breakup the halo debris will be less pronounced than the length of the Gabbard arms because the same amount of energy will produce a lesser change in the radial direction.

A velocity component in the crosstrack direction will cause a change in the orbital inclination of the satellite. Even when performed at the orbital nodes—the most efficient locations—inclination changes require considerable energy. When performed at even moderate latitudes, the amount of energy associated with an inclination change increases dramatically. Crosstrack velocity components of even 100 m/s or more can result in very small inclination changes, often masked by the inaccuracy of the normal NORAD element sets. Consequently, crosstrack velocity components are often estimated by the magnitudes of the observed in-track and radial velocity components. The effects of crosstrack velocity components are not depicted on a Gabbard diagram which concentrates on in-plane orbital changes.

A common occurrence in Gabbard diagrams for low altitude satellite breakups is the collapse with time of the left (lower period) arms. This collapse actually represents the normal orbital decay of debris which causes a circularization effect of the debris orbits (a greater retarding force occurs near perigee thereby lowering apogee). As the apogees of these debris fragments begin to decrease, the upper left arm of the Gabbard diagram begins to collapse toward the lower left arm. This phenomenon is most apparent for breakups that have fragments with orbital periods less than 95 minutes. Figure 3.16 shows an example of a breakup with the left arm collapsed due to drag effects after more than 23 years. A dotted line has been added to show the original position of the upper arm for the retrograde debris.

Three example Gabbard diagram problems will now be presented. For each of the Gabbard diagrams, the following three questions will be answered:

1. Did the parent satellite have an elliptical or a circular orbit?
2. Did the breakup occur at perigee, apogee, or somewhere in between?
3. Are there any notable characteristics of the diagram that might be of importance in analyzing the breakup event?

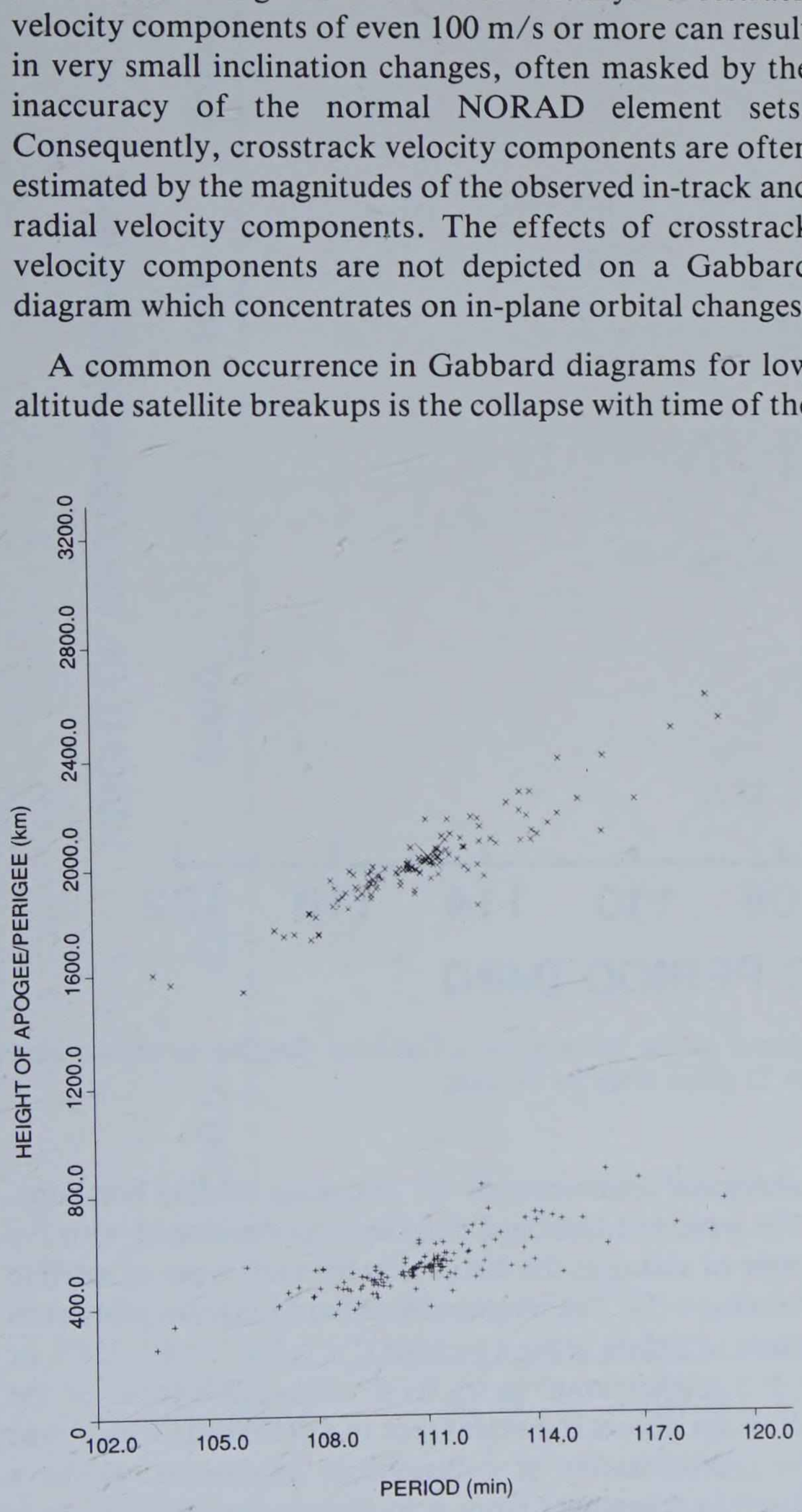


Figure 3.15 In the general case of a satellite in an elliptical orbit, the slope of the debris arms is a function of the value of the true anomaly at the time of the fragmentation. The above Gabbard diagram is for satellite 1977-65B which broke up at a true anomaly of 108 degrees.

Example 1

See Figure 3.17. The parent satellite was in a nearly circular orbit (e = 0.01) of 912 km by 742 km at the time of the fragmentation event. Consequently, there is little significance to whether the event occurred near apogee or perigee. Actual breakup altitude was 750 km. The collapse of the left arm has commenced. Noticeable halo debris is present, suggesting a moderately energetic event. This was a Delta second stage breakup.

Example 2

See Figure 3.18. Again, the parent satellite was in a virtually circular orbit of 444 km by 424 km (e = 0.001). The breakup altitude of 437 km is impossible to discern from the Gabbard diagram alone. There is an unmistakable posigrade asymmetry. No fragments were ejected in a retrograde direction. There are also no noticeable radial components. Although not reflected in the Gabbard diagram, all debris from this event had a decrease in orbital inclination as well. Consequently, all debris fragments were ejected forward and to the left of the velocity vector. This marked asymmetry is characteristic of the Kosmos 699-class breakups, of which this was the first.

Example 3

See Figure 3.19. This time the parent satellite was in an obvious elliptical orbit at the time of the breakup. Apogee

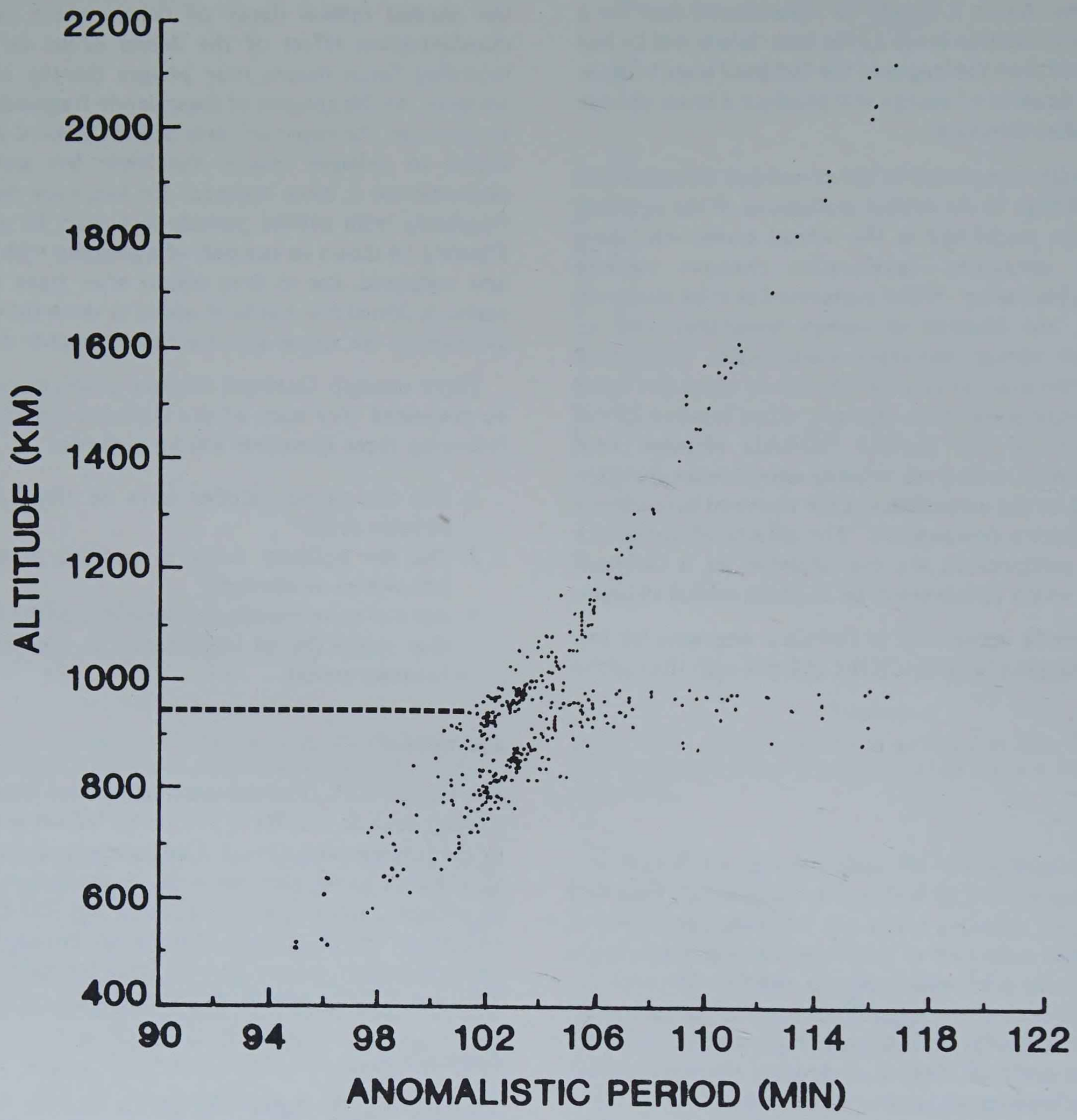


Figure 3.16 The near-term effects of orbital decay result in the collapse of the left arm on a Gabbard diagram as shown here for satellite 1961-Omicron more than 23 years after its breakup.

was 873 km and perigee was 580 km (e = 0.02). Equally obvious by the slope of both arms is the conclusion that the breakup did not occur near apogee or perigee. Actual breakup altitude was 666 km (true anomaly of 293 degrees). The event was again highly asymmetrical; that is, all debris was ejected in a retrograde direction. This was the second breakup of Kosmos 1220, a member of the Kosmos 699 class.

Weighted Gabbard Diagrams

The Gabbard diagram is a powerful tool for debris analysis, but a slight modification to it produces additional opportuntities for analyzing satellite breakups. The weighted Gabbard diagram was developed with the hope of aiding in the distinction between types of satellite breakups (1). The weighted Gabbard diagram plots each piece of debris using a symbol ("1", "2", "3", "4", or "5") proportional to its RCS value. This form of the diagram allows the researcher to note trends which may be representative of collisions or explosions. When a satellite fragments from a hypervelocity collision, it is postulated that the larger pieces of debris are an indirect result of the collision and the smaller pieces are a direct result of the collision. These observations allowed the development of four hypotheses which are used to judge

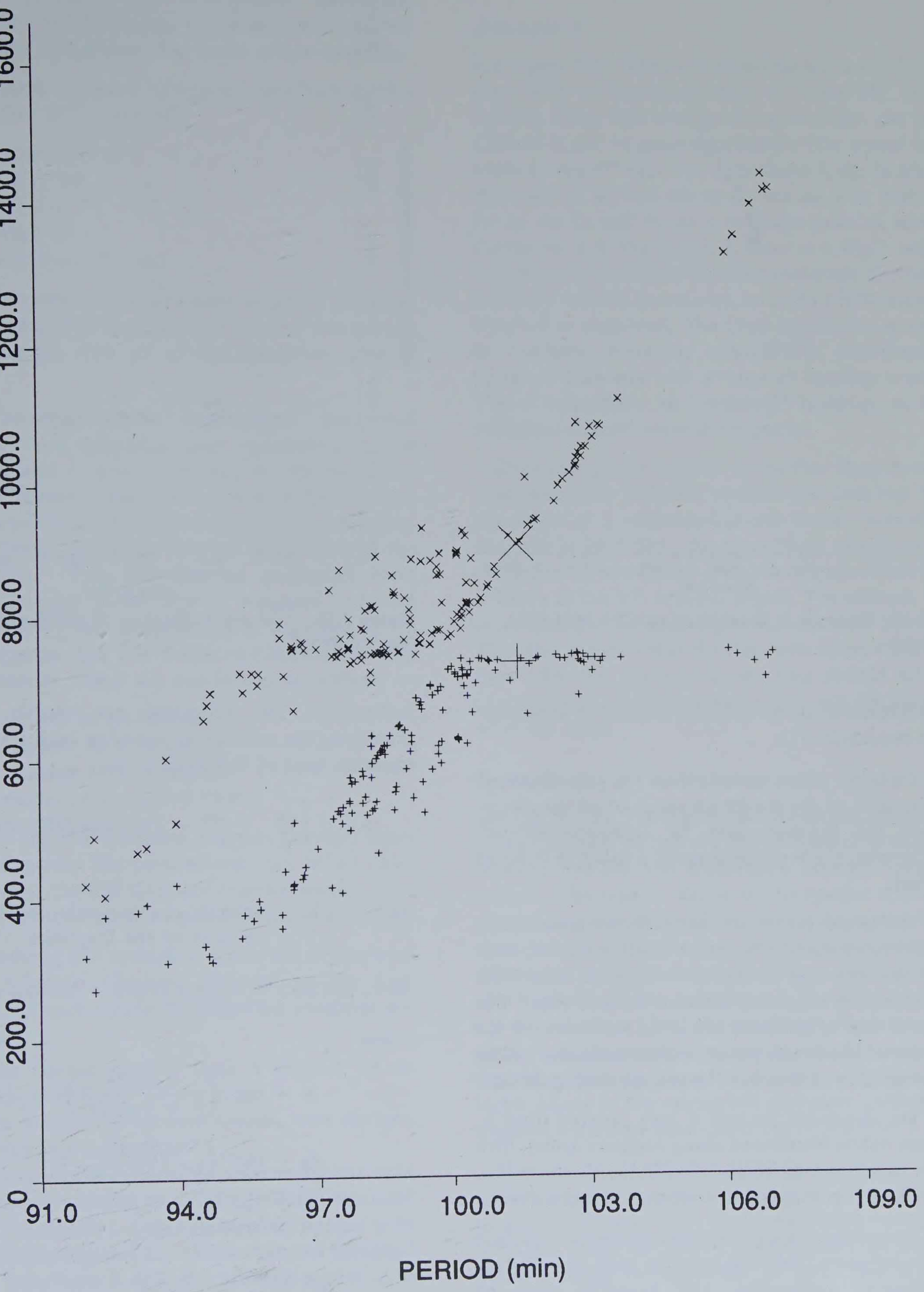


Figure 3.17 Example 1: Breakup of satellite 1975-04B (second event).

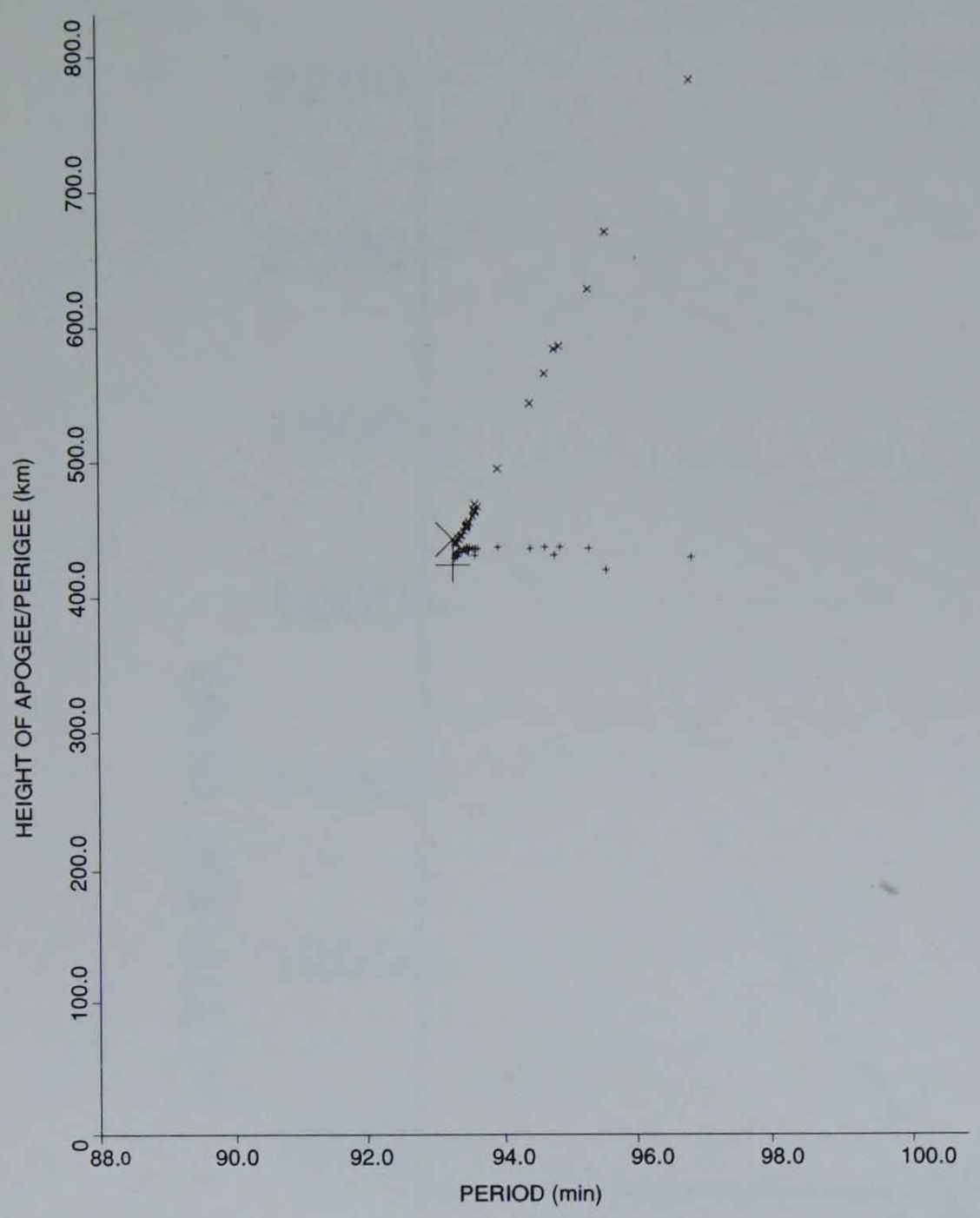


Figure 3.18 Example 2: Breakup of satellite 1974-103A (first event).

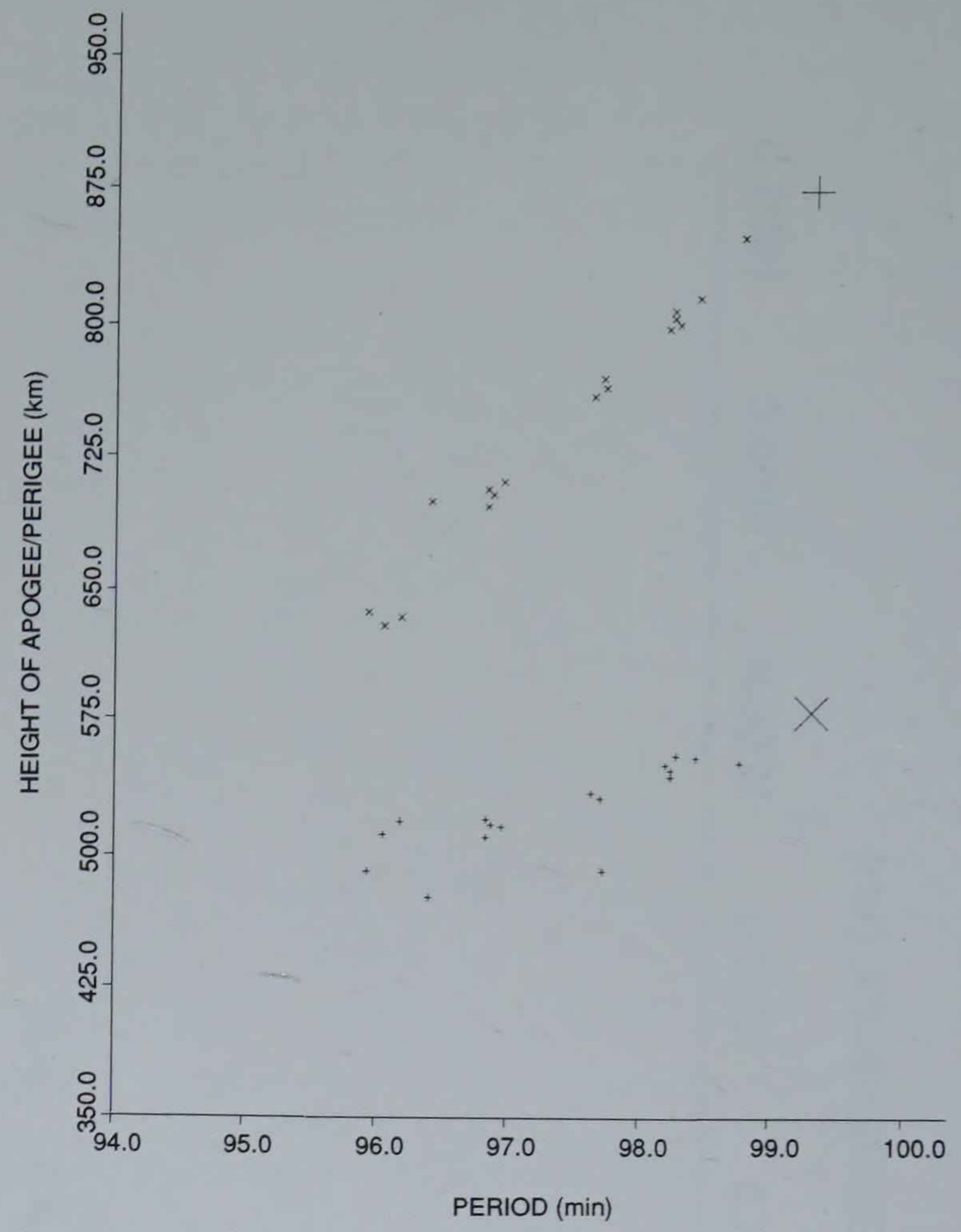


Figure 3.19 Example 3: Breakup of satellite 1980-89A (second event).

whether a breakup shows collision-induced or explosion-induced tendencies (1):

1. If the larger pieces (greater than 1 m^2) are dispersed over 50% of the maximum range of all the pieces, then the breakup may be explosion-induced; otherwise, the breakup suggests a collision-induced event.
2. If the larger pieces are distinctly asymmetrically distributed about the parent satellite's orbit, then the breakup may be explosion-induced; otherwise, the breakup suggests a collision-induced event. The ejecta that might have imparted velocities on the order of kilometers per second for collisions will be too small to be measured by present sensing devices.
3. If the dispersion pattern is very ordered (that is, most debris distributed along compact arms), then the breakup may be collision-induced; otherwise, the breakup suggests a explosion-induced event.
4. If the average velocity imparted decreases as particle size increases, then the breakup may be collision-induced; otherwise, the breakup may be explosion-induced.

This last hypothesis is very similar to the first, except that the last hypothesis includes the dispersion into new inclinations. This hypothesis can roughly be seen by examining the velocity imparted to each fragment. The equation used in reference 1 is

$$\Delta V = \left[V_o^2 + V^2 - 2VV_o \cos(DP) \cos(di)\right]^{1/2} \tag{3.17}$$

where V_o = velocity of the parent satellite
V = velocity of the fragment

Also, $\cos(DP) = \sin(\phi_o) \sin(\phi) + \cos(\phi_o) \cos(\phi)$

where

$$\phi = \tan^{-1}\left(\frac{e \sin(f)}{1 + e \cos(f)}\right)$$

$$\phi_o = \tan^{-1}\left(\frac{e_o \sin(f)}{1 + e_o \cos(f)}\right)$$

$di = |i_o - i|$
f = true anomaly.

Most of the weighted Gabbard diagram hypotheses are null hypotheses (i.e., rejection of the hypothesis only rules out the acceptance of one alternative but does not necessarily prove the other). Yet, the series of hypotheses

cascade in such a way as to make a suggestive, although subjective, observation. The subjectiveness makes it difficult to establish any statistically significant conclusions (as will be shown in the next section), but it does provide insight into the cause of the breakup.

The weighted Gabbard diagrams described in this section use five RCS intervals:

1 = less than 0.01 m^2
2 = 0.01-0.10 m^2
3 = 0.10-1.0 m^2
4 = 1.0-10.0 m^2
5 = greater than 10.0 m^2

Six diagrams actually comprise each weighted Gabbard diagram analysis: five diagrams for the five size groups and one diagram with all of the characters plotted together.

It should be noted that the "larger pieces" mentioned earlier in the four hypotheses are represented by the characters 4 and 5. Unfortunately, at this point the following deficiency arises: some breakups have few or no pieces larger than 1 m^2. For this reason the debris in the 3 group may sometimes have to be considered the "larger pieces." This inconsistency prompted John Gabbard to suggest a new type of weighted Gabbard diagram; namely, the proportionally weighted (PW) Gabbard diagram. The PW Gabbard diagram has only four size intervals which are distributed as follows:

5 = largest 5% of the debris
4 = next largest 10% of debris
3 = next largest 35% of debris
2 = remainder of the debris (50%)

The use of the PW Gabbard diagram provides more consistent diagrams for comparison, but in all cases analyzed to date, the PW Gabbard diagram produces the same results as the original weighted Gabbard diagrams.

In the following two examples, debris will be analyzed using the weighted Gabbard diagram in the four hypotheses. For each sample the following questions will be addressed:

1. Did the parent satellite have a circular or an elliptical orbit?
2. Did the breakup occur near apogee, near perigee, or somewhere in between?
3. Using hypothesis 1, does this breakup appear to be an explosion-induced or collision-induced breakup?
4. Using hypothesis 2, does this breakup appear to be an explosion-induced or collision-induced breakup?
5. Using hypothesis 3, does this breakup appear to be an explosion-induced or collision-induced breakup?
6. By looking at the answers for the last three questions, was the breakup probably explosion-induced or collision-induced?
7. Are there any characteristics of the diagram that might be of interest?

Example 1

See Figure 3.20. The parent satellite had a nearly circular orbit with an apogee/perigee of 1,014/961 km (e = 0.0036). Since this orbit is almost circular, the breakup altitude is not of great significance (the actual breakup altitude was 977 km). For hypothesis 1, the 5s are hardly dispersed at all and the 4s do not go over half way as far as the 2s and 3s, so a collision-induced breakup is suggested. For hypothesis 2, there is a slight indication that more 4s were thrown in the posigrade direction, but it is not a marked asymmetry, so again a collision-induced breakup is suggested. The third hypothesis is awkward to evaluate, requiring considerable experience with Gabbard diagrams over a range of breakup conditions. This is marginally an "ordered" breakup, so again a collision-induced event is suggested.

Even though the answers to the first three hypotheses were less than definite, overall this breakup has the earmarks of a collision-induced event. Actually, this example is 1981-53A, the most likely candidate for an accidental hypervelocity collision in space. Note that the collapse of the left arm has begun. The collapse is more pronounced in the smaller particles as would be expected. This also suggests that the data was taken a substantial time after the breakup event. One should always be cautious when analyzing data which was not taken soon after the event.

Example 2

See Figure 3.21. The parent satellite had an elliptical orbit with an apogee/perigee of 2,027/536 km (e = 0.097). The breakup altitude was somewhere between apogee and perigee. The relative slopes of the apogee arm and the perigee arm can be used to narrow down the breakup altitude regime. In this case, the breakup occurred at an altitude of 1,450 km (true anomaly = 108 degrees). See also Figure 3.15. For hypothesis 1, the most energetic 4s are dispersed over half the maximum dispersion of any piece from the breakup, suggesting the breakup may be explosion-induced. There is also a clear asymmetry of the larger pieces in the retrograde direction, calling for an explosion-induced assessment for hypothesis 2.

Hypothesis 3 will be difficult to judge, but the unevenness and thickness of the arms show a high level of disorderedness. Thus the breakup may be explosion-induced. From the above observations, an explosion-induced cause is suggested. In fact, this is satellite 1977-65B, a Delta second stage breakup. Very few small pieces are shown, due in part because this breakup occurred at a high altitude and the resolution of the tracking system is degraded.

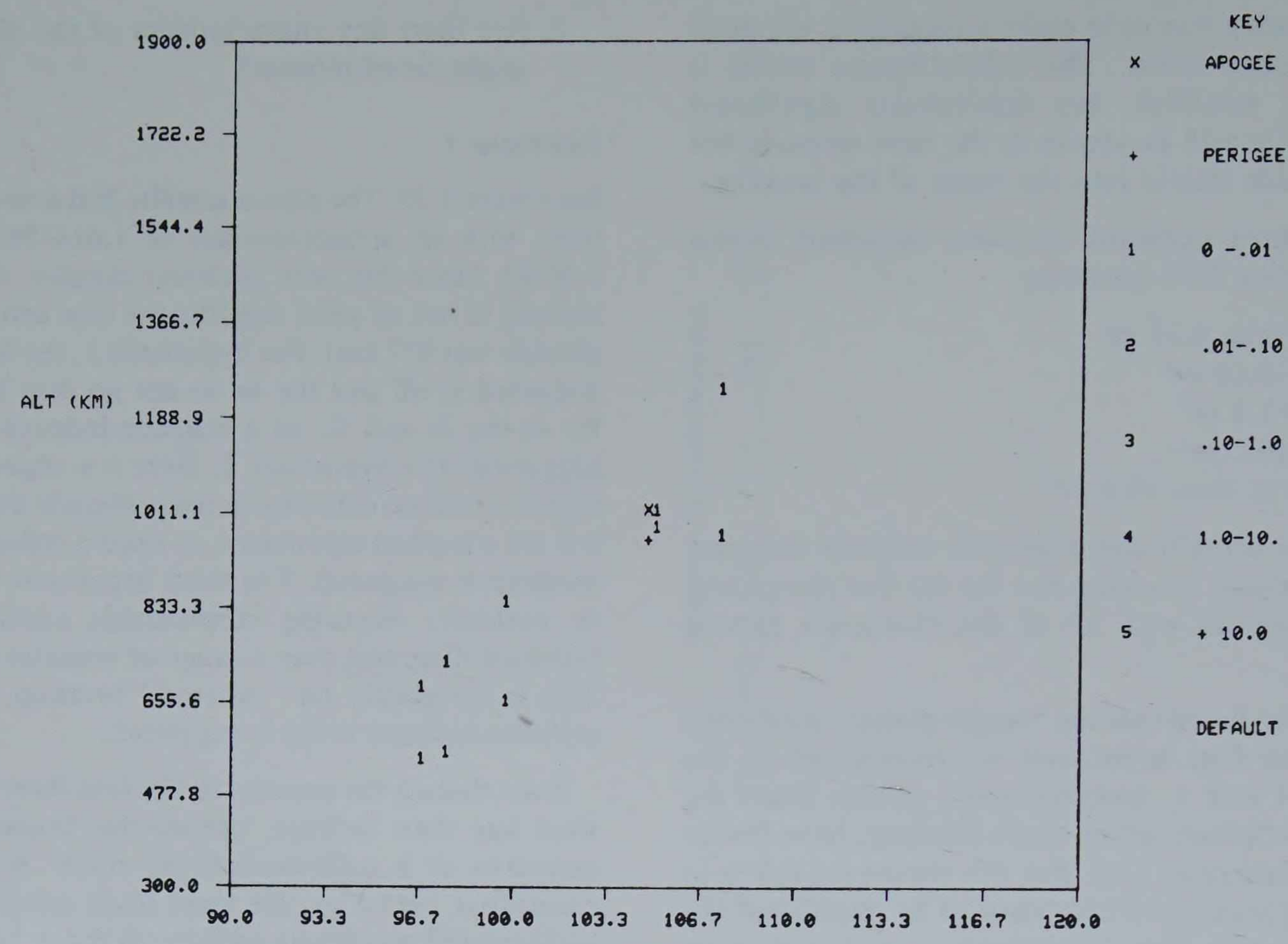


Figure 3.20A Example 1: Weighted Gabbard diagram for 1981-53A (December 1984) — size range 0.0 – 0.01 m².

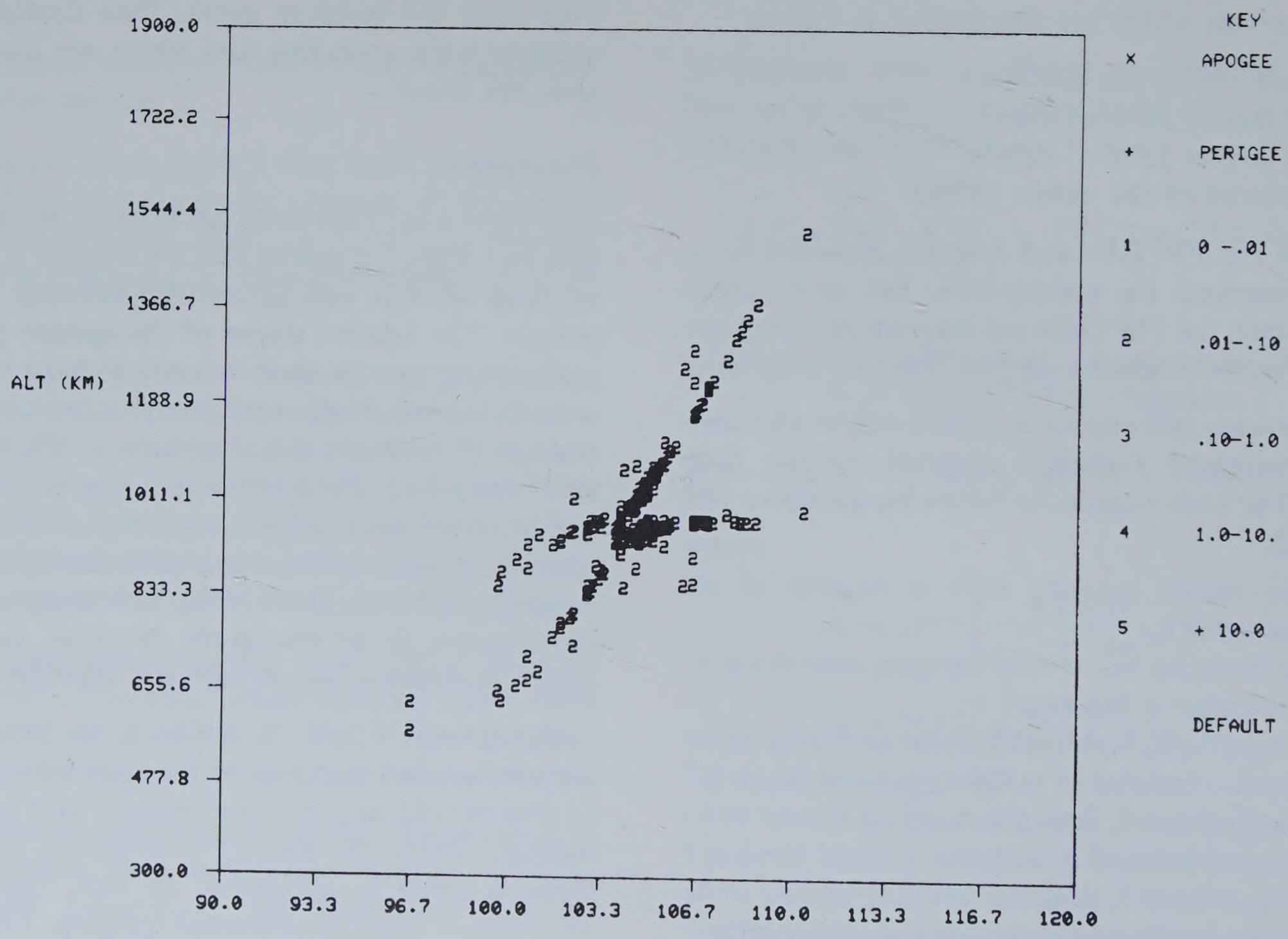


Figure 3.20B Example 1 (Continued): Weighted Gabbard diagram for 1981-53A — size range 0.01 – 0.10 m².

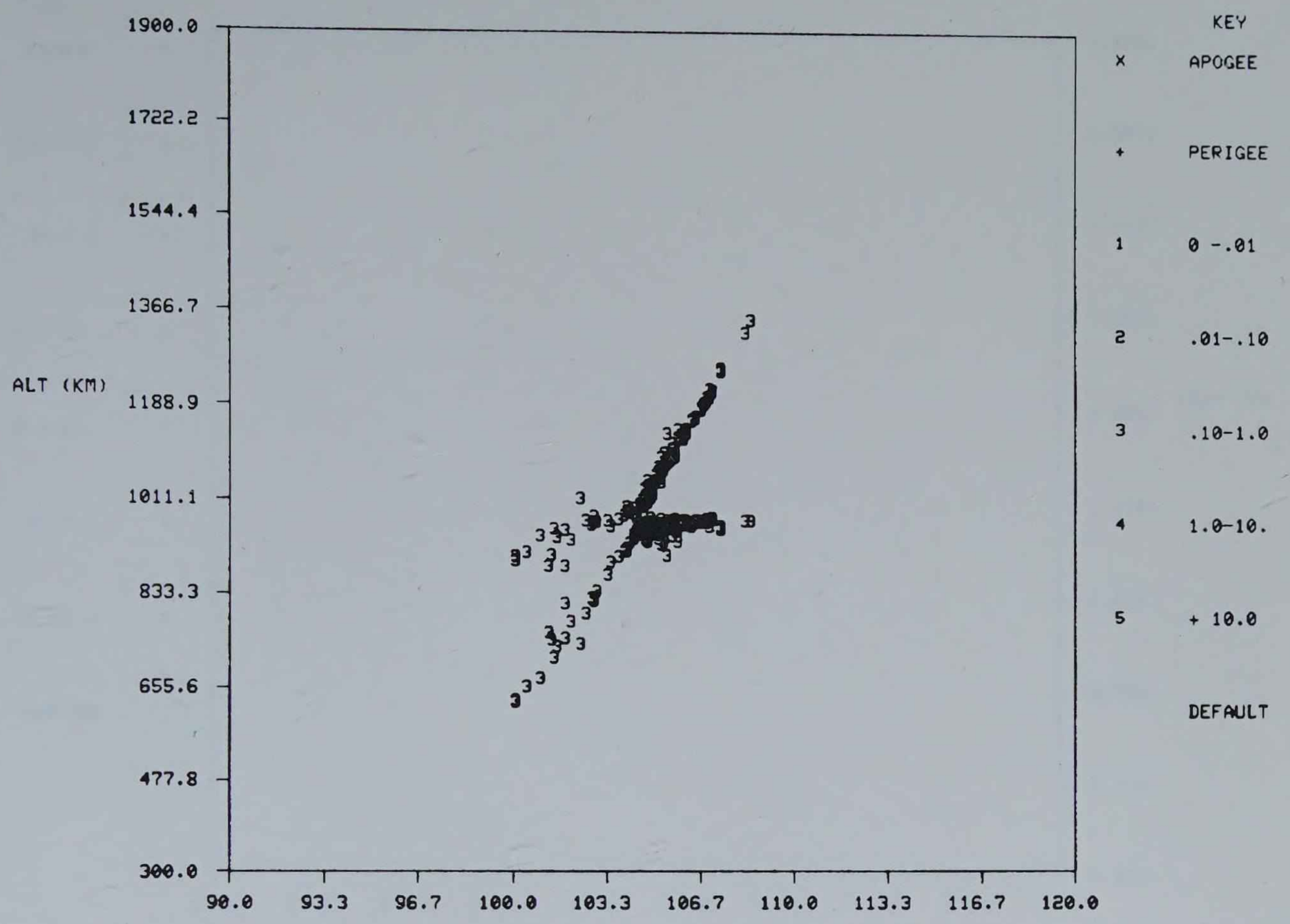


Figure 3.20C Example 1 (Continued): Weighted Gabbard diagram for 1981-53A — size range 0.10 – 1.0 m².

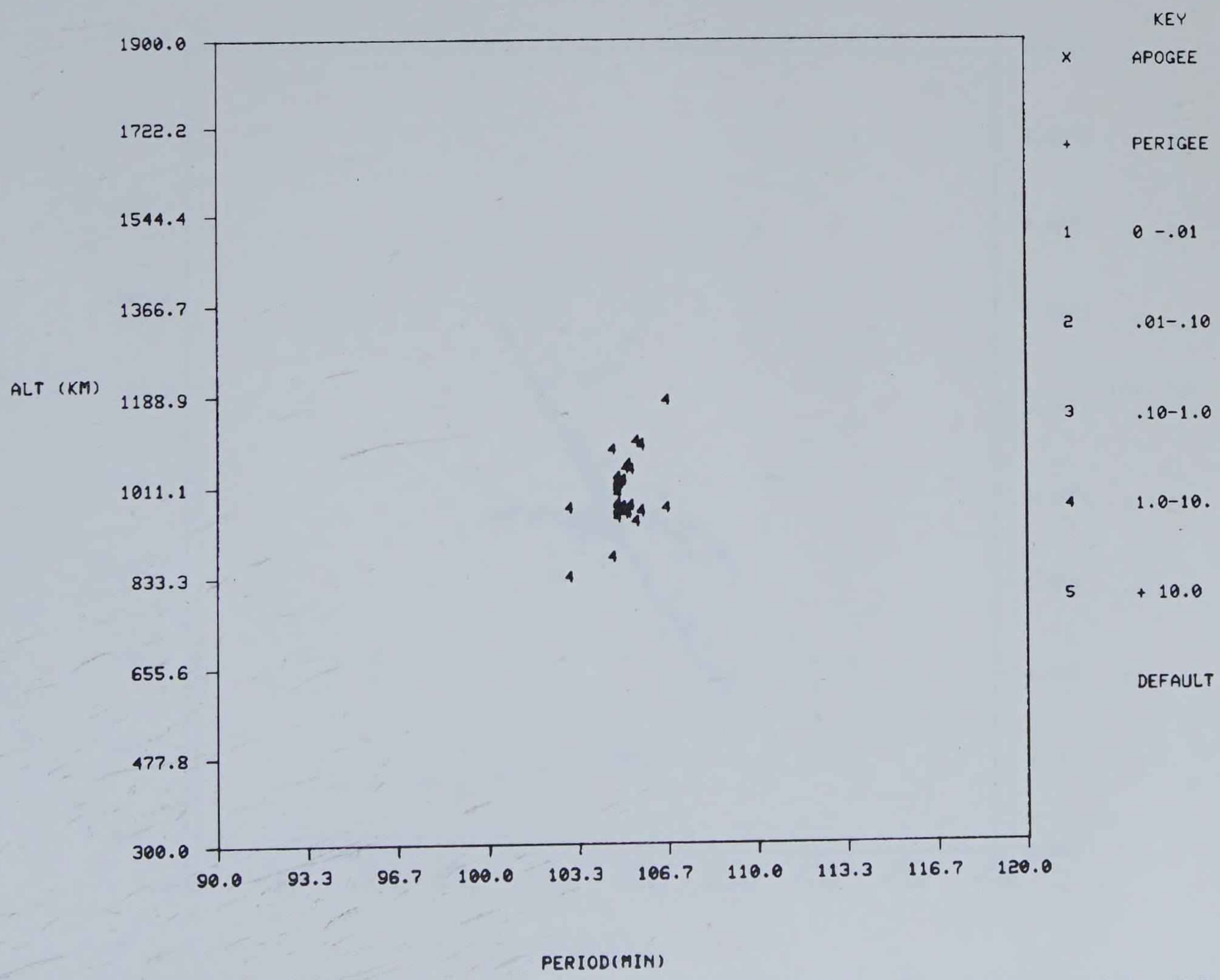


Figure 3.20D Example 1 (Continued): Weighted Gabbard diagram for 1981-53A — size range 1.0 – 10.0 m².

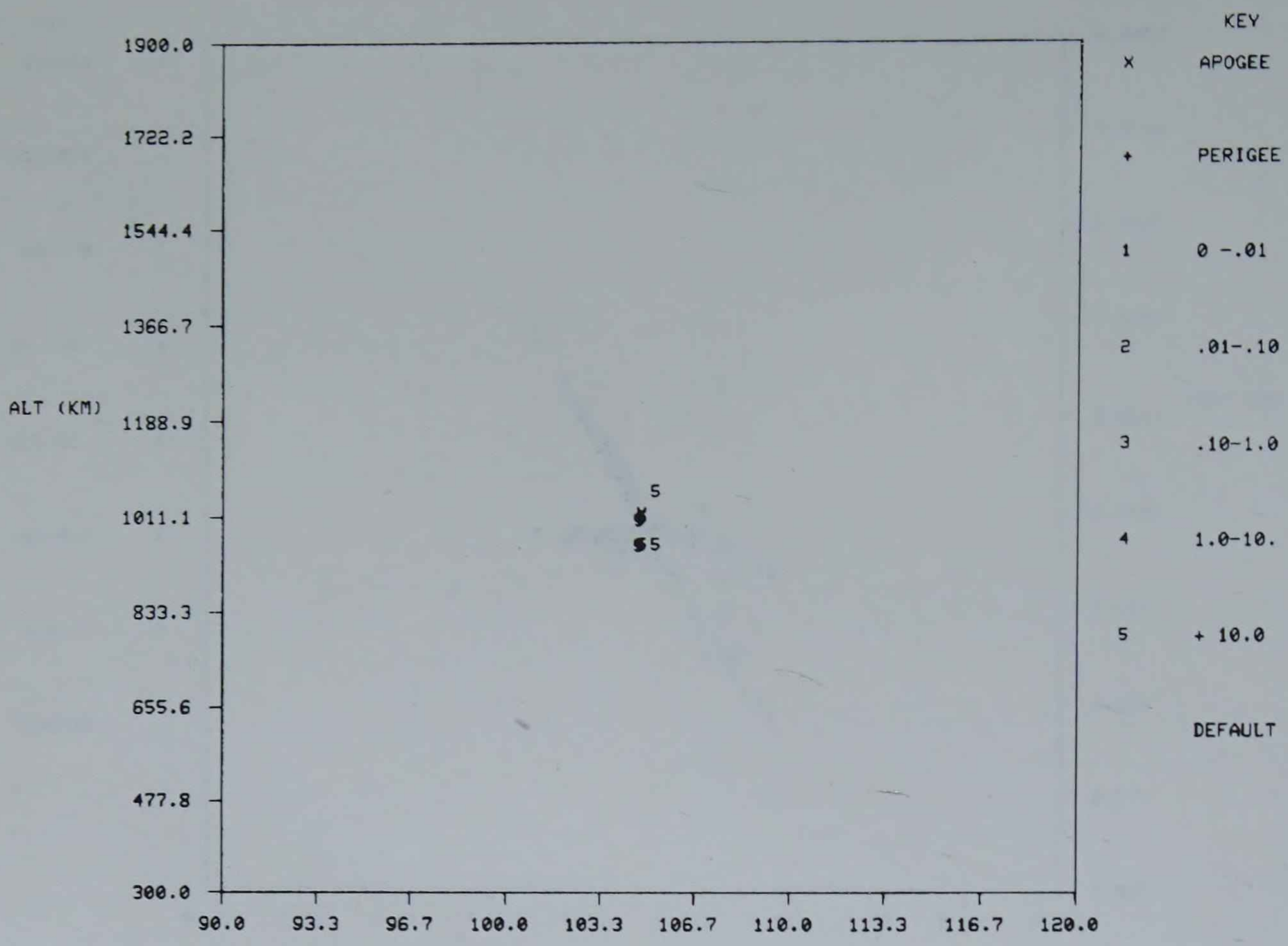


Figure 3.20E Example 1 (Continued): Weighted Gabbard diagram for 1981-53A — size range 10 m² and greater.

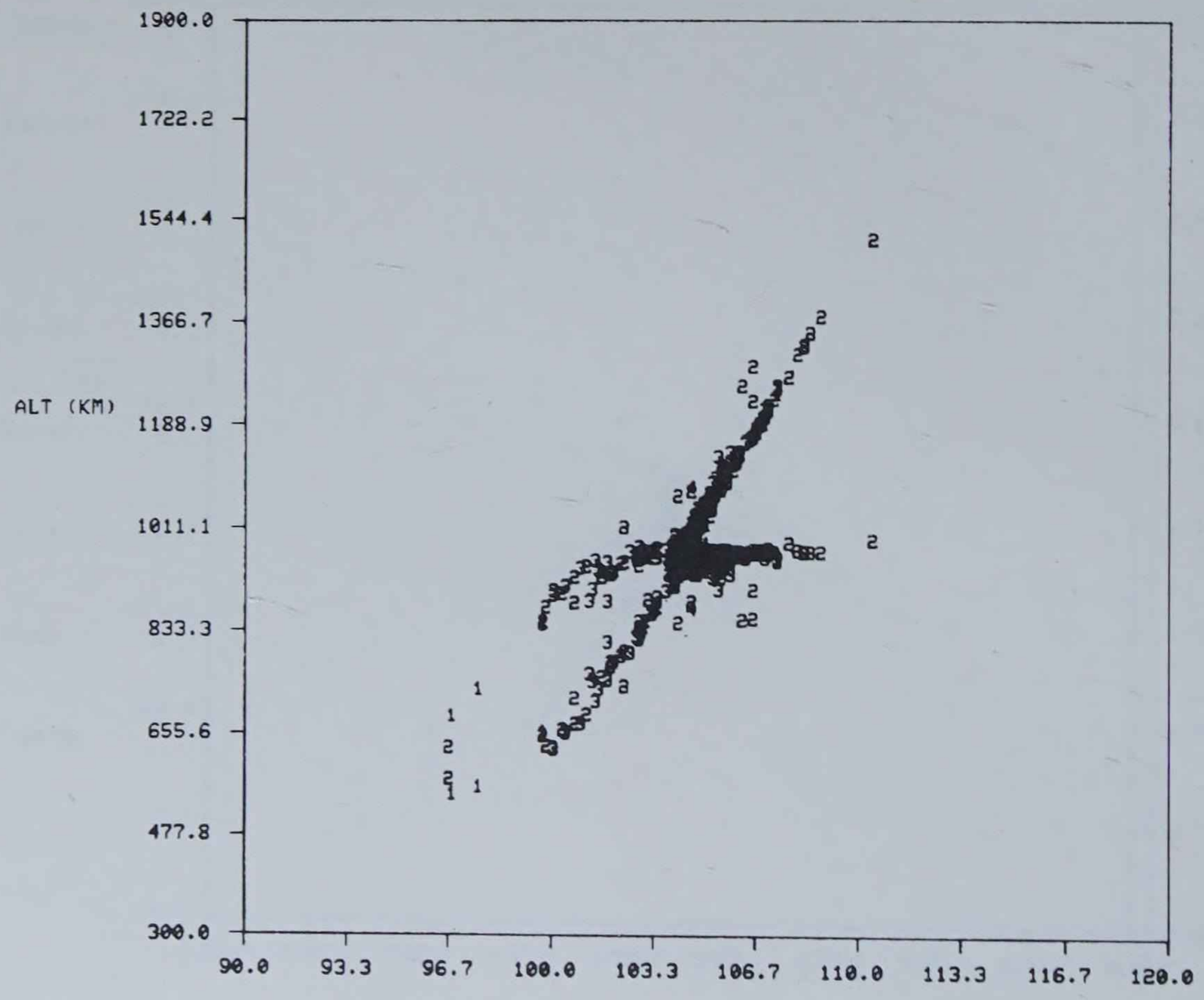


Figure 3.20F Example 1 (Continued): Weighted Gabbard diagram for 1981-53A — all size ranges.

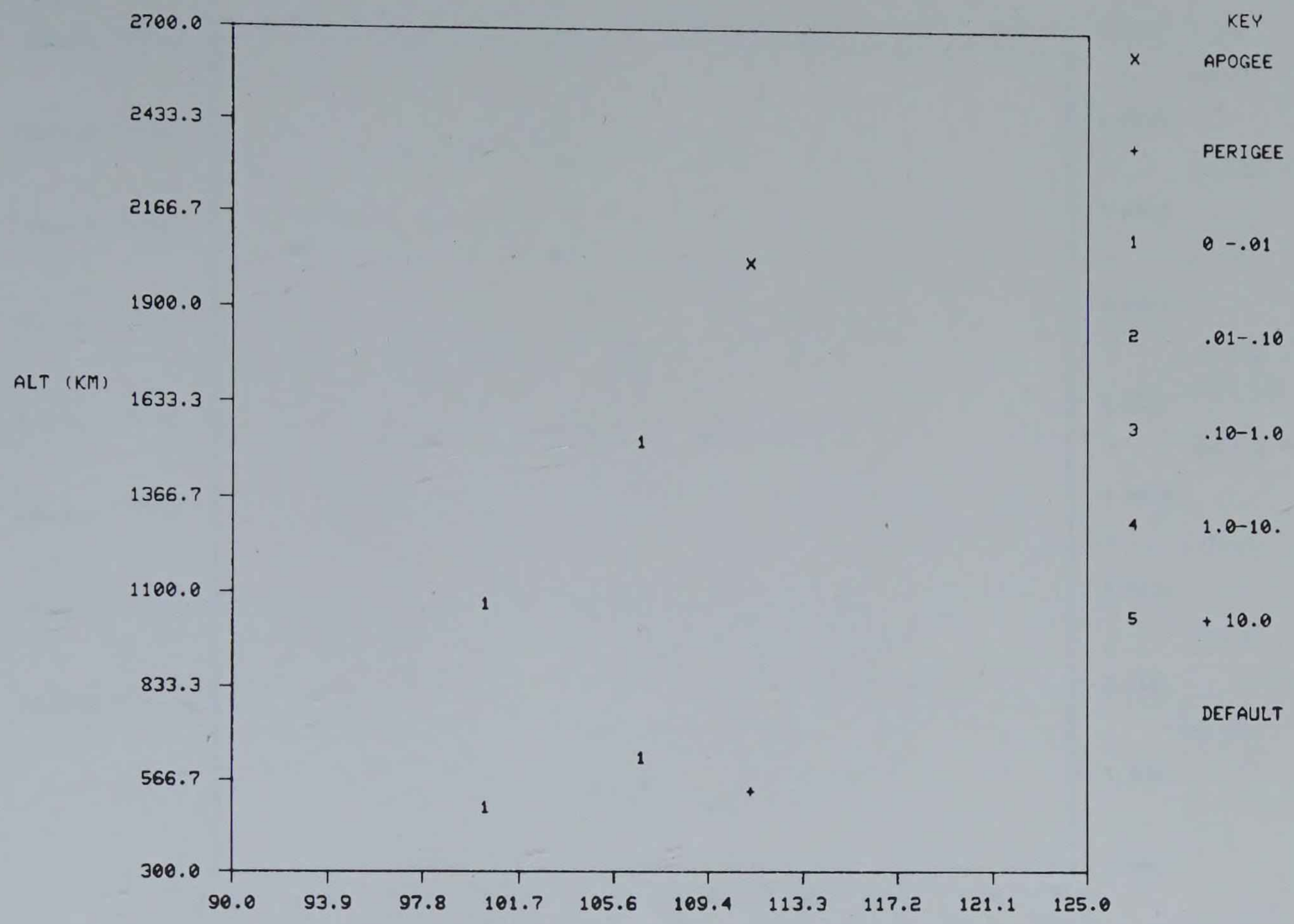


Figure 3.21A Example 2: Weighted Gabbard diagram for 1977-65B (December 1984) — size range 0.0 – 0.01 m².

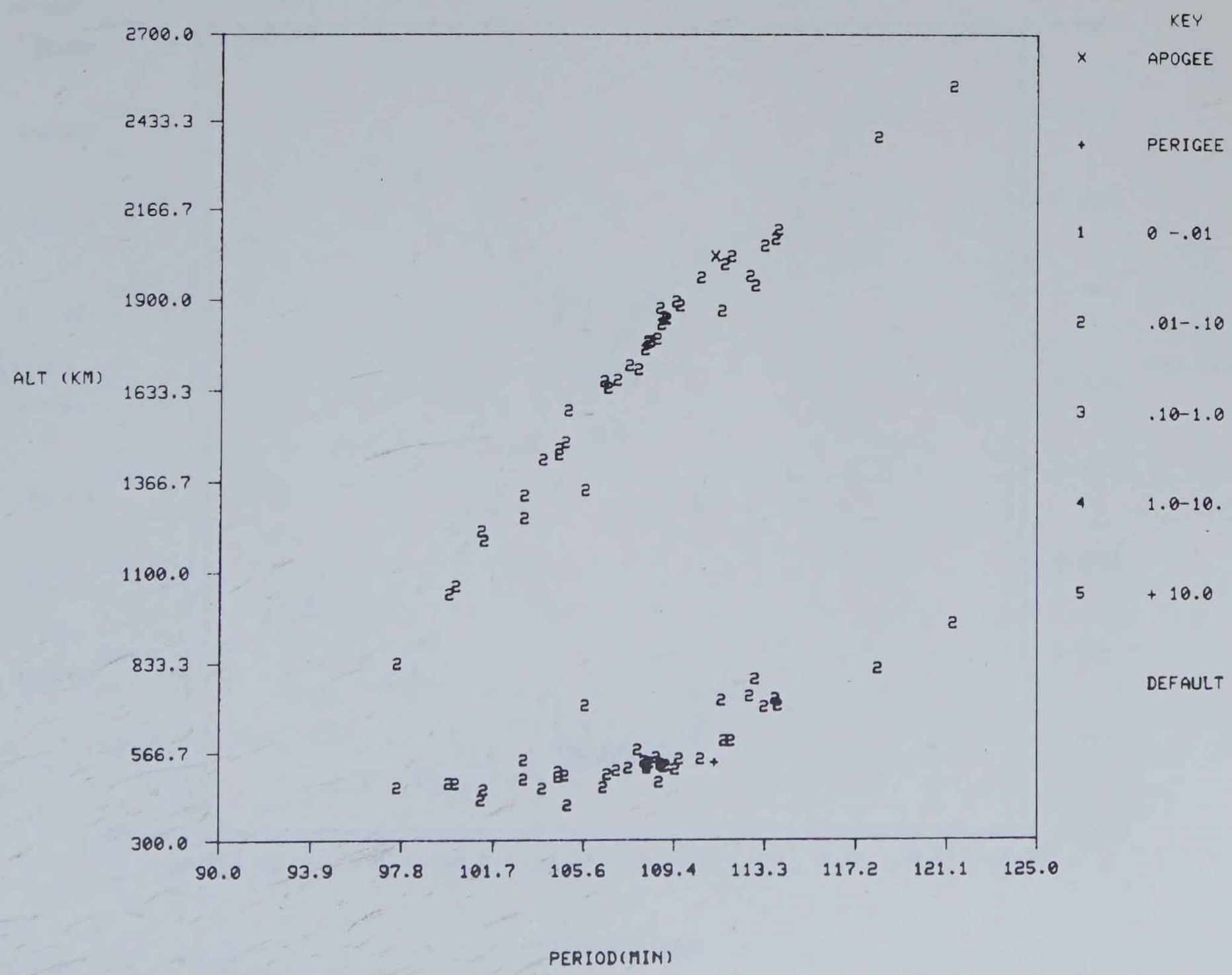


Figure 3.21B Example 2 (Continued): Weighted Gabbard diagram for 1977-65B — size range 0.01 – 0.10 m².

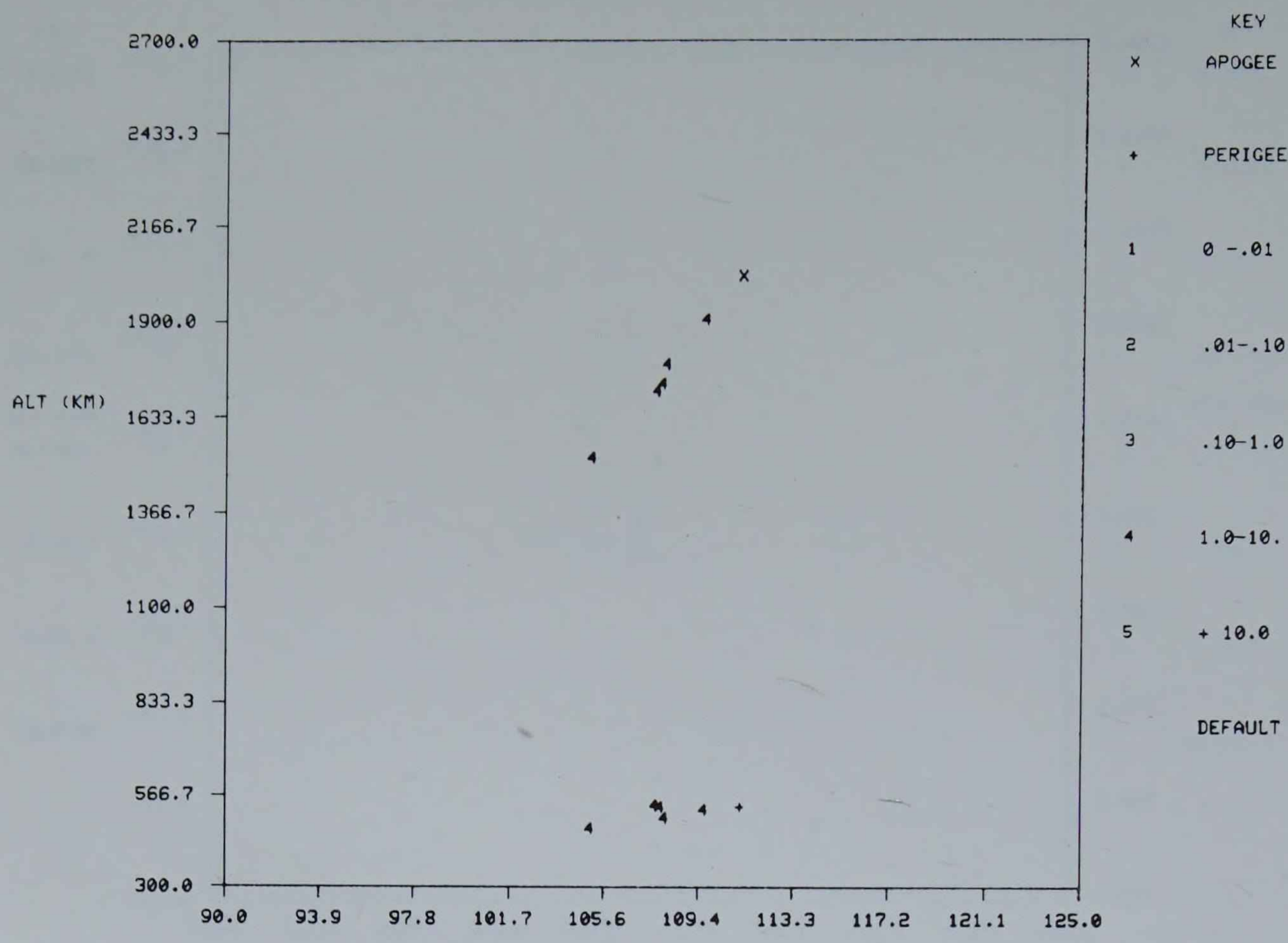


Figure 3.21C Example 2 (Continued): Weighted Gabbard diagram for 1977-65B — size range 0.10 – 1.0 m².

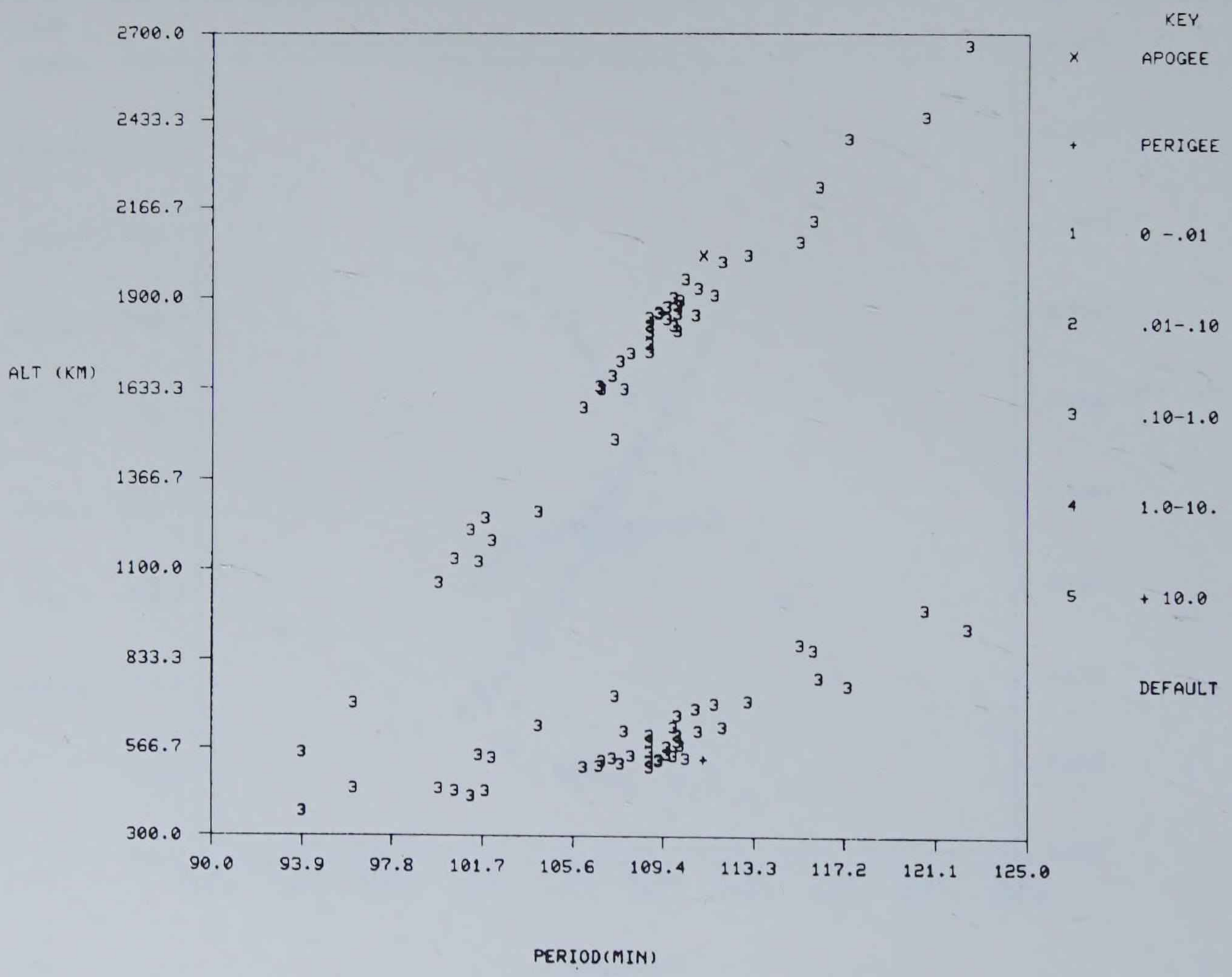


Figure 3.21D Example 2 (Continued): Weighted Gabbard diagram for 1977-65B — size range 1.0 – 10.0 m².

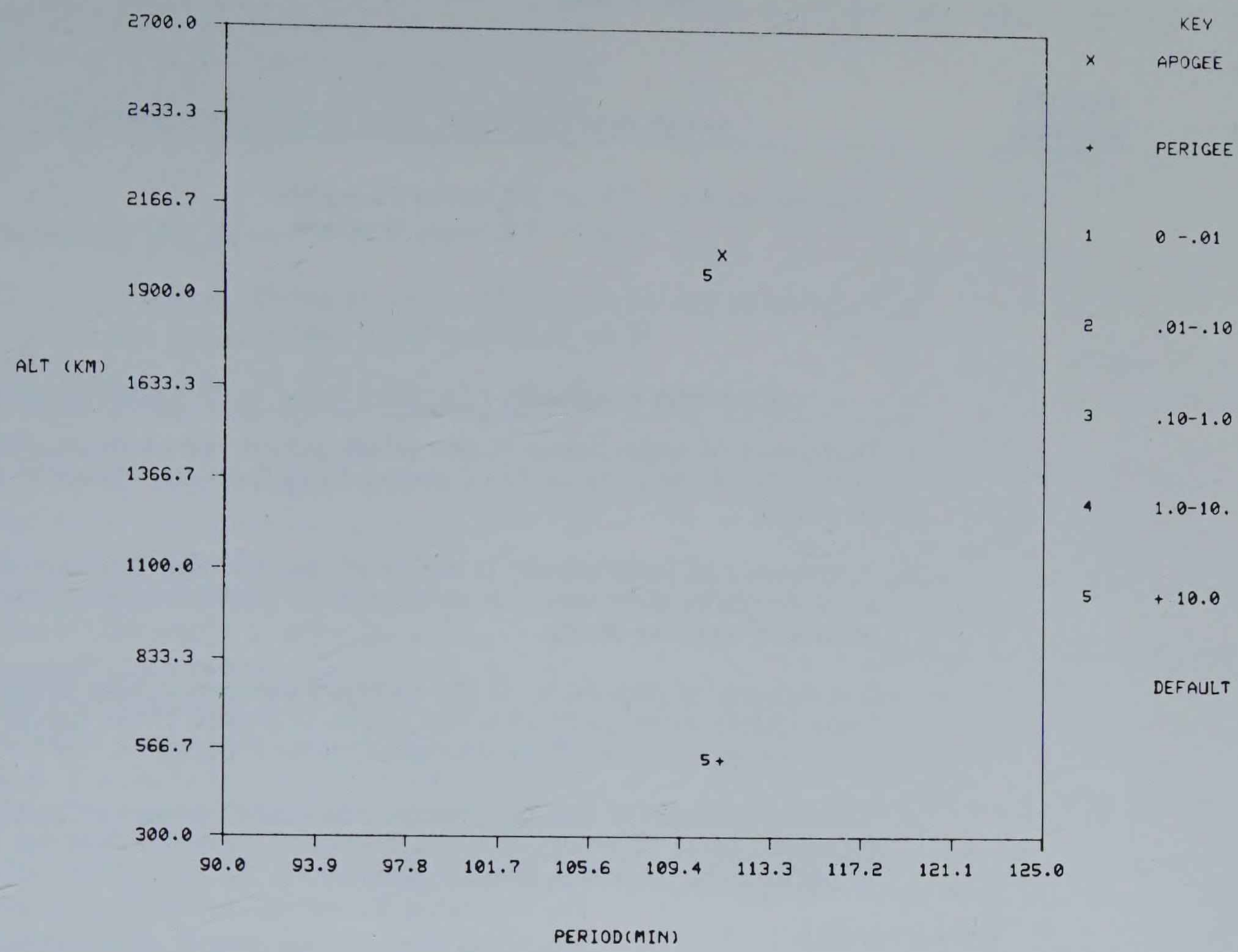


Figure 3.21E Example 2 (Continued): Weighted Gabbard diagram for 1977-65B — size range 10 m² and greater.

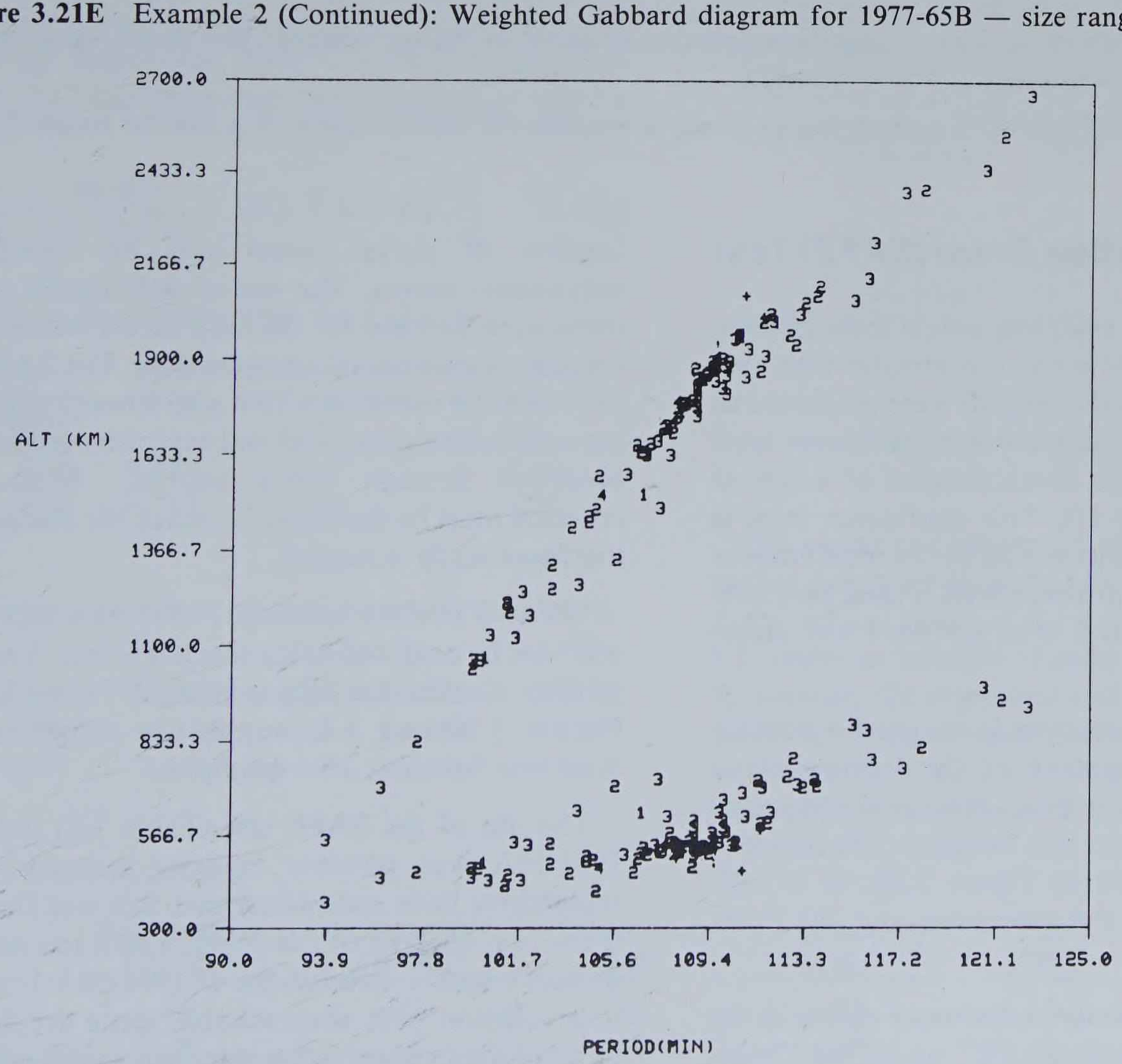


Figure 3.21F Example 2 (Continued): Weighted Gabbard diagram for 1977-65B — all size ranges.

SAFE Test

MAXIMUM POINTS AVAILABLE	POINTS SCORED	MASS DISTRIBUTION (total of 50 points possible)
25	____	a. Exponential Fit: If b < 2.0, score 25 points If b > 2.0, score 0 points
25	____	b. Polynomial Fit: If A_1 < 0.15, score 25 points If A_1 > 0.15, score 0 points
		WEIGHTED GABBARD DIAGRAM (total of 50 points possible)
10	____	a. Dispersion of large pieces: If any pieces greater than 1 m² are dispersed over 50% of the total range of pieces, score 0 points; otherwise score 10 points
15	____	b. Asymmetry of large pieces: If the pieces greater than 1 m² are distinctly asymmetrically distributed about the parent satellite, score 0 points; otherwise score 15 points
15	____	c. Orderedness of dispersion: If the Gabbard diagram is very ordered (most debris along compact arms), score 15 points; if the debris is dispersed in a very disordered manner, score 0 points
10	____	d. Velocity analysis: If average velocity imparted decreases as particle size increases, score 10 points; if average velocity imparted does not decrease as particle size increases, score 0 points
	____	TOTAL POINTS

High point value suggests a collision-induced breakup, whereas low point value suggests an explosion-induced breakup.

Figure 3.22 This SAFE Test form is employed as a tool to evaluate the possible cause of a satellite fragmentation.

Satellite Fragmentation Event (SAFE) Test

A number of methods for analyzing debris from satellite breakups have been presented in this chapter thus far. Some of these debris analysis methods were combined to form the SAFE test which calculates a confidence level that a debris cloud has the characteristics of a typical collision-induced breakup (1). This confidence level is derived by dividing the points scored by the total number of points possible. The confidence level is used here only for conceptual purposes and does not have any mathematical significance.

Each of six separate categories is assigned a number of points. When a characteristic of the debris analysis implies a collision-induced breakup, that breakup receives the full points available from that category. The standard SAFE test form is shown in Figure 3.22. It is self-explanatory for each of the categories and the point breakdown.

All categories parallel analyses discussed earlier in the chapter except the "Polynomial Fit" under the "Mass Distribution" section. It was found that the different families of curves could also be classified using polynomial curves. The use of polynomial curves also eliminates the need for the shift factor which inherently contains a number of uncertainties. The SAFE test has proved to be useful as a first step toward distinguishing between collision-induced and explosion-induced satellite breakups through debris analysis. More objective criterion must be developed to make the distinction more mathematically stringent.

The two satellite breakups, 1981-53A and 1977-65B, will now be analyzed using the SAFE test. The mass and velocity distribution data is given in Tables 3.6 and 3.7. Figures 3.20 and 3.21 supply the weighted Gabbard diagrams for these two examples.

The use of the SAFE test (Table 3.8) indicates that 1981-53A was possibly collision-induced. Although, researchers have speculated that this was the case, this is the first analysis of the debris which has attempted to quantify such a conclusion. If 1981-53A broke up due to a collision with nontrackable space debris, it would be an ominous observation since this would mark an early start to a phenomenon predicted to begin sometime in

the 1990s. Breakup 1977-65B was known to be explosion-induced and the SAFE test produced the appropriate results. Other more objective analysis methods are being researched and developed to aid in the study of satellite breakups, their resulting debris, and the cause of the event.

Debris Heading Plots

In the SAFE test the velocity imparted to each piece of debris was calculated geometrically using the law of cosines; this velocity may be separated into three orthogonal components. One useful combination of components assigns the first axis in the direction of the radius vector in the orbital plane. The second axis, perpendicular to the first, points in the direction of the velocity vector which is located in the orbital plane of the parent satellite. This axis is co-directional with the velocity vector for the parent satellite in a circular orbit. For a parent satellite in a noncircular orbit, the direction of the second axis will differ from that of the velocity vector by the flight path angle of the satellite at the time of the breakup. The third axis is perpendicular to the first two axes and is, therefore, normal to the orbital plane.

These components may be found geometrically by using the law of cosines and the law of sines, but this method is cumbersome. A more sophisticated approach, assuming an impulsive fragmentation, uses equations developed by Meirovitch from Lagrange's planetary equations (37). The following three equations will be used:

$$\Delta a = \frac{2}{n}\left[\Delta V_r \frac{e\sin(f)}{(1-e^2)^{1/2}} - \Delta V_t \frac{a}{r}(1-e^2)^{1/2}\right] \qquad (3.18a)$$

Table 3.6 Mass Distribution Data for SAFE Test.

Satellite Breakup	Spacecraft Density (kg/m³)	Shift Factor	Constant Term for Exponential (b)	Constant Term for Polynomial (A_1)
1981-53A	0.189	0.0095	1.07	−0.064
1977-65B	0.027	0.0068	4.13	−0.207

Table 3.7 Change in Velocity Results for SAFE Test (km/s).

Satellite Breakup	(1)	(2)	(3)	(4)	(5)
1981-53A	0.081	0.068	0.066	0.050	0.030
1977-65B	0.457	0.456	0.448	0.491	0.581

$$\Delta e = \frac{(1-e^2)^{1/2}}{na}\left[\Delta V_r \sin(f) + \Delta V_t \frac{a}{er}\left(1-e^2-\frac{r^2}{a^2}\right)\right] \qquad (3.18b)$$

$$\Delta i = \Delta V_n \left[\frac{r\cos(\omega+f)}{na^2(1-e^2)^{1/2}}\right] \qquad (3.18c)$$

where Δa = semimajor axis of the parent satellite minus the semimajor axis of the piece of debris
n = mean motion of the parent
f = true anomaly of the parent at the time of breakup
r = radial distance at breakup
ΔV_r = delta velocity along radius sector
ΔV_t = delta velocity along velocity vector
Δe = difference in orbital eccentricity (parent-object)
Δi = difference in orbital inclination (parent-object)
ΔV_n = delta velocity normal to the orbital plane
ω = argument of perigee of the parent

From equation 3.18c the normal component to the orbital plane may be found directly. To find ΔV_r and ΔV_t, equations 3.18a and 3.18b must be solved simultaneously. The equations for the changes in the three orthogonal velocity components follow:

$$\Delta V_r = \frac{1}{e\sin(f)}\left[\frac{n\Delta a(1-e^2)^{1/2}}{2} - \Delta V_t\left(\frac{a(1-e^2)}{r}\right)\right] \qquad (3.18d)$$

$$\Delta V_t = \frac{an}{r}\left[\frac{\Delta a(1-e^2)^{1/2}}{2} - \frac{ea\,\Delta e}{(1-e^2)^{1/2}}\right] \qquad (3.18e)$$

$$\Delta V_n = \Delta i\left[\frac{na^2(1-e^2)^{1/2}}{r\cos(\omega+f)}\right]. \qquad (3.18f)$$

The radial and tangential velocity components of the ejected debris are plotted to show the dispersion of debris in the orbital plane at the time of the breakup. Figure 3.23 shows an example of an in-plane debris heading plot. By plotting the tangential and normal components, the debris dispersion perpendicular to the orbital plane may be examined. Figure 3.24 is an example of the out-of-plane debris heading plot. There are, however, difficulties

Table 3.8 SAFE Test Results.

Satellite Breakup	Exponential Fit (25)*	Polynomial Fit (25)*	Dispersion (10)*	Asymmetry (15)*	Order (15)*	Delta V (10)*	Total Score
1981-53A	25	25	10	15	15	10	100 points
1977-65B	0	0	10	0	0	0	10 points

*Maximum Points Available

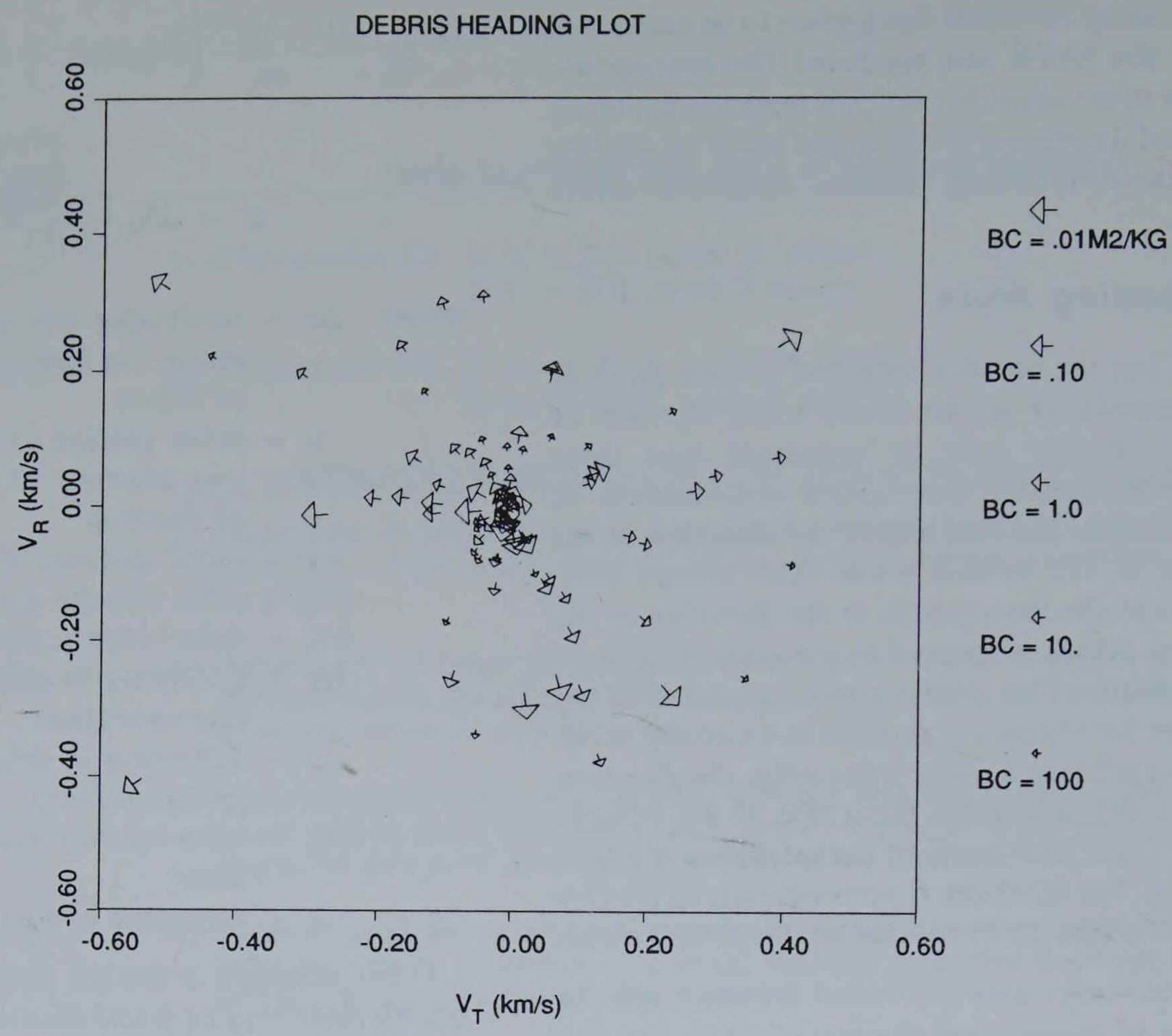


Figure 3.23 An in-plane heading plot depicts the radial and tangential components of the debris ejection velocities.

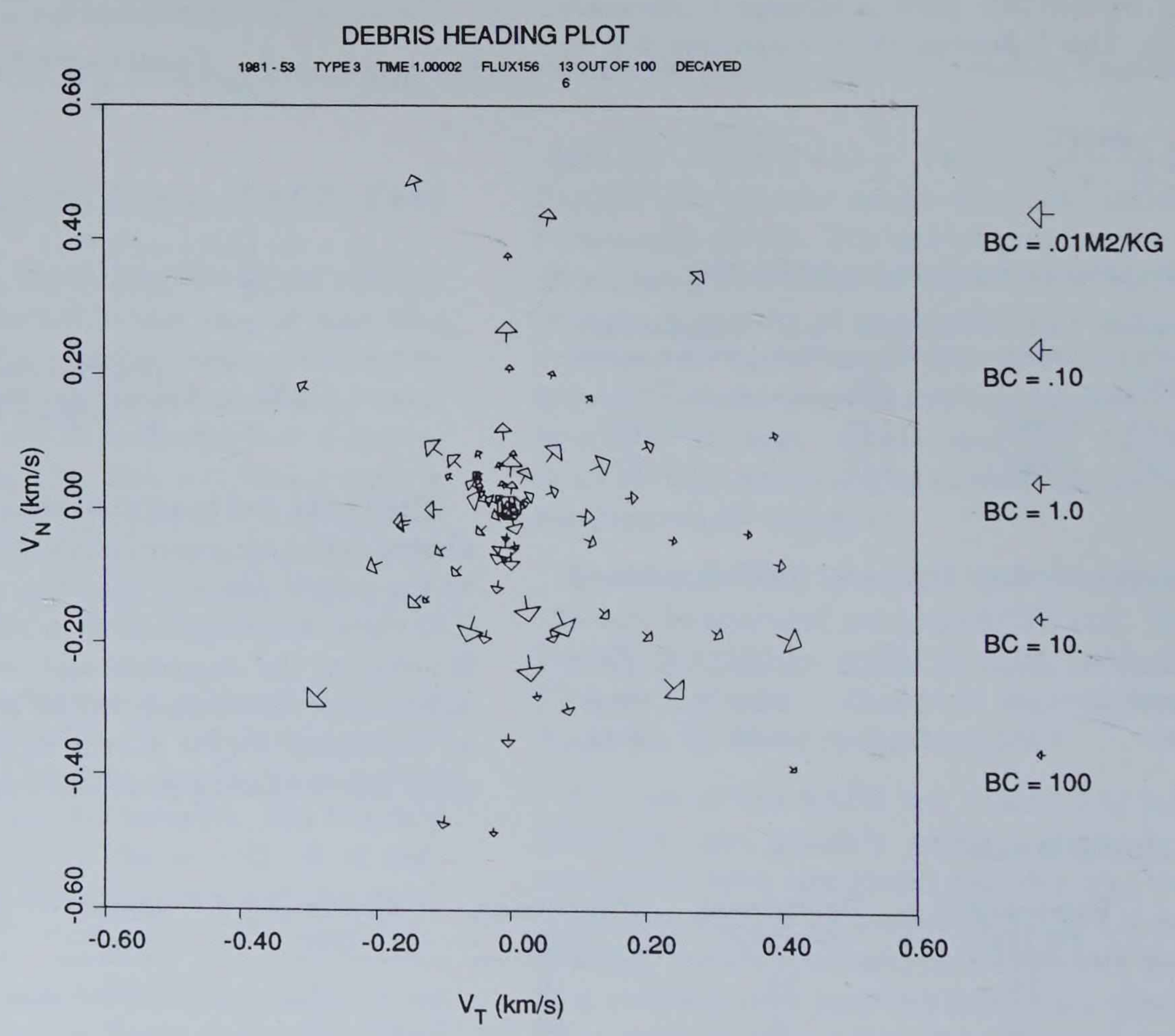


Figure 3.24 An out-of-plane heading plot identifies the normal and tangential components of the debris ejection velocities.

in the use of debris heading plots. The calculation of the delta velocities is complicated by the fact that different methods of calculating these values may give significantly different results. This difference occurs because of imperfect orbital element data.

Later it will be shown that determination of the breakup time and location is a statistical procedure which leaves some uncertainty about the epoch. When calculating the velocity imparted to the debris fragments, one might logically assume that they were all in the same place at the same time. Unfortunately, this may be incorrect "computationally" due to inaccuracies in the debris orbital elements and/or the derivation of the breakup epoch. Forcing each debris fragment to have the same radius vector as the parent satellite at the epoch time may be accomplished by using the equation for radial distance:

$$r = a_o (1 - e_o^2) / \left[1 + e_o \cos(f_o) \right] \qquad (3.19)$$

$$r = a_i (1 - e_i^2) / \left[1 + e_i \cos(f_i) \right]$$

where
- r = radius vector at breakup
- a_o, a_i = semimajor axis of parent and the N fragments (i = 1 to N)
- e_o, e_i = eccentricity of parent and the individual fragments
- f_o, f_i = true anomaly of parent and the individual fragments

All quantities are "known" except the true anomaly values of the fragments which may be solved for easily. In the substitution process, however, this true anomaly is often undefined. This inequality manifests itself in providing an argument to the inverse cosine whose absolute value is greater than one. Adjusting other orbital parameters to obtain realistic results has also been investigated. Another approach which may be used involves fixing the argument of perigee and longitude of the ascending node (50).

The total velocity (vector sum of the three orthogonal components) has been calculated fairly consistently for breakups using a variety of different methods; obtaining consistent results for the breakdown of the velocity components in the orbital plane has proven difficult. The dependence of the calculations on true anomaly appears to be an important consideration, which when neglected, causes drastic variations in the components. On the other hand, when the imparted velocity normal to the orbital plane is calculated, the results generally agree quite well regardless of which particular method of calculation is used.

Treating a Debris Cloud as a Continuum

Thus far, analysis of debris has been conducted by determining the state (size, location, velocity, density, etc.) of each object from a fragmentation event. This form of analysis is a natural extension of the observation of the parent satellite before breakup. Each object can be seen as a part of the mass of the parent satellite, each with a slightly different dynamical state. An excellent way of showing how each debris fragment is related to the parent is to plot the data in a Gabbard diagram. However, there are problems with this "classical" approach. As more debris fragments are generated, this mode of analysis may become computationally cumbersome. Additionally, the capabilities of sensing and tracking devices create artificial boundaries on these analyses. Nontrackable debris fragments do not show up on Gabbard diagrams, yet they may pose a substantial hazard to space operations. By treating a debris cloud as a continuum, all fragment sizes may be depicted.

The treatment of a debris cloud as a continuum may take either of two forms: (1) an envelope analysis, or (2) a statistical mechanics analysis. In the envelope analysis, the debris cloud is created and then analyzed as a whole to determine overall characteristics of the group of particles as a function of time. The techniques of basic orbital mechanics are used to develop this analysis. The statistical mechanics approach treats a debris cloud as an ensemble of particles in a phase space of location and momentum as a function of time. Characteristics of the debris cloud are derived by considering it as a single system, in much the same way that the macroscopic properties of a thermodynamic system (e.g., temperature and pressure) are determined by treating billions of molecules as a single system.

Envelope Analysis

Ross (22) considered the motion of "pellet clouds" after their instantaneous ejection from a spinning container. Using the classical orbital perturbation equations as developed by Moulton (23), the shape of the cloud of particles was examined over time for various orbits and ejection scenarios. When the particles were ejected within the orbital plane, the particles eventually aligned themselves in a shallow ellipse with the major axis aligned with the velocity vector of the parent satellite. Particles ejected out of the orbital plane were found to return to two points on the orbit of the parent satellite. These particles otherwise remain off of the original orbit. Due to the unique ejection circumstances, this phenomenon can manifest itself as an apparent pulsation in the size of the debris cloud.

In 1974, a master's thesis by Fuss expanded on the dynamics of a cloud of debris fragments (24). In that study the dispersion of debris fragments was investigated with and without orbital perturbations. The debris was assumed to be ejected instantaneously and randomly in

all directions. Fuss discovered three levels of dispersion for the debris cloud, represented by three simple geometrical shapes. With no perturbations taken into account, the cloud of particles will, after a few revolutions, form a pinched torus with the particles randomly distributed throughout. The time it takes for the particles in essence to be randomly distributed is roughly equal to the "reunion time." The reunion time is the time it takes the fastest particle to overtake the slowest particle. This pinched torus geometry agrees favorably with the observations made by Ross, which, if combined for in-plane and out-of-plane ejection, would also have predicted a pinched torus distribution.

When the Earth's oblateness and drag effects are added to Fuss's analysis, the particles no longer cross the original orbital plane along the original line formed by the breakup point and a point 180 degrees away. The distribution of particles now follows a simple torus geometry. In addition to these geometrical observations, it was discovered that particles 30 mm and 100 mm in diameter remained in orbit for significant periods of time during the simulation runs. This observation supports the claim that there may be many nontrackable objects presently orbiting the Earth.

The first two geometrical shapes remain aligned with respect to the orbital plane of the parent satellite; thus, the torus would circle the Earth at some fixed angle to the equator. Taking into account the perturbations of the orbital plane itself, this geometrical interpretation quickly breaks down. A breakup will create particles of different sizes and velocities in different orbits. These differences, in turn, cause variations in the regression of the orbital nodes and the location of the argument of perigee. Over time the once tilted torus is dismantled by individual particles having their longitudes of ascending node regress at different rates. The final dispersion pattern consists of a belt of debris which is centered about the Earth's equator and whose range in latitude depends on the initial inclination of the parent body (24).

The papers by Ross and Fuss use basic orbital mechanics to describe the envelope, or boundaries, of a debris cloud. The distribution of particles within these boundaries is roughly known, but the computational burden is still evident when trying to depict the structure of the debris cloud. The use of statistical mechanics avoids this problem by representing a debris cloud as a phase space distribution.

Statistical Mechanics Approach

The purpose of statistical mechanics is to study the macroscopic properties of a system which contains many particles (on the order of 10^{23}) and whose coordinate states are unknown or very difficult to derive (25). A system of N particles, each with s degrees of freedom, obeys Hamilton's equations of motion which are given as follows (26):

$$\dot{q}_i = \partial\mathcal{H}/\partial p_i \quad \dot{p}_i = -\partial\mathcal{H}/\partial q_i \quad i = 1, 2, \ldots, Ns \quad (3.20)$$

where q_i = spatial coordinates of particles (x, y, z)
p_i = momenta of particles (p_x, p_y, p_z)
$\begin{pmatrix} q_i \\ p_i \end{pmatrix}$ = phase space of system
$\mathcal{H}$ = Hamiltonian
(Note: $\mathcal{H}$ = total energy for a conservative system.)

A system's behavior is a trajectory in the phase space; so if we know all q_i's and p_i's at any one time, then the system's behavior is known for all times.

A system's macroscopic properties are "time averages over a segment of the trajectory in phase space but it is more advantageous to consider a large number of similar systems, each consisting of N particles and Ns degrees of freedom, but whose points are somewhat random in their phase space" (26). This group of particles is called an ensemble. The density of particles in the phase space is $D(p_i, q_i, t)$ and changes over time as

$$\frac{dD}{dt} = \frac{\partial D}{\partial t} + \sum_i \left(\frac{\partial D}{\partial p_i} p_i + \frac{\partial D}{\partial q_i} q_i \right). \quad (3.21)$$

The total derivative represents the change of the density with respect to the particle moving through the phase space. Liouville's theorem states that this quantity is zero for a conservative system. This means that in the vicinity of an object traversing the phase space the density does not change. This shows a conservation of volume in the phase space since the Hamiltonian holds for the coordinates of the phase space (26). Since the Hamiltonian is the total energy of a conservative system, this is simply another form of the conservation of energy principle.

These basics of statistical mechanics have been expanded upon in the literature and used in the analysis of satellite breakups (27-33). Reference 27 develops basic equations of statistical mechanics for Keplerian orbits. References 28-30 were written by William B. Heard of the Naval Research Laboratory; the earliest of these develops the basic approach to using statistical mechanics for the analysis of satellite breakups. The second paper analyzes the breakup of Kosmos 699 using these techniques. In the last of these papers the author expands his coverage of the satellite breakup problem by examining the asymptotic distribution of particles from a fragmented celestial body (30).

The analysis developed by Heard has been used by others interested in the dynamics of satellite disintegration

(31, 32). Heard's 1978 paper (33) is a review of his work up to that date in the area of the application of statistical mechanics to satellite breakups. This last reference will be used exclusively for the following development of the statistical mechanics approach for the analysis of satellite breakups.

To accomplish this task a general theory is developed here for the fragmentation of an orbiting object and the resulting debris. The dispersion of the debris cloud is then studied as a whole (a continuum) in a phase space representation and four basic problems are analyzed. The direct problem, which involves the dispersion of fragments from a known epoch, will be covered first. Second, the complication of having a continuous source of particles over a period of time (versus an instantaneous ejection) is investigated. Third, the dispersion of the debris cloud as time approaches infinity (asymptotic problem) is discussed. Last, the initial breakup conditions are discerned through analysis of the debris cloud's shape (inverse problem). The direct problem will be developed thoroughly, whereas the last three problems will only be discussed in relation to the direct problem.

For the direct problem, a debris cloud traveling under the influence of a gravitational field is considered. The equations of motion for each fragment are

$$\dot{\mathbf{q}} = \mathbf{X}(\mathbf{q}, \mathbf{p}, t) \qquad \dot{\mathbf{p}} = \mathbf{Y}(\mathbf{q}, \mathbf{p}, t) \tag{3.22}$$

where $\mathbf{q}$ = n-vector of coordinates
$\mathbf{p}$ = n-vector of momentum

The number of particles in a given volume of the phase space, $d\mathbf{q}\ d\mathbf{p}$, at $(\mathbf{q}, \mathbf{p}, t)$ is given by

$$dN = f(\mathbf{q}, \mathbf{p}, t)\ d\mathbf{q}\ d\mathbf{p} \tag{3.23}$$

where $f(\mathbf{q}, \mathbf{p}, t)$ = phase space density function.

The phase space density function for an instantaneous breakup follows a first order, linear partial differential equation:

$$\frac{\partial f}{\partial t} + \sum_{i=1}^{N} \left[\frac{\partial}{\partial q_i}(fX_i) + \frac{\partial}{\partial p_i}(fY_i)\right] = 0 \tag{3.24}$$

Equation 3.24 is equivalent to

$$Df/Dt = -f\Delta \tag{3.25}$$

where D/Dt, the Stokes derivative, is a differential operator of the form

$$\frac{D}{Dt} = \frac{\partial}{\partial t} + \mathbf{X} \cdot \nabla q + \mathbf{Y} \cdot \nabla p$$

and

$$\Delta = \sum_{i=1}^{N} \left[\frac{\partial X}{\partial q_i} + \frac{\partial Y}{\partial p_i}\right].$$

An initial condition is needed to solve eq. 3.25. This initial condition is

$$f(\mathbf{q}, \mathbf{p}, 0) = F(\mathbf{q}, \mathbf{p}). \tag{3.26}$$

Assuming that $f(\mathbf{q}, \mathbf{p}, t)$ can be found, another basic quantity of the ensemble can be derived; namely, the spatial density, $\varrho(\mathbf{q}, t)$. Spatial density is simply the integral of the phase space density function over all momenta:

$$\varrho(\mathbf{q}, t) = \int f(\mathbf{q}, \mathbf{p}, t)\ d\mathbf{p}. \tag{3.27}$$

The state of the debris cloud is depicted by the spatial density. It is assumed that the dispersion occurred at one point, $\mathbf{q}^*$. Thus, the initial condition prescribed earlier becomes

$$F(\mathbf{q}, \mathbf{p}) = \delta(\mathbf{q} - \mathbf{q}^*)G(\mathbf{p}) \tag{3.28}$$

where $\delta(\ )$ = the Dirac delta function
$G(\mathbf{p})$ = momentum distribution function.

The spatial density function may then be rewritten as

$$\varrho(\mathbf{q},t) = \int \delta\left[\mathbf{Q}_{-t}(\mathbf{q},\mathbf{p},t) - \mathbf{q}^*\right] G\left[\mathbf{P}_{-t}(\mathbf{q},\mathbf{p},t)\right] \exp\{-\Gamma\} d\mathbf{p} \tag{3.29}$$

where $\mathbf{Q}_t$, $\mathbf{P}_t$ = propagator functions of q_i and p_i
Γ = phase space trajectory

Through the application of two delta function theorems, the spatial density becomes

$$\varrho(\mathbf{q},t) = \frac{1}{|J|} G\left[\mathbf{P}_{-t}(\mathbf{q},\mathbf{p}^*,t)\right] \exp\left\{-\Gamma(\mathbf{q},\mathbf{p}^*,t)\right\} \tag{3.30}$$

where $\mathbf{p}^*$ = momenta at breakup, from transcendental solution of $\mathbf{Q}_{-t}(\mathbf{q}, \mathbf{p}^*, t) = \mathbf{q}^*$

$$J = \frac{\partial(Q_{-t1}, \ldots, Q_{-tn})}{\partial(P_1, \ldots, P_n)}$$

= Jacobian determinant

Thus, the spatial density is derived through the calculation of one equation (usually transcendental) and a Jacobian determinant.

The additional assumption that each debris fragment only has a small delta velocity imparted to it compared to the parent satellite's orbital velocity is valid for most realistic examples. Application of this assumption

converts the equation for spatial density into the following computationally convenient form:

$$\varrho(\mathbf{q}, t) = \frac{1}{|\det \mathbf{V}(0,t)|} G\Big[M(0,t)\mathbf{q} - Y(0,t)\mathbf{V}^{-1}(0,t)\mathbf{q}^*\Big] \exp\{-\gamma\} \quad (3.31)$$

where $M(0,t) = W(0,t) - Y(0,t)V^{-1}(0,t)U(0,t)$
n = mean motion
$s = \sin[n(t-\tau)]$
$c = \cos[n(t-\tau)]$
$D = -3n(t-\tau) + 4(1-c)$

and

$$U(t,\tau) = \begin{pmatrix} c & 0 & 0 \\ -2s & 1 & 0 \\ 0 & 0 & c \end{pmatrix}$$

$$V(t,\tau) = \frac{1}{n}\begin{pmatrix} s & 2(1-c) & 0 \\ -2(1-c) & 4s-3(t-\tau) & 0 \\ 0 & 0 & s \end{pmatrix}$$

$$W(t,\tau) = \begin{pmatrix} -ns & 0 & 0 \\ 0 & 0 & 0 \\ 0 & 0 & -ns \end{pmatrix} \quad Y(t,\tau) = \begin{pmatrix} c & -2s & 0 \\ 0 & 1 & 0 \\ 0 & 0 & c \end{pmatrix}$$

$$M(t,\tau) = \begin{pmatrix} 3n(t-\tau)+4x & 2(1-c) & 0 \\ -2(1-c) & s & 0 \\ 0 & 0 & D/s \end{pmatrix}$$

$$\gamma = \int_o^t \mathrm{Tr}\{A(t)\}dt \qquad \text{from } \dot{\mathbf{x}} = A\mathbf{x} + \mathbf{f}$$

This equation provides a solution for the spatial density of a debris cloud formed by the instantaneous release of particles in nearly circular orbits. The second general problem is the direct problem with ejection of fragments over time. With a source of particles, eq. 3.25 becomes (33)

$$Df/Dt + f\Delta = S(\mathbf{q}, \mathbf{p}, t) \quad (3.32)$$

where $S(\mathbf{q}, \mathbf{p}, t)$ = a source of S particles per unit time created in the phase space volume element dqdp at coordinate (q,p) and time t.

Developing the equations, as was done for the first direct problem, yields

$$\varrho(q,t|\tau) = \frac{1}{|\det V(\tau,t)|} G\Big[M(\tau,t)q - Y(\tau,t)V^{-1}(\tau,t)\mathbf{q}_s(\tau)\Big] \exp\{-\gamma\} \quad (3.33)$$

where $\mathbf{q}_s(\tau)$ = location of emission of particles
τ = some finite time at which particles ceased being emitted

Again, the spatial density depends on the time since breakup and the conditions at breakup. The third problem, the asymptotic problem, considers the state of the cloud created at one point as time approaches infinity. The asymptotic problem is simply an extension of the first direct problem analyzed. The results of this problem will be left for the reader to investigate in reference 33. Basically, letting time approach infinity in eq. 3.31 provides the results to the asymptotic problem.

The last problem, the inverse problem, may be the most interesting application of statistical mechanics to satellite breakup analysis. In the inverse problem, one solves for the state of the initial breakup from direct observations of the cloud of debris itself. Given the spatial density and breakup epoch, the initial momentum distribution may be calculated directly from

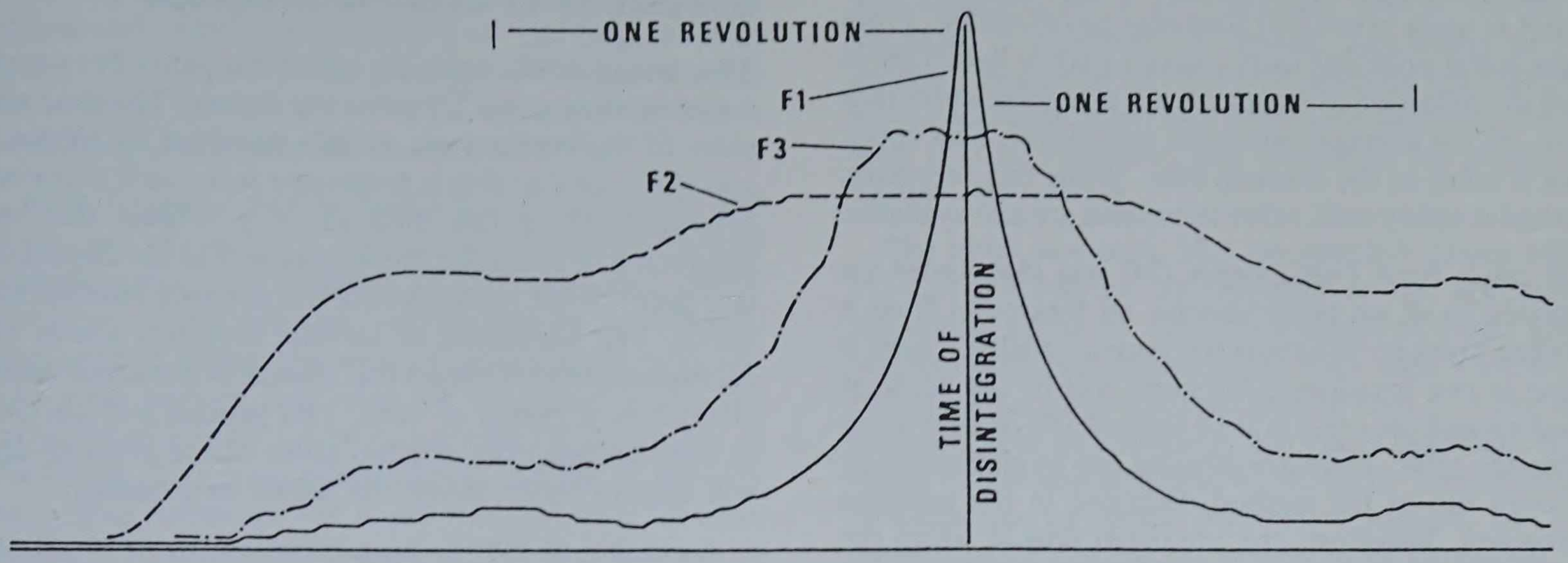
$$G(\mathbf{p}) = |\det V(0,t)|\varrho\Big[M^{-1}(0,t)\ \mathbf{p} + Y(0,t)V^{-1}(0,t)q^*\Big]. \quad (3.34)$$

It is also possible to derive the epoch conditions of the fragmentation by knowing only the low order moments of the spatial density (33). Three-dimensional Hermite polynomial expansions are used to represent $\varrho(\mathbf{q})$ and $G(\mathbf{p})$ while the known moments of $\varrho(\mathbf{q})$ are used to derive the other parameters in the equation for $G(\mathbf{p})$.

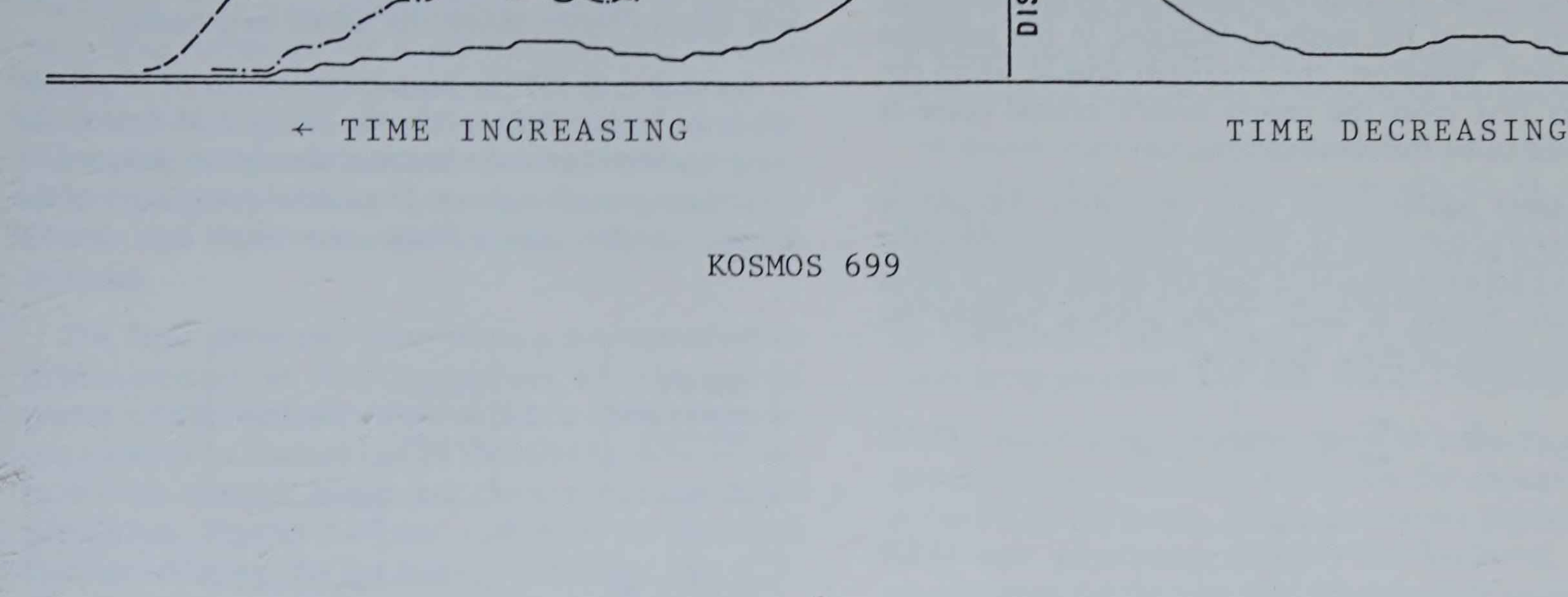
In summary, the use of statistical mechanics to investigate satellite breakups appears to have a number of advantages over the classical approaches. First, the statistical approach requires less computational effort and does not require increased effort for larger breakups. It also provides a global definition to a problem which inherently does not lend itself to such an approach. On the other hand, statistical mechanics requires the conversion of basic orbital element data sets (the common data form) into analytic functions for use in this analysis. The nomenclature of statistical mechanics may also be less widely used than the classical orbital terms. Whether or not statistical mechanics should be used in the analysis of space debris depends on what problem is being investigated.

Determining Breakup Time

When a satellite fragments the event is seldom observed directly, hence the details of the breakup, including the time of its occurrence, are not known precisely. Typically, the satellite is tracked intact during one pass near a ground-based sensor and then, at the time of the next



KOSMOS 699



ERTS-1 ROCKET BODY

Figure 3.25 These time-dependent analyses of two satellite breakups are a powerful tool in determining the time of the fragmentation event. *Courtesy of B. Kaufman, Naval Research Laboratory.*

observation, a cloud of debris will be observed in the vicinity of where the satellite used to be. Each of the pieces of debris is then tracked separately. From the orbital element sets of each object, the position of that object at some prescribed time may be calculated. From these initial positions each object's path is backtracked until the collection of fragments are at a point where they have, on the average, minimum separation. This epoch time is taken as the breakup time. While this very basic method is widely used, other techniques are also available.

A result from Fuss's paper (24) was that under the assumption of no perturbations, all fragments from a satellite breakup will cross the parent satellite's orbital plane at two locations. One point will be the point of breakup and the other will be located 180 degrees away along the orbit. The extra crossing can be eliminated by a rough use of the method described in the previous paragraph. Therefore, the computed time at which the objects first cross the parent body's orbital plane is assumed to be the breakup time.

A more sophisticated time dependent method is developed in reference 31. Instead of only minimizing the distance between objects to find the epoch time, a series of three criteria is used. These criteria require the maximization of three functions:

$$F_1 = \sum \frac{1}{|\vec{r}_i - \vec{r}_j|^2 + \delta^2} \tag{3.35}$$

$$F_2 = \frac{1}{\sum_{i \neq j}^{N} |\vec{r}_i - \vec{r}_j|^2} \tag{3.36}$$

$$F_3 = \text{number of points such that } |r_i - r_j| \leq d_1 \tag{3.37}$$

where r_i, r_j = position vectors of the ith and jth fragments, respectively
N = total number of fragments
δ = measure of position uncertainty
d_1 = an arbitrary distance, usually greater than position uncertainty

The function F_1 has a δ included to prevent a small separation distance from making F_1 approach infinity. The function F_1 is not affected much by objects which are actually not a result of the breakup under analysis. This means that a large spike of F_1 is a "necessary but not sufficient condition that a breakup has occurred." The peaking of the F_2 function is a "sufficient condition" for the formulation of a breakup time since it measures the entire cluster size. The last function, F_3, simply measures "the number of close approaches within d_1." Again, as with F_1 the peaking of F_3 must occur for a breakup time to be found. A plot of these three functions for the breakup of satellites Kosmos 699 and the ERTS-1 rocket body is shown in Figure 3.25.

Simulation of Satellite Breakups

The mass and velocity distributions for each fragmentation event are generally known. The time and place of the breakup are usually provided by NORAD and the trackable debris fragments from each event are cataloged. From this data set it is evident that the simulation of a satellite breakup as well as the dispersion and decay of the resulting debris is not only possible but useful. The simulation of satellite breakups allows the accountability of nontrackable objects of a realistic debris cloud over a period of time. This process will also aid in distinguishing the original cause of the breakup and will help to better model the debris environment.

A number of models have been developed which use the same basic concepts (47, 48). Figure 3.26 depicts the program flowchart for a breakup simulation designed by one of the present authors. The orbital parameters of the parent satellite are initially converted into inertial

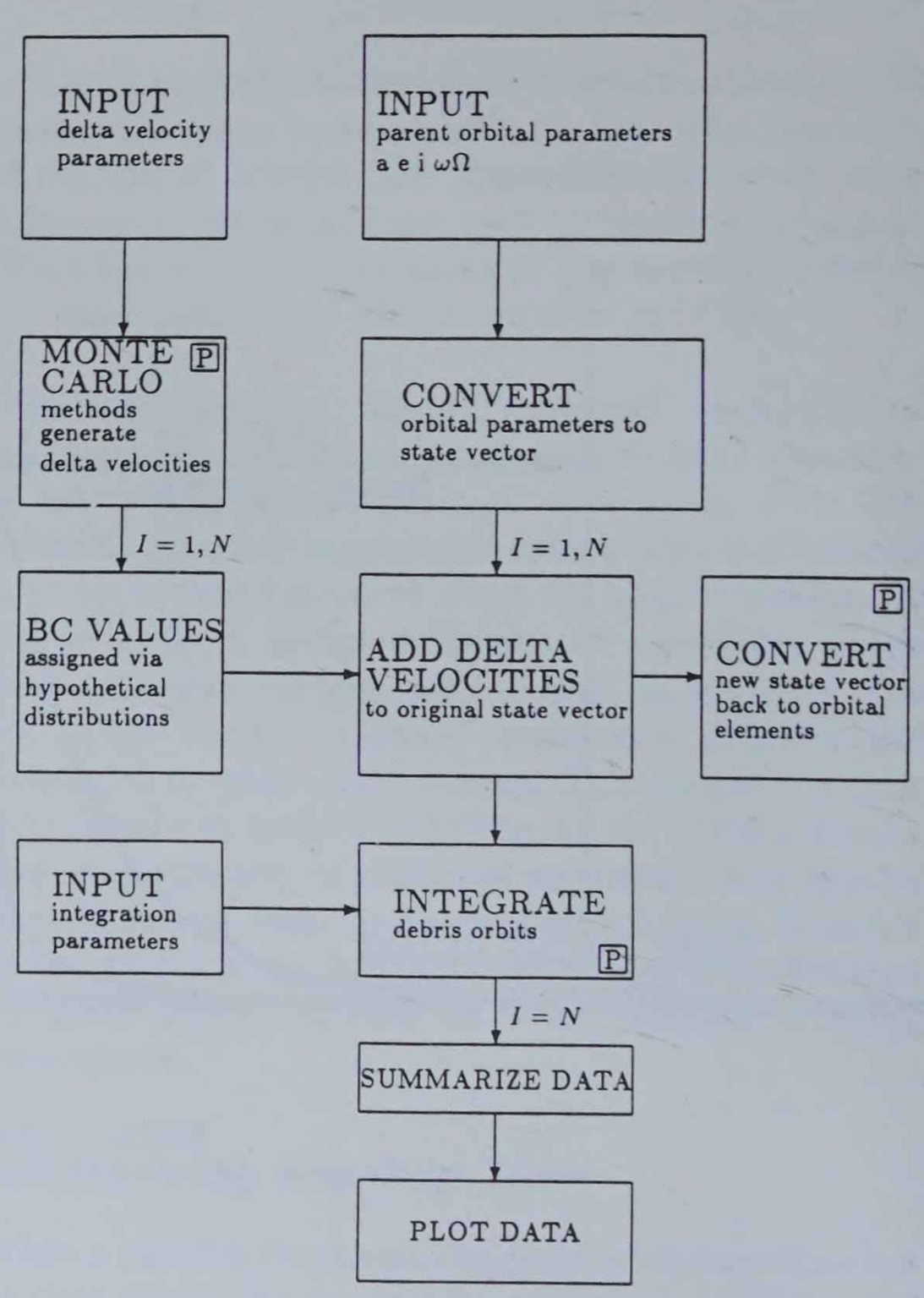


Figure 3.26 A simple satellite fragmentation simulation can not only model the numbers and orbits of the debris but also can be used to predict the evolution of the debris cloud.

coordinates, and the breakup is then simulated by replacing the parent satellite with a large number of fragments. Each fragment's state vector is then formed by adding a delta velocity component to each of the three orthogonal velocity components of the original state vector. The magnitude and proportion of delta velocities are assigned through a Monte Carlo simulation with a designated probability distribution function.

Each fragment may be assigned a delta velocity and mass to recreate a hypothetical debris cloud respresentative of a collision, an explosion, or a special condition. These new state vectors may be immediately converted to orbital elements by conventional methods. The state vectors may then be integrated under the influence of a force model to simulate the dispersion of the debris. This force model should include, at the very least, drag forces and the J_2 gravitational term for most orbits, since these forces account for the majority of secular perturbations on low altitude Earth satellites. Depending on the altitude and duration of integration, other forces, such as solar radiation pressure, solar-lunar effects, and higher order gravitational terms, might be included.

The final integrated state vectors are converted to orbital elements to allow comparison with the original parent satellite and the observed debris cloud. Particles too small to be tracked can be included in these models to provide valuable insight into the nontrackable debris population. Figures 3.27 and 3.28 show the simulated Gabbard diagrams for the breakup of satellite 1981-53A. The first diagram is the original simulated dispersion, whereas the second diagram shows the debris cloud after two weeks.

Over this 14 day period, one very small fragment decayed while a number of others lost altitude. The fragments are classified according to ballistic coefficient due to the difficulty of relating RCS and mass values as discussed earlier. The trackable objects in the simulated Gabbard diagrams (designated as plotting characters 4 and 5) are much less susceptible to drag forces than are the smaller, nontrackable objects.

By including the J_2 gravitational term into the force model, secular perturbations on the argument of perigee and the longitude of the ascending node may be seen. The original dispersion of fragments from the parent satellite may be represented in two debris heading plots: one in-plane and one out-of-plane. Figures 3.29 and 3.30 show the debris heading plots for a simulated symmetrical explosion of satellite 1981-53A.

Future Measurement Devices

Up to this point, only existing forms of measurement and analysis have been reviewed. A number of concepts are being studied to provide enhanced debris detection capabilities in the future. First, ground-based optical devices have great potential as debris detection devices. The tradeoffs for a ground-based optical system are discussed in reference 34. System parameters such as location, slew rates, detector type, aperture (A), collecting area, band pass, minimum detectable signal (s), field of view (FOV), f-number, and resolution are played off against one another.

The result is a basic 33.5 cm aperture design with a FOV of 2.4 degrees, an f-number of 1.8, a minimum detectable signal of 3.80 photoelectrons/pixel, and a resolution of 16.8 arcsec/pixel. With such a system an object with a cross-sectional area of only 6.14 cm^2 may be detected at an altitude of 800 km, a capability far in excess of that now possessed by NORAD. There are many combinations of optical parameters possible, and even more capable systems are certain to be developed.

A second approach to improved debris surveillance is to use space-based detection systems (35, 42, 43, 45). By placing the detecting devices in space, the problem of atmospheric distortion and attenuation will be eliminated. Neste has provided an excellent summary of three options for space-based debris detection systems (35). They all show great potential, but each has its limitations.

The major design criterion used in evaluating these alternatives was increased resolution for objects in the 0.1 to 10 cm size range. Weight and power requirements were also scrutinized closely. The projected debris environment for the year 1995 developed by Kessler (36) was used as the design environment for analyzing these systems. First, radar systems have been used terrestrially for years, but would require a large platform and much power to run. They provide great versatility and accuracy because the direction, intensity, and duration of the energy incident on the target may be precisely controlled. While a shorter wavelength would permit greater resolution, the significant power requirements may be prohibitive.

While the radar concept of using reflected radio energy to detect objects is well known, a second option known as lidar (light detection and ranging) is also possible. A lidar system will transmit optical energy at an object and measure the reflected energy on a mosaic detector. While lidar systems provide the same flexibility as radar systems they operate at optical wavelengths which are much shorter than radio wavelengths.

Another alternative is a passive optical device which measures the Sun's reflective energy off the object in question or measures the radiant energy of the object itself. The passive optical system could include two optical imaging cameras (to take advantage of parallax) which require much less power and weigh considerably less than

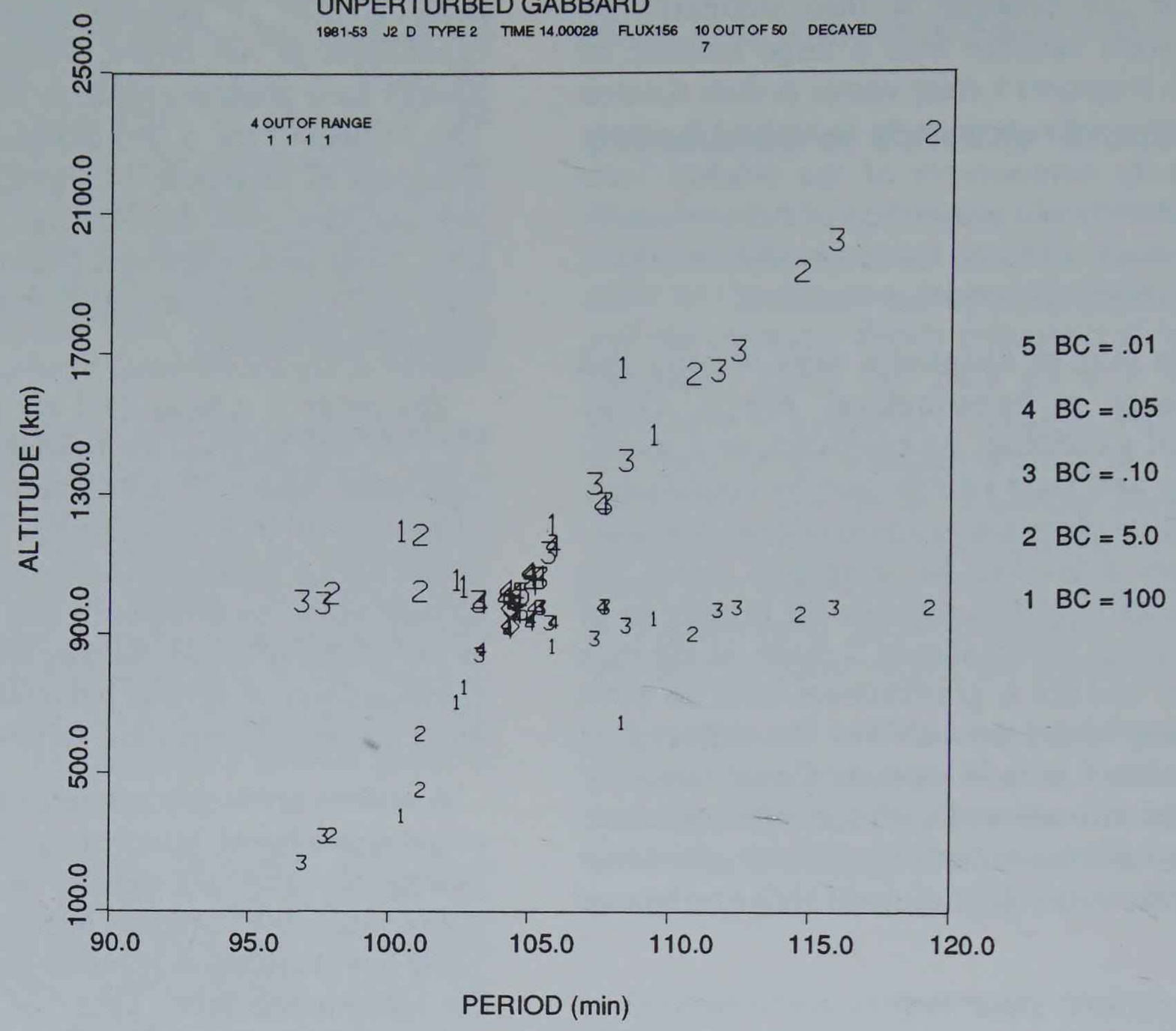


Figure 3.27 This Gabbard diagram depicts the initial distribution of debris from a simulation of the breakup of satellite 1981-53A using the model described in the text.

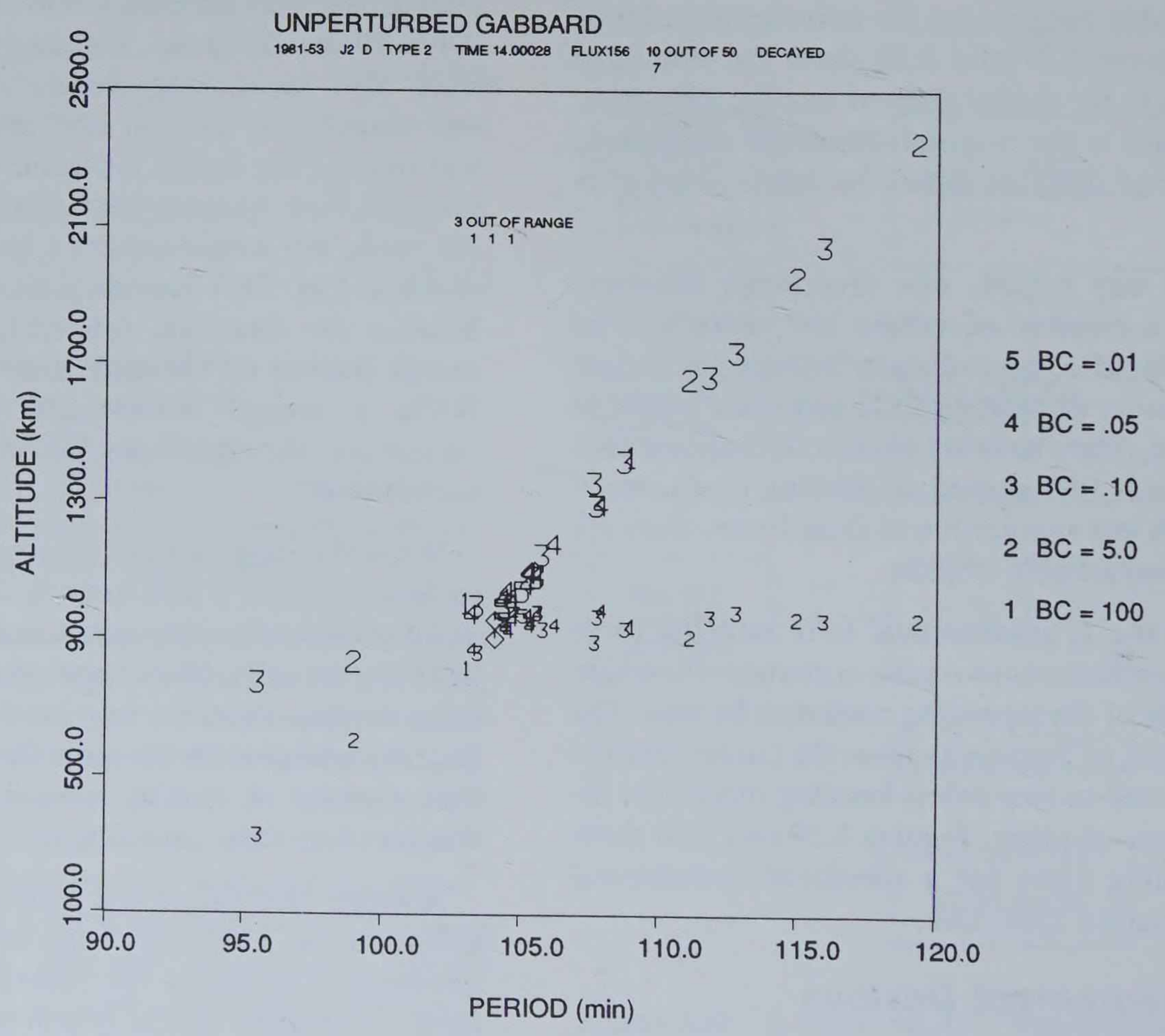


Figure 3.28 The effects of decay on smaller particles from the fragmentation of 1981-53A can be seen in this simulated Gabbard diagram of the debris two weeks after the event.

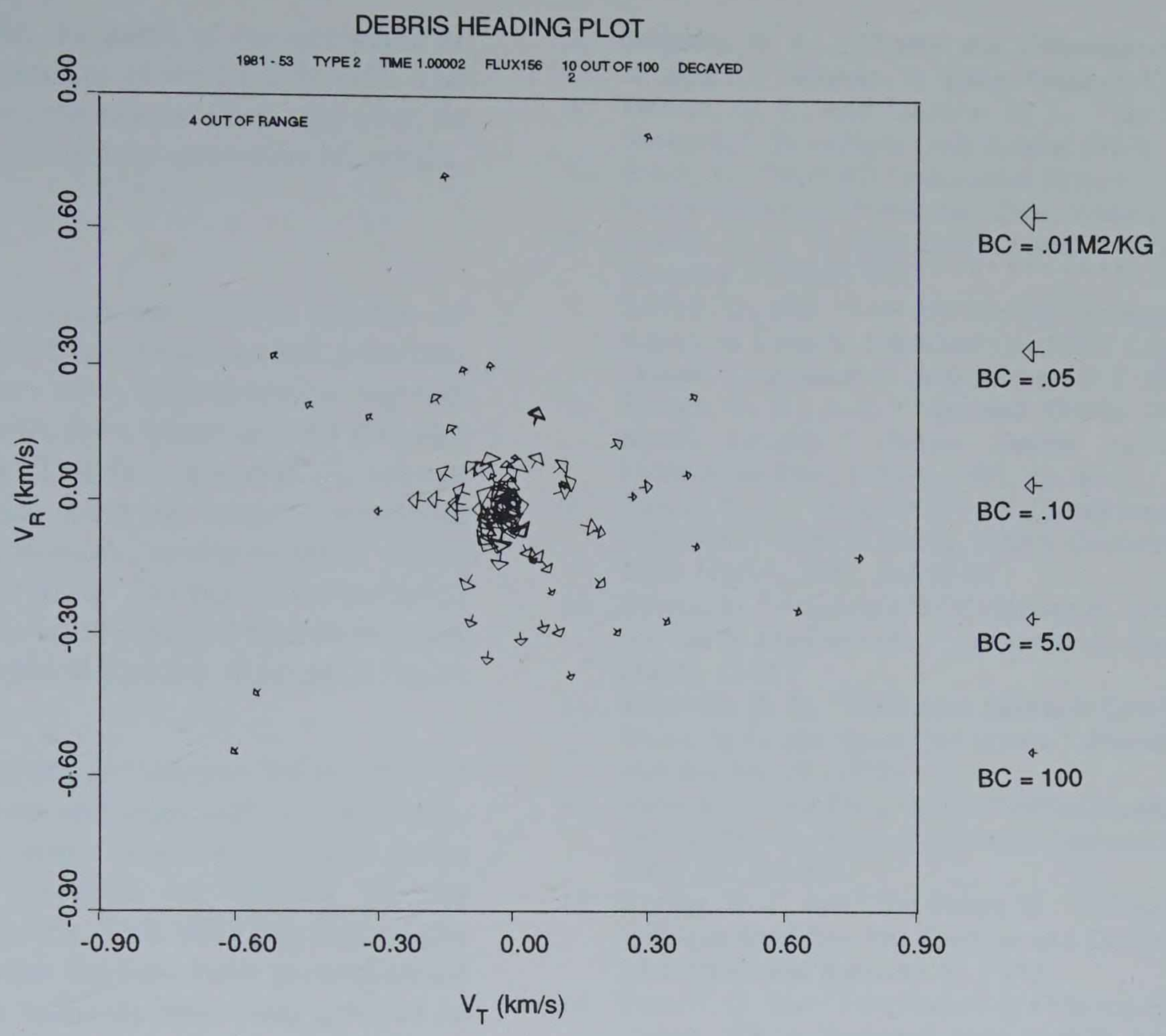


Figure 3.29 Assuming a symmetrical distribution of debris from 1981-53A, the in-plane debris heading plot should resemble the simulated graph shown here.

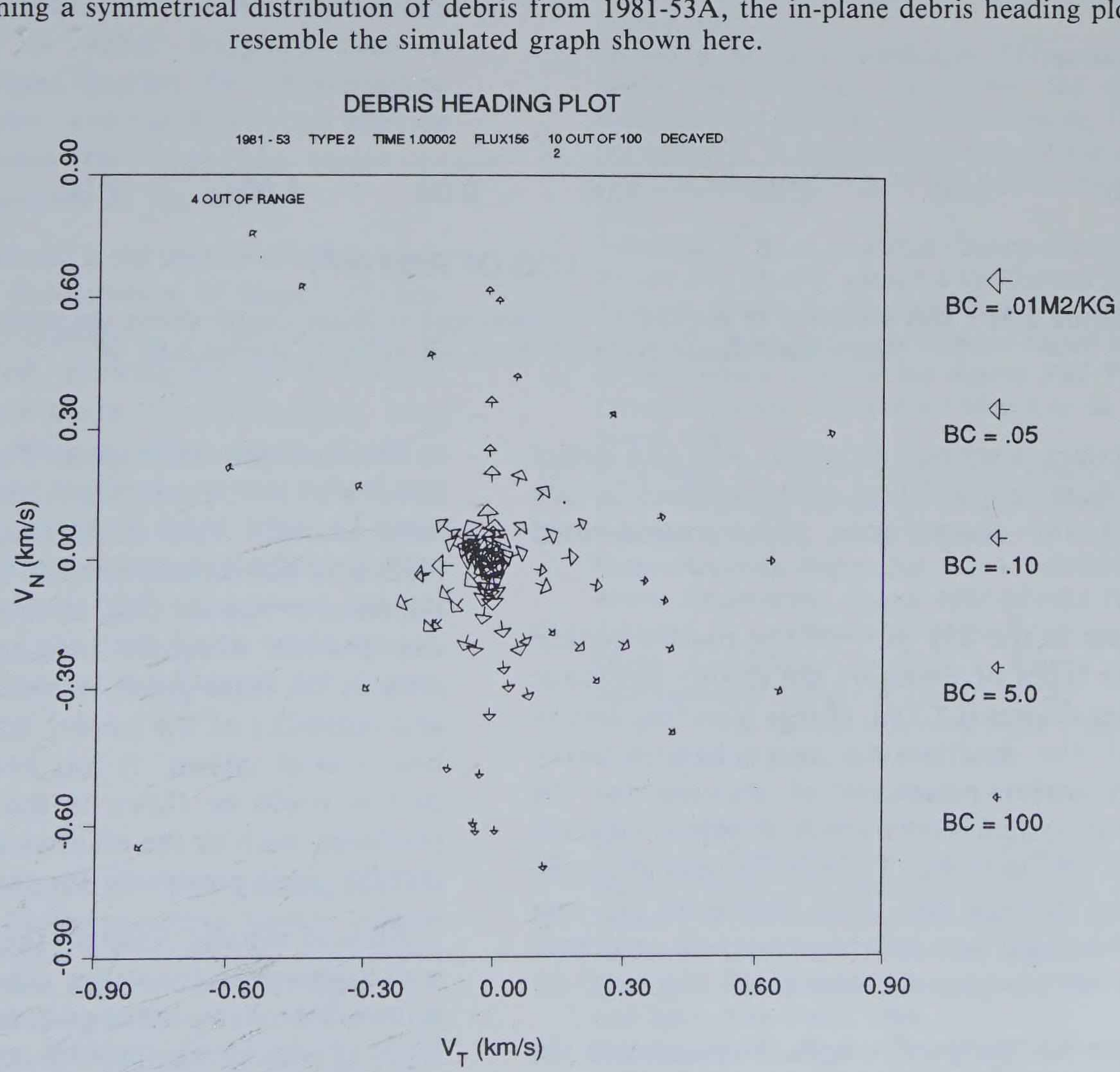


Figure 3.30 Out-of-plane debris heading plots, such as this one for 1981-53A, simulate the higher ejection velocities imparted to the smaller particles.

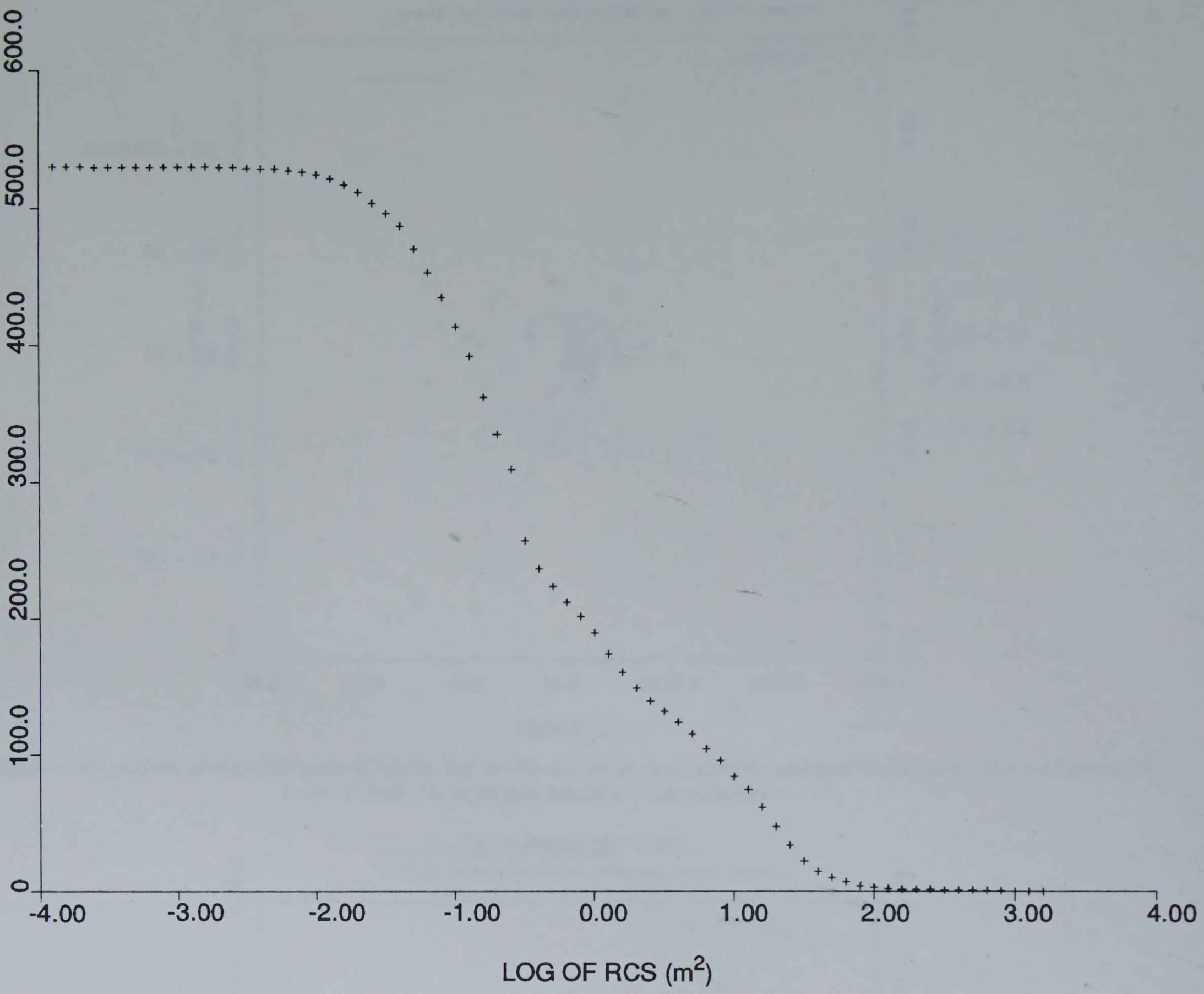


Figure 3.31 This summary of the size of the cataloged satellites clearly shows the resolution of the Space Surveillance Network drops off abruptly around 0.05 m².

the active devices described above. It will also detect objects with diameters of 10 cm or more which in turn can be used for comparisons with ground-based instruments.

The detector is the key part of the passive optical system. Three types of detectors are readily available: charge coupled devices (CCDs), charge injection devices (CIDs), and the multianode microchannel array (MAMA). A major parameter of concern for the accuracy of each system is the number of objects expected to be detected per unit time. The passive optical system should achieve an event rate in the thousands per year at 800 km while lidar and radar systems will only have rates around 100 per year for very small objects.

Components for the passive optical system and the radar systems have been used in space before. The lidar system, however, includes components which have not to date been proven in space. The lidar system is also the heaviest of the three systems, but it is projected to be the most accurate. Each of the three systems may cost $10 million to $20 million to build and each will cost about the same to operate (35). In summary, all three systems can provide adequate measurement capabilities for roughly the same price, yet the combined performance and reliability of the passive optical device make it the best overall system. It has been proposed that these devices could be flown in the future on a dedicated platform, such as the multimission modular spacecraft (MMS), used previously for the Landsat 4 mission.

An even simpler detector, the impact sensor, is not as sophisticated as the other sensing devices, yet it has proven dependable in the past. Improved designs of these types of sensors may provide more capability. The two-stage acoustic penetration and impact detector can measure not only the time of impact, but also the velocity

of the impacting particle, the angle of the projectile at encounter, and the momentum of the particle (45). The material which penetrates the sensor's foil may even be chemically analyzed to accurately determine its origin.

Summary

Debris data is currently available from a number of sources, but it is all derived from the same sensing devices. This network of radars and electro-optical devices provides the researcher with the average size and the orbit of each piece of debris. This intricate system, though reliable and accurate for tracking larger operational satellites and incoming missiles, measures small debris particles with some uncertainty. The poor size resolution for debris fragments is further amplified by uncertainties in the RCS-to-mass conversion process, as noted in Figure 3.31.

Two actions are necessary to improve the analysis of debris: enhanced awareness and improved measurements. Enhanced awareness of space debris will help to focus more attention and research on aspects of the proliferation of space debris. This will then lead to the use of better measurement devices, both ground-based and space-based. Many methods have been covered to analyze debris data. The mass and velocity distributions are traditional forms in which fragment data is scrutinized, but the Gabbard diagram, the debris heading plot, statistical mechanics, and the SAFE test provide additional insight into the probable cause of fragmentation and dispersion of the debris.

The simulation of breakups is the most promising mode of analysis due to the development of large, efficient computers. Through simulation, a wide range of scenarios may be enacted, allowing for the proving or disproving of hypotheses which otherwise might have waited for the right fragmentation event. Once a rudimentary understanding is gained, the next logical step is better evaluation of the hazard from debris to space operations. It is imperative to ascertain the hazard from space debris to save lives and to prevent further unintentional littering of the near Earth environment. Chapter 4 discusses aspects of the hazards from space debris.

References

1. Culp, R. D., and McKnight, D. S. "Distinguishing Between Collision-Induced and Explosion-Induced Satellite Breakup Through Debris Analysis." Presented at AAS/AIAA Astrodynamics Conference, Paper No. 85-370, August 1985, also *Astrodynamics 1985,* vol. 58, pt. 1, Advances in Astronautical Sciences, American Astronautical Society Publication, Univelt, Inc., San Diego, 1986, pp. 739-758.
2. *RCS Catalog*. NORAD/J5YS, Peterson AFB, Col., December 1982 through December 1984.
3. Johnson, N. L. "History and Consequences of On-Orbit Breakups." *Advances in Space Research* 5 (1985): 11-19.
4. DeVere, G. T., and Johnson, N. L. "The NORAD Space Network." *Spaceflight* (July-August 1985): 306-309.
5. Brach, D. "NORAD Operational System." *Orbital Debris,* NASA Conference Publication 2360, NASA, 1985, pp. 39-44.
6. Kessler, D. J. "Orbital Debris Issues." *Advances in Space Research* 5 (1985): 3-11.
7. Taff, L. G., et al. "Low Altitude One Centimeter Space Debris Search at Lincoln Laboratory's (MIT) Experimental Test System." *Advances in Space Research* 5 (1985): 35-47.
8. Humes, D. H., et al. "Manmade Orbital Debris Studies at NASA Langley." *Orbital Debris,* NASA Conference Publication 2360, NASA, 1985, pp. 45-68.
9. Kessler, D. J. "NORAD's PARCS Small Satellite Tests (1976 and 1978)." *Orbital Debris,* NASA Conference Publication 2360, NASA, 1985, pp. 39-44
10. Sehnal, L. "Probability of Collisions of Artificial Bodies in the Earth Environment." *Advances in Space Research* 5 (1985): 21-25.
11. Reynolds, R. C. "Man-made Debris in Low Earth Orbit - A Threat to Future Space Operations." *Journal of Spacecraft and Rockets* 20 (1983).
12. Hyland, D. "Air Force Orbital Position Management Policy." *Orbital Debris,* NASA Conference Publication 2360, NASA, 1985, pp. 393-398.
13. Kessler, D. J., and Cour-Palais, B. "Collision Frequency of Artificial Satellites: The Creation of a Debris Belt." *Journal of Geophysical Research* 83 (1972).
14. Bess, T. D. *Mass Distribution of Orbiting Man-made Space Debris*. NASA Technical Note D-8108, Langley Research Center, 1975.
15. Gurney, R. W. *Mass Distribution of Fragments From Bombs, Shells, and Grenades*. Report No. 448, Ballistic Missile Research Lab, Aberdeen Proving Grounds, 7 February 1944.
16. Bevington, P. R. *Data Reduction and Error Analysis for the Physical Sciences*. McGraw-Hill Book Company, New York, 1969.
17. Nebolsine, P. E., et al. *Debris Characterization Final Report*. Report PSI TR-399, prepared by Physical Sciences Inc. for Teledyne Brown Engineering, December 1983.
18. Su, S. -Y., *Reanalyzing the Number Versus Size Distribution of the Impact Data in the Report PSI TR-399 "Debris Characterization."* Lockheed Memo to D. J. Kessler, 14 March 1984.
19. King-Hele, D. *Theory of Satellite Orbits in Atmosphere*. Butterworth and Company, London, 1964.
20. Johnson, N. L., et al. *History of On-Orbit Satellite Fragmentations*. Report No. CS84-BMDSC-0018, Teledyne Brown Engineering, August 1984 (revised February 1986).
21. Johnson, N. L. "Artificial Satellite Breakups (Part 1): Soviet Ocean Surveillance Satellites." *Journal of the British Interplanetary Society* 36 (1983): 51-58.
22. Ross, S. "The Orbital Motion of Pellet Clouds." *Journal of Astronautical Sciences* 8 (1961): 79.
23. Moulton, F. R. *An Introduction to Celestial Mechanics*. 2d ed., MacMillan, New York, 1958.
24. Fuss, J. T. *Dynamics of Explosion Remnants in Earth-Orbits*. Master's thesis, Old Dominion University, July 1974.
25. Dennery, P. *An Introduction to Statistical Mechanics*. George Allen and Unwin Ltd., Norwich, England, 1972.
26. Eyring, H. *Statistical Mechanics and Dynamics*. John Wiley and Sons, New York, 1964.
27. Hameen-Anttila, K. A. "Statistical Mechanics of Keplerian Orbits." *Astrophysics and Space Science* 43 (1976): 145-174.
28. Heard, W. B. "Dispersion of Ensembles of Non-interacting Particles." *Astrophysics and Space Science* 43 (1976): 63-82

29. Heard, W. B. *An Analysis of the Breakup of Satellite 1974-103A (COSMOS 699).* NRL Report 7991, Naval Research Laboratory, 23 April 1976.
30. Heard, W. B. "Asymptotic Distribution of Particles From Fragmented Celestial Bodies." *The Astronomical Journal* 82 (1977).
31. Dasenbrock, R. R., et al. "Satellite Disintegration Dynamics." AAS Paper 75-040, presented at AAS/AIAA Astrodynamics Specialist Conference, 28-30 July 1975.
32. Dasenbrock, R. R., et al. *Dynamics of Satellite Disintegration.* NRL Report 7954, Naval Research Laboratory, 30 January 1976.
33. Heard, W. B. *Satellite Breakups: A Survey of a Dynamical Theory.* NRL Memo Report 3802, Naval Research Laboratory, July 1978.
34. Morgan, T. H. "Preliminary Design of an Earth-based Debris Detection System Using Current Technology and Existing Installations." *Orbital Debris,* NASA Conference Publication 2360, NASA, 1985, pp. 150-163.
35. Neste, S. L. "In Situ Orbital Debris Experiment Concepts." *Orbital Debris,* NASA Conference Publication 2360, NASA, 1985, pp. 134-149.
36. Kessler, D. J. "Proposed Preliminary Design Criteria Model Environment for the 1990's." *Orbital Debris,* NASA Conference Publication 2360, NASA, 1985, pp. 78-83.
37. Meirovitch, L. *Methods of Analytical Dynamics.* McGraw-Hill Company, New York, 1970.
38. Gabbard, J., and Wackernagel, H. "Satellite Breakups." AAS Paper 71-351, presented at the Astrodynamics Specialist Conference, 17-19 August 1971.
39. *The Long Duration Exposure Facility (LDEF) Mission 1 Experiments.* NASA SP-473, NASA, 1984.
40. Wilbeck, J. S., et al. *BMD Impact Phenomonology Data Base: Bibliography.* Southwest Research Institute, April 1982.
41. Bjork, R. L., and Olshaker, A. E. *The Role of Melting and Vaporization in Hypervelocity Impact.* RAND Memo-3490-PR, RAND Corporation, May 1965.
42. Sanguinet, J. A. "Satellite-based Instrument Concepts for the Measurement of Orbital Debris." *Advances in Space Research* 5 (1985): 59-62.
43. Reynolds, R.C. "Design Considerations for Orbiting Detectors for the Large Low-Earth Orbit Debris Population." *Advances in Space Research* 5 (1985): 63-75.
44. Carey, W. C., et al. "Space Shuttle Microabrasion Foil Experiment (MFE): Implications for Aluminum Oxide Sphere Contamination of Near-Earth Space." *Advances in Space Research* 5 (1985): 87-90.
45. Kuczera, H., et al. "Two-Stage Acoustic Penetration and Impact Detector for Micrometeoroid and Space Debris Application." *Advances in Space Research* 5 (1985): 91-94.
46. Bjork, R. L., and Olshaker, A. E. *A Proposed Scaling Law for Hypervelocity Impacts Between a Projectile and a Target of Dissimilar Material.* RAND Memo RM-2926-PR, RAND Corporation, May 1965.
47. Computer program BREAKUP. Developed by Teledyne Brown Engineering, Colorado Springs, Col., from the NASA simulation DIFRAG.
48. McKnight, D. S. *Simulation of On-Orbit Satellite Fragmentations.* Ph.D. dissertation, University of Colorado, Boulder, Col., 1986.
49. Curtis, A. R., ed. *1986 Satellite Handbook.* ARCSoft Publishing Company, 1986.
50. Bate, R. R.; Mueller, D. D.; and White, J. E. *Fundamentals of Astrodynamics.* Dover Publications, Inc., New York, 1971.
51. Roy, A. E. *The Foundations of Astrodynamics.* MacMillan Company, New York, 1965.

Chapter 4

Hazards From Space Debris

As spacecraft become larger and the missions longer in duration, the danger from orbiting space debris and meteoroids increases greatly. While the Shuttle may be expected to suffer a catastrophic collision only once every 10,000 years, a space station 100 meters in diameter may have a 10% chance of being struck by a large piece of space debris within just a 10 year span (1). Although these calculations are based on our admittedly imperfect knowledge of the numbers and masses of space debris currently in orbit about the Earth, a consensus exists that current estimates are still probably conservative. Already, during the few years that the space debris environment has been actively studied, the assumed magnitude of the debris population has been adjusted upward manyfold.

As previously noted, the design criteria for spacecraft shielding for low to medium Earth orbits are now generally driven by the space debris population instead of the meteoroid population. Meteoroids having a mass of 1 gram or greater can be expected to impact a square kilometer area less than once a year (38). This is a much smaller flux than that calculated for radar tracked space debris of the same size. Nevertheless, the space debris population is still not precisely known.

The uncertainties in our debris environment assessments include the number density, the mass, and the size of the debris. Experiments on the Long Duration Exposure Facility (LDEF) are designed to measure space debris impacts directly in order to better understand the space debris environment and to determine the resulting hazard space debris poses to operational spacecraft.

Debris measurement studies and analysis of impacts to Apollo, Skylab, and Explorer spacecraft have provided valuable insight into the debris environment. The simulation of satellite breakups discussed in Chapter 3 helps to clarify the probable state of the nontrackable debris population, which at the present time is the most poorly defined aspect of the debris population. Unfortunately, direct measurement of space debris is time-consuming, limited in its overall applications, and expensive. For these reasons, spacecraft hazards due to space debris are typically developed using a combination of observations, theory, and modeling.

First, simple impact theory is needed. The spacecraft engineer must know how much shielding is necessary, based upon mission requirements, to protect the spacecraft from a collision with a piece of orbital space debris of specific size. The hypervelocity impact tests discussed in the previous chapter are useful, but a simpler penetration approach (developed for meteoroid impacts) proves beneficial at this point. As new composites are used on spacecraft, more impact testing will have to be conducted for these new materials (1).

Before impact theory can be used to define shielding requirements, predictions must be made concerning the nature, i.e., how many and what size, of the debris which will probably impact the spacecraft. The estimated number density, mass density, mass, and velocity of impacting debris must be available to the spacecraft design engineer. These quantities are derived by using results from extrapolations of actual debris data, debris models, and space-borne impact experiments, each of which is applicable to limited areas of the total debris population assessment. Since the debris hazard is a function of orbital altitude and inclination, the combination of a number of hazard assessment procedures is necessary to produce a comprehensive representation. The projected debris environment, tempered by an appreciation of the present hazard from debris, causes even greater alarm because the aspects that lead toward an increased debris hazard are also increasing; namely, larger spacecraft, longer mission durations, and the possibility that collision-induced breakups have already occurred.

The hazard to people on Earth from reentering space debris will not be covered in this chapter, and only the special case of radioactive debris reentering the Earth's atmosphere will be examined in Chapter 5. In the early years of the space age, there was much concern about satellites dropping out of the sky. The probability of personal injury from reentering space debris was found to be less than that for meteorites (on the order of one in a thousand chances) (10). Since the total thermodynamic load on a reentering object is inversely proportional to its flight path angle, most small orbiting

fragments will never survive to the Earth's surface. Approximately 500 meteorites impact the Earth annually from the more than 10,000 meteors which enter our atmosphere. Only about 500 space debris fragments even encounter Earth's atmosphere each year with the majority of these fragments disintegrating before reaching the ground. Detailed information on research conducted in the 1970s in this area of debris hazard may be found in references 10-12.

In the last few years a number of dramatic reentries of Soviet and American spacecraft have raised the awareness of the potential hazard of reentering space debris. In 1985 the European Space Agency sponsored a workshop on this topic, in part to examine the ability to estimate the time and location of reentering space objects (43). Though it was noted that the hazard of reentering space debris to the general population is still quite low, the uncertainty associated with well-publicized reentering space objects, such as Skylab, has caused unwarranted public alarm nonetheless.

Impact Theory

For years the meteoroid environment has driven shielding requirements, but research conducted during the 1970s showed that the artificial debris environment has, for the most part, become the most probable source of spacecraft damage. A meteoroid typically has a velocity of 20 km/s or greater and a density of about 0.05 g/cm^3, whereas a piece of space debris in low Earth orbit typically has a slightly lower velocity of 7-8 km/s but a density of 2.0 to 8.0 g/cm^3. Due to the orbital nature of artificial space debris the relative velocity for a collision between an operational satellite and a piece of space debris, both in low Earth orbit, is about 9-11 km/s (15, 16, 33). Consequently, the damage expected from the impact of space debris is likely to be more severe than from meteoroids. A difference in hazards also develops because of different population sizes and because space debris may linger in orbit for years while a given meteoroid passes through the near Earth environment only once.

From current measurements the estimate of the space debris population equals or exceeds that of the meteoroid population at low altitudes and in most sizes (13). Although space debris may be made of a number of different materials having a wide variation in densities, for this section on impact theory a simplifying assumption will be made; namely, that the space debris, as well as the target structure, primarily consists of aluminum (ϱ = 2.7 g/cm^3). Considering the history of spacecraft construction, an aluminum projectile striking an aluminum target is a fairly likely scenario for a spacecraft encounter with space debris.

Bjork developed a model to describe a hypervelocity impact of this type (14; II-48). Bjork's equation was originally developed for meteoroid impacts as were three other impact theories outlined in reference 14. The other three equations provide the flexibility of analyzing many different collision scenarios which may be of importance in examining impact damage for spacecraft constructed of new and different materials. By incorporating the material characteristics of aluminum in the other three equations, results similar to those obtained using Bjork's equation are found.

The equations of Whipple, Kornhauser, and Summer are given below without further comment, while Bjork's equation, which follows, is examined in more detail. Whipple's equation is

$$P = K_1 (1/\pi\varrho\epsilon)^{1/3} E^{1/3} \qquad (4.1)$$

where
- P = penetration depth in a thick target material
- K_1 = constant of proportionality
- E = meteorite (debris) energy
- ϱ = density of target material
- ϵ = heat of fusion of target material

Kornhauser's equation is

$$h = K_2(T/E)^{1/3} (E/E_o)^{0.09} \qquad (4.2)$$

where
- h = penetration (depth of crater)
- K_2 = constant of proportionality
- T = kinetic energy of projectile
- E = modulus of elasticity of target
- E_o = reference modulus

Summer's equation is

$$P/d = 2.28(\varrho_P/\varrho_T)^{2/3} (V/c)^{2/3} \qquad (4.3)$$

where
- P = penetration depth in a thick target material
- d = diameter of projectile
- ϱ_P = density of projectile
- ϱ_T = density of target
- V = projectile velocity
- c = speed of sound in target material (5.1×10^5 cm/s for aluminum)

Of these alternative equations Summer's is the easiest to work with and uses the most convenient parameters. Bjork's equation for an aluminum-aluminum collision is given below.

$$P = 1.09 (MV)^{1/3} \qquad (4.4)$$

where P = penetration depth in cm
M = projectile mass in grams
V = impact velocity in km/s

The velocity of the projectile and target for our space debris encounter problem would be their orbital velocities. Yet, the average impact velocity of two Earth satellites at altitudes below 2,000 km has been calculated to be between 9 and 11 km/s. Additionally, satellites in near polar orbits ($i \leqslant 90°$) will generally encounter larger relative velocities than those in orbits of lower inclination. A 10 km/s value will be used as an average value to simplify calculations. A more detailed discussion of relative velocity calculations and the effect of orbital inclination on collision probability will follow later in this chapter.

Some typical results of using Bjork's equation are shown in Table 4.1. Moreover, a later Bjork paper (37) developed a penetration-to-projectile diameter ratio (P/d) for an aluminum-aluminum impact for various impact velocities. The penetration depth (in parentheses in Table 4.1) comes from the P/d ratio of 3.2 for a 10 km/s impact.

Before discussing the results from Table 4.1, it is interesting to note that the potential RCS of the 10 gram projectile may vary by an order of magnitude. Using the building block approach with a typical spacecraft density, the 10 gram particle will be represented by a 0.00049 m^2 RCS. The RCS-to-mass conversion developed by Kessler in reference 15 predicts an RCS of 0.005 m^2. Neither of these values is large enough to be reliably measured by NORAD.

Results from the Table 4.1 should seem alarming: a 10 gm (centimeter-sized) particle traveling 10 km/s may penetrate a 5 cm thick aluminum plate, which is, of course, many times the thickness of current spacecraft walls. As noted earlier, a particle of this size cannot be measured by NORAD at any altitude. Fortunately, the lethality of this situation is mitigated by the collision probability modes, which are to follow, that show such encounters have a very low probability of occurring at this time.

However, the problem of spacecraft survivability is not as simple as determining a penetration depth. Sometimes a penetration might not result in the fragmentation of the satellite; instead it may only cause a degradation of its ability to perform its mission. This is particularly true if the particle strikes an appendage such as a solar panel or hits the spacecraft at a very oblique angle. The hypervelocity tests discussed in Chapter 3 have also shown that a target may just be cratered or penetrated without a catastrophic fragmentation occurring. It can be concluded that whether or not a particular collision causes significant damage depends largely on the size and velocity of the projectile as well as on the physical construction and the importance of the area impacted (1).

Another factor whose importance was discovered in the hypervelocity impact tests is that of spacecraft internal pressurization. Those structures which were pressurized (up to 1 atmosphere) on the average sustained greater damage due to the creation of extremely high pressure waves on impact. NASA is presently in the process of developing system damage criteria which combine the physics of the hypervelocity impact with unique spacecraft functions and vulnerabilities (1). This simple impact theory merely serves to illuminate the danger of orbital debris and the importance of having a dependable, realistic debris model.

As an interesting example, one might ask if a piece of debris having an RCS value of 0.01 m^2 will penetrate a 10 cm thick aluminum skin. Assume that the debris is made of aluminum and that the parent satellite (source of the debris) had a spacecraft density of 0.03 gm/cm^3 and a characteristic thickness of 7.5 mm. Using the three RCS-to-mass conversion techniques, 0.01 m^2 may equate to 202.5 gm, 340 gm, or 30 gm (circular disk, $M = 62 \times 10^3 (A_c)^{1.13}$, and building block, respectively). Thus, the penetration depths would be 13.79 cm, 16.39 cm, and 7.29 cm, respectively. Therefore, two out of three methods indicate that the debris will penetrate, while the building block approach calculates that it will not. Note, however, that 10 cm is many times thicker than virtually all spacecraft wall structures. Therefore, all debris models indicate that the 0.01 m^2 fragment will easily penetrate a typical spacecraft wall and, in fact, will probably cause extensive damage to the vehicle.

Table 4.1 Results From Bjork's Equation.

Diameter (cm)	0.10	0.21	0.44	0.96	2.1	4.5
Mass (gm)	0.01	0.10	1.00	10.00	100.0	1000.0
Penetration (cm)	0.51 (.32)	1.09 (.67)	2.35 (1.41)	5.06 (3.07)	10.9 (6.72)	23.48 (19.40)

Debris Models

As early as 1966 the hazards from orbital debris (natural and artificial) were being scrutinized by NASA for the Apollo missions and again in the 1970s for the Skylab missions. In the early 1970s the results of these and other studies concluded that only large structures ("greater than 100 meters in diameter") had any significant probabilities of collision with man-made debris (Figures 4.1 and 4.2). More studies during the 1970s showed that the nontrackable debris could be a factor of 2.5 greater in number than the cataloged population and that collisional fragmentations could be a major source of debris by the 1990s (13). All these observations caused concern and

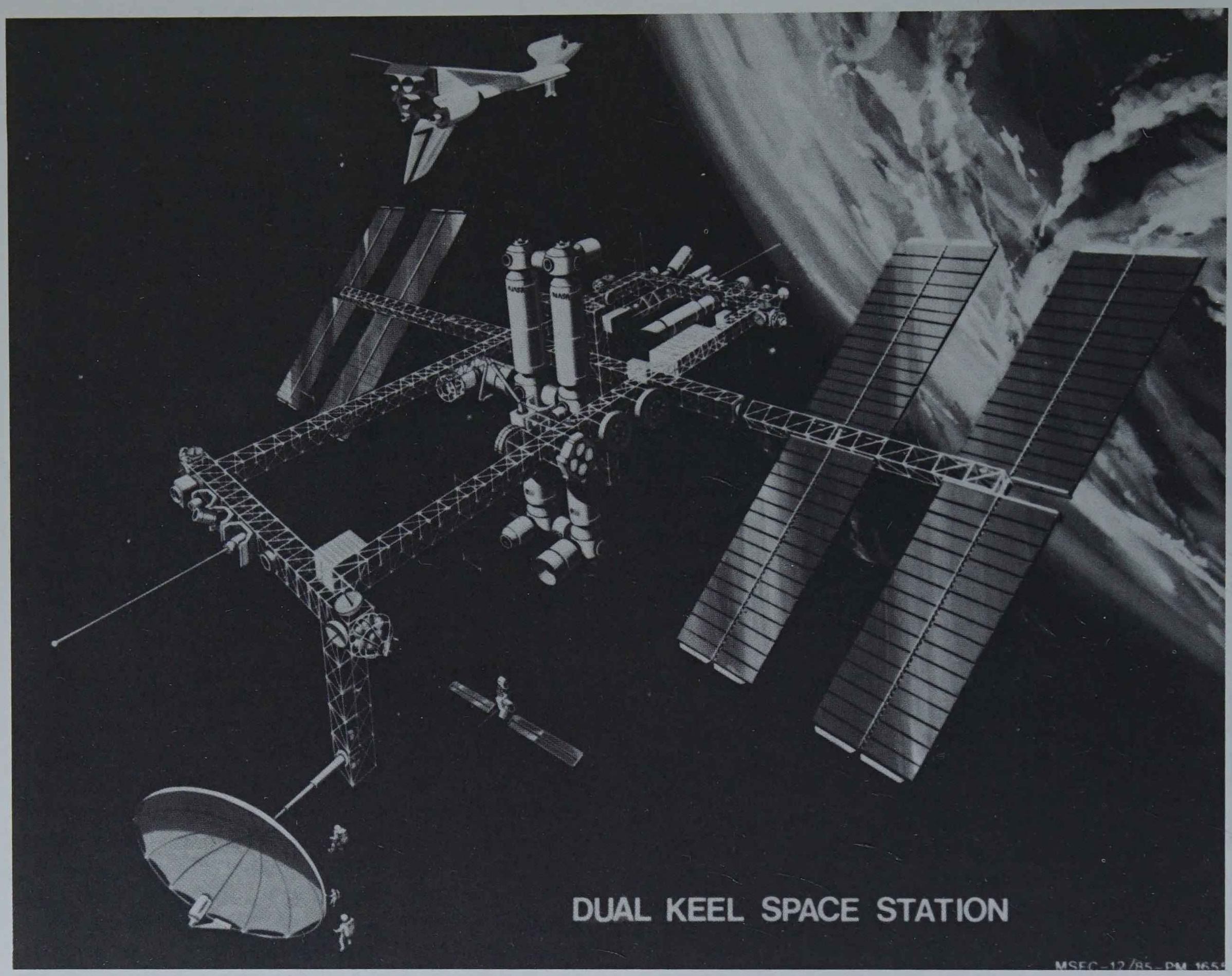


Figure 4.1 Large orbital structures with long lifetimes are exceptionally vulnerable to collisions with space debris. *Courtesy of NASA.*

prompted the aerospace community, most notably NASA, to begin to develop models for collisional probabilities to quantify the hazard to spacecraft from space debris.

Many factors must be taken into account in these models. The hazard due to space debris can generally be said to be a function of the size of the spacecraft, the size and number of debris fragments in the orbital regime traversed by the spacecraft, and the duration of the spacecraft's mission (18). The size of the spacecraft and the length of its mission are reasonably well-known quantities. Yet, some ambiguity still exists since size must be measured relative to the approaching projectile. This approach angle may vary greatly and thus the area of the spacecraft exposed to the debris may also vary. For example, assume that there are two objects at the same altitude but with inclinations of 60 and 30 degrees, respectively. The collision angle may be either 30 or 90 degrees. This difference in collision angles equates to relative velocities of 3.62 km/s and 9.90 km/s for objects with an orbital velocity of 7 km/s. Thus, the relative velocity between two objects of known altitude and inclination may vary considerably, adding another uncertainty in the survivability analysis.

The major problem in the development of debris models is estimating the size and number of debris fragments at a given altitude. Although NORAD provides a catalog of all the Earth satellites which its tracking system detects, two problems remain. First, the tracked debris is measured and given an average RCS value. This value, as mentioned earlier, may vary due to fragment shape, fragment orientation, and measurement inaccuracies. Additionally, the radar measurements tell the observer almost nothing of the composition of the fragment. Since most satellites are made of a wide variety of materials with various radar reflectivity properties,

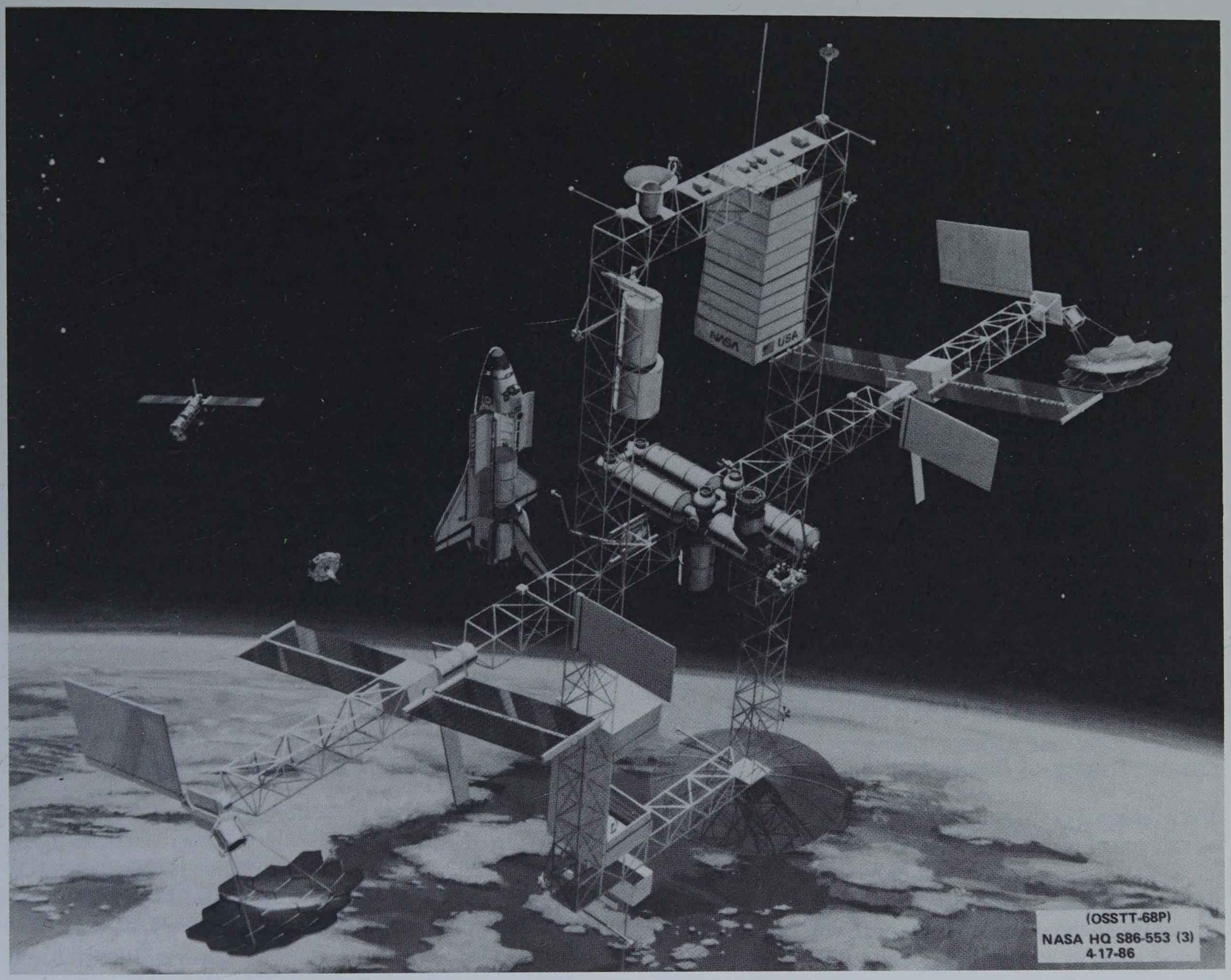


Figure 4.2 Maneuvering complex structures like this space station will be difficult but possibly necessary to avoid large pieces of space debris. *Courtesy of NASA.*

knowing the parent satellite does not clearly identify the makeup of individual fragments.

The second problem with debris-tracking capabilities is that a large number of potentially lethal fragments are not detected by NORAD. The contribution of unobserved debris to the collision hazard represents the major unknown in current collision hazard assessments. Correction factors to the observed population have been derived by examining the raindown of debris through the atmosphere, extrapolation of ground-based explosion experiments, extrapolation of space-borne impact experiments, and the optical measuring of space debris from the Earth. The average correction factor of all these techniques is about 5 to 10 for low to medium Earth orbits.

In developing debris models, three major concepts usually play an important role. First, atmospheric drag and solar pressure are the primary disturbing forces exerted on debris and are presently the only mechanisms cleansing the near Earth environment of debris. This decay process is accelerated by increased solar activity (20, 41). Second, debris at high altitudes may be affected only minimally by atmospheric drag and thus may stay in orbit for thousands of years or longer. This situation has the potential for creating a "self-regenerative" belt of debris (15). Third, debris which is too small to be tracked by radar has been measured optically while still in orbit or as it reentered the Earth's atmosphere. In the latter case, radar detection of debris ionization trails has proved valuable.

These phenomena hint at the existence of large reservoirs of debris at much higher altitudes to produce such a large flux of low altitude debris. These reservoirs are analogous to the hypothesized Oort cloud, consisting

of primordial debris left over from the formation of the solar system, which is believed to orbit the Sun at distances beyond Pluto and may be the source of new comets. Another indication of a larger amount of debris circling the Earth is seen in the cataloging of pieces of debris years after a breakup because the fragment finally decays to a low enough altitude to be detected by NORAD. Recent improvements in the NORAD network overall sensitivity have also contributed to the increase in the known artificial debris population. An appreciation of the raindown effect (21) provides insight into why debris models are so difficult to develop: namely, the present environment is not completely known; it is ever changing due to natural effects; and unfortunately, it is ever increasing due to mankind's continuing space activities.

The four approaches to the calculation of hazard from space debris, discussed below, depict a variety of technical and philosophical concepts even though they all use the same foundations. The unique characteristics of collision hazards at geosynchronous altitudes are also covered in the succeeding sections. This subject deserves special attention due to the importance of satellites in this regime and the special traits of geostationary orbits.

Kinetic Theory of Gases Approach

The collisional probability of Earth-orbiting satellites may be calculated through the use of kinetic theory of gases concepts (20). A number of assumptions are made about the arrangement of satellites in Earth orbit to approximate the spatial density of the objects. First, the orbital plane of all the debris fragments are the same as the parent satellite or of the trackable debris cloud. This is primarily true only for a short period of time after the creation of the cloud. Second, some pattern of decay of nontrackables must be assumed. Third, a ratio of nontrackables to trackables must be selected. Finally, the orbital planes of known satellites are assumed to be randomly distributed about the Earth.

The satellites distributed about the equatorial plane are measured in angular terms. The space is divided into toroidal sectors, ΔS, formed by the intersection of spheres of different altitudes and planes of different latitudes. The average number of particles per unit volume per unit time in the "toroidal belt" is the spatial density. Using the catalog of space objects tracked by NORAD, the spatial density may be calculated. By examining the *SATCAT,* the known population peaks between 800 and 1,000 km with smaller peaks at 1,400 km and 3,700 km evident. The spatial density of trackable objects versus altitude is very well known but it is how this spatial density is used to calculate collisional probabilities which produces the difference between various debris models.

The frequency of collision may be given as

$$C = \frac{1}{2} \sum AVD^2 \Delta S \qquad (4.5)$$

where
A = effective cross-section
V = relative collision velocity
ΔS = volume of toroid
D = spatial density

As developed by Sehnal (20) the relative velocity is approximated by

$$V = 7.0(1 - \cos i_1 \cos i_2) \text{ km/s} \qquad (4.6)$$

where i_1 and i_2 are the orbital inclinations of the two colliding objects. This equation will always give values less than or equal to 7 km/s. There are other methods which have produced larger values for the average relative velocity between a satellite and a piece of space debris in low Earth orbit. By using the tracked debris population provided by NORAD, the average relative velocity may be calculated through numerical simulation of possible encounters or through direct averaging (16, 33). Both of these methods derive an average collision velocity of approximately 10 km/s. Figures 4.3 and 4.4, adapted from reference 33, show the range of relative velocities for various altitudes and orbital inclinations.

The effective cross section, A, is the sum of the average radar cross section (RCS) of the two particles upon impact. The average RCS value taking into account all the trackable objects has been calculated to be 2.9 m² (23). Using a more recent database, the authors calculated the average radar cross section of all Earth-orbiting objects

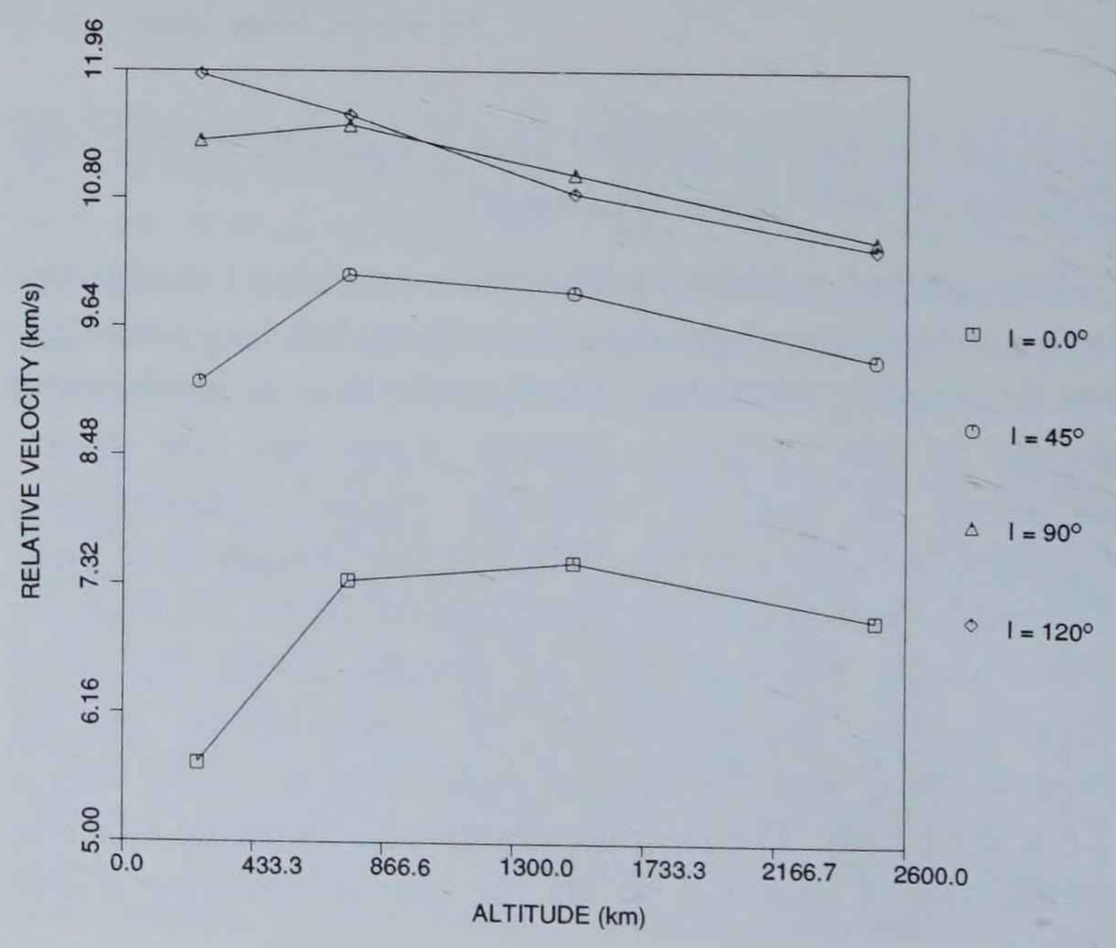


Figure 4.3 The average relative velocity expected between an object and a piece of space debris is a function of both the altitude and inclination of the object.

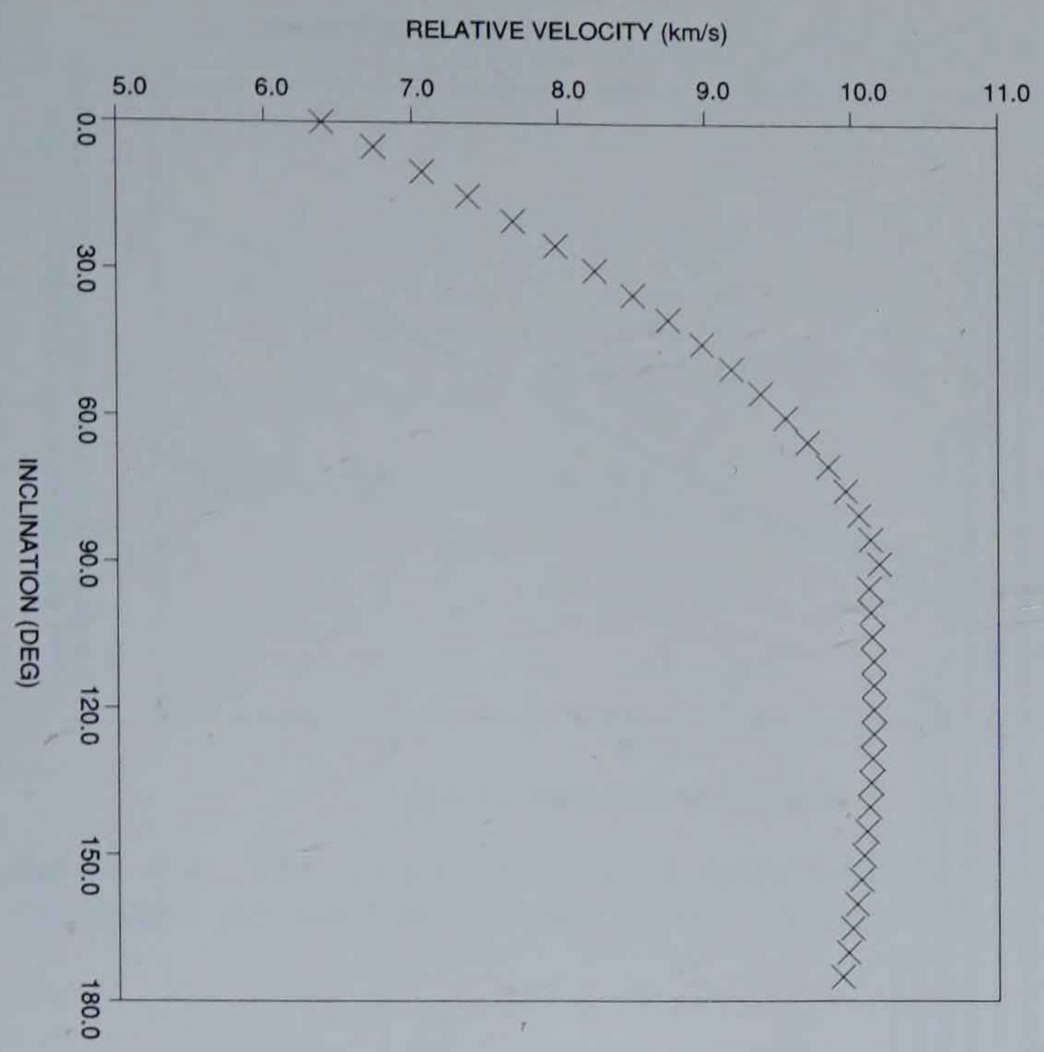


Figure 4.4 Across all altitudes, high collision velocities can be expected for objects in retrograde orbits.

and found it to be 4.42 m² as of 1 April 1987 (Figure 4.5). This change in average RCS for debris is probably due, in large part, to improved measurements and data reduction rather than to a physical change in the environment.

Using the model, the largest collision frequency will occur in the region most populated with debris; namely, 800 to 1,000 km altitude. The theory estimates that there is a 63% probability that a major collision will occur within one decade using the 1978 debris population (20). The known satellite breakup presently considered to be the most likely subject of an accidental hypervelocity collision took place at an altitude of about 1,000 km in 1981.

This model provides a very good physical approach to the collisional hazard problem with the use of simple geometrical concepts. The assumptions used to determine the one collision per decade estimate are limiting but valid. With an assumed increase in spatial density one would expect that collisions would be more probable now than in 1978. Despite the simplicity of this model, its results compare very favorably with more sophisticated models.

Hazard as Function of Altitude Approach

Again, in developing a collisional model the spatial density must be calculated. The trackable population is taken from the NORAD database while the nontrackable population must be estimated. A common way to predict the nontrackable debris population is to extrapolate data taken during terrestrial explosion tests (25). The mass distribution shown in eq. 4.7 is taken from reference 26:

$$N = \begin{cases} 1.71 \times 10^{-1} M_t \exp(-0.02056 M^{1/2}), & M > 1936 \text{ gm} \\ 8.69 \times 10^{-4} M_t \exp(-0.05756 M^{1/2}), & M < 1936 \text{ gm} \end{cases} \quad (4.7)$$

where N = cumulative number of fragments with masses greater than M
M_t = total mass of pre-explosion target.
M = mass of fragment

A series of "compartments" are formed to contain debris fragments. Each compartment is defined by the parameters of the fragment which are known. Kessler and Su (25) selected the semimajor axis, the eccentricity, and the object size as the pertinent parameters. One may select a different combination of parameters to provide insight into an alternate area of concern, but as selected, the model calculates collisional hazard as a function of altitude. No matter which parameters are selected, the resolution within the compartments must be chosen carefully. For example, the width of the compartments associated with small values of orbital eccentricity must be much smaller, since most satellites have nearly circular orbits ($e = 0$).

The collision analysis proceeds using eq. 4.8 which is developed in reference 30:

$$C_{ij}/t = S_i S_j V \sigma_{ij} \Delta U \quad (4.8)$$

where ΔU = volume element
$S_i S_j$ = latitude-averaged spatial densities of compartments d_i and d_j (d being the size of the object)
V = relative velocity
σ_{ij} = collision cross section = $(d_i + d_j)^2/4$
C_{ij} = number of collisions between objects in compartments d_i and d_j
t = time

This approach is very similar to the one developed in the first section, but is more versatile. By summing the collisions over certain size and volume elements, characteristic collision rates can be calculated. Using 1983 NORAD debris data and results from laboratory experiments to extrapolate down to millimeter-sized objects, a collision rate of 0.26 collision per year is obtained for all altitudes below 2,500 km (25). Similarly, looking only at objects greater than 4 cm in diameter, the average collision rate is reduced to 0.04 collision per year. The lower collision rate is expected for the larger objects since there are considerably fewer of them.

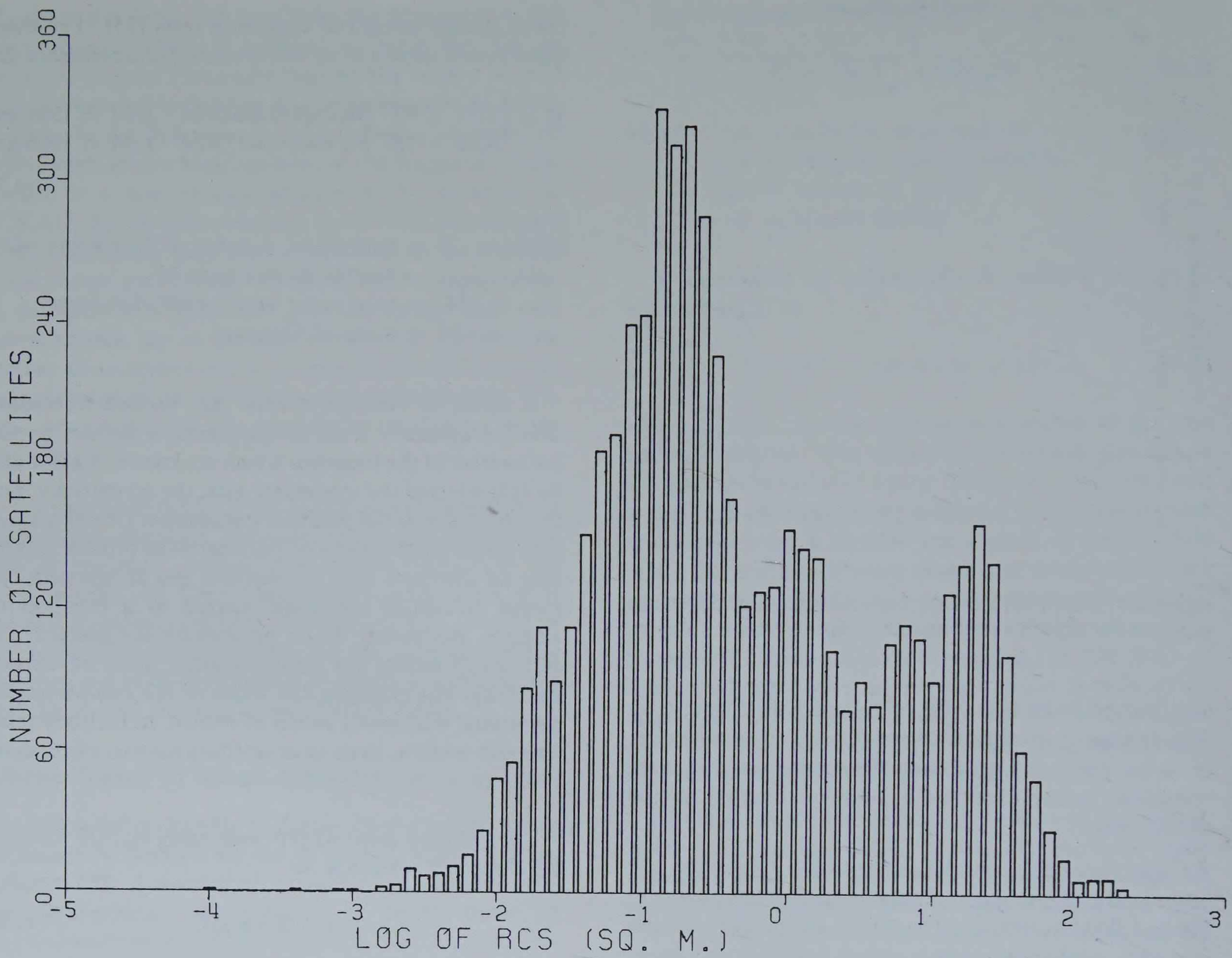


Figure 4.5 A recent examination of the *NORAD Satellite Catalog* indicated that the average radar cross section for Earth satellites is about 5 square meters.

Once the collision rate is found, a probability distribution may be developed to calculate collision probabilities. The Poisson probability distribution, also known as the law of rare events, is a good choice due to the infrequency of expected collisions (25). The Poisson distribution is given as

$$P_k = \frac{C^k \exp(-C)}{k!} \tag{4.9}$$

where k = number of collisions
C = average collision rate
P_k = probability of k collisions per year

Assuming the average collision rate is small, the probability of no collisions is the largest, the probability of one collision is smaller (an exponential decrease), and so on until the probability of N collisions is infinitesimal, where N is the number of particles in the model. The summation of all the probabilities from zero to N collisions will equal to one, since it represents all the possible outcomes of the event (25). Once a collision takes place, the two objects involved may be estimated through a series of probability calculations. After a collision is perceived, the same Poisson probability distribution is used to find the probable altitude of the collision. Next the sizes of the objects are estimated, again using the probability distribution.

A collisional hazard model may end at this point, but it is likely that a collision will create even more debris. From reference 25 the mass ejected due to a collision is

$$M_e = V^2 M_p \tag{4.10}$$

where M_e = ejected mass
V = collision velocity
M_p = projectile mass

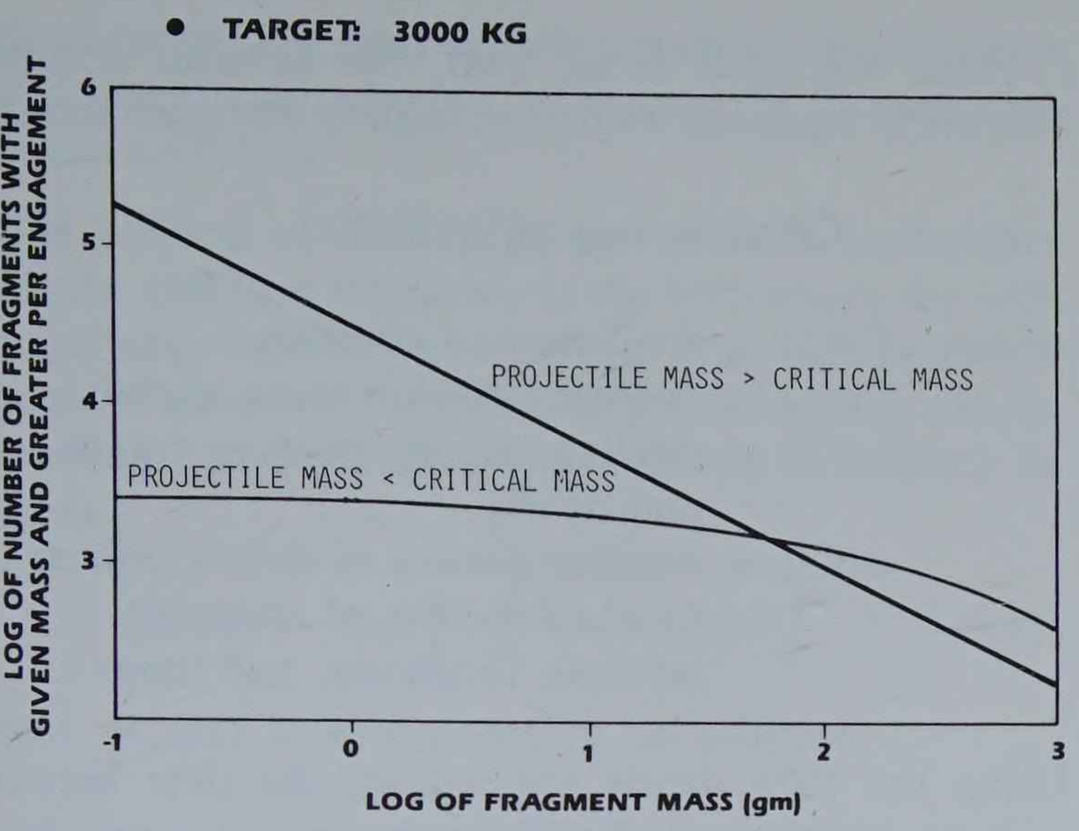


Figure 4.6 The critical mass in a hypervelocity collision determines the mass distribution of the resultant debris.

As discussed earlier, the mass distribution of the ejected mass is

$$N = 0.4478\ (M/M_e)^{-0.7496}. \qquad (4.11)$$

When the projectile mass is greater than a certain percentage of the target mass, a collision will result in a catastrophic fragmentation. When the projectile mass is less than this critical mass, the cratered target combines with the ejecta mass to form the complete mass distribution.

This critical percentage is greatly dependent upon the fabrication and composition of the colliding objects and upon the relative velocity at impact (15). If a typical spacecraft is impacted by a debris fragment (at 10 km/s) whose mass is at least two orders of magnitude smaller than its own mass, then a noncatastrophic collision will result. The subsequent ejecta mass will be at least 100 times as massive as the impacting debris particle. If the mass of the impacting object exceeds the 1% cutoff, the result will be a catastrophic fragmentation with the ejecta mass being constrained only by the mass available from the two colliding objects. Figure 4.6 illustrates the different debris distributions resulting from a 3,000 kg target being struck by two different projectiles: one less than the critical mass and one greater than the critical mass. Using these characteristics, even nonperfect observational data can give insight into the nature of the breakup.

Hazard as Function of Altitude and Inclination Approach

The model developed in the last section may be modified to calculate the hazard as a function of orbital altitude and inclination (latitude). In the previous development, however, the spatial density was latitude-averaged, eliminating the hazard distinction for different latitudes. A similar model, developed by V. Chobotov of Aerospace Corporation, uses a spatial density which is dependent on both altitude and inclination (16).

The collision probability in Chobotov's development is calculated in a manner similar to that used in the earlier approaches. The result is

$$P = 1 - \exp(-FA_s\Delta t) \qquad (4.12)$$

where P = probability of collision
F = number of encounters per unit time per unit area
A_s = projected area of spacecraft
Δt = time interval

For very small probabilities (less than 0.1) the probability may be approximated by the exponential term. Thus

$$P = FA_s\Delta t \qquad (4.13)$$

Using 1981 NORAD debris data, this approach was used to calculate encounters between trackable objects and the Shuttle under typical missions. Table 4.2 shows the results. Under the present development, the above encounters may be converted into collision probabilities by using a 10 meter radius for the Shuttle.

Taking into account the orbital inclination of the target satellite has shown an interesting trend; namely, that the likelihood of collision increases as the orbital inclination increases. Thus, retrograde orbits have a higher probability of colliding with trackable debris. This fact is a direct consequence of the distribution of debris in low Earth orbit. Mission planners should pay special attention to this phenomenon, particularly for satellites in polar orbits. Kosmos 1275, considered by many to have been a victim of an accidental hypervelocity collision, was not only in a 1,000 km high orbit but also operated in a near polar orbit of 83 degrees inclination.

Path Integral Approach

The three debris models already discussed have much in common. They all basically calculate a collision rate between orbiting objects using the data provided by NORAD, often extrapolated to include nontrackable

Table 4.2 Encounters and Collision Probabilities for 4-Day Shuttle Missions.

Inclination	Number of Encounters	Collision Probability (10^{-6}/yr)
28.5	67	15.3
57.0	79	18.0
98.0	108	24.7

debris. This collision rate is then used to derive a collision probability through the use of a simple probability distribution, usually the Poisson distribution function. All of the models show that the hazard arising from collision with debris depends on the size of the target, the size and number of projectile objects, and the target's mission duration.

A slightly different approach, yielding nearly identical results to these models, uses a path integral formulation for calculating collision probabilities (44). Instead of looking at bins of debris described by an altitude and/or orbital inclination, the hazard is examined along a specific orbit, i.e., path. This approach was employed by Kessler and Su in reference 25. In addition to using a path integral formulation, this approach also introduces another new concept. That is, that the velocity distribution of debris can be used in the calculation of collision probabilities. This approach accommodates the calculation of "the hazard increase introduced by a specific debris deposition event" (44).

From Reynolds et al. (44), the familiar collision frequency equation written in slightly different terms is

$$\dot{C}(\vec{r},t) = \sigma_{TOT}\, n(\vec{r},t)\, V_r(\vec{r},t) \qquad (4.14)$$

where $\dot{C}(\vec{r},t)$ = frequency of collision
σ_{TOT} = average collision cross section
$V_r(\vec{r},t)$ = relative velocity between target and debris
$n(\vec{r},t)$ = number density of debris objects (n is a function of altitude, latitude, longitude, and time)

Using the 1976 debris population, the time between collisions (reciprocal of collision frequency) is calculated for a large range of collision cross sections. Assuming, a 5% annual growth of debris from 1976 to 1996, the time between collisions for 1996 can be projected. These results are plotted in Figure 4.7 The figure shows the typical sizes for the spacecraft for a variety of missions. The greater hazard for large spacecraft in long term orbits

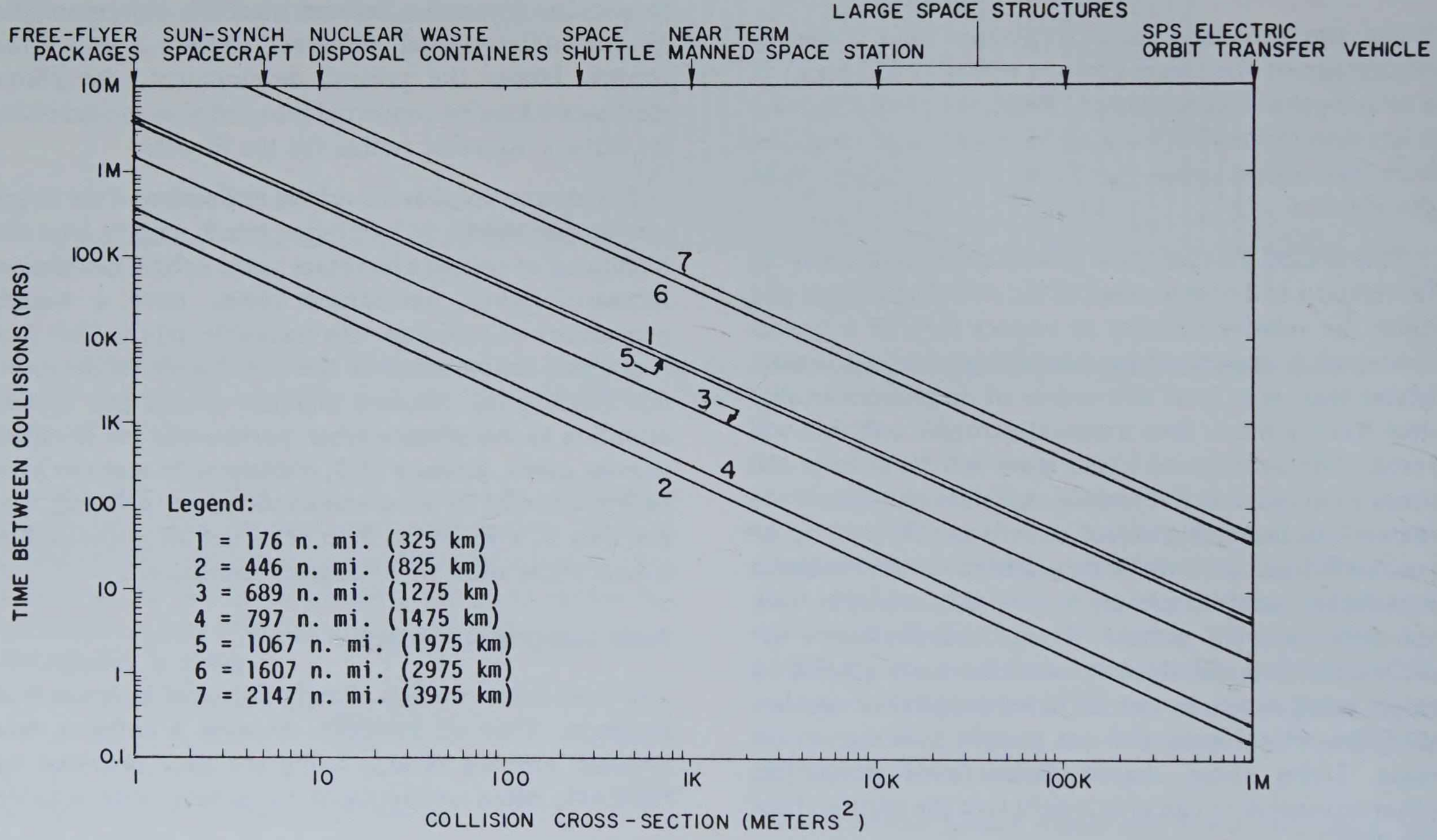


Figure 4.7 This chart by Reynolds using a 1976 satellite database predicts the probabilities of collision for a variety of spacecraft in the year 2006. *Courtesy of R. C. Reynolds and N. H. Fischer.*

is clearly seen. The most densely populated debris region (800-1,000 km altitude) has, of course, the shortest time between collisions.

The method of calculating the collision probability from the collision frequency is the area where the path integral approach differs from the other debris hazard models. The collision probability relationship can be calculated by integrating the collision frequency as follows:

$$P_{NC}(t_o) = \exp\left[-\int_o^{t_o} \dot{C}\left(\vec{r}(t),t\right)dt\right] \qquad (4.15)$$

where $P_{NC}(t_o)$ = probability of no collision
t_o = elapsed time.

Therefore, the collision probability can be written as

$$P_C(t_o) = 1 - P_{NC}(t_o)$$

where $P_C(t_o)$ is the probability of at least one collision.

It should be noted that the spatial density used in this development kept its dependence on altitude and latitude and a velocity distribution was formed for each debris fragment compartment. A typical Shuttle mission is again used to show characteristic collision hazards. Table 4.3 summarizes the time between collisions for a series of Shuttle inclinations at an altitude of 300 km.

These numbers compare favorably with all the previous models, i.e., the Shuttle may expect one catastrophic collision every ten thousand years with the present debris population. Additionally, all models show greater hazards for orbits of higher inclination, peaking around i = 120 degrees.

Hazard to Geosynchronous Satellites

The hazard to geosynchronous satellites from space debris is an area of increasing concern. Most space-faring nations and organizations with assets in the geostationary ring have recognized this problem and some have begun to remove inactive (failing) spacecraft from the regime to mitigate the cluttering in this unique natural resource. The removal of inactive satellites is not yet a general policy, but it may become necessary in the near future since about 20 satellites and their associated launch debris are added to the already crowded geostationary ring annually (35).

This policy of creating a disposal orbit for useless satellites, a sort of elephant's graveyard in space, has not been internationally accepted due to a number of recognized drawbacks. First, the removal of a satellite from geostationary orbit may create more of a hazard to other satellites than it would eliminate. For example,

Table 4.3 Time Between Collisions for the Shuttle.

Inclination	Time Between Collisions (10^4/yr)
28.5	2.7
56.0	2.0
98.0	1.4

the byproducts of rockets may present a hazard to other spacecraft; also, during rocket firing there is always the possibility of an explosion. Furthermore, due to solar-lunar perturbations and solar radiation pressure, an object in a disposal orbit, even as much as 100 km above geostationary altitude, will eventually migrate back into the lower geostationary ring.

Second, the implementation of this policy is not without expense. Maneuvering satellites out of the geostationary ring requires propellents which could in many cases be used to extend the operational lifetime of the satellite, thus providing additional revenues. The reliability of a growing number of geostationary communications satellites is greater than their station-keeping fuel supplies.

The four modeling approaches outlined earlier in this chapter have only dealt with low Earth orbits. In these orbits objects will be traveling between 7 to 8 km/s with widely varying inclinations. Therefore, as previously discussed, relative collision velocities will have an average range between 9 and 11 km/s. Objects in low Earth orbit are also transient in nature since drag and solar pressure acting on them will cause these objects to reenter the Earth's atmosphere in a comparatively short time.

In contrast, the orbital velocity of geosynchronous satellites is only 3.075 km/s with very small inclinations for active satellites, i.e., usually less than 5 degrees. With these orbital parameters, the average relative velocity will be only about 100 to 500 m/s between geosynchronous objects, with a maximum of 800 m/s. At geosynchronous altitudes the smallest particle which can be detected and tracked by the NORAD space surveillance network is about 1 meter in diameter. Even without any satellite breakups at geosynchronous altitudes, as many as 2,000 nontrackable pieces of debris may be regularly passing through the geostationary ring (27).

In geostationary orbit each object remains relatively fixed above one point on the equator. The station-keeping fuel needed to keep from drifting away from this point is typically a few percent of the spacecraft mass per year. Some orbital regions above the Earth's equator are much more in demand than others for obvious commercial and strategic reasons. At these points there is an increased risk of collision due to longitudinal bunching. It has been calculated that the collision hazard for the FLTSATCOM satellite located at 100 degrees west longitude is about a

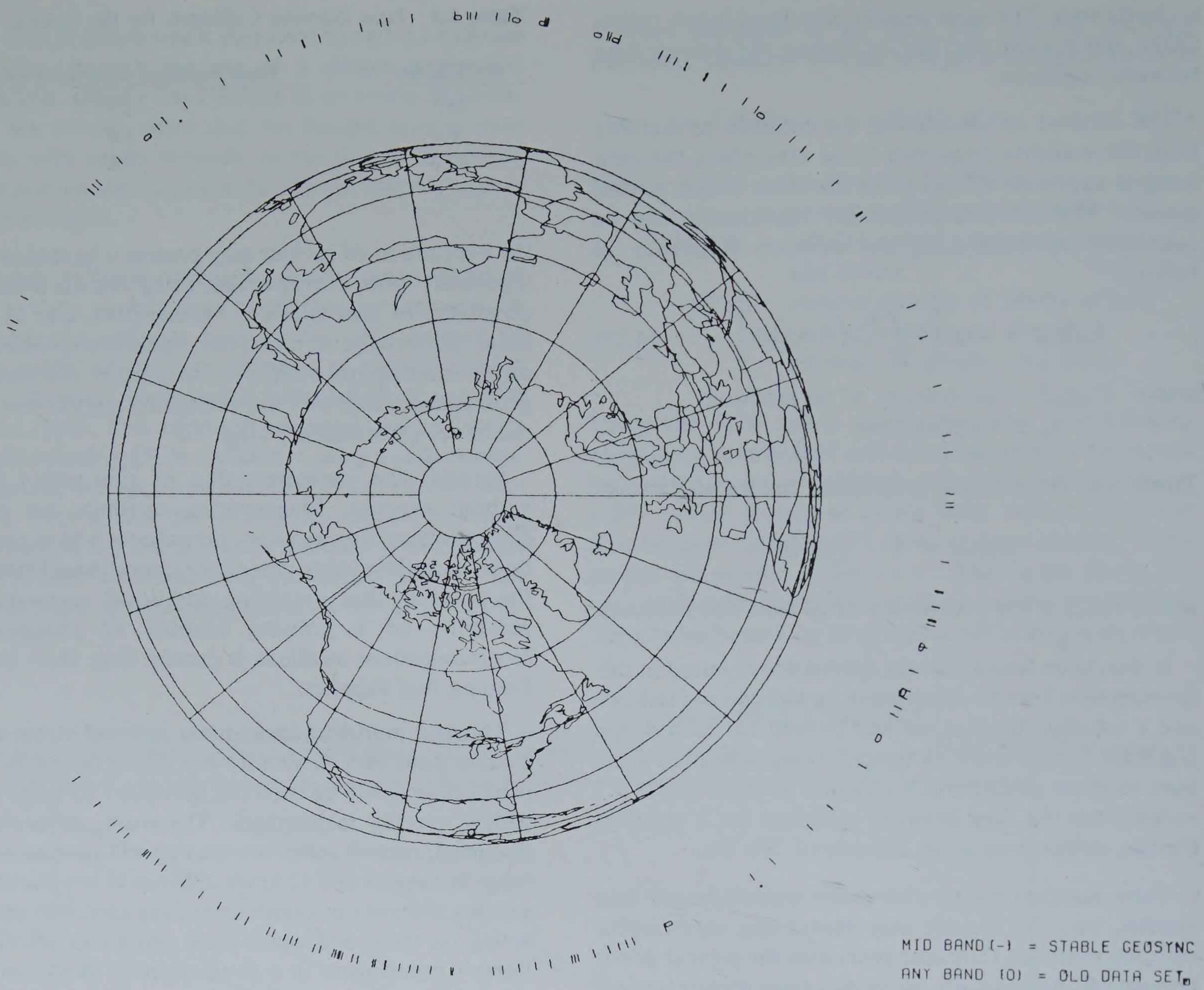


Figure 4.8 As of 1 July 1987, the distribution of geosynchronous satellites was relatively uniform, although some pockets of higher density do exist.

hundred times greater than for the average geosynchronous satellite (16). The importance of this grouping of satellites at certain points on the geostationary ring is highlighted by examining the dimensions of the ring itself. The length of the geostationary band, the circumference of a circle with a radius of about 43,000 km (35,785 km plus the radius of the Earth), is about 265,000 km. There are over 300 trackable objects in near geostationary orbits, providing 900 km between satellites if they were evenly spaced. Figures 4.8 and 4.9 show the populations of active and inactive satellites about the geostationary ring. Obviously, the satellites are nearly uniformly distributed, but there are a number of more densely populated regions.

In addition to having areas of high demand, there are also longitudes to which satellites are naturally attracted. The gravitational field of the Earth causes the migration of objects toward longitudes 105 degrees west and 75 degrees east. Unfortunately, these libration points are also in areas of commercial and strategic significance where operational spacecraft are often stationed. Although this drift rate about the libration points is very slow, these regions may constitute areas of increased probability of collision in the future.

Besides the longitudinal drifting, geosynchronous satellites also experience the slow inclining of their orbits due to solar and lunar perturbations. A maximum inclination of 15 degrees may be expected. Thus, inactive satellites will oscillate along the equator and across the equator in a slow periodic fashion. This situation has caused the geostationary ring to be likened to a "shooting gallery" (27) in which inclined satellites pass through the geostationary ring twice each day.

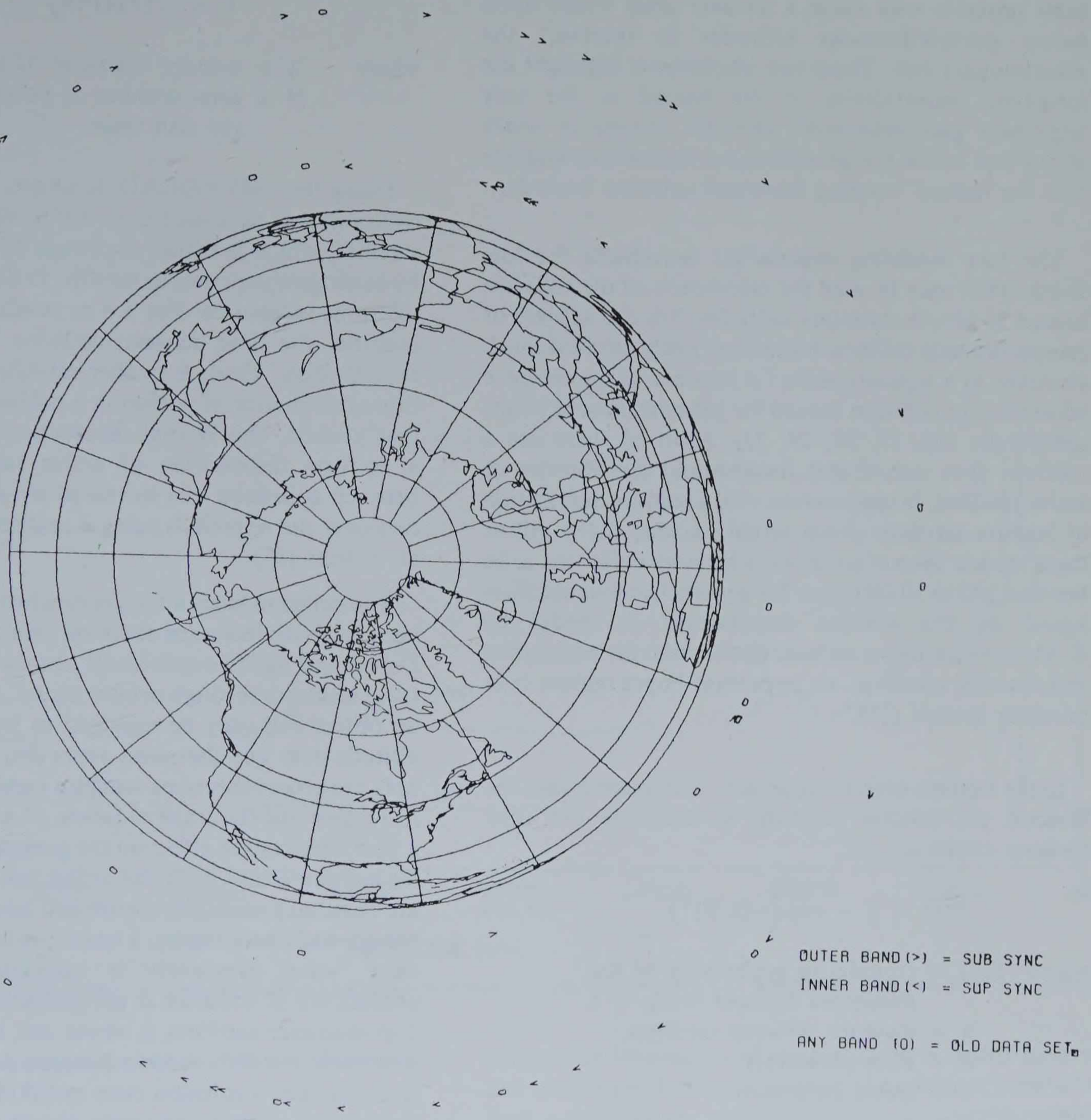


Figure 4.9 This figure illustrates the position of nearly geosynchronous satellites and their direction of motion relative to the geostationary belt. These are the satellites which pose collision hazards to the geosynchronous regime.

With the growing number of inactive satellites, spent rocket stages, and assorted launch debris, the collision hazard to operational geostationary spacecraft is of concern. The hazard to active satellites is already great enough at this time to require the use of collision avoidance maneuvers (16). The Air Force Satellite Control Facility presently watches for objects that pass closer than a few hundred kilometers to a group of essential communications and surveillance satellites. If the pass is estimated to be in the tens of kilometers, the owner of the satellite is notified and the two objects are closely watched.

Once it appears that the objects will pass within less than ten kilometers, means to avoid the encounter are reviewed. Actual maneuvers may be conducted if estimates of the separation distance close further. As noted by V. Chobotov, "for certain objects the position error can be equal to or greater than the predicted miss distance" (16). This observation points out a difficult aspect of the study of collision hazard to geosynchronous satellites. Besides poor size resolution of geosynchronous objects, satellite orbital parameters are not usually known precisely.

When a satellite is placed into a geosynchronous orbit, usually a rocket body is left in a transfer orbit. These rocket stages may intersect the geostationary ring at their apogee points creating a hazard to operational spacecraft. The same perturbations which could make a disposal

orbit unstable may cause a transfer orbit which starts below geosynchronous altitudes to intersect the geostationary belt. These two phenomena highlight the long-term uncertainties of the hazard at the very important geosynchronous altitude: objects in orbits above and below the geostationary region may migrate into the regime, creating increased collision hazards.

The four modeling approaches introduced for low Earth orbits may be used for calculation of the collision hazard at geosynchronous altitudes, but the subject of geosynchronous collision hazard has justly received much attention as a separate entity. A number of papers have addressed the collision hazard for geosynchronous orbits specifically (16, 17, 28, 29, 35). Most of these use a uniform (but unrealistic) longitudinal distribution of active satellites, in conjunction with a realistic distribution of inactive satellites (from actual tracking data). All of these models determine the time between collisions to be between 500 to 10,000 years for geosynchronous satellites based on the present population. A model by B. McCormick uses a realistic distribution for both active and inactive satellites, an important improvement over previous models (17).

In the realistic-realistic approach, McCormick uses the Weibull distribution function to calculate the time between collisions, i.e.,

$$F(x) = 1 - \exp\left(-(x/\beta)^{\gamma}\right) \qquad (4.16)$$

where $F(x)$ = cumulative probability of the minimum distance being $< x$
x = distance between satellites
β = scale parameter
γ = shape parameter

This function is appropriate for this application since as the separation distance approaches a very large number, the cumulative probability approaches one. This probability approaches one since it encompasses all physical collision situations: from no separation distance to an extremely large distance between the satellites. The probability also tends toward zero as the separation distance approaches zero. In other words, the probability of the center of mass of two satellites being in the same location at the same time is infinitesimally small for the present population. A collision is then defined as occurring when the average diameter of the target and the projectile combined exceed the separation distance. Thus the probability of collision is equal to the cumulative probability, F(x), times the total number of potential collisions per unit time. The time between collisions is simply the inverse of the probability of collision per year and can be calculated by

$$T = 1/\left(F(x)*N\right) \qquad (4.17)$$

where x = average diameter of satellites
N = total number of potential collisions per unit time.

Using the 1983 NORAD database, the time between collisions was calculated to be 600 to 900 years for a 50 m satellite, which is within the range of values calculated by other geosynchronous satellite collision models using the same target size. For a 5 m satellite, which is more realistic, the time between collision increases to over 10,000 years. Thus, a smaller satellite has a one in ten thousand chance of suffering a collision during a year-long mission. This Weibull distribution was also used with a uniform distribution of active satellites. The time between collisions was increased by almost a factor of two over the approach using a realistic distribution for all objects (17).

The collision hazard for geosynchronous satellites has been receiving increased attention over the past few years. Debris and inactive spacecraft cannot be removed from these altitudes through orbital decay. At these altitudes, an object will only be expected to lose 1 kilometer of altitude over one thousand years due to drag (27). Not only are geosynchronous satellites expensive and difficult to replace but the fragmentation of a satellite will have a very long-lasting effect on the geosynchronous regime. By assuming that both the active and inactive satellites are essentially randomly distributed (see Figure 4.8) about the geostationary region, a lower probability of collision than found previously is calculated. The present probability of collision at geosynchronous altitudes for 5 m diameter satellites is about one in one million for a one year mission. A 50 m diameter satellite may expect to experience a collision once every 10,000 years. Thus, the hazard using a randomly distributed population is smaller by a factor of from two to ten compared to using realistic distributions of active and inactive satellites. This trend has been noted by many scientists and is in part a manifestation of the longitudinal bunching and libration point problems.

Over the last ten years the capability and desire of the space faring countries to launch geosynchronous missions has led to a constantly rising collision hazard. It is estimated that by the year 2000 the chance of collision will increase by over three orders of magnitude from the present hazard to a 5% chance of collision per year.

An increase in the debris population at geosynchronous altitudes could be cataclysmic. The estimated fragment addition from just one satellite breakup could increase the probability of collision markedly. The mere addition of 1,000 debris fragments (tens of thousands can be expected from a collision-induced breakup of moderate

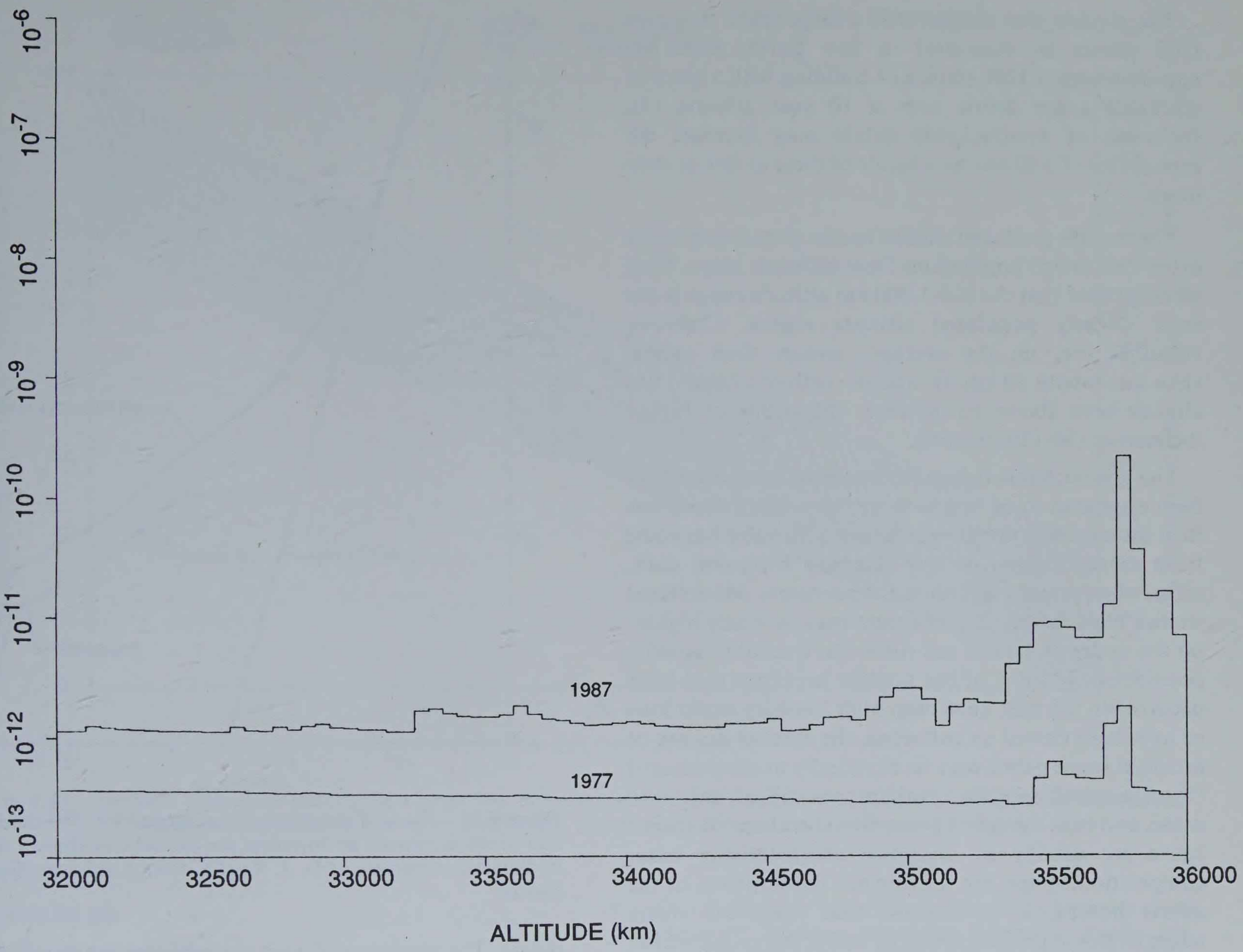


Figure 4.10 The spatial density at geosynchronous altitudes increased by about two orders of magnitude between 1977 and 1986.

magnitude) could increase the probability of collision by a factor of four (35).

A recent examination of known Earth satellites does show a significant increase in spatial density at geosynchronous altitudes even though no satellite fragmentations have been observed at these altitudes. Figure 4.10 overlays the satellite spatial densities for 1977 and 1986 in the near geosynchronous region. In 1977 the maximum spatial density in the geostationary region was less than one order of magnitude greater than the average background hazard at high altitudes. By 1986 the spatial density was over two orders of magnitude greater than the 1977 level.

Summary

All hazard models, no matter how they are formulated, show the dependence of hazard on the target's size, the debris environment (size and number) in the target's orbital regime, and the time in orbit for the target. An interesting illustration of the tradeoffs in debris hazard calculations is the examination of the collision hazard to Sun-synchronous satellites (19). Sun-synchronous satellites are placed in slightly retrograde orbits and usually at altitudes below 1,200 km. These parameters suggest a higher probability of collision than is associated with the typical low altitude, low inclination orbits. Yet, due to the characteristically smaller size of most Sun-synchronous spacecraft, the debris hazard is mitigated, and the collision probability is comparable to that of the Shuttle in posigrade orbits (about one collision every ten thousand years).

The formulations of all the debris hazard models use the same basic concepts. These concepts are summarized well by Kessler in the development of the collision probability between Jupiter's outer moons (30). The derivation is general enough, however, to be used as the basis for a variety of collision hazard models. Kessler also consolidates some earlier work (31, 32) conducted on collision probabilities.

The models also suggest that a large space structure (100 meters in diameter) in low Earth orbit has approximately a 10% chance of colliding with a piece of trackable space debris over a 10 year mission (1). Inclusion of nontrackable debris may increase the probability of collision by a factor of three to five or even more.

The models produced similar results even though they often used debris populations from different years. They all concluded that the 800-1,000 km altitude range is the most densely populated altitude region. Collision velocities are, on the average, greater than orbital velocities (about 10 km/s), and the collision hazard has already been shown to increase with orbits of higher inclination (90-120 degrees).

The nontrackable debris environment has historically been estimated to be two to three times more numerous than the trackable debris population. This value has come from extrapolations of low intensity explosion data, actual observations, and impact experiments. More recent studies have shown that this ratio may be much higher, on the order of five to ten times the trackable satellite population. If some of the satellite breakups that have occurred in the past have been high intensity explosions or have been caused by collisions, the number density of artificial space debris may be drastically underestimated (1). Almost 40 satellite breakups are still of unknown cause, and even the debris pieces from breakups of known cause are usually of unknown characteristics (size, composition, shape, etc.). From this development of the debris hazard, it is obvious that there are many uncertainties in the calculation of collisional probabilities: the extent of the nontrackable debris population, the collision fragmentation process itself, the physical characteristics of debris, and the cause of many breakups.

It is with this cautious background that a projected low Earth debris environment is introduced. Figure 4.11 displays the projected latitude-averaged debris flux for 1995 (15). Again it can be seen that the space debris population exceeds the meteoroid population at most altitudes over most particle sizes.

Figure 4.12 summarizes the magnitude of the debris hazard for low Earth orbit satellites now and in the future (42). The time between collisions will decrease and the collision probability will increase by an order of magnitude over the next 25 years. This hazard will increase for all types of satellites. The probability of collision for the Space Shuttle in a 1 year mission is projected to be only one in two-hundred by the year 2010.

The hazard from debris is much different for geosynchronous satellites than for low Earth satellites. At geosynchronous altitudes the debris population is much smaller in number and the collision velocities much lower, but there is no secular removal mechanism for

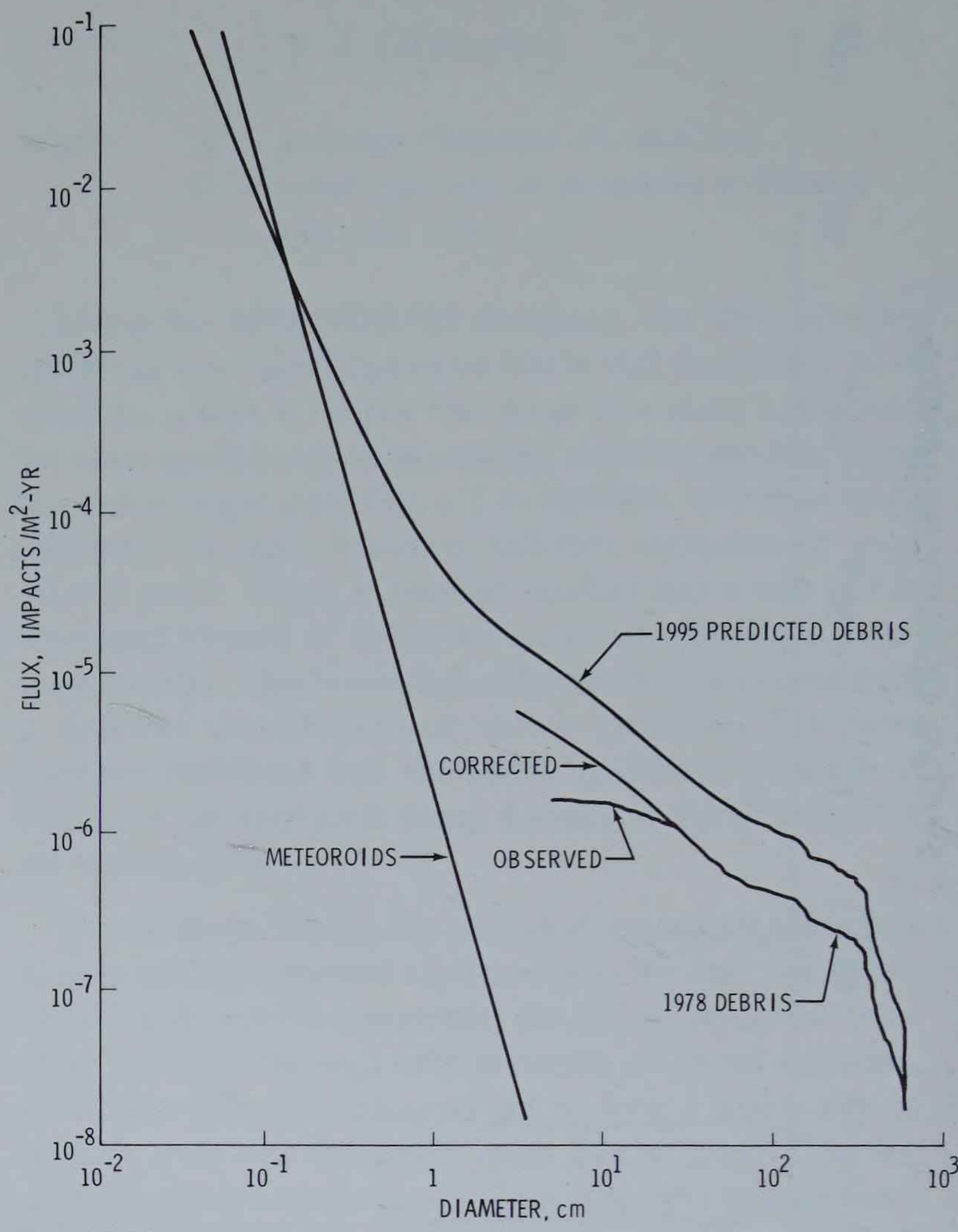


Figure 4.11 The artificial debris flux projected for 1995 exceeds that of the meteoroid environment for all particles above 1 mm in diameter. *Courtesy of D. J. Kessler, NASA Johnson Space Center.*

debris. The resulting collision probabilities are thus lower than for most low Earth satellites, yet the potential for long-term problems is quite high. The large, strategically important satellites in the geostationary ring would be very sensitive to just one breakup of the magnitude of the many Delta second stage fragmentations. The debris would linger nearly indefinitely. In addition, the debris pieces would tend to migrate toward the stable points on the ring while their orbital inclinations would vary slowly and periodically. This phenomenon could be disastrous and difficult to correct. As the vital sectors of the geosynchronous region become more and more crowded, the potential for such a catastrophe increases.

The models of the debris environment and the hazard from the debris provide valuable insight into our present situation. They illustrate the escalating population and collision hazards of the debris environment which, in the future, may lead to a curtailing of certain types of space activities. It is time to begin to develop methods to mitigate the severity of the space debris hazard to future space operations. Past, present, and proposed efforts to control the space debris environment are the subject of the next chapter.

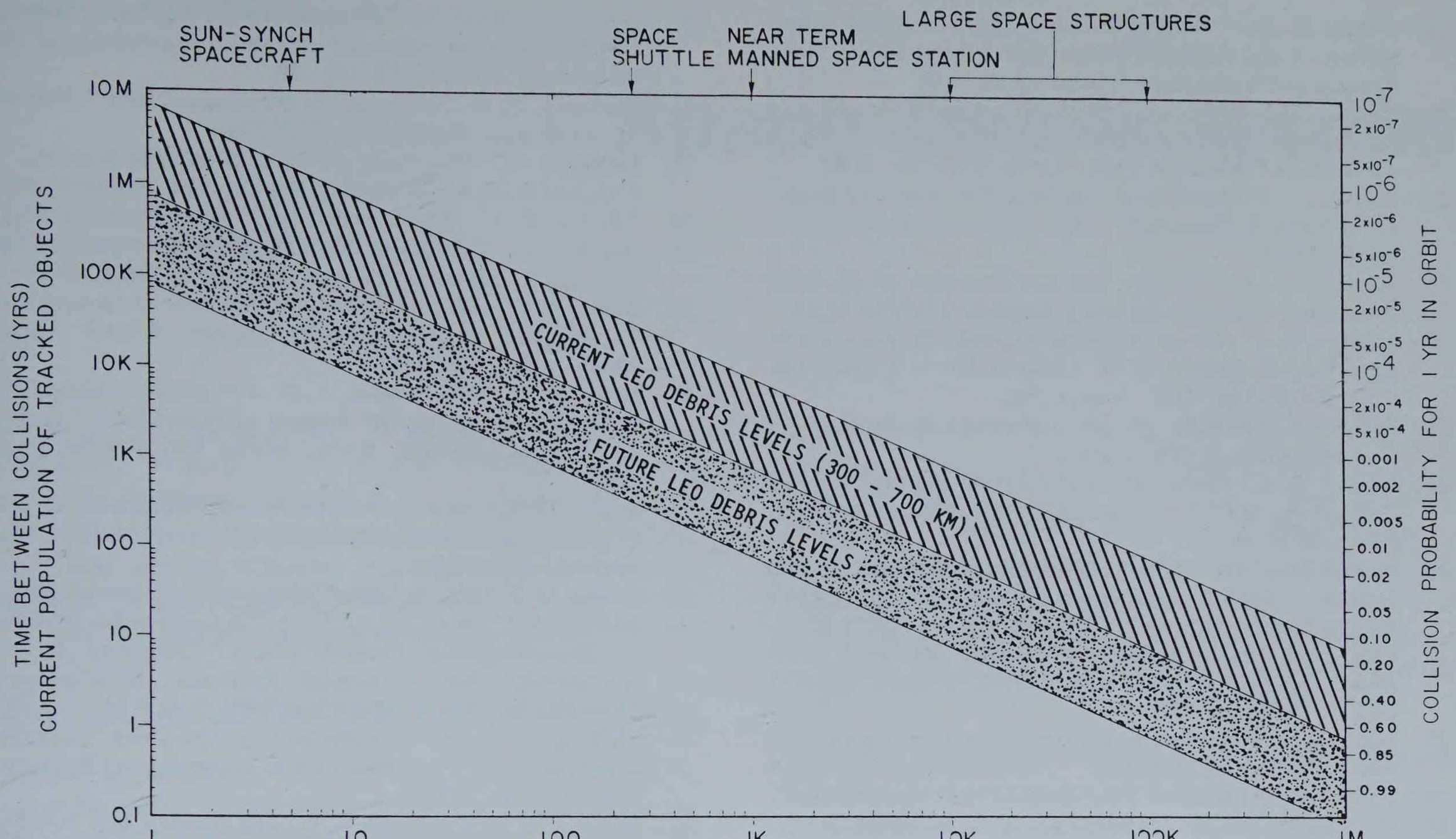


Figure 4.12 The time between collisions for a large, low altitude space structure and a member of the currently tracked satellite population is approaching unacceptable levels. *Courtesy of Edgecombe, Fischer, and Denning.*

References

1. *Orbital Debris.* NASA Conference Publication 2360, NASA, 1985.
2. Beck, A. J., and Bamford, R. "Solid Particle Environment and Protection for the Galileo Orbiter." *Orbital Debris,* NASA Conference Publication 2360, NASA, 1985, pp. 276-278.
3. Davis, E. E., and Sperber, R. "Space Debris Protection for a Reusable Orbital Transfer Vehicle." *Orbital Debris,* NASA Conference Publication 2360, NASA, 1985, pp. 279-286.
4. Kowalski, R. "Parametric Analysis: SOC Meteoroid and Debris Protection." *Orbital Debris,* NASA Conference Publication 2360, NASA, 1985, pp. 287-288.
5. Clanton, V. S., et al. "Hypervelocity Impacts on Skylab IV/Apollo Windows." *Orbital Debris,* NASA Conference Publication 2360, NASA, 1985, pp. 177-190.
6. Clanton, V. S., and Gooding, J. L. "Survey of Probable Micrometeor-sized Earth Orbital Debris Fragments in the NASA-JSC Cosmic Dust Sample Collection." *Orbital Debris,* NASA Conference Publication 2360, NASA, 1985, pp. 190-219.
7. Kessler, D. J. "Impacts on Explorer 46 From an Earth Orbiting Population." *Orbital Debris,* NASA Conference Publication 2360, NASA, 1985, pp. 220-232.
8. Grun, E., and Zook, H. A. "In Situ Detection of Micron-sized Dust Particles in Near-Earth Space." *Orbital Debris,* NASA Conference Publication 2360, NASA, 1985, pp. 233-245.
9. Cour-Palais, B. "Hypervelocity Impact Investigations and Meteoroid Shielding Experience Related to Apollo and Skylab." *Orbital Debris,* NASA Conference Publication 2360, NASA, 1985, pp. 247-275.
10. Edgecombe, D. S. "Orbital Debris Policy Issues, Battelle Involvement and Some Personal Observations." *Orbital Debris,* NASA Conference Publication 2360, NASA, 1985, pp. 402-409.
11. Drago, V. J., and Edgecombe, D. S. *A Review of NASA Orbital Decay Reentry Hazard.* Report No. BMI-NLVP-TM-74-1, Battelle Columbus Laboratories, Columbus, Ohio, 7 March 1974.
12. Edgecombe, D. S. *Skylab Special Analyses.* Report No. BMI-NLVP-LR-78-1, Battelle Columbus Laboratories, Columbus, Ohio, 25 April 1978.
13. Kessler, D. J. "Orbital Debris Issues." *Advances in Space Research* 5 (1985): 3-11.
14. Townsend, G., and Jensen, J. *Orbital Flight Handbook.* NASA SP-85, NASA, 1963.
15. Kessler, D. J., and Cour-Palais, B. "Collision Frequency of Artificial Satellites: The Creation of a Debris Belt." *Journal of Geophysical Research* 83 (1978): 2637-2646.
16. Chobotov, V. A. "Classification of Orbits With Regard to Collision Hazard in Space." *Journal of Spacecraft and Rockets* 20 (September-October 1983).
17. McCormick, B. "A New Technique for Predicting Geosynchronous Satellite Collision Probability." AAS Paper 85-374, presented at AAS/AIAA Astrodynamics Specialist Conference, August 1985.

18. Rugge, H. R. "Man-made Space Debris." AIAA report written by the Natural Environmental Panel of the Space Systems and Technology Workshop II, 1984.
19. Kessler, D. J. "Proposed Preliminary Design Criteria Model Environment for the 1990's." *Orbital Debris*. NASA Conference Publication 2360, NASA, 1985, pp. 78-83.
20. Sehnal, L. "Probability of Collisions With Artificial Bodies in the Earth Environment." *Advances in Space Research* 5 (1985): 21-25.
21. Johnson, N. L. "History and Consequences of On-Orbit Breakups." *Advances in Space Research* 5 (1985): 11-19.
22. Johnson, N. L. *History of On-Orbit Satellite Fragmentations*. Report CS-84-BMDSC-0018, Teledyne Brown Engineering, Colorado Springs, Col., August 1984.
23. Sehnal, L. *Bulletin of the Astronomical Institute of Czechoslovakia* 32 (1981): 310-315.
24. Kessler, D. J. "Sources of Orbital Debris and the Projected Environment for Future Spacecraft." AIAA Paper 80-0855R, July-August 1981.
25. Kessler, D. J., and Su, S. -Y. "Contribution of Explosion and Future Collision Fragments to the Orbital Debris Environment." *Advances in Space Research* 5 (1985): 25-35.
26. Bess, T. D. *Mass Distribution of Orbiting Man-made Space Debris*. NASA Technical Note D-8108, Langley Research Center, December 1975.
27. Suddeth, D. H. "Debris in the Geostationary Orbit Ring, 'The Endless Shooting Gallery.' " *Orbital Debris,* NASA Conference Publication 2360, NASA, 1985, pp. 349-364.
28. U.N. Committee on Peaceful Uses of Outer Space. "Physical Nature and Technical Attributes of the Geostationary Orbit." Prepared by the A/AC, 29 August 1977, pp. 105-203.
29. Hechler, M., and Van der Ha, J. C. "The Probability of Collisions on the Geostationary Ring." *Journal of the AIAA* 18 (July-August 1981).
30. Kessler, D. J. "Derivation of the Collision Prob-ability Between Orbiting Objects: The Lifetimes of Jupiter's Outer Moons." *Icarus* 48 (1981): 39-48.
31. Opik, E. J. "Collision Probabilities With the Planets and the Distribution of Interplanetary Matter." *Proceedings of the Royal Irish Academy* 54: 165-199.
32. Wetherill, G. W. "Collisions in the Asteroid Belt." *Journal of Geophysical Research* 72: 2429-2444.
33. McKnight, D. "Discerning the Cause of Satellite Breakups." Presented at the AAAS meeting, Boulder, Col., 1-5 April 1986.
34. Johnson, N. L. "The Crowded Sky." *Spaceflight* 24 (1982).
35. Hechler, M. "Collision Probabilities at Geosynchronous Altitudes." *Advances in Space Research* 5 (1985): 47-57.
36. Bjork, R. L., and Olshaker, A. E. *The Role of Melting and Vaporization in Hypervelocity Impact*. RAND Memo RM-3490-PR, May 1965.
37. Bjork, R. L., and Olshaker, A. E. *A Proposed Scaling Law for Hypervelocity Impacts Between a Projectile and a Target of Dissimilar Material*. RAND Memo RM-2926-PR, May 1965.
38. *Space and Planetary Environment Criteria Guidelines for Use in Space Vehicle Development*. NASA Technical Memo 82478, NASA, January 1983.
39. Kessler, D. J. "Junk in Space." *Natural History* (March 1982).
40. Mueller, A. C., and Graf, O. F., Jr. "A Study of the Lifetime of Geosynchronous Transfer Orbits." Presented at the AAS/AIAA Astrodynamics Specialist Conference, Provincetown, Mass., 25-27 June 1979.
41. McKnight, D. S. *Simulation of On-Orbit Satellite Fragmentations*. Ph.D dissertation, University of Colorado, Boulder, Col., 1986.
42. Edgecombe, D. S.; Fischer, N. H.; and Denning, R.S. "Policy Considerations in the Management of Orbital Debris." Presented at SDIO/IST Space Experimentation Workshop, Orlando, Fla., 17-19 June 1986.
43. *Re-entry of Space Debris*. Proceedings of an ESA workshop held at the European Operations Centre, Darmstadt, FRG, on 24-25 September 1985.
44. Reynolds, R. C., et al. "Man-made Debris in Low Earth Orbit - A Threat to Future Space Operations." *Journal of Spacecraft and Rockets* 20, no. 3 (May-June 1983).

Chapter 5

Space Debris Issues

Contrary to popular belief, during the last 20 years the worldwide annual space launch rate has remained virtually unchanged (Figure 5.1), yet during this same time interval the known Earth satellite population has increased sixfold. Clearly, this trend cannot continue without adversely affecting legitimate interests in the exploration and exploitation of space.

Recognition of the Space Debris Problem

The sheer immensity of space is the largest obstacle to the recognition of the space debris issue. For centuries the terrestrial seas, similarly thought to be nearly infinite in expanse, were the object of man's abuse and indiscriminate activity. The dumping of refuse and toxic materials into the seas was not only accepted, but often encouraged: better to pollute the seas than man's own habitat. The relief of man's burden was immediate and the consequences of his actions hidden - for a while at least. Because of the vastness of the oceans, few vessels ever encountered the effects of dumping, let alone were affected by it.

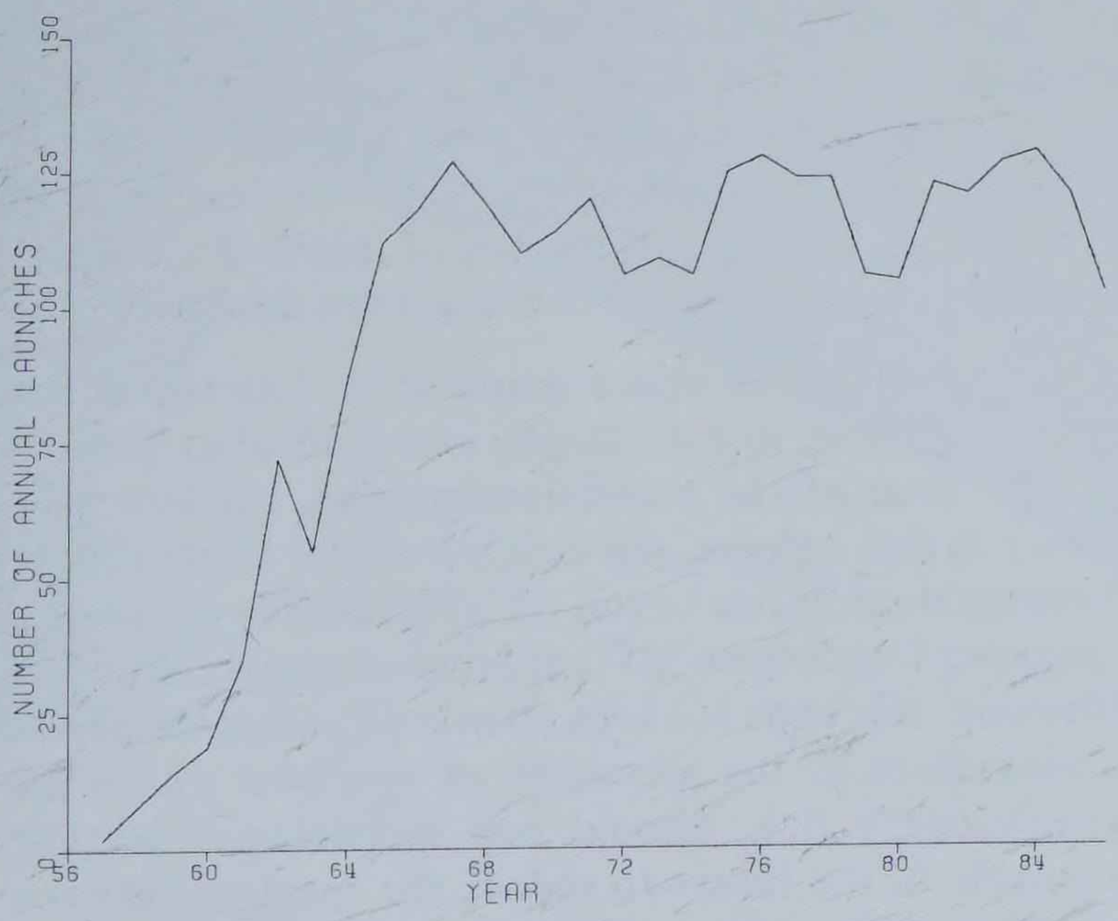


Figure 5.1 The international space launch rate has remained virtually unchanged for the past 20 years.

But the seas are finite after all, and eventually the signs of disease began to appear. Marine life began to disappear, beneficial coral reefs began to die, sightings of oil slicks and surface garbage became more frequent, and finally birds and even people who fed from the sea began to die. Not until people were directly threatened did the seafaring nations of the world come together to devise new regulations concerning their treatment of the seas.

So it has been with space. Spacefaring nations have yet to be touched by the space debris problem except in rare incidents of minimal importance. The replacement of a Shuttle window is not the thing about which crusades are made. However, the danger presented by the pollution of the sea of space is no less threatening to the future of mankind than is the pollution of the terrestrial seas. It has been said that the Earth is the cradle of man and that man must leave his cradle to grow. The pollution of space, then, threatens this evolution.

The state of space debris today should not be viewed apocalyptically. By all accounts space debris today does not pose a significant long-term hazard to operations in space. As water on a stove will continue to boil after the heat has been removed, the problem of space debris cannot be solved overnight. More importantly, if we wait until serious side effects of space debris manifest themselves, we may be too late.

In the United States, NASA has taken the leading role in the aerospace community to draw attention to the growing space debris problem. In July 1982, the NASA Lyndon B. Johnson Space Center hosted the first national conference dedicated to the issue of orbital debris. Participants included not only representatives from NASA and DOD—the primary users of space in the United States —but also from industry and a number of research and scientific organizations (1).

In 1981 NASA implemented a 10 year space debris assessment plan. Its goal is to lay a foundation for eventual U.S. and international agreements on the space debris issue (2). To this end the program plan is divided into three major areas: debris environment assessment,

debris hazard assessment, and space object management studies.

Before any estimate of the potential hazards of space debris can be made, the extent of the space debris environment must be better defined. NASA has adopted a three-pronged approach to tackling this task. First, ground experiments, primarily radar and optical tracking experiments and fragmentation tests, will be conducted with emphasis on understanding the nature of existing small orbital debris and debris mass and velocity distributions, respectively. Second, in situ experiments will be conducted. These experiments may call for dedicated sensors (radar, optical, infrared, or lidar) or they may merely take advantage of other planned flight activities, e.g., examining Shuttle surfaces and material brought back from Earth orbit. Finally, NASA envisions integrating this data into a three-dimensional, time dependent mathematical model which translates launch traffic models and the above noted data into particle flux as a function of impacting size and velocity on any particular spacecraft, i.e., as a function of orbital altitude and inclination.

The overall objective of the debris hazard assessment is to translate debris impact rates into spacecraft failure rates. This is accomplished by performing impact and systems damage assessment studies and by developing mission success assessment algorithms. These algorithms, an ambitious undertaking, will be designed for both engineering design studies and to determine the overall environmental cost to the spacecraft community. It is hoped that the spacecraft designer will be able to input the nature of a particular subsystem, its size, mission duration, and location in space, and obtain a reliability factor for that subsystem.

The final element of the forward-looking NASA program centers on the issue of space object management. To date this potentially effective technique has primarily been applied to the geostationary orbit. Space object management includes not only the control of the space environment, but also an assessment of the effectiveness of adopted control measures.

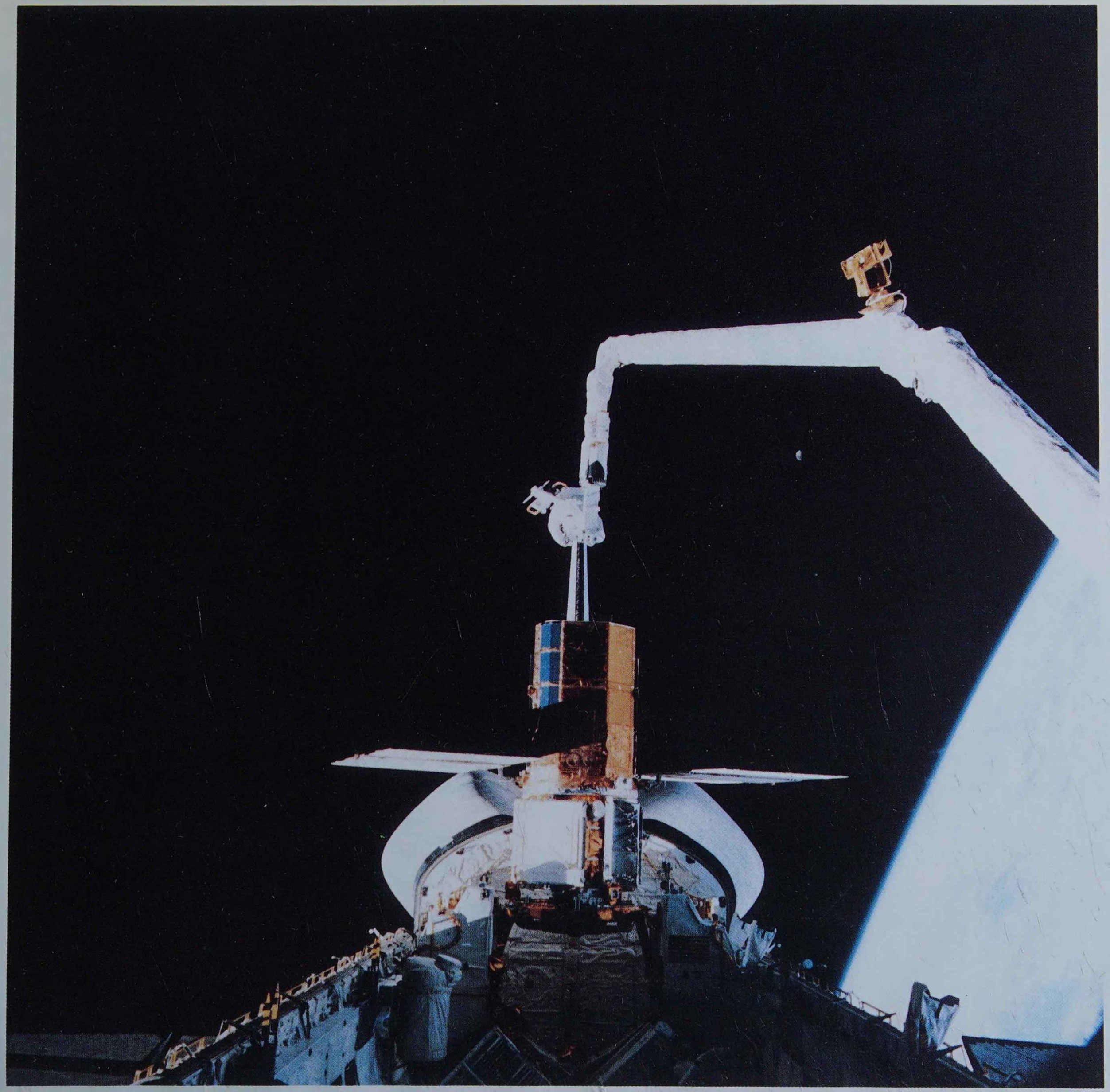
For its part, DOD has taken a much more cautious approach to the space debris question. Estimates made by DOD in 1982 indicated that space debris would probably not constitute a threat to DOD missions until after the year 2000 (3). Like NASA, DOD suggested emphasis now be placed on better defining the current debris environment. According to DOD, any proposed solution to the space debris problem should be examined critically with an eye toward cost effectiveness and international participation.

A year prior to the NASA space debris conference, the American Institute of Aeronautics and Astronautics (AIAA) issued a position paper on space debris (4). Their conclusions addressed both the near term and far term issues:

> At the present time, the collision hazard posed by space debris is real but not severe. However, continuation of present design and operational practices and procedures ensures that the probability of collision will increase and will eventually reach unacceptable levels, perhaps within a decade.
>
> The space debris issue should be faced by all space users, and coordinated action should be taken immediately if the future of space is not to be seriously restricted.
>
> Design to tolerate debris impact (bumpers) or to provide evasive capability may provide a measure of protection to particular satellites, but the most effective approach is to eliminate the need for such action by constraining the generation of further debris.
>
> The space debris problem can be forestalled by immediate action in five major areas:
>
> - Education
> - Technology
> - Space vehicle design
> - Operational procedures and practices
> - National and international space policies and treaties
>
> There is an immediate need for an international dialog to be initiated on the space debris issue, with the goal of forming responsible groups to coordinate research and recommend policy.
>
> Corrective action must begin now to forestall the development of a serious problem in the future.

Specifically in the area of operational procedures and practices, the AIAA recommended that consideration be given to safe spacing of satellites, avoidance of crowding specific orbit locations, limitation of planned explosions (e.g., ASAT tests) to low altitudes to allow fragments to reenter quickly, and the planning of launch trajectories for early reentry of spent rocket stages and dead payloads.

The international space community concern about space debris has, to date, largely been limited to the very narrow issue of the geostationary orbit. As indicated earlier in this volume, the concern of the International Telecommunications Union (ITU) is actually with radio frequency interference (RFI) at geosynchronous altitudes. However, this issue has been translated into space object management by the allocation of positions within the geostationary ring. Should new technologies become available in the future to reduce the spacings between satellites without increasing the potential for RFI, greater spacecraft densities will probably be allowed. Spacecraft spacings have already been reduced in recent years as





communications satellites employ higher frequency uplinks and downlinks. Removal of inactive geostationary payloads is also encouraged but not yet officially endorsed. An exception is the INTELSAT organization which has implemented a policy of geostationary satellite desynchronization.

At its plenary meetings in 1984 and 1986, the Committee on Space Research (COSPAR), an international scientific organization specializing in space research of all kinds, held workshops devoted exclusively to the topic of space debris. Although the majority of participants were from the United States, papers from Czechoslovakia, the European Space Operations Center, and West Germany indicated the awakening recognition of the space debris problem around the world. Notably absent from international forums on space debris has been the Soviet Union.



Figure 5.2 A piece of space debris was responsible for this dramatic impact found on a retrieved louver from the Solar Max satellite. *Courtesy of NASA.*

Living With the Present Environment

The easiest course of action - the path of least political and economic resistance - is simply to ignore the issue of space debris and to continue operational practices well-established during 30 years of space activity. While this philosophy may prove workable through the near term, (perhaps to the end of this century,) there is little doubt that such a policy would not be successful in the long term. However, minor alterations in space activities could be implemented with only small efforts which would increase the probability of mission success during this period of increasing space debris.

Wherever possible, the mission designer could select orbital parameters which would mitigate the probability of collision with space debris. Although mission requirements and orbit types are often intimately related, some missions can accommodate a surprisingly wide range of altitudes or inclinations. Low altitude navigation satellites operated by both the United States and the U.S.S.R. currently orbit the Earth at altitudes of 1,000-1,100 km. Such satellites could be moved into the less densely populated altitudes of 1,200-1,300 km without significantly affecting spacecraft design or mission performance. Likewise, a number of low altitude communications, intelligence, and geodetic satellite constellations could be modified to take advantage of regions of space less susceptible to space debris encounters. More difficult to modify are the orbits of photographic reconnaissance satellites which must fly at very low altitudes and Sun-synchronous satellites (meteorological and remote sensing) whose orbital inclinations are dictated by their altitudes.

Another countermeasure to the debris hazard would be the redesign of spacecraft to tolerate impacts by larger pieces of debris. Since there are fewer larger particles, the probability of mission failure due to space debris could be lowered. Present-day satellites already incorporate shielding requirements into spacecraft design; thus only more stringent requirements would be necessary. Aluminum louvers returned from Solar Max provide graphic evidence of the desirability of a reliable particle bumper system. Figure 5.2 illustrates the penetration of an outer louver 0.14 mm thick by a piece of space debris. Figure 5.3 indicates the extent of the spray pattern on a second louver spaced 3 mm behind the first. A dual wall structure of this type can be very effective in absorbing space debris impacts without endangering spacecraft viability and without further degrading the environment with significant secondary debris.

Of course certain parts of the spacecraft such as solar panels and antennas cannot be shielded effectively. In these cases, redundancy is a viable option. For example, designing solar panels to be 10% to 20% larger than needed for power generation will compensate for solar cells destroyed by hypervelocity impacts with space debris. Auxiliary antennas could be provided to ensure mission continuance in the event one is struck by space debris. These added costs will be far less than any active measures taken to combat space debris.

Reduction of spacecraft size will, of course, also decrease the probability of collision with space debris. However, spacecraft are already, in general, as compact as possible because of weight and size restrictions imposed by the launch vehicle. Because a collision from space debris is more likely to occur from a direction near the plane perpendicular to the radius vector than near the plane perpendicular to the velocity vector, spacecraft design which minimizes cross-sectional area along the

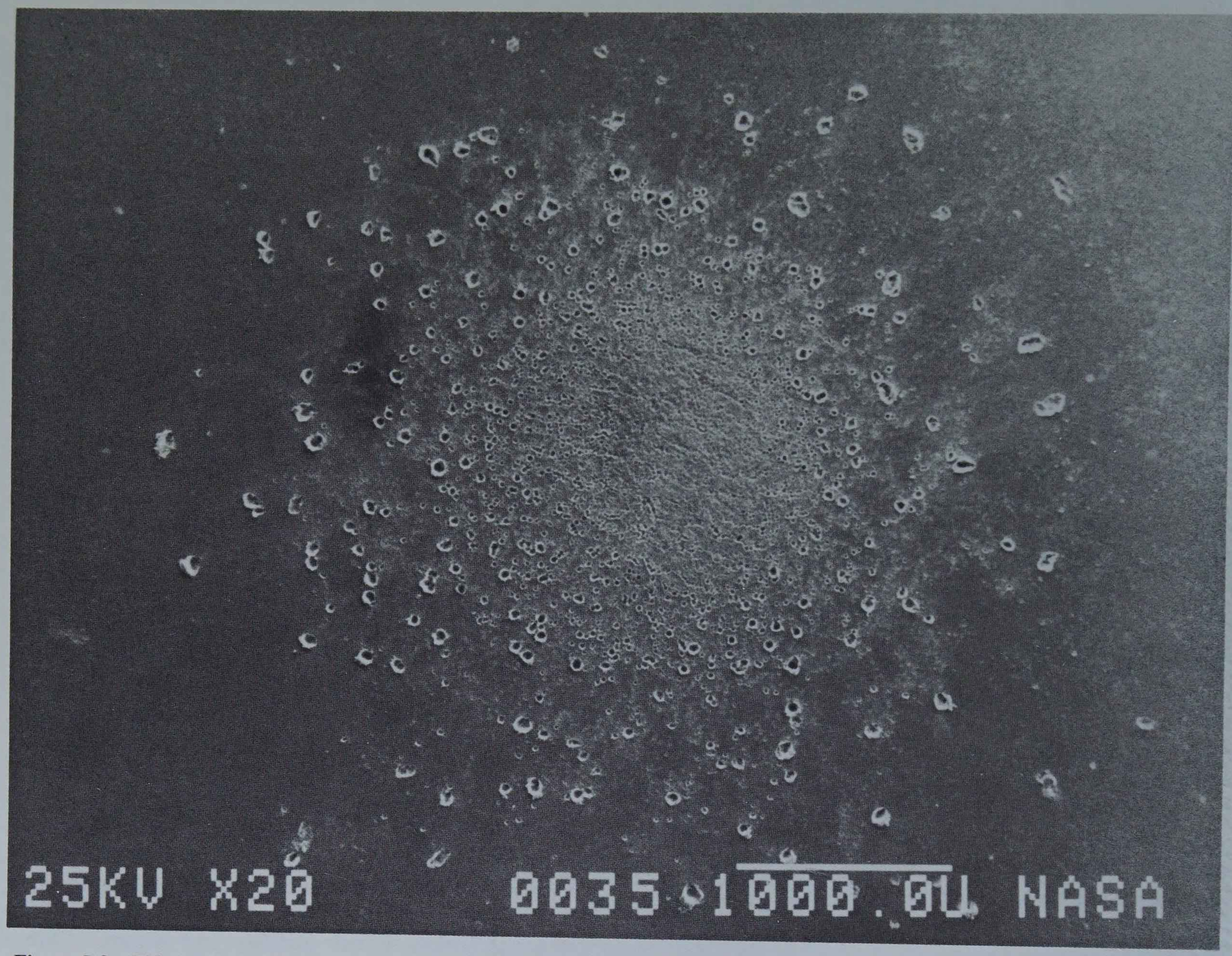


Figure 5.3 This photograph graphically illustrates the hazards of secondary ejecta generated by a hypervelocity collision. This Solar Max surface was positioned 3 mm behind the louver shown in Figure 5.2. *Courtesy of NASA.*

velocity vector will reduce the probability of collision with space debris. This technique also has the added benefit of reducing atmospheric drag.

Alternatively, special shields could be aligned with the most probable directions of colliding space debris. Figure 5.4 shows some of the impact absorbing properties of a tile from the Shuttle *Atlantis*. The crater was probably caused by a hypervelocity impact of a small piece of orbital debris.

Another relatively inexpensive means of reducing the probability of collision is to perform collision avoidance maneuvers. As noted previously, this technique has already been implemented in the geostationary orbit and is available as required for manned spacecraft. Most spacecraft have inherent collision avoidance capabilities by virtue of their attitude control or main propulsion systems. Even gravity gradient stabilized satellites might be successfully maneuvered along the radius vector without adversely affecting their delicate passive attitude control systems. Perhaps not surprisingly, collision avoidance maneuvers are being seriously considered for use by structures as large as NASA's space station when the vehicles are threatened by significantly massive pieces of orbiting debris.

The technique of maneuvering to avoid collisions would benefit from a more sensitive surveillance system which would then warn a satellite of an impending close approach. Improved ground-based radar and optical sensors would add little to the present capabilities due to the inherent limitations of most of these systems. However, space-based surveillance systems, already planned for deployment in the next decade, could provide much more timely and accurate warnings for the relatively few active satellites.

A more responsible action, and one which is still economically palatable, is to overlay a debris acceptance

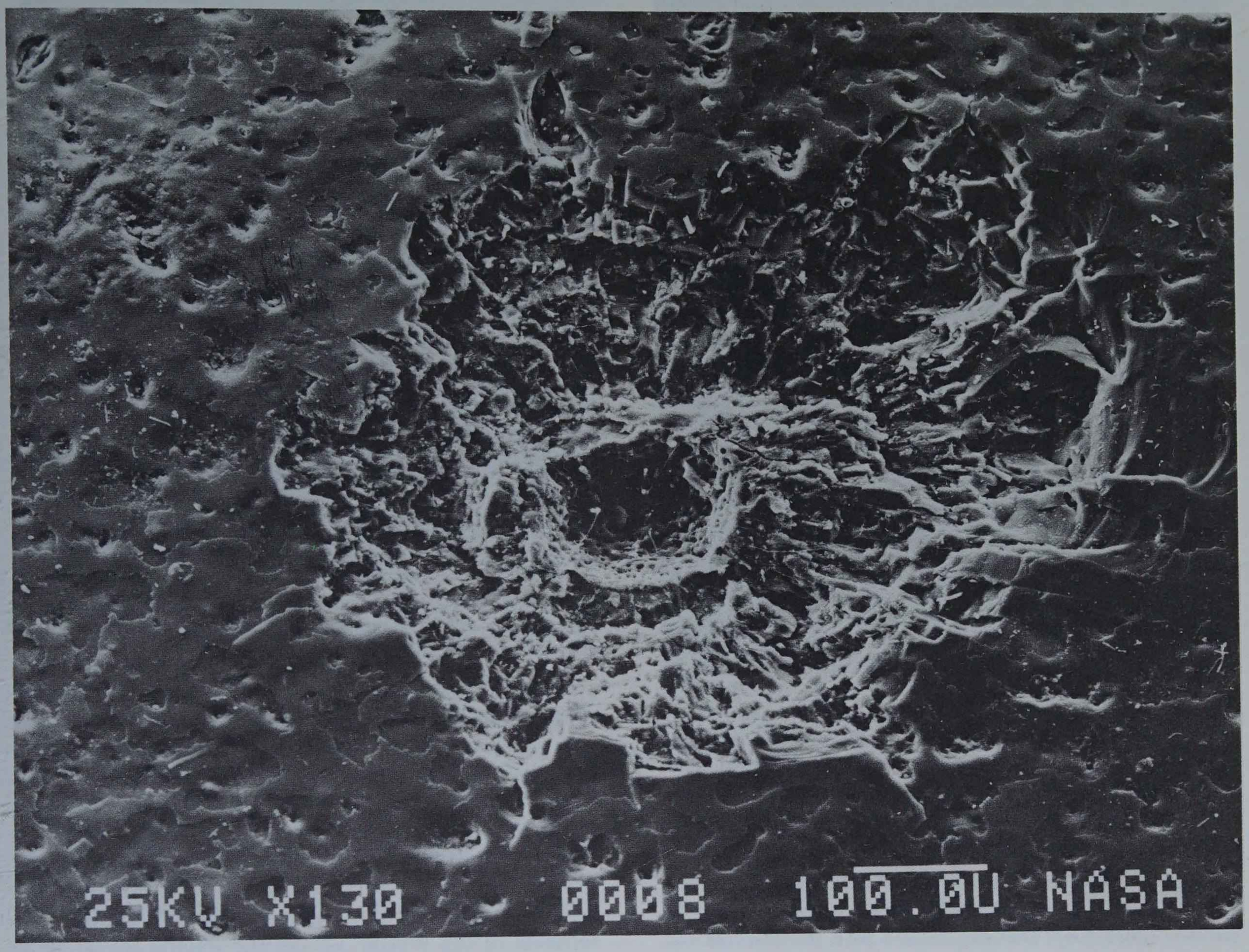


Figure 5.4 A scanning electron microscope photograph of a thermal tile from the Space Shuttle *Atlantis* revealed a hypervelocity impact crater probably caused by a collision with space debris. *Courtesy of NASA.*

program with a vigorous debris control program. Nature remains remarkably resilient to man's activities. If debris generation can be controlled, the environment at lower altitudes will in time cleanse itself. This is possible, however, only if control policies are instituted before the debris environment becomes self-regenerative, i.e., the Kessler syndrome is initiated. In this regard the recommedations of the AIAA pertaining to judicious selection of planned explosions and orbits designed to accelerate the natural decay process are welcome.

Awareness of debris generation mechanisms, as discovered with the Delta second stages, can itself promote good debris control policies. Alternatives to aluminum impregnation in solid rocket propellents and even the matter of using paint less vulnerable to atomic oxygen would also go a long way toward curbing the debris environment. Better design of rocket body and payload separation mechanisms could also reduce the amount of debris now routinely being created.

A more subtle way of controlling the environment is through the refurbishment of existing spacecraft. Instead of replacing failing satellites with more satellites, the simple act of refueling or fixing satellites on-orbit could lower the annual launch rate and mitigate the growth of space debris. In 1984 the world was amazed at the apparent ease with which NASA astronauts repaired the crippled Solar Max satellite and placed it back on duty (Figure 5.5). Not only was the cost of the repair considerably less than the cost of a new satellite, but the repair mission was accomplished following the completion of the primary mission: deployment of the long duration exposure facility (LDEF). Many techniques and procedures were refined during the revitalization of the Solar Max satellite which will help in future satellite repair missions and space construction in general (6, 7).

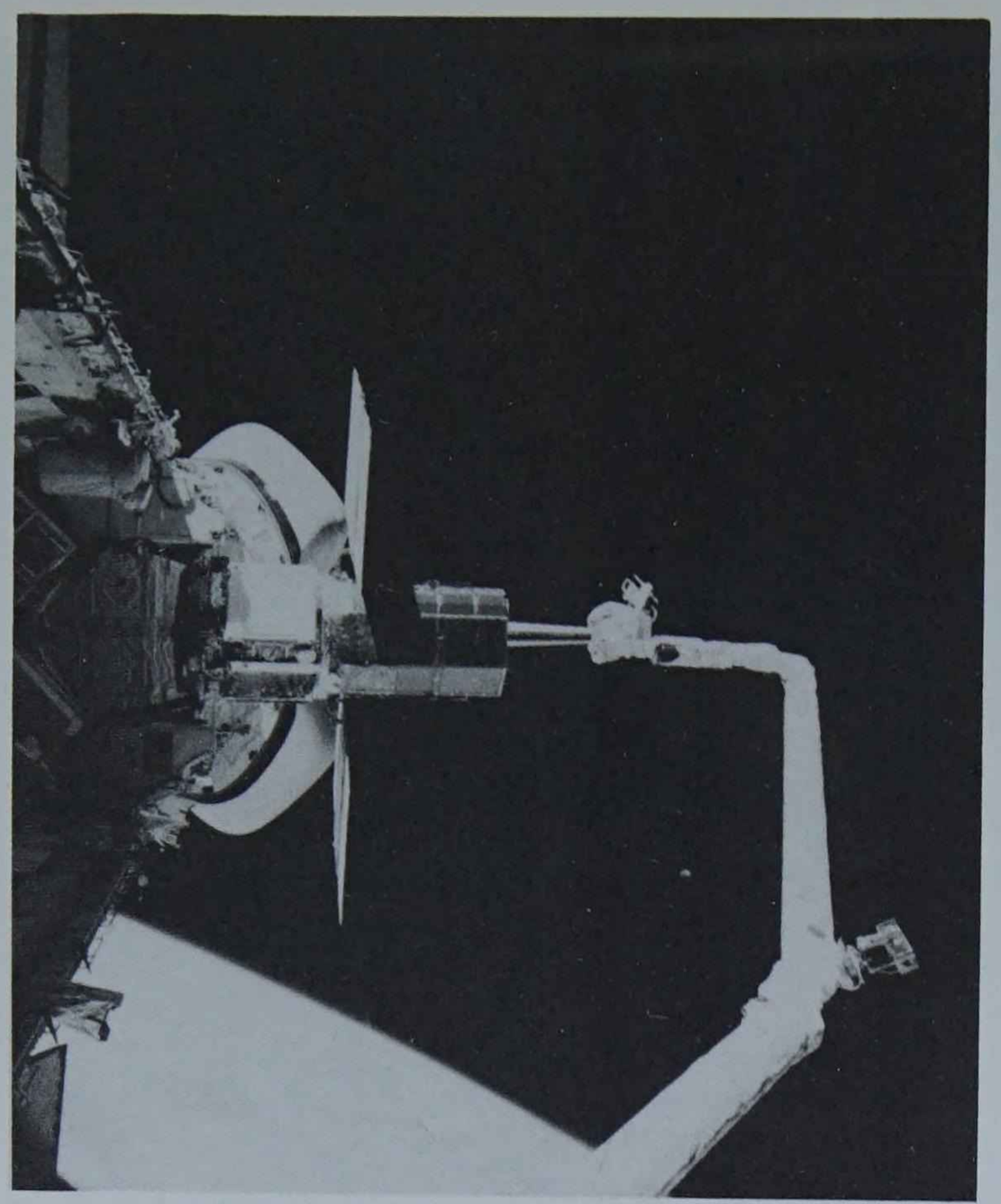


Figure 5.5 Retrieval of old satellites and large pieces of space debris with the Space Shuttle is possible but generally not economically feasible. See Plate 2. *Courtesy of NASA.*

The very nature of the Shuttle system is having its own impact on controlling the debris environment. By taking multiple payloads into low altitude orbits and returning to Earth, fewer spent rocket bodies are being left in Earth orbit (Figure 5.6). Our experience with the Shuttle will ultimately lead to advanced shuttles and reusable orbital transfer vehicles (OTVs) which will eliminate the need for high altitude transfer stages. Had Shuttle-OTV combinations been around in the early 1970s, the known Earth satellite population as of 1 January 1986 could have been reduced by 15% merely by the elimination of the Delta second stage breakups.

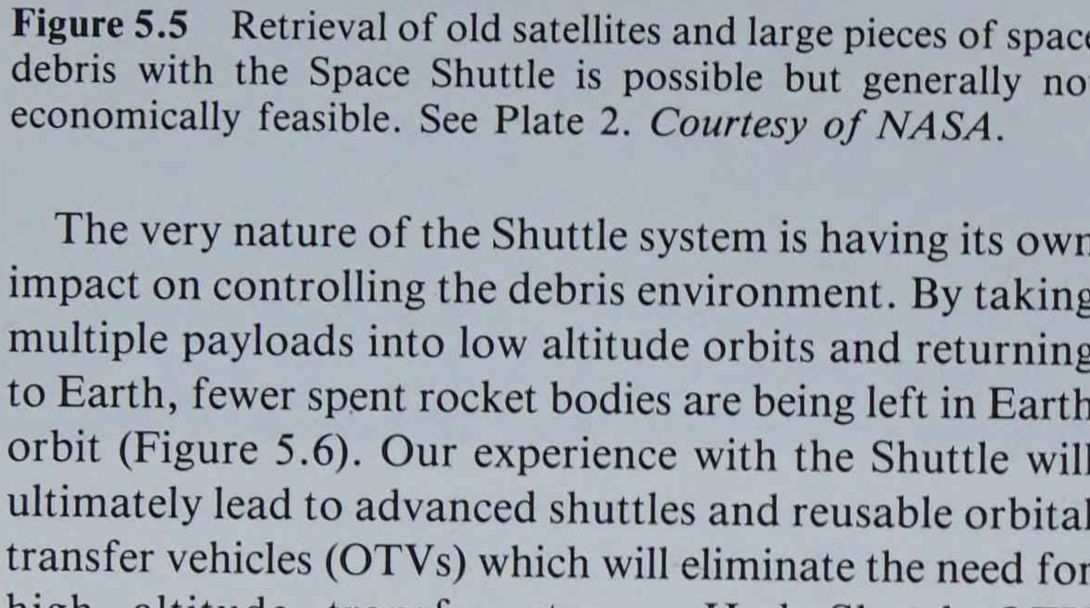


Figure 5.6 By returning to Earth, the Space Shuttle reduces the number of spent stages left in Earth orbit. *Courtesy of NASA.*



Figure 5.7 Satellite retrieval can be astronaut-assisted or carried out using automated proximity operations vehicles (POVs). See Plate 3. *Courtesy of NASA.*

Cleaning Up the Environment

Although resilient, the space environment will require a little help if the debris problem is to be reduced as well as curtailed within the near term. The most obvious example of cleaning up the environment is the removal of inactive satellites from Earth orbit. Although this is seldom feasible from an economic standpoint, the retrieval of the Westar VI and the Palapa B2 satellites in 1984 was graphic evidence of cost effectiveness under special circumstances (Figure 5.7). This mission, too, was performed after the deployment of two new geosynchronous communication satellites from the Shuttle cargo bay, thereby reducing overall mission cost. Westar VI and Palapa B2 have since been refurbished on Earth and now await a relaunch into space, possibly by a Chinese launch vehicle.

Under certain circumstances, factors other than cost may be the motive for the removal of satellites from Earth orbit. One reason may be safety. The planned controlled reentry of Skylab and the deorbiting of most Soviet space stations (two suffered fates similar to Skylab, and like Skylab, caused no damage) are illustrative of the concerns associated with the debris arising from large space objects reentering the atmosphere. In fact the daring rescue of the completely disabled Salyut 7 space station in 1985 was prompted in large measure by the Soviet concern for its unpredictable eventual reentry.

A less well-known threat is that posed by Earth satellites carrying radioactive materials. As of 1 August

Table 5.1 Radioisotope Power Supplies in Earth Orbit.

	Name	Launch Date	Fuel Type	Orbit (1 Jan 86) Mean Altitude (km)	Orbit (1 Jan 86) Orbital Inclination (degrees)	Comments
U.S.	Transit 4A	29 Jun 61	^{238}Pu	930	66.8	SNAP 3
	Transit 4B	15 Nov 61	^{238}Pu	1030	32.4	SNAP 3
	Transit 5BN1	28 Sep 63	^{238}Pu	1095	89.9	SNAP 9A
	Transit 5NB2	5 Dec 63	^{238}Pu	1085	90.0	SNAP 9A
	Nimbus 3	14 Apr 69	^{238}Pu	1100	99.8	SNAP 19
	Transit OI-1X	2 Sep 72	^{238}Pu	770	90.0	SNAP 29
	LES 8	15 Mar 76	^{238}Pu	35785	22.8	Carried 2 advanced RTGs
	LES 9	15 Mar 76	^{238}Pu	35785	22.7	Carried 2 advanced RTGs
U.S.S.R.	Kosmos 80-84	3 Sep 65	^{210}Po?	1500	56.1	One of the five payloads carried a RTG
	Kosmos 86-90	18 Sep 65	^{210}Po?	1500	56.1	One of the five payloads carried a RTG

1987, more than four dozen potentially hazardous radioactive satellites, carrying over a metric ton of highly enriched uranium-235, plutonium-238, and assorted fission products, were orbiting the Earth. The threat posed by these radioisotope thermoelectric generators (RTGs), reactors, and even exposed fuel cores extends not only to contamination during eventual reentry into the Earth's atmosphere, but also to other Earth-orbiting satellites, including manned spacecraft.

Despite their cost and safety restrictions, nuclear power supplies have long been considered a desirable method for power generation on a variety of near Earth and deep-space missions. Attributes of nuclear power supplies include compactness, reliability, endurability, low mass-to-power ratios, and the ability to perform in environments hostile to other power generation methods. Nuclear power supplies are primary candidates whenever high electrical demands (greater than 10 kilowatts) are required, particularly over many months or years. However, low power requirements (below 1 kWe) can also be met by nuclear power sources to promote longevity, to supplement other power generation systems, and to operate under varying environmental conditions.

In the United States nuclear power supplies for space are as old as the space age itself. The Atomic Energy Commission established a program to develop Systems for Nuclear Auxiliary Power, commonly called SNAP. By January 1959 the first complete thermoelectric generation device, SNAP 3, powered by Po-210 and producing 2.5 watts of electricity, was delivered by the Martin Company. Slightly more than 2 years later a modified SNAP 3, loaded with Pu-238, was successfully orbited aboard a U.S. Navy navigation satellite. In the years to follow similar devices were installed on meteorological, communications, and deep-space satellites. In the case of the last, nuclear power supplies for spacecraft journeying to Mars or beyond proved superior to solar-powered generators which are at a disadvantage due to decreased solar radiant flux at great distances from the Sun.

In contrast, after orbiting two experimental RTGs in 1965, the Soviet Union concentrated on higher power reactor systems which would operate at very low altitudes above the Earth. The Soviet system was designed to circumvent the undesirable drag effects of large solar panels at the designated operational altitude of 250 km and to overcome the substantial electrical storage problem associated with a high drain payload which must operate in the Earth's shadow as well as in sunlight.

The 54 radioisotope power supplies, nuclear reactors, and fuel cores now in orbit about the Earth pose both near term and far term hazards (Tables 5.1 and 5.2, Figure 5.8). Unfortunately, all but a few of these satellites reside in the most densely populated regions of cis-Earth space near 1,000 km altitude. Here the probability of colliding with another Earth-orbiting object is accentuated. As noted previously, a Soviet navigation satellite, which explosively fragmented in this altitude regime in 1981, is considered to be a prime candidate for the first case of catastrophic collision in space.

A disquieting situation already exists with the only U.S. space reactor, SNAP 10A. Since late 1979 SNAP 10A has spawned pieces of debris on at least six occasions. The nature of this debris and the cause of its liberation are currently unknown. Since SNAP 10A remained attached to the final stage of its launch vehicle, either the rocket body or the payload may be the source of the debris. The possibility that SNAP 10A was struck by another space object in 1979 has not been dismissed.

Table 5.2 Nuclear Reactors in Earth Orbit.

	Name	Launch Date	Fuel Type	Fuel Mass (kg)	Orbit (1 Jan 86) Mean Altitude (km)	Orbit (1 Jan 86) Orbital Inclination (degrees)	Comments
U.S.	SNAP 10A (SNAPSHOT)	3 Apr 65	^{235}U	11	1290	111.4	Operated 43 days.
U.S.S.R.	Kosmos 198	27 Dec 67	^{235}U	50	920	65.1	Operated 2 days.
	Kosmos 209	22 Mar 68	^{235}U	50	905	65.3	Operated 6 days.
	Kosmos 367	3 Oct 70	^{235}U	50	970	65.3	Failed soon after launch.
	Kosmos 402	1 Apr 71	^{235}U	50	990	65.0	Operated 8 days.
	Kosmos 469	25 Dec 71	^{235}U	50	980	64.5	Operated 10 days.
	Kosmos 516	21 Aug 72	^{235}U	50	975	64.8	Operated 31 days.
	Kosmos 626	27 Dec 73	^{235}U	50	945	65.4	Operated 46 days.
	Kosmos 651	15 May 74	^{235}U	50	920	65.0	Operated 71 days.
	Kosmos 654	17 May 74	^{235}U	50	965	65.0	Operated 74 days.
	Kosmos 723	2 Apr 75	^{235}U	50	930	64.7	Operated 44 days.
	Kosmos 724	7 Apr 75	^{235}U	50	900	65.6	Operated 66 days.
	Kosmos 785	12 Dec 75	^{235}U	50	955	65.1	Operated 1 day.
	Kosmos 860	17 Oct 76	^{235}U	50	960	64.7	Operated 24 days.
	Kosmos 861	21 Oct 76	^{235}U	50	960	64.9	Operated 60 days.
	Kosmos 952	16 Sep 77	^{235}U	50	950	64.9	Operated 22 days.
	Kosmos 1176	29 Apr 80	^{235}U	50	920	64.8	Operated 134 days. Fuel core ejected into similar orbit.
	Kosmos 1249	5 Mar 81	^{235}U	50	940	65.0	Operated 106 days. Fuel core ejected into similar orbit.
	Kosmos 1266	21 Apr 81	^{235}U	50	930	64.8	Operated 8 days. Fuel core ejected into similar orbit.
	Kosmos 1299	24 Aug 81	^{235}U	50	945	65.1	Operated 13 days. Fuel core ejected into similar orbit.
	Kosmos 1365	14 May 82	^{235}U	50	930	65.1	Operated 136 days. Fuel core ejected into similar orbit.
	Kosmos 1372	1 Jun 82	^{235}U	50	945	64.9	Operated 71 days. Fuel core ejected into similar orbit.
	Kosmos 1412	2 Oct 82	^{235}U	50	945	64.8	Operated 40 days. Fuel core ejected into similar orbit.
	Kosmos 1579	29 Jun 84	^{235}U	50	945	65.1	Operated 90 days. Fuel core ejected into similar orbit.
	Kosmos 1607	31 Oct 84	^{235}U	50	950	65.0	Operated 93 days. Fuel core ejected into similar orbit.
	Kosmos 1670	1 Aug 85	^{235}U	50	950	64.9	Operated 82 days. Fuel core ejected into similar orbit.

Table 5.2 continued on next page

Table 5.2 Nuclear Reactors in Earth Orbit (Continued).

Name	Launch Date	Fuel Type	Fuel Mass (kg)	Orbit (1 Jan 86) Mean Altitude (km)	Orbit (1 Jan 86) Orbital Inclination (degrees)	Comments
Kosmos 1677	23 Aug 85	^{235}U	50	940	64.7	Operated 61 days. Fuel core assumed ejected into similar orbit.
Kosmos 1736	21 Mar 86	^{235}U	50	960	65.0	Operated 92 days. Fuel core ejected into similar orbit.
Kosmos 1771	20 Aug 86	^{235}U	50	960	65.0	Operated 56 days. Fuel core ejected into similar orbit.
Kosmos 1860	18 Jun 87	^{235}U	50	950	65.0	Operated 50 days. Fuel core ejected into similar orbit.
			1461 Total			

After the reentry of the radioactive Kosmos 954 over Canada in 1978, a Soviet spokesman, Leonid Sedov, announced that the spacecraft had apparently collided with another object in early January of that year and had suffered a sudden depressurization. Sedov did not mention difficulties with Kosmos 954 in November and December as evidenced by its orbital behavior, but, if his statement is correct, then the occurrence in January may have prevented any last minute Soviet action which could have boosted the reactor to its normal, higher altitude storage orbit.

The destruction of a radioactive satellite by hypervelocity collision not only will prevent any future opportunity to dispose of the satellite but also may create more immediate hazards to manned and unmanned spacecraft. A hypervelocity collision with a spent Soviet nuclear reactor may produce as many as 1,000,000 particles with a diameter of 1 mm or more. Some of these particles will be injected into orbits with perigees well below the current 900-1,000 km storage altitude, into regions populated by large, manned spacecraft. Even if these particles do not strike other spacecraft, they will begin to decay at an accelerated rate and reenter the Earth's atmosphere much quicker than previously calculated. Furthermore, the very small particles at all altitudes will be subjected to stronger solar radiation effects and will also decay at a faster rate.

Statistically, with the current population estimate of small and large Earth satellites, most of the present-day nuclear power supplies and fuel cores will decay naturally without experiencing a catastrophic collision. However, if the satellite population continues to grow at the present rate, the probability of collision before reentry reaches a virtual certainty. Since the number of satellite payloads orbited each year is not projected to diminish significantly at least through the end of the century, control of satellite fragmentations - now the primary factor behind the satellite population growth - must be aggressively pursued.

After several hundred years, radioactive satellites will begin to enter the lower altitude regimes, which, by then, may be populated by very large structures, both manned and unmanned. The probability of collision of one of these radioactive satellites with another satellite increases with the cross-sectional area of the second satellite. The impact of a spent fuel core with a space station could be devastating. In addition to the structural damage, radioactive contamination will be likely since the half-life of uranium-235 is in excess of 700,000 years.

Even without collisions of any kind, the nuclear power supplies will eventually return to Earth and be distributed into the atmosphere. Already over 1,450 kg of reactor fuel have been placed into orbit (Figure 5.9). The mass of contaminated reactor and other spacecraft materials is many times this number. With no further program setbacks, the mass of radioactive fuel orbited each year should average 150 kg, resulting in more than 3 metric tons of highly toxic fuel and fission products in orbit by the end of the century.

As a recourse, retrieval of the majority of nuclear power supplies in space could be accomplished with a very modest program. More than 90% of the radioactive materials in orbit today are of Soviet origin and circle the Earth at an orbital inclination of about 65 degrees and mean altitudes between 900 and 1,000 km. By taking advantage of natural orbital perturbations, all of these objects could be retrieved within a span of only a few years.

At their present altitudes and inclinations, the precession of their orbital planes due to the oblateness of the Earth amounts to about 2.6 degrees per day.

Figure 5.8 As of 1 August 1987, more than four dozen satellites carrying radioactive materials were in orbit about the Earth.

However, the orbital plane of a platform at the same inclination, but at a lower altitude of 300 km, will precess 3.6 degrees per day. Hence, the orbital plane of each reactor or fuel core will coincide with that of a low altitude platform at least once each year. The total change in velocity required to rendezvous with an object at 950 km and return to the 300 km platform is only 700 m/s.

The Soviet Union already possesses the technological expertise and experience to accomplish retrieval of their spent nuclear payloads. Using a Salyut-type vehicle as a base and a modified Kosmos 929-type spacecraft as a propellent reserve, an automated orbital transfer vehicle could make repeated trips to the higher altitude nuclear power supply graveyard and return payloads for storage in the Salyut-type vehicle. The Kosmos 929-type spacecraft may need to be replaced periodically as additional propellents are required.

Once many or all of the old reactors have been recovered and stored in the Salyut-type vehicle, that spacecraft could be sent on an Earth escape trajectory toward the Sun or out into deep space. This entire operation can be performed by remote control or can be

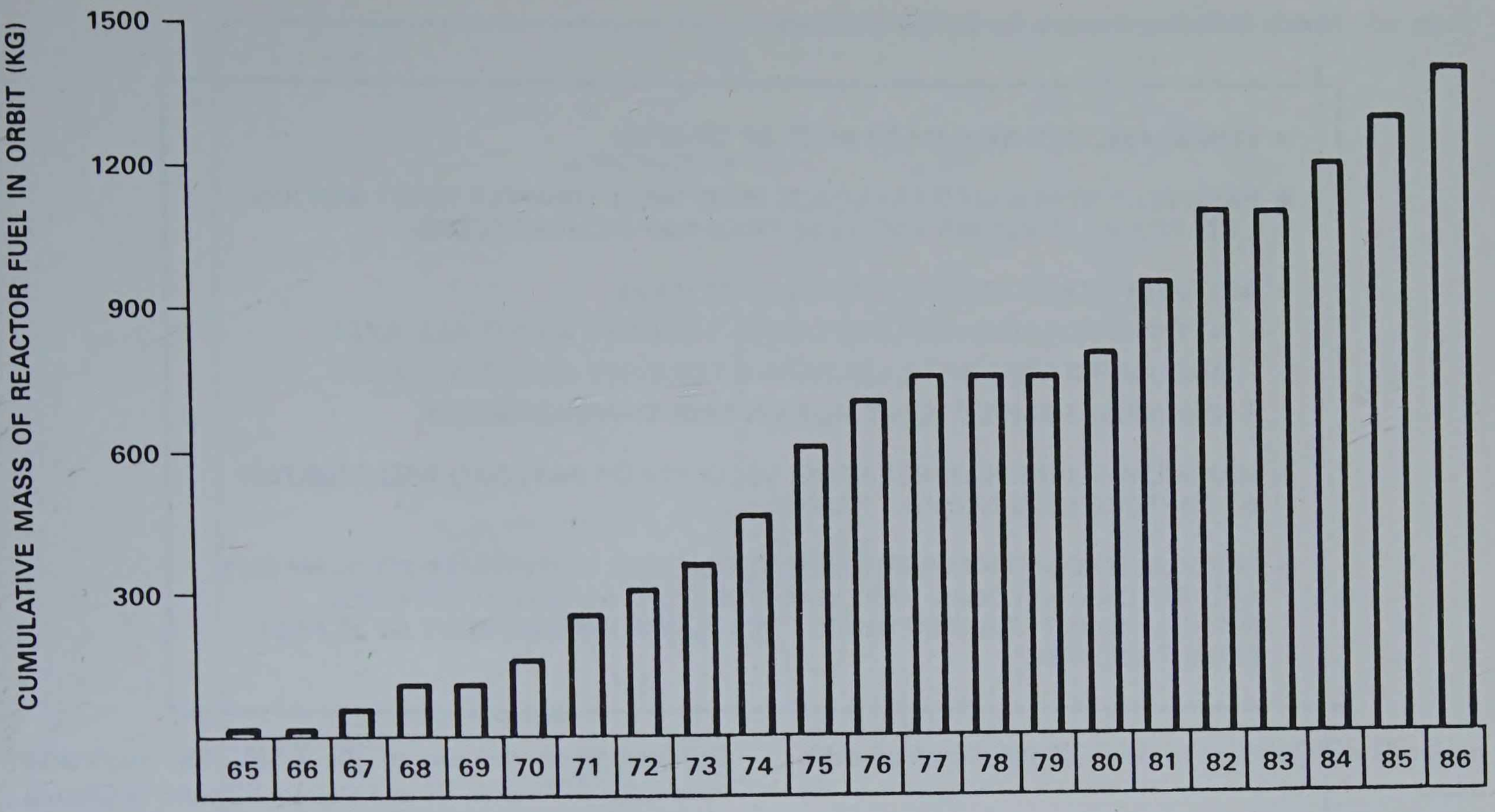


Figure 5.9 The amount of radioactive materials now in orbit about the Earth exceeds 1,450 kg. By the end of the century this amount will probably approach 3 metric tons. *Courtesy of Teledyne Brown Engineering.*

assisted in low Earth orbit by man. When the Soviet Union deploys its large, permanent space station in the 1990s, there is reason to believe that its orbital inclination may be 65 degrees. In this event, the cleanup operations could be facilitated. Alternatively, a low altitude platform could be visited by Soviet cosmonauts, using either the Soyuz TM spacecraft or the new space plane now under development.

Storage orbits are rarely the answer to debris problems. They are not a solution; they merely postpone the problem. Current storage orbit practices, particularly regarding radioactive satellites, are insufficient to ensure the protection of continued space activities and of the Earth's biosphere in both the near term and the far term. The authors recommend that alternatives to storage orbits, even those for geostationary satellites, be investigated and implemented. What appear to be useless orbits today may be essential to some future space operations.

In general, the on-orbit cleanup of space debris is not a viable option. Each of the 6,000+ pieces of space junk now known to be in orbit about the Earth resides in a unique orbit, and considerable energy is usually required to transfer from one orbit to another. Even objects in the same orbital altitude and inclination will likely reside in different orbital planes. Translating from one orbital plane to another is an energy intensive maneuver which is rarely economically attractive.

Despite this discouraging situation, concepts for the removal of large debris (nonoperational payloads and spent rocket bodies) have been offered in recent years. The bulk of the concepts envision use of the Shuttle as the primary means of transport. Two designs, one, a graduated approach to debris retrieval developed as a service extension of the Shuttle program and, the other, a reusable debris hauler which uses the Shuttle only for transportation to and from its working environment, are described in more detail below.

Satellite Services is seen as "an extension of the Space Transportation System (STS) which will provide on-orbit services and operational capabilities that exploit the uniqueness of the STS and the advantages of human presence on-orbit" (5). Close proximity retrieval and retrieval of payloads in higher altitude LEO are under investigation. Between 1982 and 1993 possibilities exist for the retrieval of at least 150 active satellites which could be refurbished in space or repaired on the ground. These

Table 5.3 Shuttle RMS Requirements for Satellite Retrieval.

- SPIN-STABILIZED PAYLOADS MUST BE DE-SPUN
- PASSIVELY-STABILIZED PAYLOADS MUST HAVE GRAPPLE POINT MOTION LESS THAN ± 15 INCHES AND LESS THAN 0.05 INCHES/SECOND
- ACTIVELY-STABILIZED PAYLOADS MUST HAVE
  - ATTITUDE DEAD-BAND LESS THAN ± 1 DEGREE ABOUT ALL AXES
  - ANGULAR RATE LIMIT LESS THAN 0.1 DEG/SEC ABOUT ALL AXES
  - MAXIMUM GRAPPLE POINT MOTION LESS THAN ± 3 INCHES
- MAXIMUM ALLOWABLE RELATIVE VELOCITY OF PAYLOAD AND ORBITER AT CAPTURE LESS THAN 0.1 FT/SEC
- PAYLOAD SHOULD HAVE SUFFICIENT CONTROL AUTHORITY TO DAMP OUT AND RETURN TO LOCAL VERTICAL/HORIZONTAL (LVLH) ATTITUDE WITHIN 2 MINUTES AFTER DIRECT RCS PLUME IMPINGEMENT AT 35 FEET FROM THRUSTER

retrievals may amount to over 700,000 kg of on-orbit mass.

The Shuttle itself, even with its remote manipulator system (RMS), is ill-equipped for most retrieval operations. Table 5.3 summarizes some of the constraints imposed upon the use of the RMS. The successful recoveries of Westar VI and Palapa B2 were facilitated by the fact that control of the satellites was still possible. Both satellites were maneuvered into Shuttle accessible orbits and despun via ground control. Such operations of course would not be possible for inactive satellites.

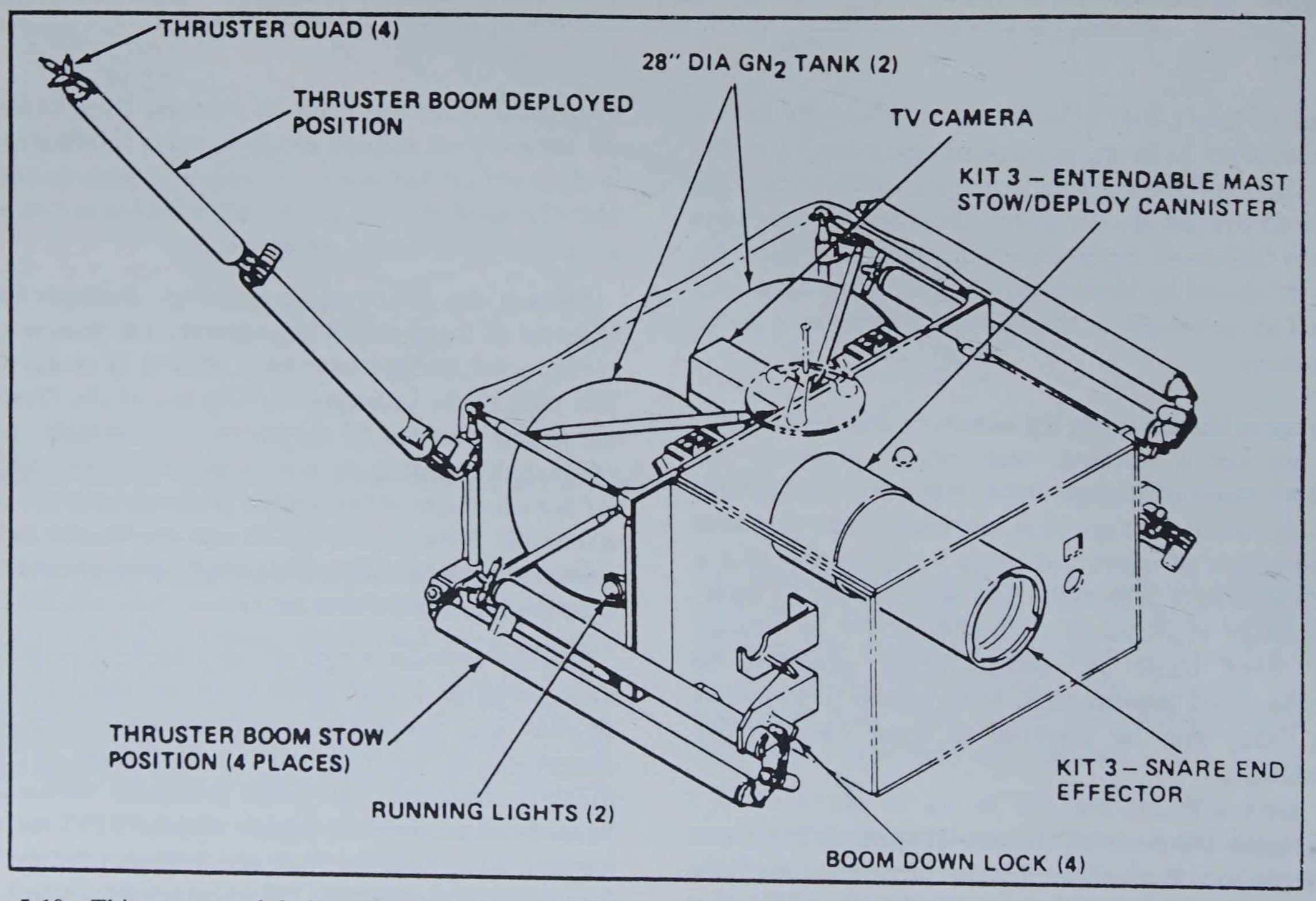


Figure 5.10 This conceptual design of a proximity operations vehicle (POV) could bring a 5,000 kg satellite to the Space Shuttle from a distance of up to 1 km. *Courtesy of Satellite Services, Grumman Aerospace.*

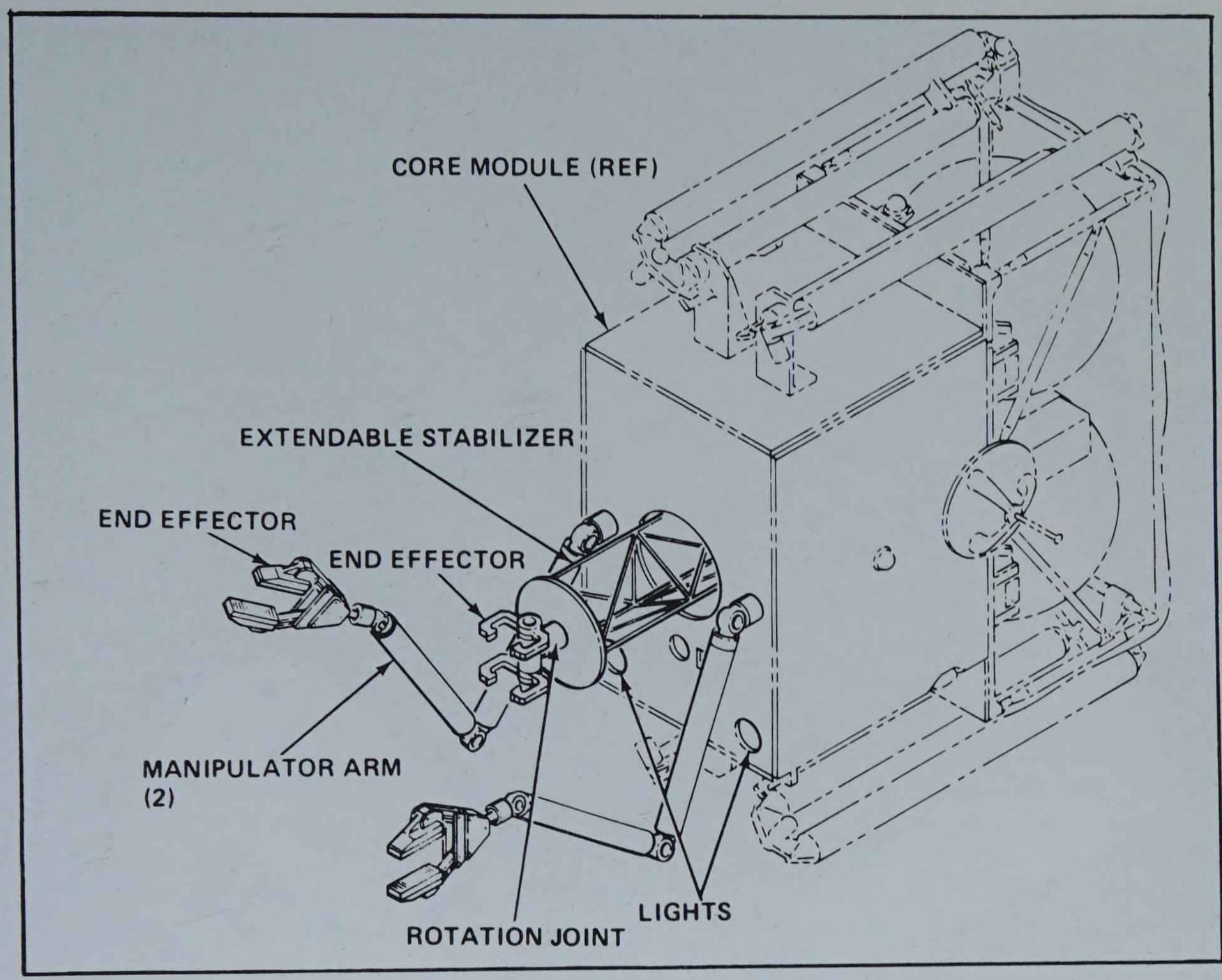


Figure 5.11 A more advanced POV design would incorporate a manipulator arm capability. *Courtesy of Satellite Services, Grumman Aerospace.*

For uncooperative satellites which are in orbital regimes accessible to the Shuttle, a proximity operations vehicle (POV) has been designed. From a stand-off distance of up to 1,000 m, Shuttle astronauts could guide the 500 kg POV to the satellite and effect the capture by remote control via a television system and a snare end effector. The POV could then maneuver the satellite with a mass of up to 5,000 kg within reach of the Shuttle RMS and deliver it in an attitude stable mode suitable for the RMS. This system would minimize the dangers to both the astronauts and the Orbiter when retrieving tumbling satellites. A Grumman Aerospace conceptual design of a POV is shown in Figure 5.10. A more advanced model (Figure 5.11) of the POV could employ two manipulator arms, much like those used on the *Discovery's* manned EVA pods in the science fiction epic film *2001, A Space Odessey*.

Shuttle astronauts have already aptly demonstrated the feasibility of capturing satellites and returning them to the Shuttle bay (Figure 5.12). Likewise, the technology to build POVs or similar devices is already at hand. The primary obstacles are opportunities, safety, and economics. While it seems logical to encourage returning the Shuttle to Earth with a full cargo bay rather than an empty one, the Shuttle flight program must be carefully tailored to permit satellite retrieval following deployment of the Shuttle's original payload. Orbital constraints of the primary mission can easily prevent such opportunities, particularly if the recommedations earlier in this volume for the judicious selection of orbital planes for geosynchronous transfer orbits are accepted.

The safety of the Shuttle crew is of paramount concern. Many of the large inactive payloads and rocket bodies pose a potential threat of the release of toxic fluids, of damage to the Orbiter during reentry, and even of explosion. No Shuttle astronaut is likely to volunteer for a mission to retrieve a Delta second stage, given the volatile history of that rocket body. Almost all liquid rocket stages will contain residual propellents to some degree and thus may behave unexpectedly when exposed to the gravitational forces of reentry. One of the requirements for retrieving Westar VI and Palapa B2 was the expenditure of virtually all propellents before retrieval. This was done over a period of months prior to the mission.

When the objective of a retrieval mission is simply to remove the satellite from orbit and not necessarily to refurbish it for reuse, an alternative exists which poses considerably less hazards to the crew: de-orbiting the

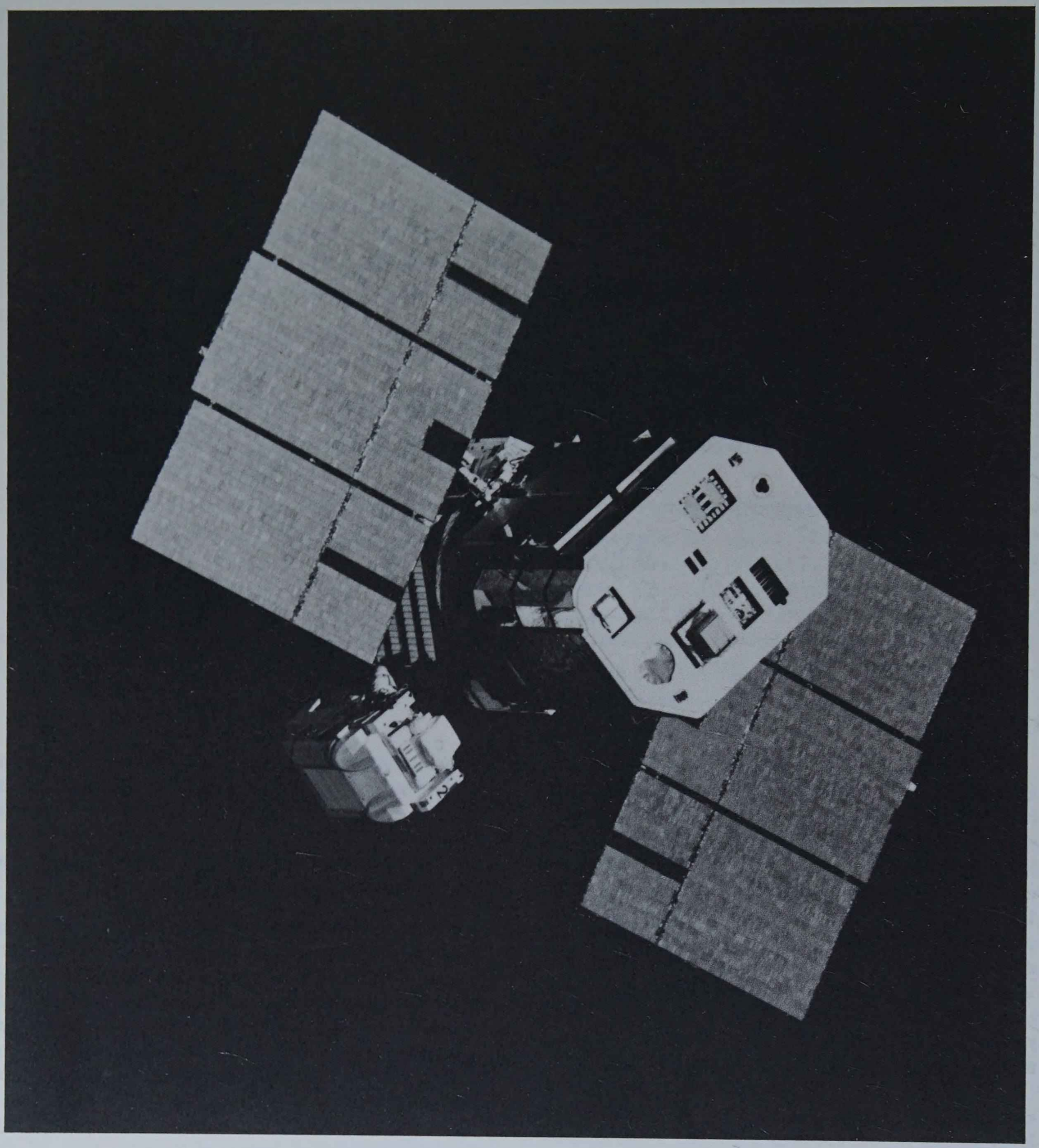


Figure 5.12 Retrieval and repair of satellites, such as Solar Max shown here, will contribute to reducing the growth of space debris. *Courtesy of NASA.*

satellite. Using a technique similar to the POV, a Shuttle astronaut could affix a small propulsion unit to the satellite. From a circular orbit of 500 km (near the maximum Shuttle operating altitude), a change in velocity of only 115 m/s is needed to ensure rapid reentry. More capable units could propel themselves to even higher altitudes, rendezvous with the target satellite with the aid of telerobotics, and then de-orbit.

The third and perhaps major obstacle existing today is simply economics. The expense of rendezvousing with a satellite after completion of the primary mission may still be tens of millions of dollars. This includes in part the cost of crew training, the equipment required, and the day(s) in space devoted to the operation when other experiments or activities must be put aside. For future missions the cost of incorporating a de-orbit capability into the initial spacecraft/rocket body design will probably be more cost effective than a Shuttle retrieval mission at a later date.

An even broader question is the magnitude of the benefit gained by removing large derelict space objects from low Earth orbit. Certainly, the removal of a single rocket body will reduce the chances of collision now and in the future. However, this solitary removal is statistically insignificant. To measurably lower the probabilities of collision with space debris, a much larger number of satellites must be removed.

If an objective is to cleanse a specific region of space, a less demanding task may be effective. Assume that a large permanent space station is to be deployed at an altitude of 500 km. From this altitude most satellites will decay within 4 to 10 years, depending strongly upon solar activity. Prior to the establishment of the space station, if large objects only in the 500 km altitude regime are removed, then the major future threat to the space station will come from higher altitude satellites decaying to 500 km. Thus a more realizable goal might be the removal each year only of large objects decaying down to 500 km. Satellites in highly elliptical and geosynchronous transfer orbits could be excluded from the set of target satellites not only because their removal is considerably more difficult but also because the time spent in the 500 km region is so short the probability of collision with the space station is quite small. An offsetting factor is the possible longer orbital lifetime of the highly elliptical satellite which may result in a larger probability of collision integrated over time.

To this point only the removal of large satellites has been addressed. While these satellites will certainly cause greater damage upon collision and are themselves sources of secondary debris by collisions with even smaller satellites, their relatively few numbers make them statistically less of a threat to functioning satellites. Of primary concern are those satellites between 1 mm and 10 cm in diameter which now populate near Earth space in vast numbers. A single piece of debris only a few centimeters in diameter impacting a spacecraft at hypervelocities will carry the destructive force of a hand grenade.

Several concepts have been offered as means of eliminating significant quantities of small debris. Don Kessler has calculated that a system - of any type - which merely retards a piece of debris whenever it passes within a radius of a few tens of kilometers of a platform will eventually make a significant contribution to cleaning up the space environment. This retarding force, which will accelerate the natural decay process, might be effected in a variety of ways. Because most debris develops a charge in space, a magnetic field could be useful in slowing down the debris. Large collecting areas of special fine-mesh nets or foam material could be deployed. Unlike the analagous fly-paper, capture is not mandatory; only the slowing down of the debris is necessary. Care, of course, must be taken with the design of the system that the impact of the debris with the device does not generate more particles than are eliminated.

A large portion of this chapter has dealt with means to mitigate the space debris problem in the future through technical and programmatic measures. If present policies are allowed to continue, space debris will become a significant hazard by the turn of the century. The contribution to the debris population from specific space systems serves to illuminate this prediction.

By examining the change in the spatial density of satellites in the region of space between 16,000 and 20,000 km, two major trends are evident. Figure 5.13 shows the spatial density of cataloged satellites in this altitude band for 1977 and 1987. First, the dramatic increase in spatial density around 19,000 km is due to the fielding of the Soviet GLONASS navigation system. Launchings into this region did not begin unitl 1982 and will continue for many years to come. At this altitude the spatial density is over an order of magnitude greater than neighboring altitudes and nearly two orders of magnitude greater than the 1977 level. As the spatial density increases so does the probability of collision.

The second observation from Figure 5.13 is that the baseline across the 4,000 km wide altitude band has grown by about a factor of four since 1977. This increase can be attributed in part to the many geosynchronous transfer stages still in orbit. Thus, as one region of space, such as the geostationary belt, is developed, other areas may be adversely affected.

Summary

The central space debris issue today is a simple one: recognition of the problem. Space debris has not yet reached a level which normally manifests itself in visible ways nor endangers routine space operations. However, continuance of the current unrestrained growth of the space debris population will ensure that space debris will someday pose significant hazards to both man and machine. Because of our imperfect knowledge of the space debris environment, simulations cannot predict with

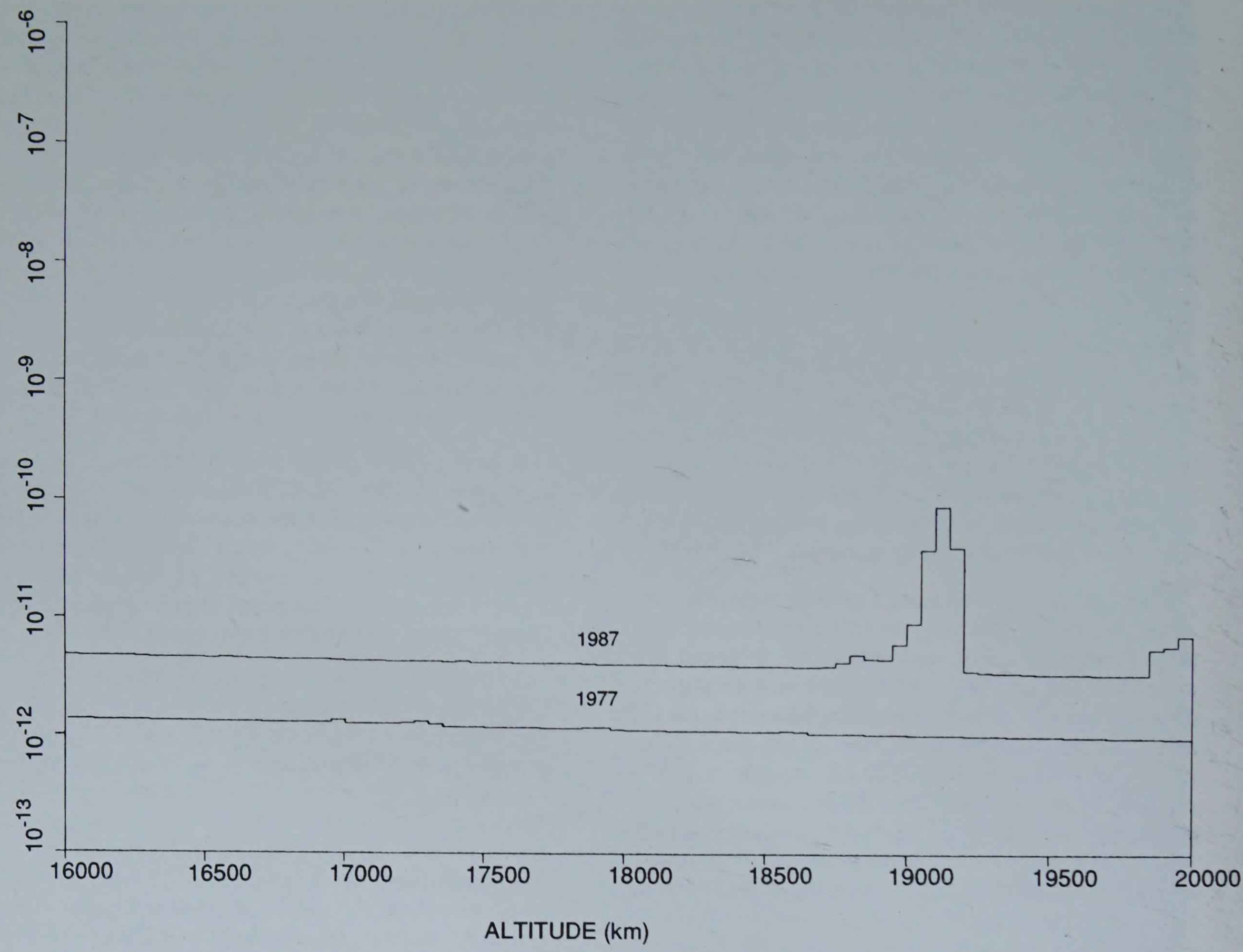


Figure 5.13 The recent deployment of Soviet GLONASS satellites in nearly circular orbits around 19,000 km has already had a visible effect on the spatial density in that orbital regime.

any confidence when this problem will become severe. But like a chain reaction, once natural collisions begin, the environment will start to deteriorate at an accelerated rate. At that time intervention by man may be too little, too late.

The first requirement in reducing the potential hazards of space debris - and one which has virtually no economic impact - is to curb the unnecessary creation of orbital debris. Intentional satellite fragmentations must be stopped immediately or, at the very least, carefully designed to ensure rapid decay of all debris. Operational launch debris should also be curtailed and eliminated whenever possible. Most operational debris is generated needlessly and without awareness of its potential adverse effects. The redesign of rocket bodies to deorbit themselves or the adoption of new launch procedures to take advantage of natural decay forces should be encouraged.

The retrieval of large satellites, while commendable, will have little consequence on the growth of the debris population. The energies and expense required for such missions can normally be put to better use by investigating techniques and technologies to remove the greater number of small satellites. An exception to this rule is the removal of radioactive satellites from Earth orbit because of the special dangers they pose.

An international effort should be initiated to better define the near Earth environment. Debris measurements can be made by a host of terrestrial sensors and can be an integral part of satellites deployed in different regions in space. If warranted, dedicated space-based debris monitoring platforms could be designed and operated by such august bodies as the United Nations, the International Astronautical Federation, or the Committee on Space Research of the International Council of

Scientific Unions. The data collected from these investigations should then be made available to the world scientific community for the purpose of determining the extent of the space debris problem and of finding efficient, cost effective ways of improving the space environment.

In the words of the American Institute of Aeronautics and Astronautics (AIAA), "corrective action must begin now to forestall the development of a serious problem in the future."

References

1. *Orbital Debris.* NASA Conference Publication 2360, NASA, 1985.
2. *Orbital Debris.* NASA Conference Publication 2360, NASA, 1985, pp. 8-21.
3. Hyland, D. "Air Force Orbital Position Management Policy." *Orbital Debris,* NASA Conference Publication 2360, NASA, 1985, pp. 393-398.
4. Wolfe, M. G. "Space Debris: An AIAA Position Paper." *Orbital Debris,* NASA Conference Publication 2360, NASA, 1985, pp. 365-371.
5. Adornato, R. J. "Satellite Services and Orbital Retrieval." *Orbital Debris,* NASA Conference Publication 2360, NASA, 1985, pp. 299-315.
6. Grady, K. J. "The Dynamics of the Solar Maximum Mission Spacecraft Capture and Redeployment on STS 41-C." Presented at the Annual Rocky Mountain Guidance and Control Conference, February 1985.
7. Lane, J. F. "On-orbit Repair of Solar Maximum Mission Observatory." Presented at the Annual Rocky Mountain Guidance and Control Conference, February 1986.

Illustrations

PLATE

1	Figure 1.5	
2	Figure 5.5	
3	Figure 5.7	

FIGURE PAGE

Frontispiece	Soviet antisatellite tests have been a significant contributor to the artificial space debris population since 1968. *Painting by William Hartmann, courtesy of Donald J. Kessler.*	
1.1	The known Earth satellite population.	1
1.2	Satellite fragmentations account for almost half of all known Earth satellites now in orbit.	2
1.3	The distribution of Earth satellites at high altitudes.	3
1.4	The impact crater which appeared on a Space Shuttle window during the 1983 flight of STS-7.	4
1.5	Closeup view of the STS-7 Shuttle window impact crater. See Plate 1.	4
1.6	The growth of the Earth satellite population is governed by a variety of sources and sinks.	5
1.7	The locations of all cataloged satellites in the near Earth environment as of September 1986.	7
2.1	Examination of the STS-7 impact crater with an electron scanning microscope revealed material consistent with a fleck of spacecraft paint.	12
2.2	The rate of satellite fragmentations has increased significantly during the past decade.	13
2.3	According to the *NORAD Satellite Catalog,* the 10 most prolific satellite fragmentations have accounted for more than 2,600 known pieces of debris.	13
2.4	This schematic diagram of a Delta second stage illustrates the common bulkhead between the fuel and oxidizer tanks.	18
2.5	The altitude regime between 900 and 1,000 km is the most populous.	19
2.6	Despite numerous investigations, the causes for almost half of all satellite fragmentations are still unknown.	23
2.7	The regimes of most satellite fragments are relatively narrow and easily defined.	23
2.8	Calculation of the spatial density of known Earth satellites is necessary to evaluate the collision hazard in near Earth orbits.	23
3.1	The worldwide NORAD Space Surveillance Network provides frequent coverage of low altitude satellites.	26
3.2	The overall sensitivity of the NORAD Space Surveillance Network is highly dependent on the altitude of the satellite.	28
3.3	The sensitivities of specific NORAD radars.	28
3.4	The Long Duration Exposure Facility (LDEF), deployed in 1984 by the Space Shuttle.	30
3.5	The mass of an Earth satellite can be approximated by its average cross-sectional area.	32
3.6	This hypervelocity impact target was designed to simulate a typical spacecraft structure.	35
3.7	The mass ratio (projectile/target) during this hypervelocity impact test was 9%.	36
3.8	The same projectile type impacted a more massive target at the same velocity (mass velocity of 3%).	36
3.9	Hypervelocity impact tests have revealed the maximum ejection velocities of debris as a function of particle diameter.	37
3.10	A Gabbard diagram for a satellite in a circular orbit is depicted by a single point.	38
3.11	For an elliptical orbit the Gabbard diagram plots the apogee (x) and the perigee (+) against the orbital period.	38
3.12	When a satellite in a nearly circular orbit fragments, the resultant debris is distributed in a characteristic X-pattern.	39
3.13	Satellite 1971-15A was in an elliptical orbit near perigee when it fragmented.	40
3.14	When a satellite in an elliptical orbit fragments near apogee, the result is a Gabbard like this one for satellite 1976-126A.	40
3.15	In the general case of a satellite in an elliptical orbit, the slope of the debris arms is a function of the value of the true anomaly at the time of the fragmentation. This Gabbard diagram is for satellite 1977-65B which broke up at a true anomaly of 108 degrees.	41
3.16	The near-term effects of orbital decay result in the collapse of the left arm on a Gabbard diagram as shown here for satellite 1961-Omicron more than 23 years after its breakup.	42

Illustrations *Continued*

FIGURE		PAGE
3.17	Example 1: Breakup of satellite 1975-04B (second event).	43
3.18	Example 2: Breakup of satellite 1974-103A (first event).	44
3.19	Example 3: Breakup of satellite 1980-89A (second event).	44
3.20A	Example 1: Weighted Gabbard diagram for 1981-53A (December 1984) — size range 0.0 – 0.01 m^2.	46
3.20B	Example 1: Weighted Gabbard diagram for 1981-53A — size range 0.01 – 0.10 m^2.	46
3.20C	Example 1: Weighted Gabbard diagram for 1981-53A — size range 0.10 – 1.0 m^2.	47
3.20D	Example 1: Weighted Gabbard diagram for 1981-53A — size range 1.0 – 10.0 m^2.	47
3.20E	Example 1: Weighted Gabbard diagram for 1981-53A — size range 10 m^2 and greater.	48
3.20F	Example 1: Weighted Gabbard diagram for 1981-53A — all size ranges.	48
3.21A	Example 2: Weighted Gabbard diagram for 1977-65B (December 1984) — size range 0.0 – 0.01 m^2.	49
3.21B	Example 2: Weighted Gabbard diagram for 1977-65B — size range 0.01 – 0.10 m^2.	49
3.21C	Example 2: Weighted Gabbard diagram for 1977-65B — size range 0.10 – 1.0 m^2.	50
3.21D	Example 2: Weighted Gabbard diagram for 1977-65B — size range 1.0 – 10.0 m^2.	50
3.21E	Example 2: Weighted Gabbard diagram for 1977-65B — size range 10 m^2 and greater.	51
3.21F	Example 2: Weighted Gabbard diagram for 1977-65B — all size ranges.	51
3.22	SAFE Test form.	52
3.23	An in-plane heading plot depicts the radial and tangential components of the debris ejection velocities.	54
3.24	An out-of-plane heading plot identifies the normal and tangential components of the debris ejection velocities.	54
3.25	These time-dependent analyses of two satellite breakups are a powerful tool in determining the time of the fragmentation event.	59
3.26	A simple satellite fragmentation simulation can not only model the numbers and orbits of the debris but also can be used to predict the evolution of the debris cloud.	60
3.27	This Gabbard diagram depicts the initial distribution of debris from a simulation of the breakup of satellite 1981-53A.	62
3.28	The effects of decay on smaller particles from the fragmentation of 1981-53A can be seen in this simulated Gabbard diagram of the debris two weeks after the event.	62
3.29	Assuming a symmetrical distribution of debris from 1981-53A, the in-plane debris heading plot should resemble the simulated graph shown here.	63
3.30	Out-of-plane debris heading plots, such as this one for 1981-53A, simulate the higher ejection velocities imparted to the smaller particles.	63
3.31	This summary of the size of the cataloged satellites clearly shows the resolution of the Space Surveillance Network drops off abruptly around 0.05 m^2.	64
4.1	Large orbital structures with long lifetimes are exceptionally vulnerable to collisions with space debris.	70
4.2	Maneuvering complex structures like this space station will be difficult but possibly necessary to avoid large pieces of space debris.	71
4.3	The average relative velocity expected between an object and a piece of space debris is a function of both the altitude and inclination of the object.	72
4.4	Across all altitudes, higher collision velocities can be expected for objects in retrograde orbits.	73
4.5	A recent examination of the *NORAD Satellite Catalog* indicated that the average radar cross section for Earth satellites is about 5 square meters.	74
4.6	The critical mass in a hypervelocity collision determines the mass distribution of the resultant debris.	75
4.7	The probabilities of collision for a variety of spacecraft in the year 2006.	76
4.8	The distribution of geosynchronous satellites.	78
4.9	The position of nearly geosynchronous satellites and their direction of motion relative to the geostationary belt.	79
4.10	The spatial density at geosynchronous altitudes increased by about two orders of magnitude between 1977 and 1986.	81
4.11	The artificial debris flux projected for 1995 exceeds that of the meteoroid environment for all particles above 1 mm in diameter.	82

Illustrations *Continued*

FIGURE		PAGE
4.12	The time between collisions for a large, low altitude space structure and a member of the currently tracked satellite population is approaching unacceptable levels.	83
5.1	The international space launch rate has remained virtually unchanged for the past 20 years.	85
5.2	A piece of space debris was responsible for this dramatic impact found on a retrieved louver from the Solar Max satellite.	87
5.3	The hazards of secondary ejecta generated by a hypervelocity collision are illustrated by this view of a Solar Max surface.	88
5.4	A scanning electron microscope photograph of a thermal tile from the Space Shuttle *Atlantis* revealed a hypervelocity impact crater probably caused by a collision with space debris.	89
5.5	Retrieval of old satellites and large pieces of space debris with the Space Shuttle is possible but generally not economically feasible. See Plate 2.	90
5.6	By returning to Earth, the Space Shuttle reduces the number of spent stages left in Earth orbit.	90
5.7	Satellite retrieval can be astronaut-assisted or carried out using automated proximity operations vehicles (POVs). See Plate 3.	90
5.8	As of 1 August 1987 more, than four dozen satellites carrying radioactive materials were in orbit about the Earth.	94
5.9	The amount of radioactive material now in orbit about Earth exceeds 1,450 kg.	95
5.10	Conceptual design of a proximity operations vehicle (POV).	96
5.11	Advanced POV design.	97
5.12	Satellite retrieval and repair.	98
5.13	Semisynchronous satellite spatial density.	100

Tables

TABLE		PAGE
2.1	Deliberate satellite breakups.	14
2.2	Propulsion-related satellite breakups.	17
2.3	Satellite breakups of unknown cause.	21
3.1	NORAD space surveillance sensors.	27
3.2	Future NORAD space surveillance sensors.	27
3.3	Trackable mass versus satellite mass (circular disk).	33
3.4	Trackable mass versus actual mass (building block).	33
3.5	Comparison of fragment mass values.	33
3.6	Mass distribution data for SAFE test.	53
3.7	Change in velocity results for SAFE Test (km/s).	53
3.8	SAFE Test results.	53
4.1	Results from Bjork's equation.	69
4.2	Encounters and collision probabilities for 4-day Shuttle missions.	75
4.3	Time between collisions for the Shuttle.	77
5.1	Radioisotope power supplies in Earth orbit.	91
5.2	Nuclear reactors in Earth orbit.	92
5.3	Shuttle RMS requirements for satellite retrieval.	96

Glossary

ADCOM	Aerospace Defense Command
AEDC	Arnold Engineering and Development Center (Tennessee)
AFB	Air Force Base
AIAA	American Institute of Aeronautics and Astronautics
A/M	Area-to-Mass ratio
ASAT	Antisatellite
BMEWS	Ballistic Missile Early Warning System
CCD	Charge Coupled Device
CID	Charge Injection Device
COSPAR	Committee on Space Research
DOD	Department of Defense
ECS	Experimental Communications Satellite
EORSAT	Electronic Intelligence Ocean Reconnaissance Satellite
ERTS	Earth Resources Technology Satellite (also known as Landsat)
ESA	European Space Agency
EVA	Extra-Vehicular Activity, i.e., spacewalk
FLTSATCOM	Fleet Satellite Communications (U.S. Navy satellite)
FOV	Field of View
GEO	Geostationary Earth Orbit
GEODSS	Ground-based Electro-Optical Deep Space Surveillance system
GLONASS	Global Navigation Satellite System (U.S.S.R)
GPS	Global Positioning System (U.S.)
GSFC	Goddard Space Flight Center (NASA)
ITU	International Telecommunications Union
LDEF	Long Duration Exposure Facility
LEO	Low Earth Orbit
MAMA	Multi-Anode Microchannel Array
MMS	Multi-Mission Modular Spacecraft
NASA	National Aeronautics and Space Administration
NORAD	North American Aerospace Defense Command
OTV	Orbital Transfer Vehicle
PARCS	Perimeter Acquisition Radar Characterization System (North Dakota)
POV	Proximity Operations Vehicle
PW	Proportionally Weighted, as in PW Gabbard diagram
RAE	Royal Aircraft Establishment (United Kingdom)
RCS	Radar Cross Section
RFI	Radio Frequency Interference
RMS	Remote Manipulator System
RTG	Radioisotope Thermoelectric Generator
SAFE Test	Satellite Fragmentation Event Test
SATCAT	Satellite Catalog (NORAD)
SNAP	Systems for Nuclear Auxiliary Power
SPADATS	Space Detection and Tracking System
STS	Space Transportation System, i.e., Space Shuttle
UHF	Ultra High Frequency
VHF	Very High Frequency

Index

Aluminum oxide, 10, 24
American Institute of Aeronautics and Astronautics (AIAA), 86, 89, 101
Antisatellite testing
  Soviet, 13, 14, 15, 22
  U.S., 13, 14, 15
Apollo, 1, 67, 69
Ariane, vii, 16, 22
Artificial debris
  derelict, 11
  fragments, 12
  operational, 9, 10, 100
Atlas rocket, 16, 32
Atmospheric drag, 5, 31
Ballistic coefficient, 5, 9, 11, 31
Bjork's equation, 68-69
Breakup time, 58-60
CCDs/CIDs, 64
Collision with STS-7, 4, 12
COSPAR, 6, 87
Debris cloud, 26, 55-58, 60-61
Debris flux, 9, 29, 31, 82
Debris heading plots, 53-54, 83
Debris models, 69-71
Delta rockets, vii, 12-13, 16-18, 22-23, 45, 82, 89-90, 97
Delta velocity, 11, 34-35, 41, 44, 61
ECS 1, 20
ECS 2, 20
EORSAT (Kosmos 699-type), 16
European Space Agency (ESA), 10, 68
Explosion data, 33-34
FLTSATCOM, 77
Fragmentation events
  collision-induced, 18
  deliberate, 13, 23
  propulsion-related, 16, 18, 22
Gabbard diagram, 25, 31, 37-44, 55
Gabbard diagram (weighted), 25, 42, 52, 62
Gemini, 11
GEODSS, 26-27, 29
Geosynchronous/geostationary, 2, 6, 9-10, 20, 77-80, 86, 88
GLONASS, 99-100
Hamilton's equations of motion, 56
Hazard, 1, 7, 67, 71, 73, 75, 77, 82, 87
Himawari rocket (1977-65B), 40, 45, 49-53
Hypervelocity impact data, 11, 29, 33-37, 87-88
INTELSAT, 87
International Telecommunications Union (ITU), 6, 86
Kinetic theory of gases, 72-73
Kornhauser's equation, 68
Kosmos 397 (1971-15A), 40
Kosmos 699 (1974-103A), 16, 44, 56, 60
Kosmos 862 (1976-105A), 22
Kosmos 886 (1976-126A), 40
Kosmos 954 (1977-90A), 93
Kosmos 1220 (1980-89A), 42
Kosmos 1275 (1981-53A), 22, 45-48, 52-53, 75
Lagrane's planetary equations, 53
Landsat 1 (ERTS 1) rocket (1972-58B), 59-60
Landsat 2 rocket (1975-04B), 43
Liouville's theorem, 56
Long Duration Exposure Facility (LDEF), 29-30, 67, 89
Mass distribution, 13, 25, 31, 33-34
Measurement devices, 61
Meteoroids/meteorites, 1, 29, 67-68
Molniya, 2, 6, 16
NASA, vii, 7, 8, 13, 69-70, 85-86
NOAA 3 rocket (1973-86B), 38-39
NORAD, vii, 1, 3-4, 6, 10, 17, 22-23, 25-26, 30, 41, 60-61, 69-72, 77
Nuclear reactors, 91-93
Oort cloud, 71
Orbital decay (see atmospheric drag)
Orbital transfer vehicle (OTV), 90, 94
P-78, 19-20
Pageos, 12, 20
Palapa B2, 90, 96-97
PARCS, 30-31
Perturbation theory, 31, 37-38, 61
Poisson probability distribution, 74, 76
Probability of collision, 5, 9-10, 18, 20, 75-77, 80, 83, 88
Proximity operations vehicle (POV), 90, 96-98
Radar cross-section (RCS), 25-26, 28-29, 31-32, 64, 69, 72-74
Radars, 6, 25-27, 30-31
Radioisotope thermoelectric generators (RTGs), 91
Remote manipulator system (RMS), 96-97
SAFE test, 34, 52-53, 65
Salyut space station: 1, 11
Saturn rocket, 16
Semisynchronous, 2, 6, 16, 99-100
Simulation, 60-63, 65
Skylab, 1, 11, 67-69, 90
SNAP, 91
Solar cycle, 5, 12, 31
Solar Max, 10-12, 87-89, 98
Solar pressure, 6, 10
Space launch rate, 1, 85
Space shuttle 4, 16, 67, 75-77, 88-90, 95-98
Space station, 5, 31, 70, 76, 88, 99
Space telescope, Hubble, 5
SPADATS, 25-26
Spatial density, 31, 57, 81, 99-100
Sputnik, 1
Statistical mechanics, 25, 56-58
Strategic Defense Initiative (SDI), 13, 19
Summer's equation, 68
Sun-synchronous, 18, 22, 81
Titan rocket, 16
Velocity distribution, 33-35, 37
Weibull distribution, 80
Westar VI, 90, 96-97
Westford Needles experiment, 11
Whipple's equation, 68

O9-BKT-039

ISBN 0-89